UNIVERSITY OF SOUTHAMPTON

FACULTY OF MEDICINE

Cancer Sciences

B-CELL RECEPTOR INDUCED AUTOPHAGY AND PHAGOCYTOSIS IN CHRONIC LYMPHOCYTIC LEUKAEMIA

Volume 1 of 1

by

ANNABEL RACHEL MINTON

MRes, BSc (Hons)

ORCID ID 0000-0002-2640-990X

https://orcid.org/0000-0002-2640-990X

Thesis for the degree of Doctor of Philosophy

February 2022

UNIVERSITY OF SOUTHAMPTON

Abstract

FACULTY OF MEDICINE

CANCER SCIENCES UNIT

THESIS FOR THE DEGREE OF DOCTOR OF PHILOSOPHY

B-CELL RECEPTOR INDUCED AUTOPHAGY AND PHAGOCYTOSIS IN CHRONIC LYMPHOCYTIC LEUKAEMIA

By Annabel Rachel Minton

Chronic lymphocytic leukaemia (CLL) is a common mature B-cell malignancy with a highly heterogeneous disease course, tightly linked to features of the B-cell receptor (BCR). Higher surface immunoglobulin (sIg)M signalling capacity is associated with poorer outcomes, and inhibitors targeted against BCR-associated kinases induce dramatic clinical responses. In normal B cells, the BCR has a dual capacity to induce intracellular signalling responses, and internalise soluble or particulate antigens for presentation to T-helper cells. These processes are subject to cross-talk, as BCR signalling can be required for antigen internalisation, in addition to regulating antigen presentation machinery expression. There remains a clear need to understand BCR-mediated signalling and antigen internalisation/presentation pathways in CLL cells.

One process with important links to both signalling and antigen presentation is autophagy. Autophagy is tightly regulated by signalling pathways and upregulated in many types of cancer, resulting in breakdown of non-essential, damaged or misfolded proteins/organelles, thereby protecting cells from effects of starvation or stress. However, autophagy also plays specialised roles in the immune system, including antigen processing and presentation, and is known to be activated via BCR signalling in normal B cells.

My initial hypothesis was that BCR stimulation induces autophagy in CLL cells. Using bead immobilised anti-IgM/D, I demonstrated that BCR stimulation increased autophagy markers (LC3B-II, GABARAPL2 p62 and pATG13). Inhibitor studies demonstrated that autophagy induction was dependent on autophagy regulators VPS34 and ULK1/2, and the BCR signalling kinase SYK. Confocal analysis revealed autophagosome turnover following sIgM stimulation (LC3B/LAMP colocalisation), confirming that BCR stimulation induces active autophagy in CLL. An unexpected observation from imaging studies was that anti-IgM coated beads were internalised by CLL cells. I therefore developed a quantitative, flow cytometry assay, to confirm that CLL cells efficiently internalised anti-IgM-coated beads. Internalisation required SYK activity, but not VPS34, and appeared to be mediated by a phagocytic process, requiring actin remodelling but not dynamin. These results demonstrate for the first time that CLL cells can internalise particulate antigen via sIgM.

I performed RNA-seq analysis to probe consequences of sIgM stimulation/autophagy inhibition in CLL cells, demonstrating that anti-IgM treatment results in strong activation of antigen presentation pathways. I therefore investigated the capacity of CLL cells to present antigen from anti-IgM-coated beads, via MHC-II, to T cells. This demonstrated that CLL cells could present particulate-derived antigen to a similar extent as soluble. Both processes appeared independent of autophagy. Presentation from soluble antigen required SYK activity, but SYK inhibition did not affect antigen presentation from particulate antigen, despite inhibiting phagocytosis. Therefore, internalisation of particulate antigen may not be required for presentation, and in fact B cells may secrete proteases to liberate antigen extracellularly.

In summary, these results provide important new insight into the function of the BCR in CLL as a dual mediator of signalling and antigen presentation. Autophagy is a target of signalling, but does not appear to play a key role in either phagocytosis or MHC-II Ag presentation. The ability of CLL cells to present particulate antigen may be particularly important for pathobiology. However, it does not seem to be affected by currently used kinase inhibitors, including ibrutinib, and further analysis of the pathways involved may reveal new targets for therapies aimed at depriving CLL cells of potential T-cell help.

List of Contents

List of Figures

List of Tables

List of Accompanying Materials

An accompanying dataset for this thesis is available under DOI: **10.5258/SOTON/D2139**

RNA-seq data files are available at ArrayExpress (https://www.ebi.ac.uk/arrayexpress/) under accession: **E-MTAB-11195**

Research Thesis: Declaration of Authorship

Print name: Annabel Rachel Minton

Title of thesis: B-cell receptor induced autophagy and phagocytosis in Chronic Lymphocytic Leukaemia

I declare that this thesis and the work presented in it is my own and has been generated by me as the result of my own original research.

I confirm that:

1. This work was done wholly or mainly while in candidature for a research degree at this University;
2. Where any part of this thesis has previously been submitted for a degree or any other qualification at this University or any other institution, this has been clearly stated;
3. Where I have consulted the published work of others, this is always clearly attributed;
4. Where I have quoted from the work of others, the source is always given. With the exception of such quotations, this thesis is entirely my own work;
5. I have acknowledged all main sources of help;
6. Where the thesis is based on work done by myself jointly with others, I have made clear exactly what was done by others and what I have contributed myself;
7. Parts of this work have been published as:

BCR signaling contributes to autophagy regulation in chronic lymphocytic leukemia (Smith *et al.*, 2020) DOI: 10.1038/s41375-019-0557-y

B-cell receptor dependent phagocytosis and presentation of particulate antigen by chronic lymphocytic leukemia cells (Minton *et al.*, 2022) DOI: 10.37349/etat.2022.00070

Signature: Date: 28/02/2022

Acknowledgements

The work presented in this thesis could not have been realised without the help and support from numerous other people, who contributed in many different forms. Firstly, I would like to thank my first supervisor, Dr Andrew Steele, for his optimistic outlook and continued supportiveness throughout the course of my PhD, despite challenges. I also owe special thanks to Dr Lindsay Smith, who offered invaluable training and assistance, as well as a keen enthusiasm for the autophagy section of this project, that both inspired and motivated me in this area. Autophagy is a complex area, and I am grateful for all of this support, and on top of this- couldn't have had a better time at Autophagy UK with anyone else.

I am also extremely grateful to my current primary supervisor, Professor Graham Packham, for adopting me for the final year of my PhD, through an extremely challenging time for everyone and at a time where results slowed and progression was challenging. The support and understanding provided has allowed me to complete my PhD with a set of results I can be proud of, and for this I cannot thank him enough. Dr David Tumbarello also provided invaluable feedback on the autophagy components of this project as well as additional assistance. The final part of this project was undertaken in a collaboration with Professor Ludwig Munthe at the University of Oslo, who has also been invaluable to this project. Professor Munthe has given his time in meetings and provided ideas and feedback on the components of the project involving the cell line modified by his group, and previously published on with CLL, which he kindly gifted to us for the final chapter of this PhD.

While these individuals provided primary supportive roles, the entire Southampton CLL group has been a wonderful, kind and energetic environment to work within, and I would like to thank them all hugely for all of the help and support. In particular, I would like to thank Dr Karly-Rai Rogers-Broadway, for all the help in setting experiments and reagents back up once we were able to return to work, and for moral support during this, as well as making coordinating lab cleans fun. I would also like to thank Dr Dean Bryant and Lara Buermann for their support in the RNA seq portion of this thesis. The challenges presented in the last year have truly highlighted the role of a kind and supportive lab group , when returning to work emphasised how important small lab conversations on a day to day basis were.

In addition to this, none of this could have been achieved without patient samples, therefore I would like to kindly thank all patients for donation of samples and the technical support team involved in collection, processing and storage of CLL samples, in particular Isla Henderson, for all the assistance in sample ordering. I would also like to thank Professor Francesco Forconi for providing patient samples and clinical data, and Professor Freda Stevenson for valuable feedback in group meetings.

Definitions and Abbreviations

AID: Activation-induced cytidine deaminase

Ab: Antibody

Ag: Antigen

AKT: Protein kinase B

ATG: Autophagy

ATG (3/5/7 etc): Autophagy related gene/protein

BAF: Bafilomycin A1

Bcl-2: B cell lymphoma 2

BCR: B-cell receptor

BM: Bone Marrow

BSA: Bovine Serum Albumin

BTK: Bruton tyrosine kinase

Caspases: Cysteinyl aspartic acid-proteases

cDNA: complementary DNA

CCL: CC Motif Chemokine Ligand

CLL: Chronic Lymphocytic Leukaemia

CML: Chronic Myeloid Leukaemia

CXC: chemokine receptor type

CXCL: C-X-C motif chemokine ligand

DAG: Diacylglycerol

DAPI: 4',6-diamidino-2-phenylindole

Delta: δ

DLBCL: Diffuse large B cell lymphoma

DMSO: Dimethyl sulphoxide

DNA: Deoxyribonucleic acid

DTT: Dithiothreitol

EBV: Epstein-Barr virus

EBSS: Earls Balanced Salt Solution

EDTA: Ethylenediaminetetraacetic acid

ELISA: Enzyme-linked immunosorbent assay

ERK: Extracellular signal–regulated kinase

F(Ab)2: Enzyme digest of whole Ab to leave the Fragment antigen-binding portion

FBS: Foetal bovine serum

FCR: Fludarabine, cyclophosphamide and rituximab in combination

FCS: Forward scatter

FcγR : Fc Gamma Receptor

FcγRIIb: Fc gamma-receptor II-b

FITC: Fluorescein isothiocyanate

FL: Follicular lymphoma

GC: Germinal centre

GSEA: Gene-set enrichment analysis

HBSS: Hank's Balanced Salt Solution

HCQ: Hydroxychoroquine

HRP: Horseradish peroxidase

iCa2+: Intracellular calcium

IGHV : Immunoglobulin Heavy Chain Variable Region

IGHV: Immunoglobulin heavy chain variable

IKK: I-κB kinase

IL: Interleukin

IP3: Inositol-1,4,5-triphosphate

ITAMS: Immune receptor tyrosine activation motifs

JAK: Janus kinase

JNK: c-Jun N-terminal kinase

LAP: LC3-Associated Phagocytosis

LIR: LC3-Interacting Region

LN: Lymph node

mAB: Monoclonal Antibody

MCL-1: Myeloid cell leukaemia 1

M-CLL: Mutated IGHV CLL patient subgroup

MHC I / HLA I: Major Histocompatibility Complex Class I / Human Leukocyte Antigens Class I

MHC II / HLA II: Major Histocompatibility Complex Class II / Human Leukocyte Antigens Class II

miR: MicroRNA

mRNA: Messenger RNA

NF-κB: Nuclear factor-κB

NLCs: Nurse-like cells

PAGE: Polyacrylamide Gel Electrophoresis

PARP: Poly ADP ribose polymerase

PBMC: Peripheral Blood Mononuclear Cells

PBS: Phosphate Buffered Saline

PCR: Polymerase chain reaction

PE: Phycoerythrin

PercP: Peridinin-chlorophyll Protein Complex

PH: Pleckstrin homology

PI: Propidium iodide

PI3K: Phosphatidylinositol-3-kinase

PIP2: Phosphatidylinositol 4,5-bisphophate

PIP3: Phosphatidylinositol (3,4,5)-trisphosphate

PKC: Protein kinase C

PLC-γ2: Phospholipase C-γ2

PMA: Phorbol 12-myristate 13-acetate

PS: Phosphatidylserine

pSTAT6: Phosphorylated Signal Transducer and Activator of Transcription 6

qPCR: Quantitative polymerase chain reaction

R10 media: RPMI 1640, Glutamine, penicillin/ streptomycin, foetal bovine serum

RNA: Ribonucleic acid

ROS: Reactive oxygen species

RT: Reverse transcription

SHIP: SH2-containing inositol-5-phosphatase

SHM: Somatic hypermutations

SHP: SH2-containing phosphotyrosine phosphatase

sIg: Surface immunoglobulin

siRNA: small interfering RNA

SOCs: Suppressor of cytokine signalling proteins

SSC: Side scatter

SYK: Spleen tyrosine kinase

TACI: Transmembrane activator CAML interactor receptor

TCR: T-cell receptor

Th cell: T helper cells

U-CLL: *IGHV* unmutated Chronic Lymphocytic Leukaemia

Zap-70: Zeta-chain-associated protein kinase 7

Chapter 1 : Introduction and Background

1.1 Introduction

The overall goal of this thesis is to explore the functions of the B-cell receptor (BCR) in chronic lymphocytic leukaemia (CLL) as a dual regulator of intracellular signalling and antigen internalisation/presentation. Autophagy has important links to both BCR signalling and antigen presentation in normal B cells and was a particular focus of the study. Therefore, this section will introduce the key topics of CLL, B cell biology and development, BCR signalling and antigen internalisation pathways, T-cell interactions and autophagy.

1.2 Chronic Lymphocytic Leukaemia

1.2.1 Background

Chronic Lymphocytic Leukaemia (CLL) is an incurable B-cell malignancy that displays a high degree of clinical heterogeneity, with stark contrast in treatment outcomes between patients with indolent or progressive disease (Kipps *et al.*, 2017a). A CLL diagnosis is typically made by the presence of > 5×10^9/L clonal B cells in the peripheral blood for a minimum of 3 months (Kipps *et al.*, 2017b; Hallek *et al.*, 2018), with this lymphocytosis often being the only manifestation at first diagnosis. CLL is the most prevalent adult leukaemia in Western society, largely affecting older individuals, with incidence increasing exponentially over the age of fifty. The median age at diagnosis for CLL is 72 years, with an average incidence between 1975-2014 in the US of 4.82/100,000 people per year (Howlader N, 2015). However, as the average population age gradually increases, the incidence of CLL prevalence and impact is escalating, particularly in older population groups (Brenner, Gondos and Pulte, 2008; van der Straten *et al.*, 2020). There is a high level of variability in disease progression between individuals, with the impact on lifespan and health ranging from mild to severe. Patients with more indolent forms of the disease may live a near normal lifespan, compared to age-matched controls, requiring little or no treatment (Badoux *et al.*, 2011; Hallek *et al.*, 2018; Tresckow *et al.*, 2019). However, individuals with more progressive forms of the disease show poorer outcomes; presenting symptoms much sooner after diagnosis, and experiencing significantly shortened lifespans even with treatment. Treatment using standard chemotherapy, or combinations such as FCR, can prolong lifespan but is rarely curative. These treatments can still result in relapses and resistance of the tumour population to drug.

1.2.2 Prognostic markers

The most widely used prognostic marker for CLL is the mutational status of the expressed immunoglobulin heavy chain variable (*IGHV*) region genes. *IGHV* mutation occurs as a part of B cell maturation, where chromosomal recombination of the V (variable), D (diversity) and J (junctional) segments form the V region of the heavy and light immunoglobulin chains. The V regions form the antigen binding cleft, and it is recombination of these that results in a wider repertoire of BCRs available to encounter an antigen they have affinity to. When a B cell encounters antigen that its current BCR can bind to, a further round of affinity finetuning occurs in the form of somatic hypermutation. This results in a mutated *IGHV* region. Thus, unmutated *IGHV* correspond to B cells that have not encountered antigen and undergone a germinal centre (GC) reaction, and mutated *IGHV* corresponds to a post antigen exposure/ GC reaction B cell This process is covered more fully in section 1.4 of this thesis, but a summary illustration is shown in Figure 1. CLL cases are separated into two major prognostic groups with expression of unmutated or mutated *IGHV* genes (U-CLL and M-CLL, respectively). The outcome of U-CLL is significantly worse than M-CLL, with M-CLL patients displaying a significantly longer median lifespan in comparison with the much shorter median lifespan for patients with U-CLL (Damle *et al.*, 1999; Hamblin *et al.*, 1999).Other markers of progressive disease include cell surface expression of CD38 or CD49d, or aberrant intracellular expression of the ζ -chain-associated protein kinase 70 kDa (ZAP-70) (Rosenwald *et al.*, 2001; Orchard *et al.*, 2004). In addition to these prognostic markers, genetic markers such as 17p, 11q, and 13q also correlate with clinical outcome (Quijano *et al.*, 2008).

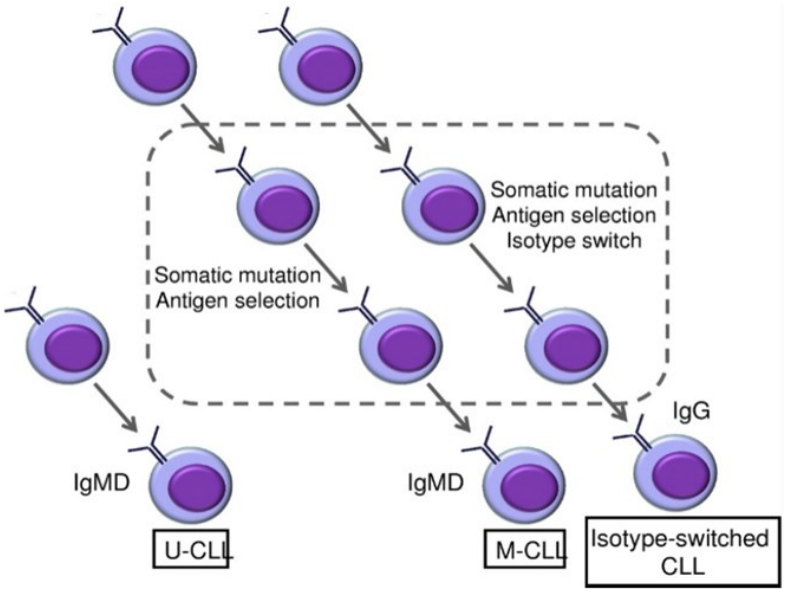

Figure 1. Formation of the 2 major subsets of CLL and a minor isotype switched variant
U-CLL is thought to derive from pre-GC B cells and lack SHM, whereas M-CLL derives from post-GC cells with SHM. A third smaller subset is thought to derive from infection or antigen engagement and a class-switched isotype. Illustration adapted from Stevenson et al., 2011.

TP53, encoding the tumour suppressor protein p53, is one of the most widely studied tumour suppressor genes, known to be dysregulated in many forms of cancer. In CLL, patients with p53 protein alterations have been shown to have significantly poorer prognosis, usually a consequence of del(17p) or *TP53* mutations. The differences between these disease groups has led to increasing interest in the presence of key cellular and molecular markers, which could provide potential prognostic and therapeutic targets. The genetic elements of CLL create additional complexity to the disease phenotypes and heterogeneity of clinical prognostic outcomes. Figure 2,from Kipps et al, 2017, illustrates recurringly mutated genes in CLL. The discovery that CLL is driven by activation of the B-cell receptor (BCR), and of these phenotypic differences in disease progression, has led to new research on the role of the BCR and downstream signalling in CLL (Burger and Chiorazzi, 2013)

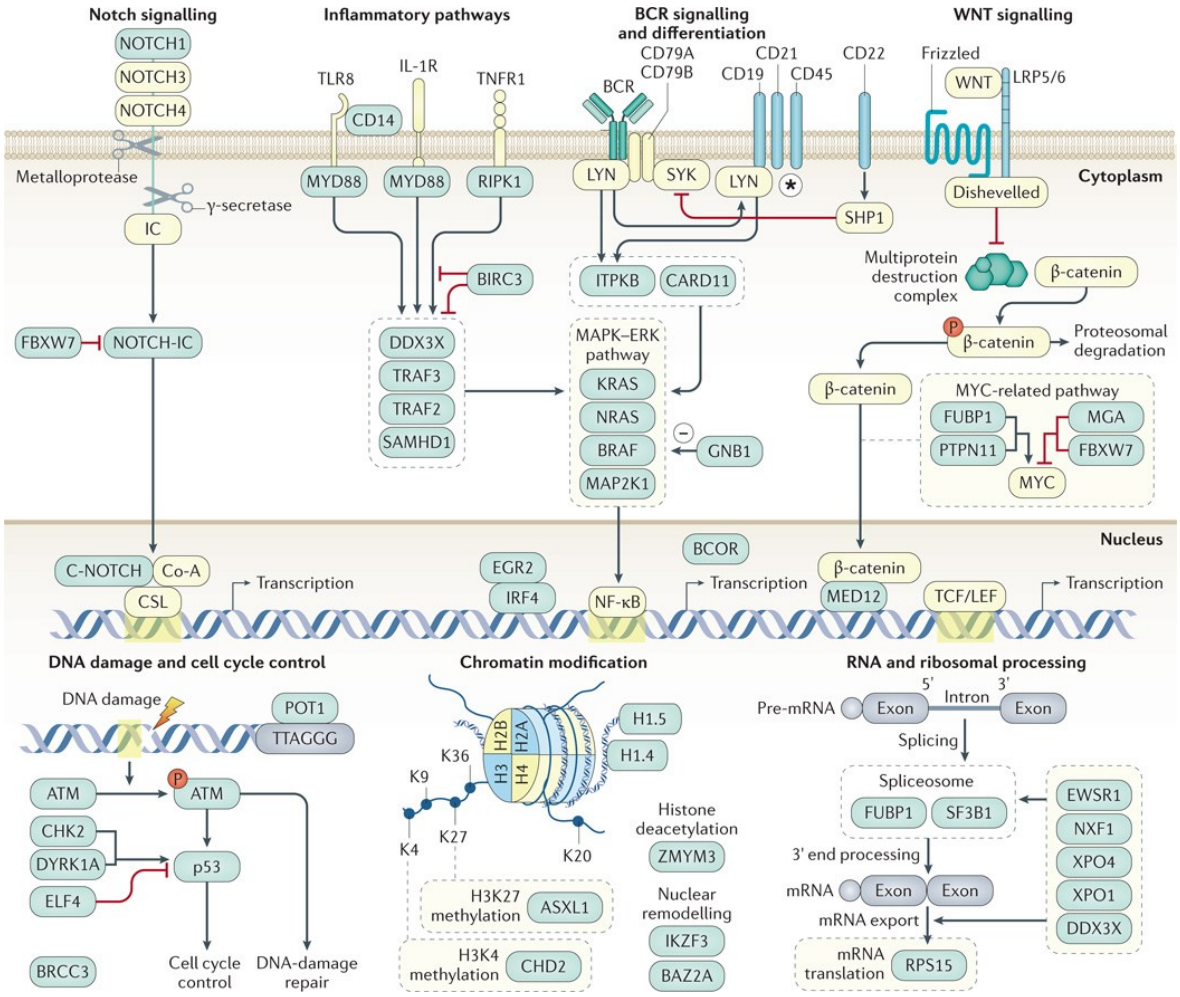

Figure 2. Somatic mutations in CLL
Recurrently mutated genes in CLL may influence a range of downstream cellular pathways including BCR signalling, cell cycle control, DNA repair, chromatin modification and RNA processing/translation. Illustration adapted from Kipps et al., 2017.

1.2.3 Treatment

The major advancement in treatment of CLL occurred with the introduction of immunochemotherapy, combining fludarabine with monoclonal antibodies, such as the anti-CD20 antibody rituximab, which showed significantly improved progression-free survival rates (Schulz *et al.*, 2002). The combination of fludarabine, cyclophosphamide, and rituximab chemoimmunotherapy (FCR) has been shown to be an effective treatment option for patients with relapsed CLL (Badoux *et al.*, 2011). However, patients with more progressive disease phenotypes still displayed reduced responsiveness to treatment with standard immunochemotherapy (Hus and Rolinski, 2015). BCR signalling capacity corresponds to disease progression in CLL (Figure 3) (D'Avola *et al.*, 2016) , with subsequent introduction of small molecule inhibitors, targeting BCR signalling, offering further significant treatment advances.

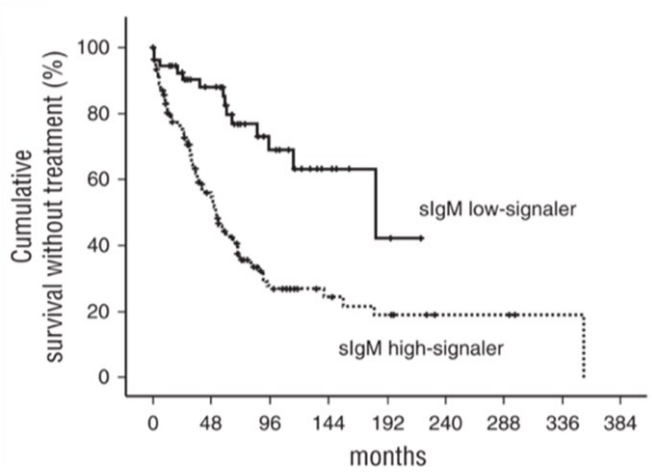

Figure 3. **The significance of sIgM-induced signalling for disease progression in CLL**
Patients with high signalling cells (>5% cell population responds to anti-IgM stimulation), termed "sIgM high-signaller", are represented by the dotted line and have worse prognosis overall compared with patients with low signalling cells (≤5% cell population responds to anti-IgM stimulation), termed "sIgM low-signaller", which is represented by the solid line. Figure from (D'Avola et al., 2016).

These new therapies target kinases associated with the BCR signalling pathway, which include the Bruton tyrosine kinase (BTK) inhibitors, ibrutinib and acalabrutinib, the phosphatidylinositol-3-kinase (PI3K) delta inhibitor, idelalisib, and the spleen tyrosine kinase (SYK) inhibitor, fostamatinib (pro-drug of R406). Clinical trials using ibrutinib report high overall response rates, in addition to long-term safety in patients (O'Brien *et al.*, 2018). However, to date these agents are not typically curative as single agent therapies, in part due to the protective effect of the tumour microenvironment which limits effectiveness and/or acquisition of genetic lesions such as C481S (BTK) (Jain *et al.*, 2015) in a proportion of patients. Mutations in BTK and PLCG2 are among those becoming an increasing clinical issue following ibrutinib treatment in CLL (Woyach *et al.*, 2017). In

an effort to combat this, the Bcl-2 inhibitor venetoclax (ABT-199) has been utilised to treat resistant CLL. CLL cells overexpress Bcl-2, a pro-survival protein that increases cells resistance to apoptotic cell death, therefore using the Bcl-2 inhibitor Venetoclax induces rapid apoptosis in CLL cells due to this aberrant Bcl-2 overexpression (Anderson *et al.*, 2016). Recent trials such as the CLARITY clinical trial, combining venetoclax with ibrutinib, show success in treating relapsed and resistant CLL cases (Waldron, Winter and Hill, 2017). However, mutations leading to resistance to this compound, such as G101V (*BCL-2*) are already becoming apparent (Blombery *et al.*, 2019).

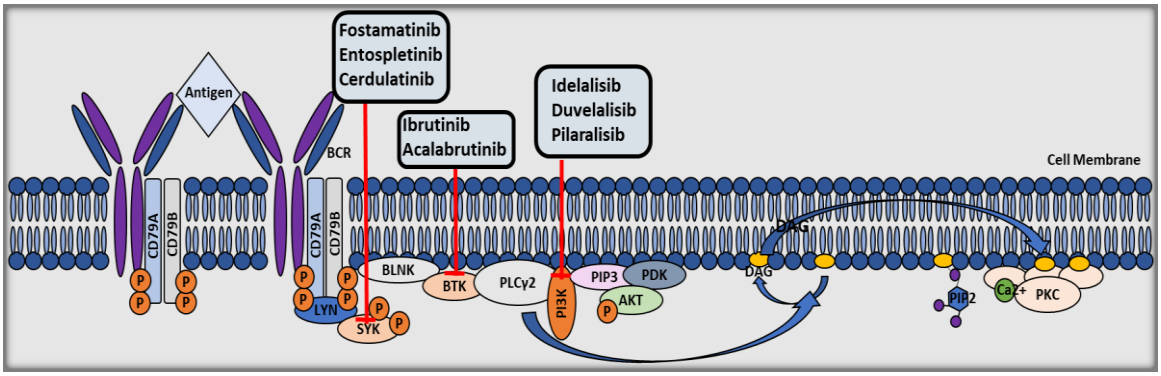

Figure 4 BCR signalling targeting drugs
The main pathways that lead to cell survival and proliferation downstream of the BCR are shown in along with drugs targeted against key signalling intermediates.

1.3 B Cell development

B lymphocytes have been characterised primarily in their role as antibody producing cells, and as such are central in the humoral immune response. As part of the adaptive immune system, they are responsible for providing protection from a large variety of pathogens, including bacterial cells and viruses. Mammalian B cell development begins in the liver or bone marrow from haematopoietic precursor cells, with maturation and functionality subsequently developing in the lymph nodes and spleen (Asma, Langlois van den Bergh and Vossen, 1984). Early developmental stages in the bone marrow are focused on functional rearrangement of immunoglobulin gene segments, in order to generate a repertoire of B cells capable of recognising a diverse range of antigens. During bone marrow development, B cells primarily express surface IgM (sIgM) Pro- B cells do not express functional BCR, instead expressing only CD79A and B. Heavy chain gene rearrangement of the immunoglobulin occurs with development of pro-B cells into pre-B cells, resulting in the expression of heavy chains and surrogate light chains on the pre-B cell, which along with CD79A and CD79B, forms the pre-B-cell receptor on the pre-B cell surface. The pre-B cell subsequently undergoes light chain gene rearrangements, differentiating into an immature B cell with a fully formed, functional BCR (Figure 5). Following migration to lymph nodes and maturation, B cells express both IgM and IgD isoforms on the cell surface (Geisberger, Lamers and Achatz, 2006). The functional goal of correct B cell development is the ability to secrete antibodies, specific to exogenous pathogens, by terminally differentiated plasma cells. Immunity and immune memory is characterised by rapid reactivation of memory B cells following re-exposure to their complementary antigen following infection. Memory B cell responses are critical for efficient immune response and protection from pathogen. Following activation and differentiation, plasma cells can then secrete large quantities of corresponding high-affinity specific antibodies to enable effective immune response and antibody-dependant phagocytosis(Tay, Wiehe and Pollara, 2019). Mutations that lead to defective B cell development, B cell selection and ultimately affect functional capacity result in a range of complications, including autoimmune diseases (characterised by the persistence of auto-reactive B cells in the periphery), B-cell malignancies, immunodeficiency, and allergies.

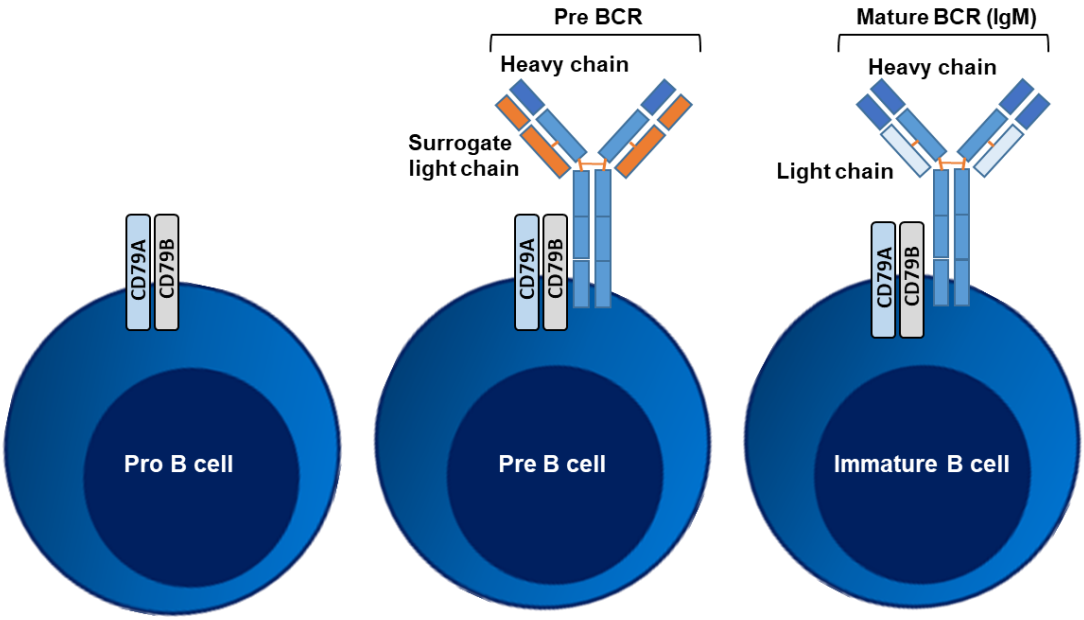

Figure 5. Maturation of the BCR and early B cell development in the BM
Ig heavy chain gene rearrangement occurs with development of pro-B cells into pre-B cells, resulting in the expression of Ig heavy chains and surrogate light chains on the surface of the pre-B cell, which along with CD79A and CD79B, forms the pre-B-cell receptor. The pre-B cell then undergoes light chain gene rearrangements as it differentiates into an immature B cell with a fully formed BCR.

1.3.1 Antigen encounter and response

Naïve B cells, which have had no previous encounter with the corresponding protein antigen to which their BCR binds, reside in the lymph nodes until encountering complementary primary antigen (Janeway CA, 2001). Following encounter with a primary antigen, such as in the case of a bacterial infection and subsequent encounter with a bacterial cell antigen, naïve B cells are activated and differentiate into antibody secreting cells. This occurs following binding of antigen to the BCR and internalisation of the BCR-antigen complex into intracellular compartments. Here the antigen can be processed by enzymatic degradation to peptide fragments, which can then be complexed with MHC-II and presented on the cell surface in order to recruit antigen-specific T-helper cells. Antigen processing and details of presentation will be covered in more detain below, in section 1.9. B cell differentiation can occur following microbial activation directly, independently of T-helper cells (Vos *et al.*, 2000), and this may enable a more rapid response. While this is important for immune function, T-cell activation causes the B cell to proliferate and subsequently differentiate into antibody secreting cells, which provides a more efficient and fine-tuned response to antigen encounter (Janeway CA, 2001). In addition to this function, some processes, such as *IGHV*

somatic hypermutation and immunoglobulin isotype switching, depend on the interaction of antigen engaged B cells with T-cells (Batista and Harwood, 2009).

The primary immune response involving naive B cells, however, displays a much slower, less specific and lower affinity response to antigens than the response elicited my memory B cells. Therefore, memory B cell responses are critical for efficient immune response and protection from pathogen re-infection following primary exposure, which forms the basis for successful vaccination and subsequent development of a repertoire of memory B cells. BCR signalling capacity differs between naïve and memory B cells, with a greater activation of signalling proteins in the BCR signalling pathway occurring in memory B cells than in naïve B cells following BCR cross-linking (Moens, Kane and Tangye, 2016). Ultimately, memory B cells play a critical role in generating a rapid antibody-mediated response to re-infection by a previously encountered pathogen. In CLL, the cell of origin for U-CLL is believed to arise from a pre-germinal centre (GC) B cell,, whereas for M-CLL is believed to be a post GC B cell (Stevenson and Caligaris-Cappio, 2004). Therefore, the differences between these two B cell subsets are not only critical in the immune response, but offers insight into CLL disease presentation and progression.

1.3.2 BCR signalling in development

The quantity of resting mature B cells is carefully controlled through BCR signalling, which induce signalling cascades that support B cell survival. Deletion of components of the BCR or prevention of BCR signalling result in cellular apoptosis induction (Kraus *et al.*, 2004). BCR signalling is also required in B cell developmental stages and differentiation (Yam-Puc *et al.*, 2018). Several major populations of B cells have been characterised in mice and humans, including B1 and B2 B cells, which in turn consist of marginal zone (MZ) and follicular (FO) B cells. MZ B cells are a pre-activated B cell subset located in the marginal zone of the spleen, and function as antibody-secreting cells. They are able to mediate antibody-based responses to antigens, independently of T-cell help, through a Toll-like receptor pathway. The pathway has been shown to rely upon mTOR activation, which then initiates MZ B cell proliferation, immunoglobulin G class switching, and differentiation to plasmablasts, which are immature plasma cells (Sintes *et al.*, 2017). B1 B cells are foetal B cells that form part of the humoral immune response, not being involved in the adaptive immune response. Instead, B1 B cells form a rapid response to pathogens while B2 B cells are produced (Quach *et al.*, 2016). Another transitional type of B cell found in the spleen are T1 B cells, which then differentiate to T2 B cells before transition to T3, FO or MZ B cells (Allman and Pillai, 2008; Martin *et al.*, 2016)

1.3.3 Germinal Centre Response

FO B cells reside in the B cell follicles of the spleen and lymph nodes, and have a distinct B cell phenotype. FO B cells recirculate in the blood, and following antigen encounter, require T-cell help to induce differentiation to plasmablasts, plasma cells or antibody-producing memory B cells (Mandik-Nayak *et al.*, 2008). This initial immune response results in the activation of antigen-specific B cells, followed by local expansion and generation of plasma cells. This response occurs outside of B cell follicles, but upon activation the circulating B cells migrate back to the B cell follicle. Within the B cell follicle, a Germinal Centre (GC) forms (Figure 6) consisting of activated, proliferating B cells, which is reliant on activation of antigen-specific B cells by T-cells recognising the same antigenic epitope. GC B cells then rapidly proliferate in dark zones of the GC, where they subsequently undergo somatic hypermutation. The newly formed GC B cells then move into the GC light zone, where they compete for their complementary antigen and signals from a subset of CD4+ T-cells, the T-follicular helper (T_{FH}) T-cells (De Silva and Klein, 2015). Signals that induce survival, proliferation and differentiation are delivered by mature follicular dendritic cells (FDC) and T_{FH} cells. These signals then initiate transcriptional programs that determine if GC B cells become memory B cells or terminally differentiated plasma cells (Hamel, Liarski and Clark, 2012). High affinity antibody-secreting plasma cells and memory B cells that have differentiated within the GC then navigate to survival niches and can persist here as longer-lived cells (Zhang *et al.*, 2018).

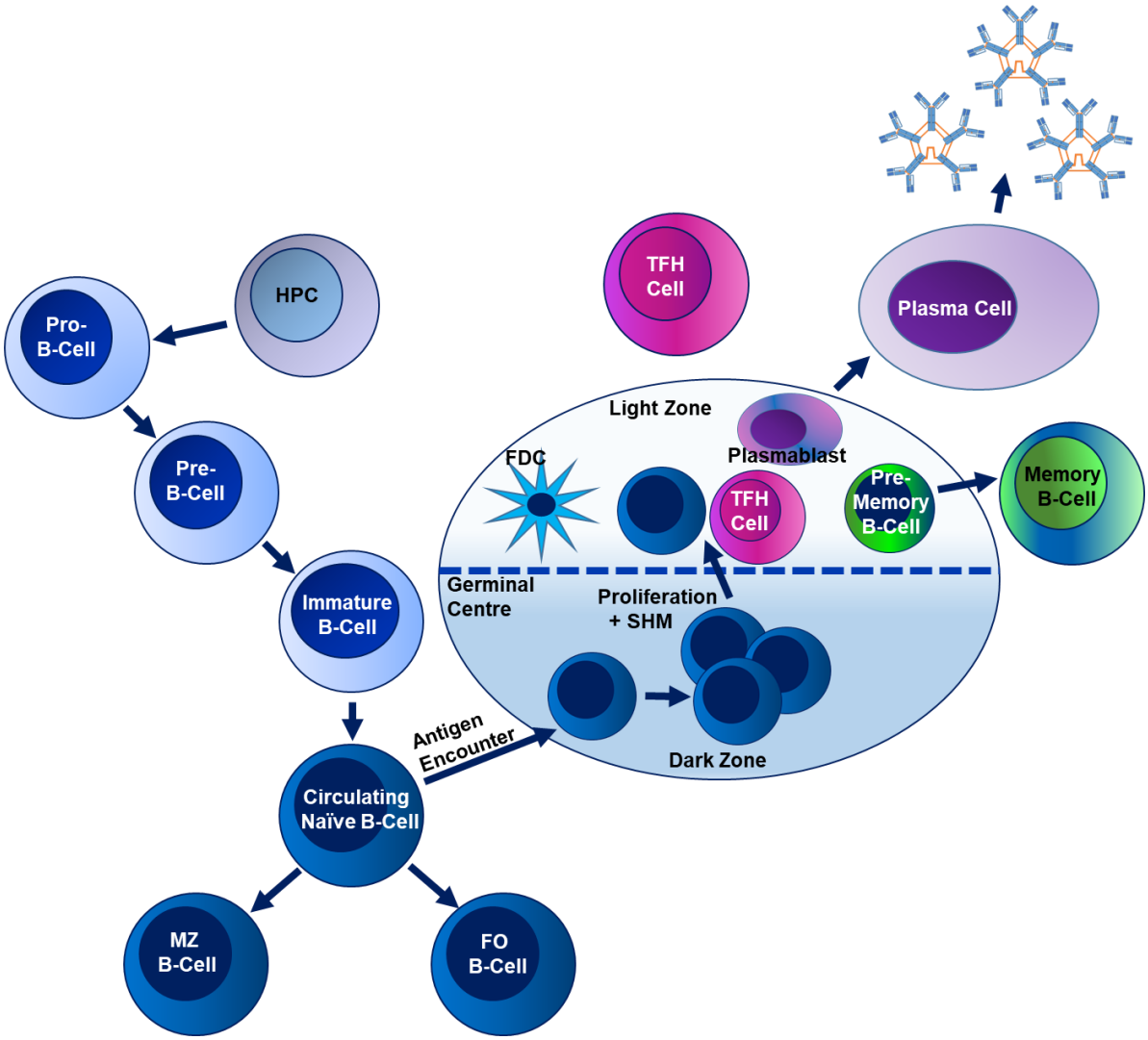

Figure 6. B cell development and proliferation.

B cell development is initiated from hematopoietic progenitor cells (HPC) in the bone marrow. At pro-B cell and pre-B cell stages, the genes encoding the BCR undergo VDJ rearrangement. From the immature B cell stage, each B cell expresses a unique, functional BCR. Immature B cells then enter the spleen and mature, developing into marginal zone (MZ) or follicular (FO) B cells. Where a circulating B cell encounters the corresponding antigen to its unique BCR , the B cell migrates to the germinal centre (GC), where they undergo proliferation and Somatic Hypermutation (SHM) in the dark zone. These B cells subsequently migrate to the light zone, where the modified BCR is selected for improved antigen binding, a process which requires help from other immune cells in the GC, including T follicular helper cells (T_{FH} cells) and follicular dendritic cells (FDCs). The selection of highest-affinity antigen binding BCR is positively regulated by the presence of peptide-MHC complexes, with higher affinity BCR capturing a greater amount of peptide-MHC, presented on the cell surface. The B cells with the greatest antigen binding capacity, presenting the greatest amount of peptide-MHC complexes, receives the most T-cell help, driving positive selection of high antigen-affinity B cells. Newly generated light zone B cells displaying unfavourable BCRs are unable to capture sufficient antigen and undergo apoptosis. Following positive selection, a subset of light zone B cells recirculate to the dark zone, where they undergo a second round of proliferation and SHM, with the potential to create higher affinity antibodies following this secondary selection. This re-migration between the GC dark zone and light zone means that B cells undergo several rounds of mutation and selection, prior to differentiation into precursor memory B cells or plasmablasts. This enables rapid generation of high-affinity memory B cells and plasma cells.

1.4 BCR Recombination and Diversification

1.4.1 VDJ rearrangement

As previously mentioned, *IGHV* mutational status in CLL offers a determinant for disease status, dividing CLL broadly into two groups, M-CLL and U-CLL. In order to understand the underlying causes for differences between these groups, it is necessary to examine the genetic basis of surface immunoglobulin expression. In pre-B cells, immune diversity is achieved through rearrangement and non-homologous end joining of variable (V), diversity (D), and joining (J) segments of the V region of immunoglobulin (Ig) genes, in order to achieve expression of a primary repertoire of Ig receptors (Rolink *et al.*, 1999). Since it would be impossible to express receptors able to recognise every possible antigen, the required receptor diversity is achieved by generating systematic variations in antigen recognition regions for B cell and T cell receptors. These antigen recognition regions are created by the combination of heavy and light chains, in the case of the BCR, and α and β chains for the TCR, which form an antigen binding site cleft between the chains (Figure 7).

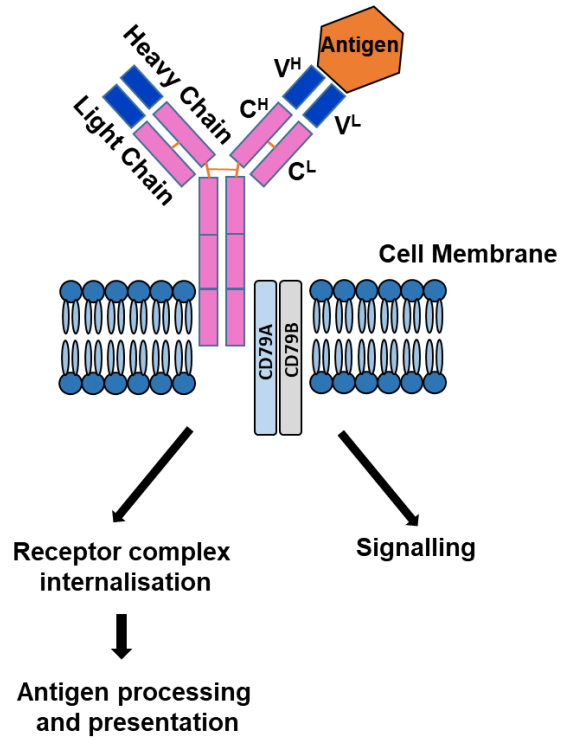

Figure 7. BCR structure
B-cell receptor structure and antigen binding site. Disulfide bridges connect the heavy(^{H}) and light(^{L}) chains, with each having a constant (C) and variable (V) region. Antigen binding occurs to the variable regions in an antigen binding cleft between heavy and light chains. The BCR comprises a tetramer of 2 heavy chains and 2 light chains, linked to the signal transduction molecules, CD79A and CD79B. Each BCR has two variable regions located on the end of the "arms" of the receptor which define antigen-binding specificity. The main functions of the BCR include induction of both positive and negative signalling as well as antigen internalisation which is critical for gaining cognate T-cell help. Signalling is initiated by phosphorylation of conserved tyrosine residues within the CD79A/B ITAM domains.

V, D and J gene segments recombine to form the BCR, with each combination leading to the expression of a different receptor complex, enabling the recognition of numerous pathogens. The V,D,J gene segment recombination sites are flanked by recombination signal sequences (RSSs). Precise DNA cleavage occurs between these RSSs and their coding regions, regulated by the proteins encoded by the recombination activating genes, RAG1 and RAG2 (McBlane *et al.*, 1995). Pre-BCR expression requires upregulation of RAG1 and RAG2 during VDJ rearrangement, and downregulation of RAG1 and RAG 2 after production of a functional VDJ recombination receptor and expression; a mechanism that ensures allelic exclusion, while preferentially selecting for clones of cells with productive VDJ rearrangements (Grawunder *et al.*, 1995). Non-Homologous end joining (NHEJ) then occurs, coordinating recruitment of the DNA ligase IV complex to DNA ends (Nick McElhinny *et al.*, 2000), which is required for recruitment of the tightly bound XRCC4-ligase IV complex (Grawunder, Zimmer and Lieber, 1998) to DNA, initiating the ligation step of NHEJ (Calsou *et al.*, 2003), which is essential in VDJ recombination (Grawunder *et al.*, 1998).

These biochemical processes result in the recombination of VDJ segments into a functional gene, encoding a new Ig receptor complex with altered antigen specificity, allowing for diversification of the surface Ig repertoire. At this stage, B cells expressing highly auto-reactive Ig receptor complexes are removed from lymphoid tissues (Hartley *et al.*, 1991). Receptor editing is one of the major ways of correcting auto-reactive receptor complexes, whereby the reactive Ig light chain undergoes rearrangement, producing a new light chain to pair with the existing heavy chain, thereby altering receptor specificity (Gay *et al.*, 1993). Alternatively, expression of the auto-reactive Ig may be silenced, to prevent autoimmunity, by arresting B cell development and inducing apoptosis. The silencing of these B cells is thought to be based on whether the sIg is auto-reactive to multi-valent, membrane bound antigen or monomeric soluble antigen (Hartley *et al.*, 1991).

Another distinct mechanism of damage control for auto-reactive antigens at this stage involves central tolerance, where B cells continue to express antigen receptors but fail to respond to antigen stimulation. These mechanisms occur as B cells develop in the bone marrow; at this stage the immature B cells carry IgM class surface antigen receptors. Subsequent B cell development predominantly occurs in the spleen and lymph nodes, along with other tissues, where B cells co-express sIgM and IgD. At this stage of B cell development, cells acquire capacity for full activation, and are able to respond productively with T-cells and antigen to produce high-affinity antibodies.

1.4.2 Somatic Hypermutation

As part of the immune response following generation of mature B cells, each expressing a unique Ig receptor, a second cycle of diversification occurs to further enhance antigen specificity. Somatic hypermutation of the V regions of the IgH or IgL leads to selection of a B cell that produces an antibody with high affinity to its target antigen. This process involves insertion of base substitutions into the region surrounding the antibody-coding sequence (Lebecque and Gearhart, 1990). Mature B cells also alter their IgH constant regions, by undergoing a DNA double stranded break dependent process known as Class Switch Recombination (CSR). A subset of GC light zone B cells undergoes class-switch recombination or differentiates into memory B cells or plasma cells in response to antigen encounter. The BCR acts as a dual regulator for signal transduction and antigen processing following antigen encounter. After an antigen binds to the receptor, a cellular signalling cascade is initiated which causes activation of processes that result in switching of surface IgM and IgD expression to expression of IgE, IgG or IgA. This occurs by altering IgH constant regions of the expressed Ig, which then function to more effectively remove pathogens in an infection model. In CLL, around 45% of cases share greater than 98% sequence homology with the germline Ig heavy chain V region (*IGHV*) sequence (U-CLL), while around 55% present with *IGHV* regions that have undergone somatic hypermutation (M-CLL) (Hamblin *et al.*, 1999). Somatic hypermutation and CSR depend on activity of activation-induced cytidine deaminase (AID). ATM kinase (11q22-23) and p53 (17p13) deletions have been linked to unfavourable prognosis in CLL. Both deletions are also significantly associated with Activation-induced deaminase (AID) levels (Leuenberger *et al.*, 2010), which have previously been linked to worse prognosis in both M-CLL and U-CLL (Patten *et al.*, 2012).

1.5 The B-cell receptor: Structure, Signalling and Function

1.5.1 BCR structure and activation

BCR activation is initiated by antigen binding, inducing receptor aggregation and clustering at the cell surface. The BCR complex consists of multiple components, with the antigen receptors formed as part of the complex made up of clonally variable heavy and light cell surface immunoglobulin chains. Five distinct immunoglobulin isotypes exist; IgM, IgD, IgG, IgA, and IgE, which may either be secreted as antibodies or form a surface immunoglobulin as part of the BCR complex (Venkitaraman *et al.*, 1991). The difference between these antigen receptors and a secreted monomeric immunoglobulin is the attachment of the antigen receptor to the carboxyl terminal of the paired heavy chains present in the BCR, which anchor the receptor to the cell membrane. While only a proportion of healthy circulating peripheral B cells display co-expression of IgM and IgD isotypes, in CLL the majority of tumour cells express sIgM and IgD, although at lower levels than healthy B cells (Dighiero *et al.*, 1980). IgG or IgA may be expressed in CLL, but this occurs rarely (Geisler *et al.*, 1991). However, a small proportion of CLL cells within sIgM/ IgD subgroups may undergo isotype switching to IgG or IgA (Cerutti *et al.*, 2002). sIgM and sIgD isotypes have been shown to have similar binding specificities, differing only in their heavy chain constant regions (Tisch, Roifman and Hozumi, 1988). Antigens with low numbers of receptor binding sites (valency) have been shown to activate IgM receptors but fail to trigger IgD signalling, whereas polyvalent antigens may elicit activation of both receptor types (Ubelhart *et al.*, 2015). In CLL, signalling through surface IgM results in a prolonged signal that supports downstream survival and chemokine responses, while signalling through IgD results in more rapid receptor internalisation and failure to induce these responses to the same extent (Ten Hacken *et al.*, 2016).

1.5.2 BCR signalling

Proteins associated with the aforementioned heavy chains include the signal-transducers, CD79A–CD79B, also termed Igα and Igβ, which are required for expression of the receptor complex on the cell surface (Hombach *et al.*, 1990). CD79A and CD79B are transmembrane proteins, with highly conserved cytoplasmic domains containing immunoreceptor tyrosine-based activation motifs (ITAMs). These ITAMs contain a characteristic consensus sequence containing two tyrosine residues, which are phosphorylated upon BCR activation to initiate a signalling cascade (Reth, 1989). CD79B (Igβ) is essential for signalling through the BCR, with deletion of this protein initiating cell death (Meffre and Nussenzweig, 2002). Upon binding of an antigen to the extracellular BCR, tyrosine phosphorylation of CD79A and CD79B on their ITAMs is initiated by the Src-related kinase (SRK) Lyn (Mkaddem *et al.*, 2017). The phosphorylated ITAMs subsequently recruit and upregulate kinase activity of Spleen Tyrosine Kinase (SYK). SYK is a cytosolic protein kinase containing two N-terminal SH2 domains, which bind to the phosphorylated ITAMs (Grucza *et al.*, 1999). This binding to phosphorylated ITAMs strongly activates SYK, enhancing enzymatic efficiency in a positive feedback loop at the receptor complex (Futterer *et al.*, 1998; Rolli *et al.*, 2002). ITAM phosphorylation and the corresponding signalling cascades must be tightly regulated in response to BCR activation, in order to prevent hyperactivity. Incomplete phosphorylation of ITAMs may alter signalling capacity, and this may be involved in maintenance of B cell anergy, where chronic antigen receptor signals drive incomplete phosphorylation of BCR ITAMs (O'Neill *et al.*, 2011). An illustration of BCR signalling following antigen binding is shown in Figure 8.

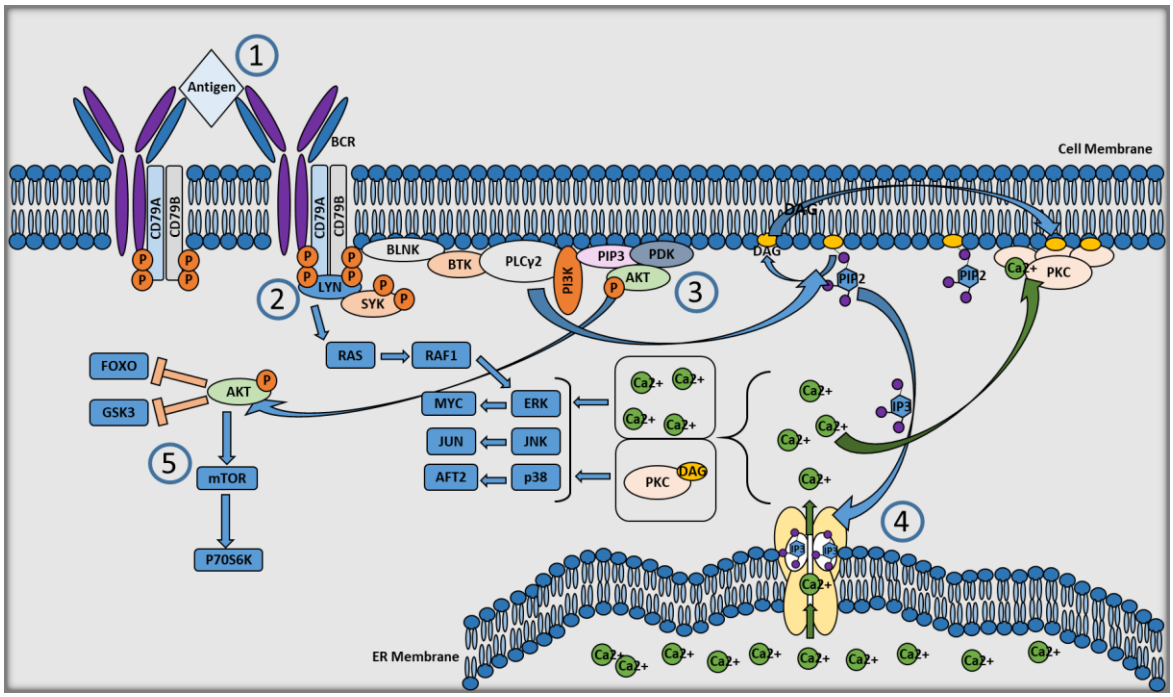

Figure 8. Structure and signalling pathway of the B-cell receptor
(1) The BCR is composed of surface immunoglobulin (sIg) molecules and associated CD79A/CD79B heterodimers. Following antigen binding to the sIg subunits and BCR aggregation, a signal response is initiated and transduced by the CD79A/B subunits. (2) BCR aggregation rapidly activates Src family Kinases such as Fyn and Lyn. A signalosome is formed from these tyrosine kinases aggregating to the CD79A/B subunits, adaptor proteins such as membrane-associated BLNK, and signalling enzymes such as Phospholipase C-γ2 (PLCγ2) and PI3K. (3) Other early effectors, such as BTK, are subsequently involved in signal transduction. Through the BLNK adaptor protein, BTK activates PLCγ2, initiating downstream responses. Membrane associated PIP3 is hydrolysed by recruited SHIP proteins, resulting in release of membrane associated PLCγ2, Btk and Akt. Activated, released PLCγ2 cleaves membrane localized phosphatidylinositol-4,5-bisphosphate (PIP2) to yield two messenger molecules; inositol-1,4,5-trisphosphate (IP3) and diacylglycerol (DAG). (4) While IP3 can dissociate from the membrane and activate IP3 receptors, promoting release of intracellular Ca2+ stores, DAG remains associated with the membrane and is involved in activation of PKC. Subsequent activation of Erk, JNK and p38 effect cellular responses. (5) Activation of the Pi3K/Akt pathway induces survival responses by inhibiting FOXO and GSK3, while activating mTOR.

Positive BCR signalling, mediated through ITAM phosphorylation, is regulated by protein tyrosine phosphatases, which act as a counterbalance to control BCR signalling. These are in turn regulated by tyrosine phosphorylation of receptor complexes containing immunoreceptor tyrosine-based inhibitory motifs (ITIMs) (Ravetch and Lanier, 2000). ITIMs counter-activate receptor complexes and may require co-localisation of the ITIM-containing receptor with an activated, ITAM-containing, receptor, in order to provide the required tyrosine kinase activity for phosphorylation of the ITIM and activation. These then recruit and activate phosphatases, such as Src homology 2 (SH2)-containing tyrosine phosphatase-1 (SHP-1) and SH2 domain containing inositol phosphatase(SHIP) 1 (SHIP-1), which act to prevent delivery of phosphorylation signals delivered through activatory receptors (Huang *et al.*, 2003). An example of a receptor containing ITIMs is FCγRIIB. In this case, the phosphotyrosine in the ITIM can then recruit several families of proteins, including the inositol

phosphatases SHIP-1 and SHIP-2 (Billadeau and Leibson, 2002), or the tyrosine phosphatase SHP-1 (Src homology region 2 containing protein tyrosine phosphatase-1)(Burshtyn *et al.*, 1997) to the plasma membrane. The SRKs involved in BCR signalling include Fyn, Lyn, and Blk, and are responsible for initiating signalling through the immunoreceptor by phosphorylating the ITAMs upon BCR activation. The two protein kinases involved in regulation of SHIP-1 and SHP-1 activity are Fyn and Lyn, which exert their opposing modes of action by phosphorylating different amino acid residues on the phosphatases (Mkaddem *et al.*, 2017). Lyn phosphorylates SHP-1 tyrosine 536 to activate the phosphatase, promoting ITIM inhibitory action through the immunoreceptor complex. However, Fyn phosphorylates SHP-1 at serine591, which inactivates the phosphatase and enables activatory signalling through ITAMs in the immunoreceptor complex. The different target substrates for SHIP and SHP-1 initiate inhibitory signals through different pathways, and deletion of either has revealed distinct protein targets for each of these phosphatases (Ono *et al.*, 1997).

Signals transmitted by the BCR influence a diverse group of cellular functions, including cellular selection, maturation, and survival, in addition to being imperative in initiating generation of antibodies (Dal Porto *et al.*, 2004). Following antigen stimulation and receptor clustering of the BCR, membrane associated Phospholipase C-γ2, Btk, and Akt are recruited to the signalosome (Bolland *et al.*, 1998), initiating downstream signalling (Figure 8). Upon PLCγ2 activation and release from the membrane, PLCγ2 cleaves membrane localized phosphatidylinositol-4,5-bisphosphate (PIP2) to yield two messenger molecules; inositol-1,4,5-trisphosphate (IP3) and diacylglycerol (DAG). IP3 is released from membrane and calcium release is stimulated (Berridge, 1993). The p110 subunit of PI3K functionally interacts with Btk, Itk and Tec kinase to produce larger and more prolonged calcium flux, with PI3K expression required for Btk function in calcium signalling (Scharenberg *et al.*, 1998). Oscillations of cytosolic free calcium ion concentrations (Ca^{2}+) provide a universal mechanism for signal control resulting in a variety of cellular processes. One form of intracellular calcium release channels are the IP3 receptors, which control calcium release from endoplasmic reticulum stores in order to transduce a signal to response pathway (Lanham *et al.*, 2003). BCR stimulation activates calcium entry across the plasma membrane that requires fully functional IP3R in order to occur (Vazquez *et al.*, 2002), suggesting a role for IP3R in calcium entry across the cell membrane in addition to release from intracellular stores. Depletion of the intracellular stores results in suppression of calcium signalling and increase in calcium entry across the cell membrane in order to replenish the intracellular stores. The strength and duration of calcium flux mediates the type of response initiated. Subsequent activation of Erk, JNK and p38 effect cellular responses, while activation of the PI3K/Akt pathway induces survival responses by inhibiting FOXO and GSK3, while activating mTORC1.

1.6 Anergy and Mechanisms of Self-Tolerance

1.6.1 Tolerance mechanisms for auto-antigens

Tolerance-mediating mechanisms for auto-reactive antigens that occur at a later stage in B cell development are termed peripheral tolerance. In fully functional B cells, engagement of BCR by a foreign antigen induces positive signals resulting in proliferation and subsequent differentiation. When the BCR is engaged consistently by an auto-antigen, a negative signalling arm is induced that effects an anergic state. Anergy is chronic BCR response without T cell help, where the BCR has affinity for auto antigens where cognate T cells are absent. This results in failure to transduce a signal and subsequent differentiation response from antigen stimulation. Induction of clonal anergy provides one mechanism of self-reactive B cell peripheral tolerance, which renders auto-reactive B cells nonresponsive to BCR cross-linking and unable to effect responses against the autoantigen (Goodnow *et al.*, 1988; Cambier *et al.*, 2007; Rosenspire and Chen, 2015). CLL patients with indolent disease phenotypes typically display an anergic BCR signalling response, characterized by reduced responsiveness to BCR stimulation and reduced sIgM expression (Mockridge *et al.*, 2007). Anergic B cells show evidence of receptor editing (Tze *et al.*, 2000), displayed by light chain rearrangement and up-regulated RAG1 and RAG2 mRNA expression. This indicates induction of further receptor editing in order to correct for the auto-reactivity of the receptor antigen. The apoptosis inhibitory genes *BCL-xL* and *BCL-2* have been linked to dysregulation of the normal mechanisms by which a self-reactive B cell would be deleted. Overexpression of Bcl-xL allows self-reactive B cells to escape into the periphery, where self-reactive B cells failing to express Bcl-xL were deleted, while cells expressing Bcl-2 were arrested at the immature stage (Fang *et al.*, 1998). These escaped cells displayed high levels of anergy, an adaptive mechanism to control signalling by these self-reactive cells. Many escaped autoreactive B cells also display loss of BIM expression, a pro-apoptotic protein that controls the fate of anergic B cells. Anergic B cells lacking BIM are therefore allowed to escape into the periphery, allowing them to accumulate sufficient differentiation signals to elicit production of autoreactive antibodies (Oliver *et al.*, 2006).

1.6.2 Anergy

Anergic B cells display heightened basal intracellular calcium levels compared to the normal calcium flux response to antigen-induced stimulation. In normal B cells, acute ligation of the BCR with complementary antibodies initiates a dual-phase calcium response; the initial response being a large increase in intracellular calcium concentration, followed by a small calcium plateau. In anergic B cells, basal calcium levels were elevated and binding of antibodies failed to induce the large calcium elevation typical of the initial phase of calcium signalling. By monitoring intracellular calcium levels, irregular calcium oscillations were noted that were subsequently quenched rapidly by extracellular calcium chelation. By transferring the anergic cells into a host system that failed to express the auto-antigen, calcium levels were restored to that of resting naive B cells (Healy *et al.*, 1997). The findings of this study indicated that the arrhythmic calcium oscillations in anergic B cells arise through continued stimulation of the self-reactive BCR, rendering reduced signalling capacity. Anergic B cells display greater phosphorylation of Erk, indicative of heightened downstream signalling in line with increased calcium flux, and require continuous binding of the auto-antigen to achieve this non-responsive signalling state. Upon dissociation of the auto-antigen, normal signalling capacity is recovered and the B cell is able to respond to further antigen stimulation (Gauld *et al.*, 2005). This increased Erk phosphorylation occurs in the absence of Akt activation (Muzio *et al.*, 2008). B cell anergy in CLL is associated with failure to induce terminal differentiation, which has been linked to reduction in expression of PRDM1 (BLIMP1) by anergic cells (Duckworth *et al.*, 2014).

1.6.3 Anergy in CLL

Anergic phenotypes are a hallmark characteristic of CLL (Packham *et al.*, 2014), but enriched in the M-CLL subgroup compared to U-CLL (Woyach, 2013; Caligaris-Cappio, 2014). CLL cells typically express reduced sIgM compared to HDB cells, but comparatively have a strong signalling response induced by BCR activation, which is elevated in U-CLL. U-CLL cells have higher sIgM levels than M-CLL and increased signal responsiveness(Stevenson *et al.*, 2011). U-CLL also downmodulate sIgM following antigen engagement to a lesser extent than M-CLL(Mockridge *et al.*, 2007). In vivo, both U- and M-CLL subtypes show evidence of constitutive engagement with antigen, consistent with the anergic phenotype, which is perhaps surprising for U-CLL subsets, corresponding to apparently naïve B cells theoretically. The antigenic source driving CLL cell engagement in vivo is thought to be a common infection (Lanemo Myhrinder *et al.*, 2008), or possibly an autoantigen (Herve *et al.*, 2005), although this remains unclear.

1.7 Phagocytosis and Endocytosis of antigen in the Immune response

1.7.1 Clathrin Mediated Endocytosis

Both phagocytosis and endocytosis are relatively well characterised cellular pathways essential to immune responses, resulting in internalisation of a molecule or cell for the purpose of recycling or breaking down the internalised particle. However, there are multiple types of endocytosis, and these differ from phagocytic pathways, requiring substantially different cellular pathway activation and responses to the internalised molecule. Each pathway has distinct roles in immune response modulation and pathogen clearance, in addition to functions in antigen presentation. There are many paths by which B cells can internalise proteins and particles that act as antigens from their environment. This is particularly important for extraction of antigens and processing for presentation to T cells. Antigens can be soluble, membrane bound or particulate, and the internalisation responses may differ for each type according to physical characteristics, therefore examining the differences can help to inform on the type of downstream response initiated. For example, particulate antigen generates a stronger GC response than soluble (Martinez-Riano *et al.*, 2018), and this is likely to be processed via phagocytic pathways rather than endocytic, due to the size of antigen particle.

Previous differences have been defined between endocytosis and phagocytosis and utilising these pathway differences I aim to characterise the observed BCR-driven internalisation pathway. Traditional receptor-mediated endocytosis, also called clathrin-mediated endocytosis (Figure 9), occurs following soluble antigen binding to receptors, and is also involved in cellular uptake and vesicular trafficking of hormones, metabolites, proteins; even in some cases viruses (Rejman *et al.*, 2004).

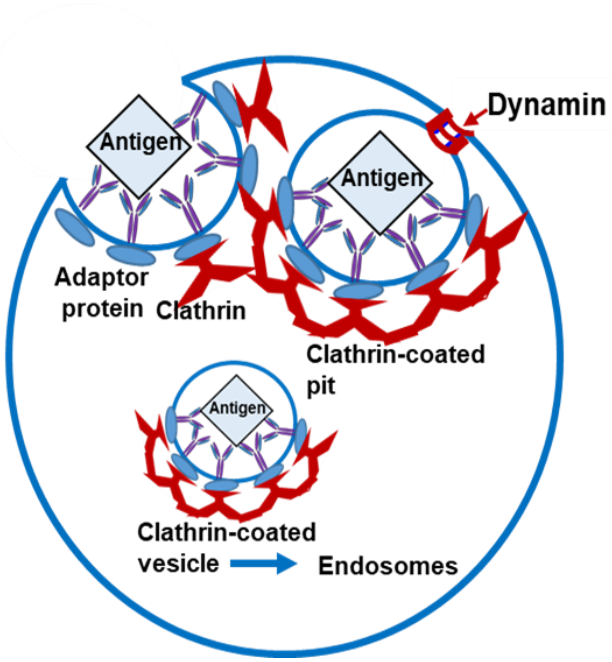

Figure 9. Clathrin mediated endocytosis

Formation of the clathrin-coated vesicle required for successful endocytosis is a complex process involving multiple stages and sequential activity of many proteins. Following antigen binding to receptor, adaptor proteins recruit clathrin to form the base of the vesicle that results from membrane invagination. Dynamin forms a cuff following sufficient inward membrane curvature, which then acts to pinch off the clathrin coated pit, forming a clathrin coated vesicle. The vesicle then associates with early endosomes, where the antigen or small molecule contained within may be appropriately processed.

Clathrin mediated endocytosis involves inward invagination and budding of the plasma membrane, forming clathrin-coated vesicles that subsequently become clathrin-uncoated and fuse with early endosomes for further processing (Mettlen *et al.*, 2009). Sequential activation of multiple proteins is required for completion of clathrin mediated endocytosis. The main classes of proteins required include adaptor proteins, which select transmembrane cargo proteins and subsequently link cargo selection to subsequent formation of polymerized clathrin coat, a group of proteins termed 'scission factors' which include the GTPase dynamin and its binding partners, with dynamin proving an essential component for clathrin-mediated endocytosis (Mettlen *et al.*, 2009). Dynamin is thought to function in early endocytosis, where it is involved in rate-limiting stages of clathrin coated pit maturation. In this function, dynamin monitors clathrin coat assembly, cargo concentration and membrane curvature generation. In a second functionality, dynamin forms a collar that catalyses membrane fission to produce the distinct clathrin coated vesicle. A third function for dynamin is also proposed, whereby it may form complexes with other late stage endocytosis drivers, possibly facilitating actin polymerisation or uncoating (Mettlen *et al.*, 2009).
A third class of proteins involved in clathrin-mediated endocytosis include auxilin and Hsc70, which subsequently facilitate the uncoating of the endocytic vesicle. Clathrin-mediated endocytosis

requires dynamin, but not downstream signalling resulting from receptor activation. It is thought to only occur for particles ≤200nm in size (Rejman *et al.*, 2004), whereas a different caveolin-mediated internalisation process becomes the predominant form of internalisation mechanism utilised for ≥500nm particles, which still requires dynamin to facilitate endocytosis, but does not require clathrin (Kiss and Botos, 2009). There is also an apparent clathrin-independent, PI3K regulated, dynamin dependent pathway involved in IL-2 receptor internalisation (Basquin *et al.*, 2013).

1.7.2 Endocytosis and Phagocytosis

By examining differential responses to particle size in macrophages, and the corresponding effect on endocytosis and phagocytosis, it has been shown that there are distinct pathways for each. Clustering of Fcγ receptors by immunoglobulin complexes leads to complex internalization in macrophages, with formation of small receptor-immunoglobulin aggregates leading to endocytosis, whereas large particulate antigen complexes induce phagocytosis. The receptor endocytosis pathway activated for small particles has been shown to be dependent on clathrin and dynamin but occurs independently of actin filament polymerisation. In the same study, large particulate antigen of greater than 3 micron diameter occurred independently of dynamin or clathrin, but required actin filament polymerisation (Tse *et al.*, 2003). Many sources in fact report that both actin filament remodelling (Ribes *et al.*, 2010) and signalling through SYK (Huang *et al.*, 2006) (Garcia-Garcia, Rosales and Rosales, 2002), are required for phagocytosis, but not for endocytosis .This is relevant in terms of the strength of GC response initiated by different forms of antigen, and therefore the strength of the overall immune response.

1.7.3 BCR mediated endocytosis

Research in B cells shows that BCR endocytosis and antigen processing are both Syk-dependent and regulated by actin filament organisation (Le Roux *et al.*, 2007). However, this study drew conclusions from using a Hen egg lysozyme and *Leishmania major* LACK Antigen, which were targeted to BCR uptake by coupling to nanoparticles, 8nm in diameter, together with an anti-BCR F(ab')2. By coupling 8nm nanoparticles to antibody, in addition to the antigen, this study may have been inadvertently studying the response of the BCR to larger, particulate antigen rather than that of soluble antigen endocytosis. Other work has shown that B cell antigen receptor endocytosis occurs into clathrin-coated pits, and that both the endocytic event and subsequent antigen presentation to T-cells requires the effector enzyme Vav, the small GTPase Rac and dynamin to occur successfully (Malhotra *et al.*, 2009). Other studies demonstrate that antigen-induced BCR endocytosis requires actin reorganization, which is Btk-dependent (Sharma, Orlowski and Song, 2009).

B cells deficient in actin binding proteins fail to internalise their BCR (Onabajo *et al.*, 2008), demonstrating the requirement for actin reorganisation in the internalisation of the BCR initiated by binding to soluble antigen. More recent work has shown that B cells require RhoG, a member of the Rac subfamily of Rho GTPases, in order to internalise particulate antigen in the form of bead-

immobilised anti-IgM. Internalisation of 1µm and 3µm anti-IgM coated beads was actin dependent, and also required signalling by Src family tyrosine kinases. Phagocytosis of particulate antigen by follicular mouse B cells was important in antigen presentation, and subsequently generating an effective humoral response against particulate antigens (Martinez-Riano *et al.*, 2018).

It is clear that endocytic pathways may be dynamic, multi-stage processes that can utilise multiple combinations of proteins, with a spectrum of requirements for different processes rather than definitive characterised pathways. Phagocytosis seems to be a better defined process, with consensus that actin remodelling and signalling are required for the phagocytic event to occur, and that this appears to predominate for large, particulate antigen, whereas endocytosis is utilised for smaller particles. The role of actin in endocytosis appears to be unclear, with conflicting results suggesting the potential for different requirements for individual combinations of factors occurring in each circumstance. Overall, it appears that by defining which major protein families are involved in the internalisation event, insight can be gained as to event functionality and subsequent responses. Thus, examining the type of internalisation or antigen capture pathway utilised helps to demonstrate the role and subsequent immune response initiated.

1.8 T cells and their role in the immune response

1.8.1 Differentiation and response to antigen encounter

Both B and T lymphocytes are involved in the acquired, or antigen dependant immune response. While B cells are involved in the humoral, antibody driven immune response, T cells are vital effectors in the innate, cellular immune response. Both types of lymphocyte produce receptors to which antigen can bind, with the receptor type utilised by T cells known as the T cell Receptor (TCR). Following T cell development, each newly differentiated naïve CD4 positive T cell possesses a unique TCR, each specific to different foreign peptide sequences presented on host HLA II /MHCII molecules (Boniface *et al.*, 1998; Marrack *et al.*, 2008). Only a very small proportion of the CD4 positive Th cells will actually express a relevant TCR specificity to a peptide:MHCII complex presented during an infection scenario (Chu *et al.*, 2010). During host infection, pathogens; including bacterial cells, viruses, or other foreign antigen containing particles, are carried to secondary lymphoid organs. Antigen presenting cells (APCs) degrade various microbial proteins into their component peptide sequences. A proportion of these peptide sequences are subsequently processed through the antigen processing pathway endomembrane compartments, loaded onto HLA-II/MHCII and presented on the APC surface membrane, where they have the opportunity to encounter their cognate TCR on a naïve Th cell. Upon interaction with an APC presenting a corresponding Peptide:MHC complex, the Naïve CD4+ T cell will engage in transduction of signalling responses that induce proliferation of the T cell, leading to subsequent expansion of the CD4 T cell population with TCRs with high affinity for the invading pathogen antigen peptide sequence (Smith-Garvin, Koretzky and Jordan, 2009).

The proliferating T cell population with affinity for the foreign peptide sequence: MHC complex then differentiate into effector cells after differentiation signalling cascades have been induced. Following stimulation of a naïve CD4 T cell as they engage with their cognate antigen presented by APCs, these T cells can differentiate into effector cells, or memory cells, with distinct phenotypes and functions, which may include aiding in B cell differentiation and proliferation, and enable maturation into antibody-producing plasma cells (Zhu, Yamane and Paul, 2010). Each naive T cell has been shown to be capable of different tendencies towards production of a certain type of effector cell, possibly due to the unique nature of each TCR (Tubo *et al.*, 2013). Several Th subgroups of effector cells have been proposed. During studies of acute models of infection, early stage infection displays naïve CD4+ T cells with antigen peptide sequence:MHCII specific TCRs, which rapidly proliferate and differentiate into Th1 effector cells. These are characterised by production

of macrophage activating cytokine IFN- γ, or into one of two subgroups of T follicular helper cells- T_{FH} cells that are involved in the process of enabling B cell activation and proliferation/ differentiation responses at the borders of T cell locations and follicles, or GC T_{FH} cells that drive affinity maturation within the germinal centre reaction (Choi *et al.*, 2011; Crotty, 2011; Lee *et al.*, 2011; Crotty, 2014). The B cell differentiation signals appear to be driven by T cell expression of BCL6, with effector cell differentiation also controlled by BCL6. Overexpression of T_{FH} cell BCL6 significantly increased the B cell proliferation in the GC following viral infection in mice (Johnston *et al.*, 2009). IL-2 receptor expression and signalling pathways also govern the T cell proliferation response, along with mutual B cell-T cell activation and proliferation in the Germinal Centre reaction (Ross and Cantrell, 2018).

1.8.2 T cells in CLL

Within CLL patient proliferation centres, CD4 positive helper T cells have been identified as among the most prominent cell types (Caligaris-Cappio, 2003), found in close proximity to CD38 positive CLL cells (Pizzolo *et al.*, 1983; Ghia *et al.*, 2002). Secretion of various cytokines by T cells can induce proliferation responses for B cells in GC reactions, with these cytokines including IL2, IL21 and IL4. In the context of CLL pathology, these may subsequently aid CLL cell survival by preventing apoptosis and increasing CLL cell proliferation responses (Panayiotidis *et al.*, 1993; Burger *et al.*, 2009; Os *et al.*, 2013; Ferrer *et al.*, 2014). In line with this hypothesis, CLL patients have been shown to have increased numbers of CD8+ and CD4+ T-cells compared to healthy donors (Gonzalez-Rodriguez *et al.*, 2010),with the greatest numbers of these T cell subsets displayed in patients with more progressive disease (Palma *et al.*, 2017) .

Given the findings regarding T cell help and the potential role for T cell engagement and response in CLL, recent work by Munthe et al investigated the capacity of CLL cells to process and present antigen through their BCR and activate CD4+ T cells, both from the patient's own T cells and a cell line reporter model (Os *et al.*, 2013). This is of particular interest, especially when considering the potential role of autophagy in antigen processing and presentation. Although, other findings in patients have shown that while T-cell numbers are increased in CLL lymph nodes, the function of these T cells appears to be impaired. The T cells showed impaired actin filament polymerisation, causing defective immunological synapse formation with antigen presenting cells (Ramsay *et al.*, 2008). This defect in formation of the synapse at the site of CLL-T cell interface was induced when healthy T cells when introduced to CLL cells, not confined to CLL patients own T cells, indicating a process driven by the CLL cells themselves. This process may rely on the ability of the CLL cells to present antigen to the T cells, engaging in subsequent synapse formation and signalling, facilitating

disease progression and an exhausted phenotype. Therefore, investigating this process within the CLL cells themselves is of clinical relevance.

1.9 Antigen Presentation in the immune response

Antigen presentation is the process by which an antigen-presenting cell (APC) encounters antigen, complexes it with major histocompatibility complex (MHC) class-I or MHC class-II, also known as human leukocyte antigen (HLA)-II / HLA-II in human systems, and displays this peptide-HLA complex on its cell surface- thus recruiting a CD4+ve (HLA-II) or CD8+ve (HLA-I) T cell response. HLA-I pathways are typically utilised for endogenous or viral antigen, typically intracellular antigenic forms, while HLA-II pathways are utilised for extracellular antigens such as in the context of bacterial infection. HLA-I pathways are also of particular relevance in the context of tumour antigen and engagement of the immune response against tumour cells, in addition to involvement in other pathways by cross presentation. An illustration of class I and II pathways is shown in Figure 10.

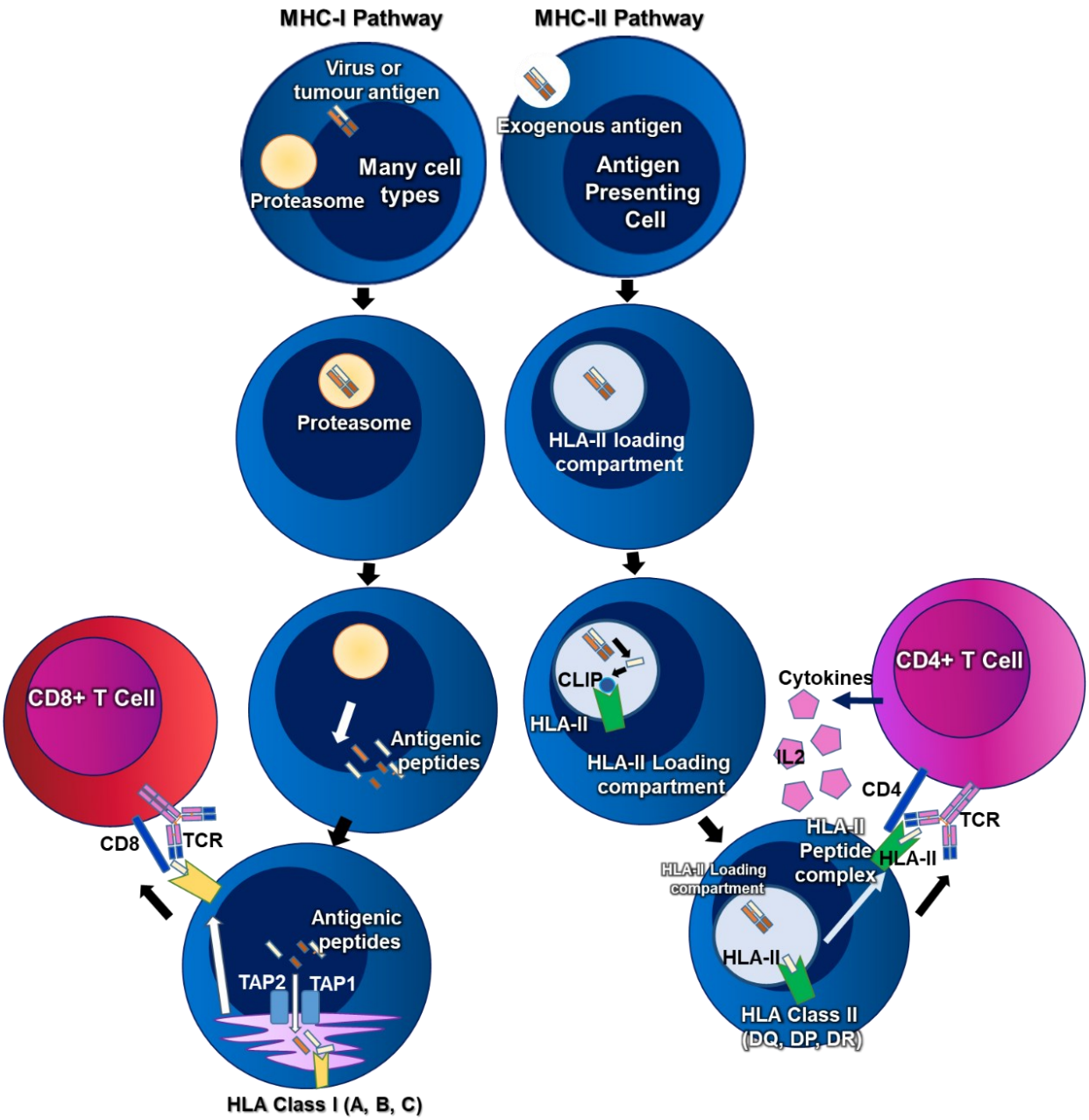

Figure 10. MHC-I and MHC-II antigen presentation pathways

Illustration of the MHC-I and MHC-II antigen processing and presentation pathways. In the MHC-I pathway, virus or tumour antigen are processed through the proteasome, complexed with MHC-I and presented to CD8+ve T cells to activate a cytotoxic T cell response. In the MHC-II pathway, an antigen presenting cell processes antigen in an MHC-II loading compartment, presenting it to a CD4+ve T cell and activating a proliferation/ differentiation response.

Mature B cells have been well characterised by their ability to recognize antigens that bind to the BCR, activating the B cell and its ability to become an antibody-producing cell. In addition to these broad features, B cells can utilize the specialized exogenous antigen presentation pathway involving major histocompatibility complex class II (MHCII). This terminology is used to refer to the form widely found in vertebrates, but the HLAII form is found only in humans, and therefore the two names are often used interchangeably to refer to the same molecule. This pathway is critical in the

process of producing high-affinity antibodies and can process BCR-bound and internalized antigens in order to present these selected peptides in complex with MHCII to CD4+ T-cells. The interaction between CD4+ T-cells and B cells presenting antigen influences the overall fate of both cell types and is responsible for mounting an effective immune response against pathogens. In order for this response to antigen to be effective, the response must be timed optimally, in addition to being specific. Four major stages are involved in the pathway that ultimately results in antigen presentation. Initially, antigen must be captured and internalised by the B cell. The B cell must then move the internalised antigen, along with MHCII, into peptide loading compartments. These are then generated into MHCII/Peptide complexes, before being transport to the cell surface via exocytosis and displayed at the cell surface.

MHC class II complexes consist of α and β subunits, which are initially assembled in the Endoplasmic Reticulum, in complex with the chaperone molecule invariant chain (CD74) (Schroder, 2016). The cytoplasmic tail of CD74 contains a motif that targets MHCII to lysosomal and endosomal compartments. Following association with lysosomal proteases, this motif is cleaved and modified to class II-associated invariant chain peptide (CLIP) which remains in association with the peptide binding groove of MHCII (Maric, Taylor and Blum, 1994). Proteins delivered through endocytosis or phagocytosis are also exposed to lysosomal proteases, creating peptide ligands that can be complexed with MHCII (Watts, 2001). Prior to conjugation of MHCII to internalised antigen peptide groups, CLIP must be removed from MHCII, which is facilitated by the molecule Human leukocyte antigen DM (HLA-DM) (Denzin and Cresswell, 1995). HLA-DM also catalyses binding of antigenic peptides to MHCII after CLIP dissociation, which occurs in lysosomal compartments.

Several pathways have been characterised that contribute to presentation of antigen in MHCII complexes, including both chaperone mediated autophagy and bulk processing through macro autophagy (Strawbridge and Blum, 2007). Other autophagic processes have been shown to facilitate antigen preservation for presentation. Non-canonical lipidation of LC3 onto a subset of macrophage phagosome membranes occurs following phagocytosis, resulting in prolonged presentation on MCHII. The subset of LC3 positive phagosomes required ROS produced by Nox2 prior to phagosome generation. (Romao *et al.*, 2013). Activation of the NAPDH oxidase Nox2 generates ROS that trigger non-canonical LC3 recruitment to bacterium positive phagosomes by LC3-associated phagocytosis (LAP) (Koster *et al.*, 2017; Gluschko *et al.*, 2018). LAP has been widely reported in macrophages (Heckmann *et al.*, 2017), with the role of particulate antigen internalisation and antigen presentation beginning to be defined in B cells (Adler *et al.*, 2017). Recent work has demonstrated the requirement of autophagy, specifically of ATG5, in B cell

response and presentation of particulate antigen in MHC-II / LAMP1 positive intracellular compartments (Arbogast *et al.*, 2018).

Another route by which antigen can be processed involves the cross-presentation pathway.
MHCII and MHCI cross presentation. Certain cell types, predominantly antigen presenting cells such as dendritic cells, can phagocytose and process extracellular antigens, but then switch to complexing these extracellular antigens with HLA class I molecules rather than the traditional class II route used for extracellular antigen. These extracellular antigenic peptide-MHC I complexes can then be presented to CD8+ve T cells, activating the cytotoxic T cell response for these extracellular antigens, rather than other CD4+ve T cell mediated responses, or even activating both pathways simultaneously. This process is known as antigen cross-presentation. This is an important part of the development of immune responses against tumours, since tumours are a source of extracellular antigens. An illustration of the cross presentation pathway is shown in Figure 11

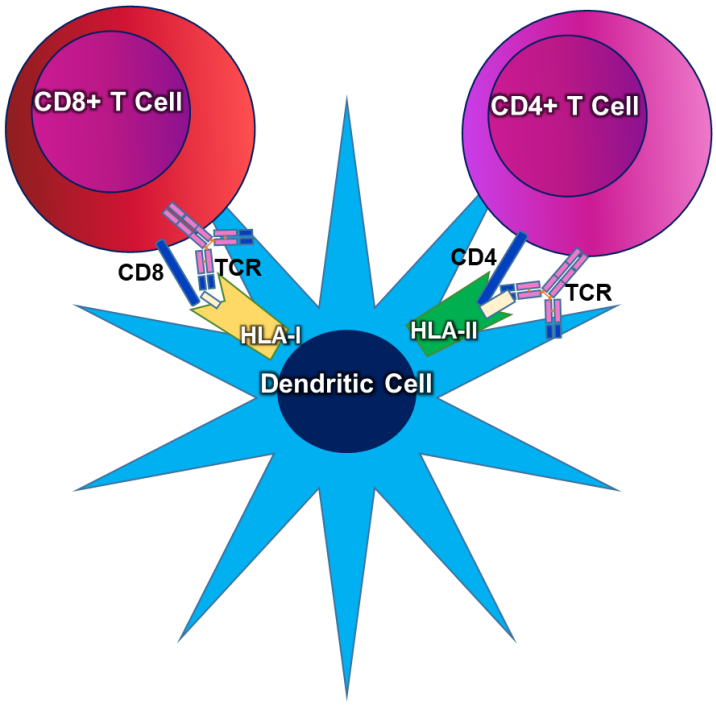

Figure 11. Cross Presentation

Antigen presenting cells, such as a dendritic cells, are capable in some circumstances of utilising both class I and class II antigen processing pathways- to initiate CD8+ve T cell cytotoxic responses against extracellular antigens. Following phagocytosis of the antigen, processing occurs and the extracellular antigen can be loaded onto class I molecules and displayed on the cell surface. These extracellular antigenic peptide-MHC I complexes can then be presented to CD8+ve T cells, activating the cytotoxic T cell response in addition to CD4+ve T cell responses.

Interestingly, stimulation of CLL cells with CpG and IL-21 combinations has been shown to induce CLL cell differentiation into an APC-like cell type, which acquire features similar to dendritic killer cells, resulting in CLL cell apoptosis. This is a distinct response in CLL compared to healthy B cells, and some of the pathways upregulated include cell adhesion, antigen cross-presentation and costimulation (Hagn *et al.*, 2014). Research has shown that CLL exhibits combinations of immunogenicity and immunosuppression phenotypes, also exhibiting immune defects including reduced CD4+ve and CD8+ve T cell function (Riches *et al.*, 2013) and reduced immune synapse formation (Ramsay *et al.*, 2008). There is interest in targeting CLL cells with antigen specific T cell based immunotherapy. However, the immunological defects present in CLL may make mounting an antitumour response challenging. Several studies have demonstrated that the immunomodulatory compound lenalidomide can reinforce effector T-cell responses in CLL, opening the possibility of combining this compound with T cell based therapies (Henry *et al.*, 2013).

1.10 Autophagy

1.10.1 Introduction

Canonical autophagy is the process of self-digestion within cells, and has important roles in maintaining cellular homeostasis. Under stress conditions, such as during starvation, autophagy is a form of self-preservation, which produces energy and amino acids from the recycling of unrequired or damaged proteins or organelles. Autophagy is also important in mediating programmed cell death. Basal levels of autophagy are necessary to maintain peripheral B cells, (Arnold *et al.*, 2016), however, this is further upregulated in CLL compared to healthy donor cells (Smith *et al.*, 2015; Gade *et al.*, 2016; Smith *et al.*, 2020), and may be involved in drug resistance (Mahoney, Byrd and Johnson, 2013). Indeed, venetoclax treatment induces autophagy, and pre-treatment with autophagy inhibitors enhances killing by venetoclax, indicating a survival mechanism contributing to treatment resistance (Smith *et al.*, 2020; Avsec *et al.*, 2021). In tumour cells, it has been shown that autophagy has both tumorigenic and tumour suppressive functions, depending on the intensity and duration of stimulus. In most cases, however, autophagy serves to promote tumorigenesis, mechanisms of which include suppression of p53 and maintenance of mitochondrial metabolism, while also increasing cancer survival and aggression(White, 2015). Interestingly, autophagy has been shown to regulate p53 by regulating DNA damage and maintenance, preventing error prone DNA damage repair mechanisms and p53 activation (Liu *et al.*, 2015). Autophagy could also regulate p53 by mitochondrial maintenance and reduction of ROS accumulation, which in turn can activate p53. Loss of autophagy has been demonstrated to result in p53 induced apoptosis under cellular stress conditions (Lee *et al.*, 2012). In the context of DNA damage whereby p53 is activated, p53 also activates autophagy, presumably as a mechanism to aid in removing misfolded and defective proteins resulting from DNA damage or mutations. Indeed, one p53 target gene is that encoding damage-regulated autophagy modulator (*Dram)*, which has been shown to induce autophagy (Crighton *et al.*, 2006) . However, the suppression of p53 by autophagy has been linked to promotion of tumourigenesis. Alternatively, the activation of autophagy by p53 suggests that autophagy is part of the protective function of p53, so the two pathways appear intrinsically linked, and can serve to both repress or activate tumourigenesis, depending on the context and level of dysregulation. The relationship between p53 and autophagy has been reviewed in detail (White, 2016; Mrakovcic and Frohlich, 2018) and is an ongoing area of research interest in cancer biology.

Several cancer varieties show deletion of essential genes regulating autophagy, such as *beclin1* (Aita *et al.*, 1999; Qu *et al.*, 2003), an essential protein involved in the process of autophagy. Constitutive activation of the PI3-Kinase/mTOR signalling pathway, which acts to inhibit autophagy, has been shown to be a common event in many cancers; driving dysregulation of autophagy induction and thus tumour cell proliferation (Tan *et al.*, 2016). In B cell acute lymphoblastic leukaemia, autophagy is downregulated, while reactivation of autophagy in a mouse model inhibited disease progression (Yuan *et al.*, 2015). In other cases, autophagy is upregulated in cancer cells as a survival mechanism in response to therapy-induced stress (DiPaola *et al.*, 2008) . The ability of cancer cells to evade the apoptotic cell death pathway has been well characterised (Fernald and Kurokawa, 2013), and is linked to their aggressive nature and ability to survive and proliferate. Research has shown that autophagy is often upregulated in tumours, and this process may serve a protective role in preventing tumour cells from undergoing therapy induced killing. Hypoxic tumour cells show upregulation of autophagy, and hypoxia in tumour cells has been associated with resistance to anti-cancer therapies (Tan *et al.*, 2016) . In chronic myeloid leukaemia (CML), tyrosine kinase inhibitors induce autophagy which rescues cells from treatment induced apoptosis. Combinations of autophagy inhibitors have been shown to target quiescent tumour cells in primary patient cells in addition to CML mouse models (Baquero *et al.*, 2019). There are three main categories of canonical autophagy; macro-autophagy, micro-autophagy and chaperone-mediated autophagy. Herein the term canonical autophagy is used to describe the process of macro-autophagy, which accounts for a large percentage of autophagy occurring to maintain cellular homeostasis.

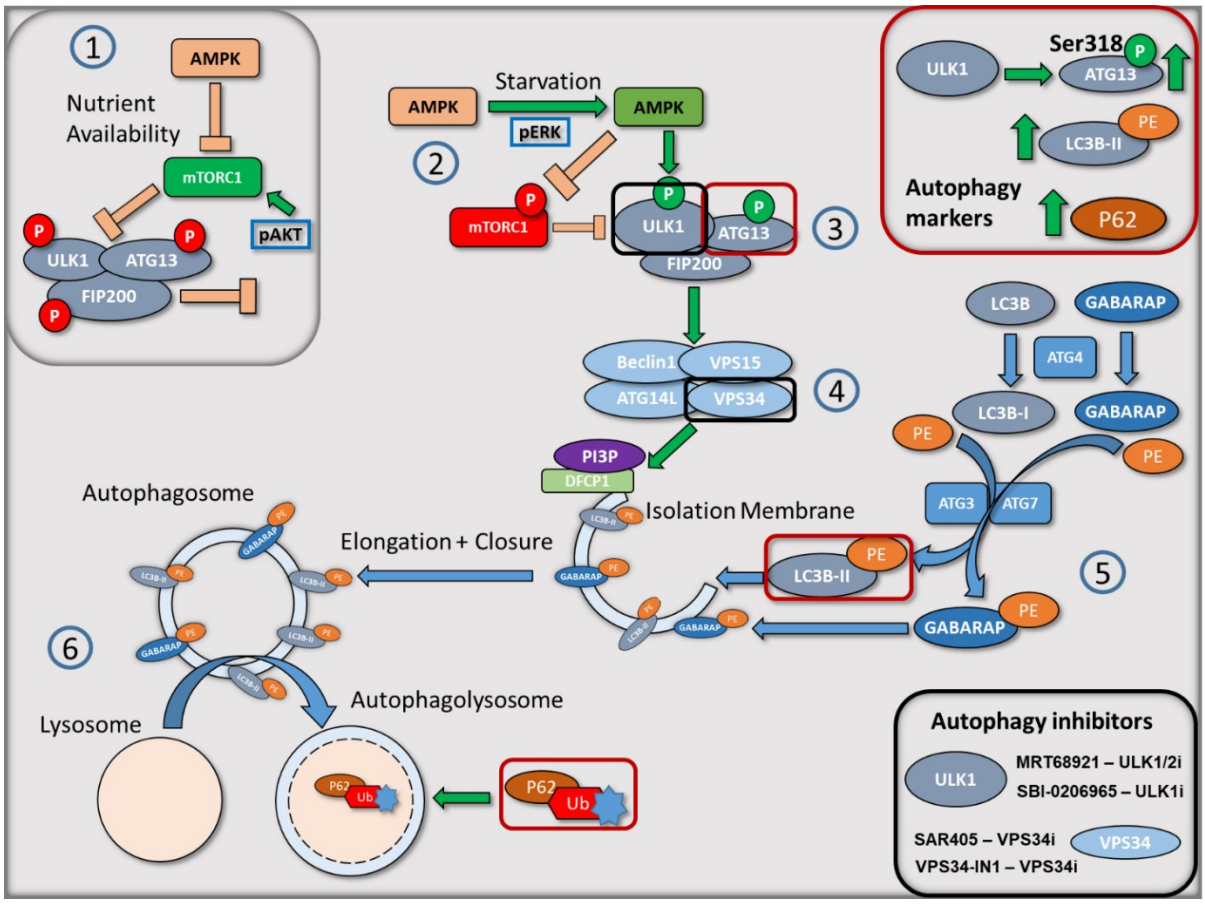

Figure 12. Canonical autophagosome biogenesis pathway

(1) Under nutrient favourable conditions, AMPK is inactive and mTORC1 is active. mTORC1 directs inhibition of the ULK1/ATG13/FIP200 complex through inhibitory phosphorylation at specific sites (ATG13 ser355), therefore autophagy cannot proceed. (2) Canonical autophagy is initiated under certain conditions, such as starvation or cellular stress. AMPK is activated, which phosphorylates mTORC1 at inhibitory regions on TSC2 and RAPTOR, preventing activity of the mTORC1 inhibitory complex. (3) When mTORC1 is inactivated by AMPK and autophagy inhibition is released, the ULK1 complex is phosphorylated at ULK1 activatory sites ser317 and ser777, in addition to ATG13 ser218, by AMPK. ATG13 is in turn phosphorylated by ULK1 at ser318, activating formation of the subsequent Beclin1/ATG14L/Vps34/VPS15 complex, (4) which directs formation of an initial membrane structure, the phagophore. (5) LC3B and GABARAP are cleaved by ATG4 soon after translation to form LC3B-I, which is then conjugated to phosphotidyletholamine(PE) by ATG3 and ATG7. These are inserted to the forming autophagosome membrane, a process aided by WIPI2, which directs the ATG12-ATG5-ATG16L1 complex to the forming autophagosome, guiding insertion of LC3B-II into the membrane. As the phagophore elongates, it nonselectively sequesters cargo and closes into a double-membrane vesicle, the autophagosome. (6) The autophagosome then fuses with a lysosome and exposes cargo to the lysosomal enzymes causing degradation of the content. Orange boxes around proteins indicates markers routinely used for measuring autophagy. Black boxes around proteins indicate inhibitor targets.

Macro-autophagy involves formation of an autophagosome, a double membrane vesicle folded around a portion of the cytoplasm to be degraded (Figure 12). The autophagosomes fuse with lysosomes, resulting in the lysosomal degradation of proteins. The process of autophagosome formation and autophagy flux is orchestrated and tightly regulated by a myriad of autophagy

proteins, many of which are bound together to form functional multi-protein complexes. These essential protein complexes consist of the ULK1 pre-initiation complex, the Beclin1-Vps34 initiation complexes, and the WIPI2 complex. Other complexes involved include ATG12-ATG5-ATG16L1 and LC3-phosphotidylethanolamine (PE) ubiquitin-like conjugation systems. Initially identified in yeast, the ATG8 family proteins are involved in autophagosome formation and elongation. ATG8 homologues in mammalian cells have been identified, including LC3A, LC3B, LC3C, GABARAP, GABARAPL1, and GABARAPL2 (or GATE-16). This family of proteins have been shown to perform at least three major functions in autophagy; inducing elongation and closure of the autophagosome membrane, recruiting cytoplasmic cargo to the autophagosome through the LC3-interacting region (LIR) motif (Slobodkin and Elazar, 2013), and lastly they may also serve as adaptors, initiating recruitment of various signalling or trafficking proteins to the autophagosome (Stolz, Ernst and Dikic, 2014).

1.10.2 Autophagosome formation and turnover

The formation, elongation and fusion of autophagosomes with lysosomes involves the microtubule associated protein LC3B, which undergoes post-translational modifications rapidly following synthesis. Cleavage occurs at Glycine120 residue following translation to remove its C-terminal 22 kDa fragment, producing cytosolic LC3B-I (Kabeya *et al.*, 2000). LC3B-I is subsequently lipidated by covalent conjugation to phosphatidylethanolamine (PE) to form membrane associated LC3B-II (Kabeya *et al.*, 2004). Since LC3B-II associates only with autophagosomes, and not with any other membrane bound organelles, measuring LC3B-II levels provides a direct correlation to the number of autophagosomes, and consequently, the amount of autophagy occurring in the cell. WIPI2 is involved in recruitment of the ATG12-ATG5-ATG16L1 complex to forming autophagosomes, or pre-autophagosomal structures, which results in the lipidation of ATG8 family proteins. WIPI2 has also been shown to have a role in autophagic clearance of pathogens. This is initiated following WIPI2 binding to the membrane of *Salmonella sp.* after cellular invasion, and subsequently recruiting the ATG12-5-16L1 complex. This complex recruitment then initiates LC3-PE conjugation and insertion into forming autophagosomes, membrane elongation and pathogen clearance by autophagosomal engulfment of the invading bacteria (Dooley *et al.*, 2014). WIPI2 is the intermediary director connecting insertion of LC3 to the membrane elongation stage, recruiting the ATG12–ATG5-ATG16L1 complex, and additionally activating it. WIPI2 also activated Class-I PI3K (Vps34) in a positive feedback loop, increasing PI3P production required for membrane elongation while simultaneously recruiting and activating insertion of LC3B-II into the forming membrane (Fracchiolla *et al.*, 2020). This is illustrated in Figure 13

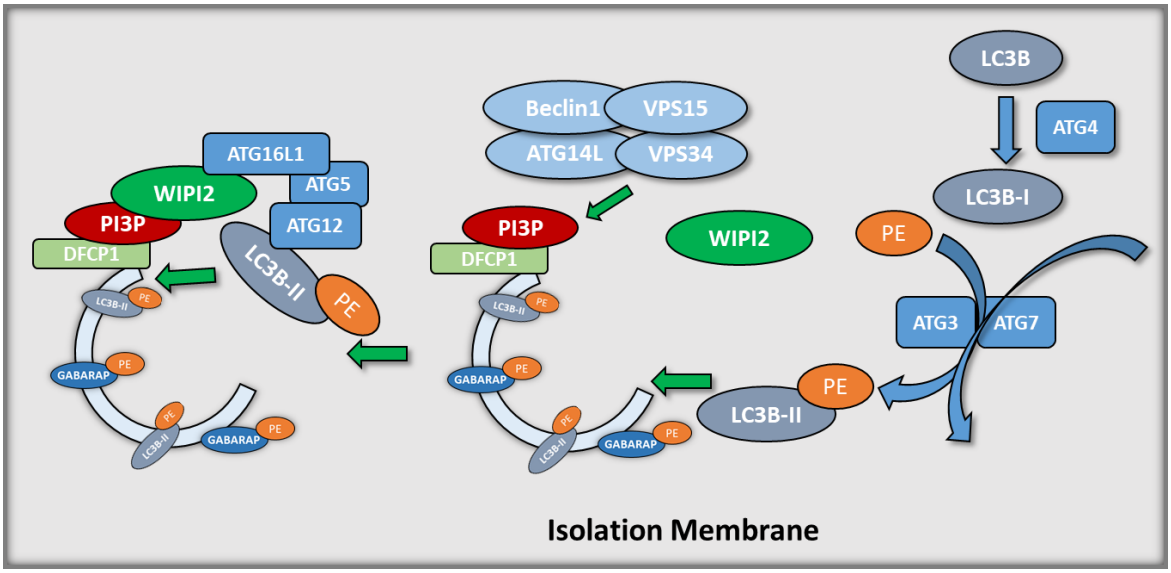

Figure 13. Role of WIPI2 in membrane elongation

WIPI2 is involved in recruitment of the ATG12-ATG5-ATG16L1 complex to forming autophagosomes, or pre-autophagosomal structures, which results in the lipidation of ATG8 (LC3) family proteins and insertion into the autophagosome membrane, allowing elongation and closure.

While LC3B has been shown to be essential for elongation of the phagophore membrane, other proteins of the γ-aminobutyric acid (GABA)-A-receptor-associated protein-like (GABARAP)/GATE-16 subfamilies are also required in the subsequent processes of autophagy. GABARAP is also conjugated to PE at a C-terminal glycine residue prior to insertion into the autophagosome membrane, a common feature of ATG8 family orthologues. Both GABARAP and LC3B are necessary for early stage autophagosome biogenesis and autophagic flux, but appear to have different roles in the formation of autophagosomes, with GABARAP being more crucial at later stages (Weidberg *et al.*, 2010). The same experiments also display that knockdown of GABARAP family proteins elicits an accumulation of ATG5-ATG16L1 puncta. This shows that GABARAP acts downstream of recruitment of the ATG12–5-16L1 complex. GABARAP is trafficked from the pericentriolar matrix (PCM) to the forming autophagosome prior to PE conjugation and insertion into the autophagosome membrane (Joachim *et al.*, 2015), a process that is dependent on a PCM reservoir of GABARAP. GM130 is a Golgi matrix tethering protein required for vesicle trafficking, and this protein binds to and sequesters GABARAP in the PCM in order to inhibit autophagy. WW domain-containing adaptor with coiled coil (WAC) is a protein with characterised involvement in transcriptional regulation by recruiting RNF20/40 and subsequently binding to RNA polymerase II, forming a complex that regulates transcriptional activity (Zhang and Yu, 2011). WAC has also been shown to positively regulate autophagy by increasing free GABARAP, preventing GM130 binding to GABARAP and allowing subsequent activation of the ULK1 complex, as GABARAP is required in the process of ULK kinase activation (Grunwald *et al.*, 2020). GM130 interacts with WAC directly and

promotes tethering to the Golgi, with GM130-WAC complex formation promoting autophagosome formation, inhibiting GM130 sequestration of GABARAP (Joachim *et al.*, 2015)

The interaction between GABARAP and the ULK1 initiation complex occurs independently of PE conjugation, likely involving a distinct GABARAP Interaction Motif (GIM) sequence (Rogov *et al.*, 2017). These GIM regions display enough sequence difference in the LIR region to generate higher specificity for interactions with GABARAP than LC3. Each member of the ULK1/ATG13/FIP200 /ATG101 initiation complex interact with the ATG8 family homologues but display high binding preference for GABARAP sub-family proteins. The purpose of the interactions between these proteins are to act as scaffold proteins, promoting complex formation and anchoring the ULK complex onto forming autophagosomes (Alemu *et al.*, 2012).

ATG4B is a cysteine protease involved in post-translational modification of both the LC3 and GABARAP subfamilies, which acts by cleaving C-terminal residues from the proteins following translation, exposing the glycine residue required for conjugation to PE. A C-terminal LC3-interacting region (LIR) motif in ATG4B is vital in allowing efficient binding to and cleavage, while also helping to stabilize cleaved GABARAP prior to PE conjugation (Skytte Rasmussen *et al.*, 2017). Akt phosphorylates ATG4B at Ser34, however, this phosphorylation appears to have little effect on autophagic flux in Hepatocellular Carcinoma Cells (HCC). While the effects on autophagy may remain unclear, this phosphorylation represses mitochondrial activity and actively reprogrammes HCC metabolic function, indicating a role for ATG4B in some forms of cancer (Ni *et al.*, 2017). MST4 kinase also phosphorylates ATG4B, instead at Ser383, with upregulation of MST4 linked to resistance to radiotherapy in some forms of cancer. Exposure to radiation induces MST4 expression and subsequently increases phosphorylation of ATG4B. The effect of this in Glioblastoma (GBM) cells corresponded to increased autophagic flux and increased cell proliferation, which, when taken with the previous findings, indicates that site-specific serine phosphorylation may exert different effects that determine final functionality. Inhibition of ATG4B reduces autophagy while also reducing tumourigenicity, improving the impact of radiotherapy treatment on GBM growth and progression in mice (Huang *et al.*, 2017). These findings further enhance the link forming between autophagy and tumourigenesis.

1.10.3 Canonical autophagy

In healthy cells, protein synthesis and autophagy work synergistically, to control cell growth in line with nutrient availability. Autophagy is regulated by a complex signalling network involving several key proteins. When cells undergo starvation, the nutrient responsive serine/threonine kinase, mechanistic Target of Rapamycin (mTOR), is inhibited (Dennis *et al.*, 2001). This causes initiation of autophagy, increasing autophagosome formation and lysosomal fusion, which subsequently increases availability of nutrients such as ATP, carbohydrates and amino acids. This increase in nutrients is detected by mTOR, which is reactivated in response to nutrient availability, generating a negative feedback loop through which autophagy can be controlled, providing homeostatic regulation during cellular stress or starvation (Yu *et al.*, 2010) . mTOR controls the activity of key translational regulators, through phosphorylation of S6 Kinase 1 (S6K1) and initiation factor 4E binding protein (4E-BP1). This regulation is dependent upon the regulatory protein Raptor, binding to a specific amino acid sequence known as the TOR signalling motif, thereby eliciting interactions between mTOR and its targets (Nojima *et al.*, 2003). Phosphorylation of 4E-BP1 impairs its ability to bind to and sequester eukaryotic initiation factor 4E (eIF4E), part of the initiation complex located at the 5' methyl-GTP cap of eukaryotic mRNA, allowing the ribosome to position at the 5' terminus and translation to occur (Richter and Sonenberg, 2005). mTOR forms mTOR Complex 1 (mTORC1) upon association with Raptor and two other proteins, mLST8 and PRAS40 (Sancak *et al.*, 2007). Inhibition of mTORC1 and another complex, mTORC2 increases autophagy in cancer cells and induces cell death (Sini *et al.*, 2010). In mammals, a complex consisting of ULK1, ATG13, FIP200 and ATG101 has been shown to promote signalling leading to autophagy (Hosokawa *et al.*, 2009; Mercer, Kaliappan and Dennis, 2009). mTORC1 has been shown to bind to the ULK1 complex through Raptor binding to ULK1, which allows mTORC1 to phosphorylate ULK1 and ATG13, repressing respective kinase activity and inhibiting autophagy (Jung *et al.*, 2009).

AMPK is a nutrient sensing protein kinase that operates globally to promote catabolic processes following metabolic stress or ATP consumption, operating in multiple ways to initiate autophagy. Firstly, AMPK is able to phosphorylate the mTORC1 complex in order to inhibit its repression of autophagy. Secondly, AMPK is able to directly phosphorylate the ULK complex to activate autophagy (Gwinn *et al.*, 2008; Alers *et al.*, 2012). ULK1 activity is inhibited by mTORC1 phosphorylation at Serine757, and activated by AMPK phosphorylation at multiple sites (Jung *et al.*, 2009). Once activated, ULK1 kinase activity is increased and phosphorylation of ATG13, which is held in complex with ULK1, occurs at Serine318, initiating autophagy. The phosphorylation of

ATG13 at ser318 can therefore be used as a readout for ULK activity, to measure canonical autophagy (Petherick *et al.*, 2015b). ULK1 also phosphorylates and activates Beclin, activating the second complex involved in autophagosome formation, containing the class-III PI3K Vps34.

Interestingly, some findings indicate that ATG13 and FIP200 act independently of ULK1 and ULK2 in autophagy induction. While ATG13 is indispensable for canonical autophagy induction, and is dependent on interaction with FIP200 for activity, the ULK1 phosphorylation sites on ATG13 have been shown to be expendable for this process in some types of canonical autophagy, with one study reporting that ULK1/2/3 knockouts displaying no effect on starvation-mediated autophagy. (Alers *et al.*, 2011). The same research also showed that, in the DT40 cells used, mTOR inhibition has a less prominent role in autophagy induction. While EBSS starvation increased LC3B-II expression significantly after 1 hour, mTOR inhibitors failed to induce autophagy to the same extent, despite validated repression of mTOR activity by the compounds used. In other cell lines, recent work has identified that mTORC1 mediated phosphorylation of ATG13 at Serine258 inhibits the autophagic function of ULK1. While this is in line with previous findings on the repressive role of mTORC1 in autophagy, it was also found that AMPK dependent phosphorylation of ATG13 at Serine224 exerts an inhibitory effect on ULK1 activity (Puente, Hendrickson and Jiang, 2016). This indicates that AMPK is also able to fine tune autophagic responses, adding an additional layer of complexity to this pathway. Additional work has shown that ATG13 and FIP200 may act independently of the ULK/ATG13/FIP200 complex to inhibit viral replication outside of traditional autophagy processes(Solvik and Debnath, 2016).

Beclin 1 is a fundamental scaffold protein involved in assembly of proteins required in regulation of autophagy. Interaction between Beclin 1 and key regulatory proteins is controlled through phosphorylation of Beclin 1 by several Serine/Threonine kinases and phosphatases. The Serine90 residue in Beclin 1 is key for initiation of autophagy, and phosphorylation at this site induces autophagy. Under nutrient rich conditions, a dephosphorylation complex is present at Ser90 which dissociates upon starvation, illustrating the role of site-specific phosphorylation in the activity of Beclin1 (Fujiwara *et al.*, 2016). In mammals, Beclin1 phosphorylation at Serine14 by ULK1 is required for induction of autophagy and activation of Vps34 (Nazarko and Zhong, 2013; Russell *et al.*, 2013). This Beclin1- Vps34 interaction network is critical for autophagy regulation. Vps34 is a Class III PI3K that phosphorylates phosphatidylinositol to generate phosphatidylinositol 3-phosphate (PI3P), and is an essential component of the Beclin1 complex regulating autophagosome biogenesis. Vps34 knockout mice display significant reduction of PI3P localisation to the autophagosome membrane, blocking both endocytic and autophagic degradation, with starvation-induced autophagosome formation blocked (Jaber *et al.*, 2012).

Phosphoinositides form a key component in autophagy regulation, with initiation of autophagy dependent on PI3P synthesis. PI3P is formed by phosphorylation of phosphoinositol on its inositol ring, with most of the free OH groups on the inositol ring able to undergo phosphorylation, with its unique functionality dependent on the combination of inositol position phosphorylation. Phosphoinositide 3-kinases are responsible for this phosphorylation, of which there are 3 classes, grouped according to the positions at which they phosphorylate the inositol ring (Rameh and Cantley, 1999). PI3K's produce PI(3)P, which has been linked to endocytosis, phagocytosis and autophagy, with key roles in autophagosome biogenesis. Double FYVE domain-containing protein 1 (DFCP1) binds to PI3P; upon starvation DFCP1 localises at the autophagosome along with LC3 and ATG5, a process dependent on Vps34 and Beclin1. This serves as a marker to define sites for autophagosome formation (Walker *et al.*, 2008). PI3P produced by Vps34 is essential in autophagosome formation, recruiting specific effectors of autophagy including WIPI2 during autophagosome biogenesis, and is therefore essential in canonical autophagy. However, a function for PI5P has also been implicated in Vps34-independent autophagy, since PI5P can regulate autophagy via PI3P effectors(Vicinanza *et al.*, 2015).

The interaction between Beclin1 and Vps34 is thought to regulate Vps34 lipid kinase activity. P300 is an acetyltransferase that directly regulates Vps34 activity by acetylating Vps34 at several specific regions, disrupting Beclin1-Vps34 complex formation and reducing Vps34 affinity for its substrate, PI. When p300 is inhibited, Vps34 deacetylation is induced, followed by increases in Vps34-Beclin 1 association and PI3P production. This demonstrates a role for p300 in regulation of Vps34 activity, with Vps34 deacetylation and subsequent activity shown to be an essential requirement in both starvation-induced autophagy and non-canonical autophagy (Su *et al.*, 2017). Knockdown of p300 reduces acetylation of several other key autophagy proteins, including ATG5, ATG7, ATG8 and ATG12, and stimulates autophagy, while overexpression of p300 inhibits starvation-induced autophagy(Lee and Finkel, 2009). Additionally, p300 activation is controlled through phosphorylation by mTORC1 (Wan *et al.*, 2017) and Akt (Huang and Chen, 2005), or inhibitory phosphorylation by several proteins, including Protein Kinase C (PKC) (Yuan and Gambee, 2000) and AMPK(Yang *et al.*, 2001). These findings suggest that post-translational acetylation may provide another key regulatory mechanism for autophagy proteins.

1.10.4 Non-canonical Autophagy

While canonical autophagy occurs as a survival mechanism when cells are under stress, recent findings indicate a much broader role for the membrane remodelling machinery involved in canonical autophagy, which can be re-purposed for a variety of processes, including within the adaptive immune response and degradation of phagocytosed molecules (Codogno, Mehrpour and Proikas-Cezanne, 2011). Non-canonical autophagy refers to the process of targeting LC3 to single-membrane structures (Florey and Overholtzer, 2012), and can occur in the absence of the described autophagy proteins that are involved in biogenesis of canonical double-membrane autophagosomes. One instance of non-canonical autophagy involves the process of LC3-associated phagocytosis (LAP), which refers to recruitment of LC3 to intracellular phagosomes. Autophagy stimulation can occur before, during adhesion and uptake of bacteria by the host cell, or during active phagocytosis. Previous research has shown upregulation of autophagy during infection, with increased autophagosome formation in macrophages in response to Toll-like receptor 4 (TLR4) stimulation by Lipopolysaccharide, a component of the cell wall of gram-negative bacteria (Xu *et al.*, 2007). In a macrophage cell line, incubation with latex bead immobilised TLR ligand induced phagocytosis and rapid subsequent recruitment of LC3B-II to the phagosome. This process requires the proteins ATG5 and ATG7, and is preceded by recruitment of Beclin 1, but does not involve the characteristic double membrane bound autophagosomes and therefore occurs independently of the stimulation of canonical autophagy. Instead, translocation of Beclin 1 and LC3B was associated with phagosome-lysosome fusion (Sanjuan *et al.*, 2007).

Subsequent research showed that a subset of human macrophage and dendritic cell phagosomes are coated in LC3B following antigen stimulation by TLR2 agonists, and that reactive oxygen species (ROS) generated by NOX2 are required for this process (Romao *et al.*, 2013). Interestingly, LAP does not appear to be dependent on ULK1 (Martinez *et al.*, 2011), or subsequent ULK1/ATG13/Fip200 pre-initiation complex, but still utilises Beclin 1, ATG5 and ATG7. In retinal epithelial cells, bursts of phagocytosis coincided with increases in LC3B-II, which associated with the forming phagosomes in an ATG5-dependent process (Kim *et al.*, 2013). Macrophages and dendritic cells detect fungal infections through the dendritic cell-associated lectin 2 (Dectin-1) receptor, which recognises fungal β-glucan (Brown and Crocker, 2016) , while Dectin-2 receptor binds and recognises mannose containing ligands exclusively (McGreal *et al.*, 2006). Recognition by either Dectin receptor triggers appropriate inflammatory responses to fungal infection, with Dectin-2 able to bind to and subsequently induce phosphorylation of FcRγ, initiating receptor endocytosis (Sato *et al.*, 2006). It

has been reported that this Dectin-2 associated ligand internalisation is a LAP-dependent process, with recruitment of LC3B to phagosomes containing fungal cells in a Syk dependent manner (Lamprinaki *et al.*, 2017). A similar, LAP-like process, targeting LC3-lipidation to single membrane structures, is also involved in micropinocytosis and entosis (Florey *et al.*, 2011).

Several varieties of chemical compounds, including lysosomotropic or ionophoric drugs, can induce non-canonical autophagic processes by creating osmotic imbalances and targeting membranes for lipidation by LC3 (Florey *et al.*, 2015). One example of such a lysosomotropic drug is Hydroxychloroquine (HCQ), which accumulates in the lysosome in a protonated form, increasing the pH in the lysosome away from the optimal pH required for lysosomal enzymes to function. This means that autophagosome turnover by the lysosome cannot occur. This occurs in a concentration-dependent manner; lower doses of HCQ inhibit autophagic flux but may not be sufficient to activate non-canonical pathways (Jacquin *et al.*, 2017). In vitro studies on the effect of HCQ in CLL, loaded in nanoparticles in combination with Chlorambucil, show an increase in drug induced CLL cell apoptosis compared to the drug alone (Mansilla *et al.*, 2010; Mezzaroba *et al.*, 2013; Capolla *et al.*, 2016), suggesting a role for autophagy in drug resistance by CLL cells. Another inhibitor of autophagic flux is the V-ATPase inhibitor, balilomycin A1 (bafA1). This inhibits turnover of canonical autophagosomes and has also been reported to inhibit non-canonical processes. Inhibiting V-ATPase activity using bafA1 does not affect lipidation of LC3-I to LC3-II in canonical autophagy, only inhibiting autophagosome turnover and therefore resulting in an accumulation of LC3B-II. However, by pre-treating with bafA1 and then treating with a range of lysosomotropic/ionophoric drugs, non-canonical drug induced LC3 lipidation was completely abolished (Florey *et al.*, 2015; Jacquin *et al.*, 2017), displaying a requirement for lysosomal V-ATPase in drug-induced non-canonical autophagy (Figure 14).

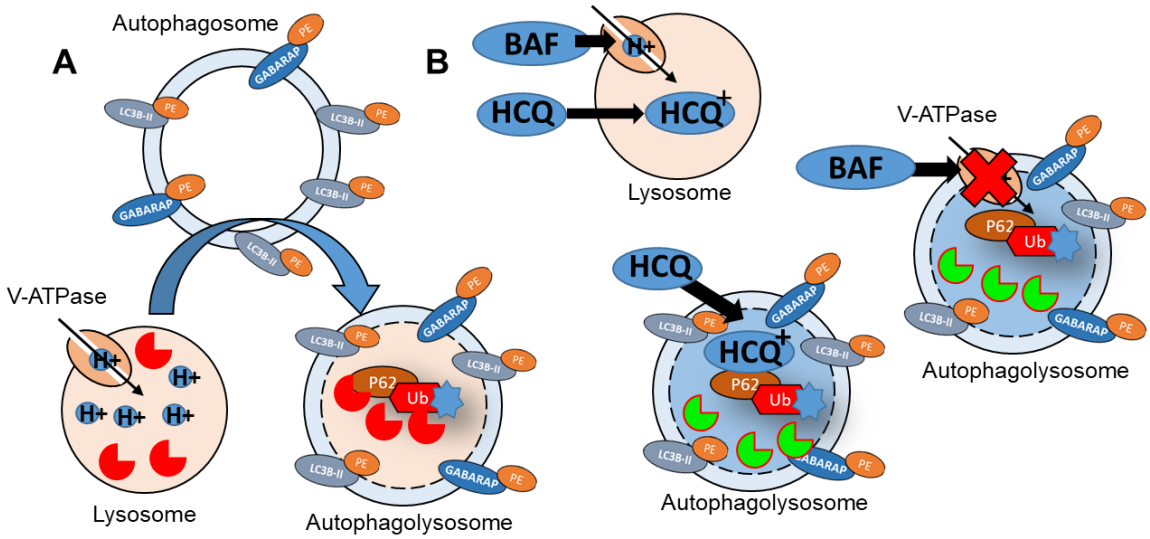

Figure 14. Illustrated mechanism of action for inhibition of autophagosome turnover, and inhibitor targets

(A) Normal mechanism of turnover for autophagosomes by fusion with lysosomes, autophagosome contents are then degraded by lysosomal enzymes. (B) Both bafilomycinA1 (bafA1) and Hydroxychloroquine (HCQ) act to inhibit turnover of the autophagosome by the lysosome, resulting in an accumulation of autophagosomes. BafA1 is a V-ATPase inhibitor, preventing H+ influx into the lysosome and therefore raising lysosomal pH, which then inhibits activity of lysosomal enzymes. HCQ accumulates within the lysosome in a protonated form, sequestering H+ ions and therefore raising the pH within the lysosomal compartment. Both therefore prevent turnover by inhibiting activity of lysosomal enzymes. There is some debate as to whether, by doing this, autophagosome-lysosome fusion is also inhibited.

While the roles of LC3B/GABARAP family proteins in canonical autophagy have been relatively well characterised, their involvement in non-canonical autophagic processes have yet to be fully elucidated. Recent findings indicate a unique role of GABARAPs, in particular for the processes directed by GABARAPL2/Gate-16 in those antimicrobial responses mediated by IFN-γ, independently from LC3B. Cells deficient in GABARAPs showed defective clearance of vacuolar pathogens, with the same response noted in mice lacking Gate-16. Gate-16 specific association with a small GTPase, ADP-ribosylation factor 1 (Arf1), was required to mediate an effective IFN induced response to pathogen clearance from the cell, with GABARAP deficiency corresponding to reduction in Arf1 activation and inactivation of vacuolar clearance (Sasai *et al.*, 2017). This demonstrates the role of GABARAP family proteins in non-canonical autophagy.

1.10.5 Autophagy in the immune response

Overall, the findings regarding the role of Autophagic proteins in non-canonical autophagy illustrates the diverse repertoire of processes that autophagy is associated with. LAP has been demonstrated in response to other surface receptors, including the previously mentioned TLR4, other TLR's and FcR-like receptors. There is great diversity of the cellular processes in which autophagy has reported roles in, with the canonical role for autophagy intricately balancing key processes necessary for cellular homeostasis and survival. In B cells, autophagy is dispensable in development but essential at basal levels for maintenance of peripheral B cells (Arnold *et al.*, 2016). In a subset of B1 cells, which exhibit higher rates of glycolysis and oxidative phosphorylation than B2 B cells, autophagy is essential for self-renewal and metabolism, and deletion of ATG7 results in selective B1a B cell death. These autophagy-deficient B1a B cells exhibit significant down-regulation of metabolic genes critical for survival, resulting in an accumulation of defective mitochondria that are unable to function (Clarke *et al.*, 2018). This shows that within subsets of B cells, autophagy is crucial for metabolic processes and cell survival.

In primary B cells, antigen stimulation through the BCR induces rapid accumulation of autophagosomes, which may then play a role in antigen presentation. Atg5 has been shown to be essential for B cell polarisation and immune synapse formation, as well as subsequent phagocytosis of particulate antigen (Arbogast *et al.*, 2018). Several lines of evidence connect the BCR signalling pathway to the co-stimulatory signalling pathway through which efficient antigen presentation and interaction with CD40 ligand expressing helper T-cells occurs (Watanabe and Tsubata, 2009). In particular, autophagic pathways have been identified as routes by which antigen can be processed and are delivered to MHC class II loading compartments for subsequent coupling to MHC-II and presentation to $CD4^+$ T cells (Crotzer and Blum, 2009), illustrated in Figure 15.

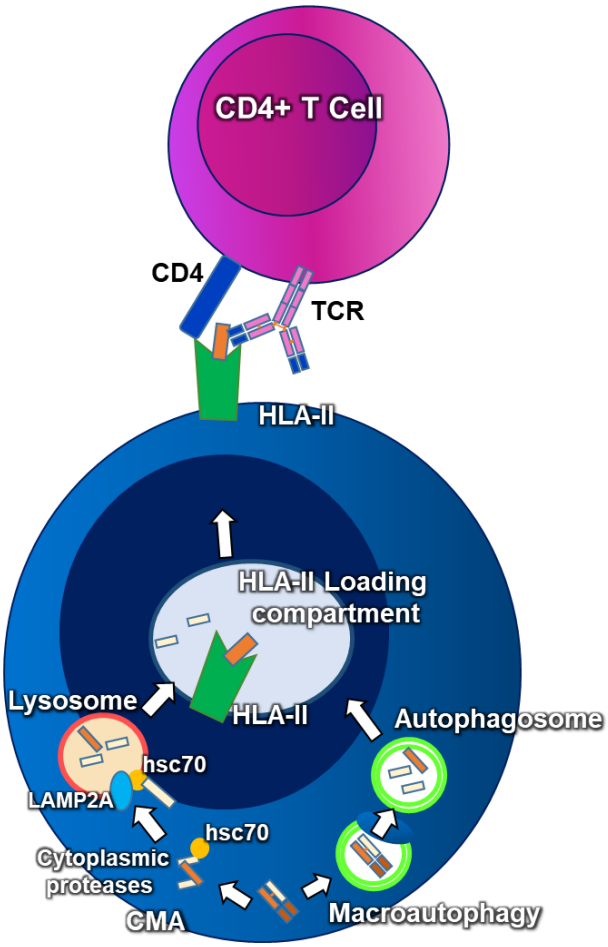

Figure 15. Illustrated potential mechanism of autophagic involvement in MHC-II mediated presentation of tumour antigen

Both macroautophagy and chaperone mediated autophagy can play a role in mediating antigen processing and delivery to the HLA loading compartment. In macroautophagy, the antigen present in cytoplasm is sequestered into autophagosomes, which fuse with lysosomes and process the antigen into peptide fragments for delivery to the HLA loading compartment. In chaperone-mediated autophagy (CMA), specific cytoplasmic proteins are transported into lysosomes via a molecular chaperone/receptor complex composed of hsc70 and LAMP-2A, which can then be delivered to the HLA loading compartment.

Autophagy has also been linked to tumour antigen processing through the cross presentation MHC-I pathway and activation of CD8 T cell response against tumour cells, although the mechanisms by which this may occur remain unclear (Li *et al.*, 2008). In this research, inhibition of autophagy abolished cross presentation, and induction of autophagy greatly enhanced cross presentation efficiency. Purified autophagosomes were shown to be efficient carriers of antigen to dendritic cells, but it was found that lysosomal turnover removed the antigen, hindering cross presentation, indicating the tumour autophagosomes were being utilised as a source of antigen prior to degradation. The uptake of these autophagosomes by dendritic cells was hypothesised, as represented in Figure 16.

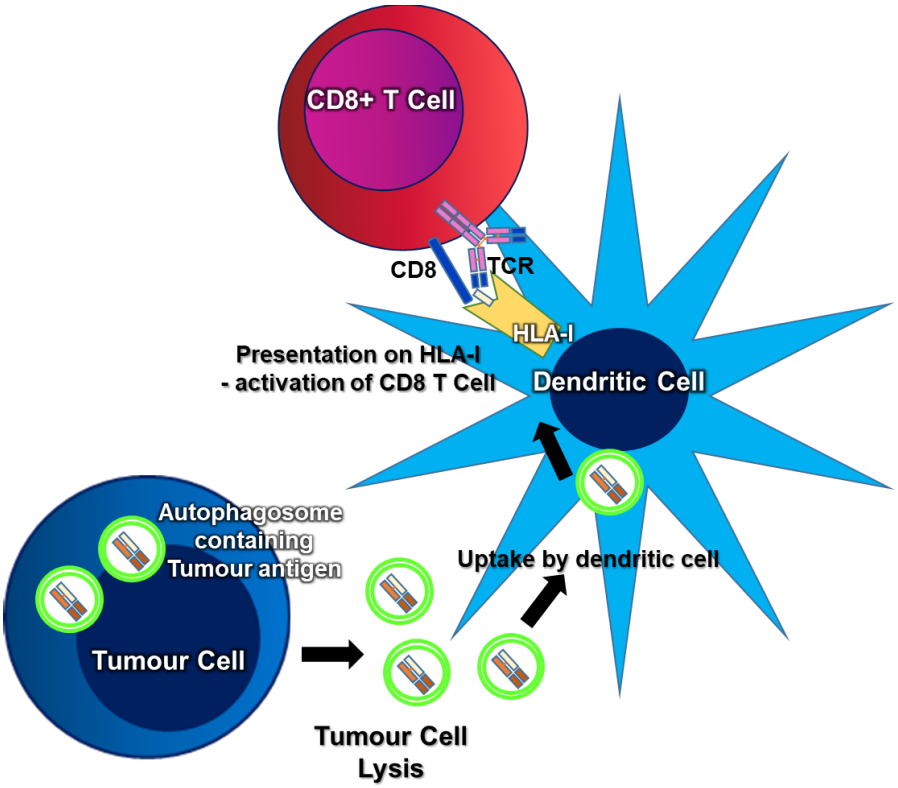

Figure 16. Illustrated potential mechanism of autophagic involvement in MHC-I mediated presentation of tumour antigen by cross-presentation

Autophagy is often upregulated in tumour cells, either as a stress response to nutrient depletion or chemotherapy, or as an elevated basal pro-survival mechanism. Autophagosomes likely contain endogenous antigen from recycling of cellular proteins or organelles, and may be released into the extracellular environment and internalised by dendritic cells. The exact mechanisms for processing of autophagosomes by dendritic cells, or how they intersect with the MHCI pathway, is unclear. Dendritic cells then present tumour peptides on MHCI for the activation of CD8+ve T cells.

Dysregulation of autophagy in primary CLL cells by the Sirtuin inhibitor, Tenovin-6, results in cytotoxicity (MacCallum *et al.*, 2013), illustrating a protective role for autophagy in CLL which requires further investigation. Moreover, autophagy induction has been demonstrated to contribute to resistance to some therapeutic agents in CLL, including the drug flavopiridol (Mahoney, 2010). In this thesis, I aim to characterise BCR-regulated autophagy and the involvement of the BCR signalling network, while investigating the relation of autophagy to bead-induced endocytosis. I aim to elucidate these processes by examining expression levels of signalling proteins and autophagy markers, localisation of these markers within the cell and the effect upon metabolic processes. Ultimately, these mechanisms could inform development of novel treatment options to improve overall prognosis of this largely incurable disease.

1.11 Project Rationale, Aims, Hypothesis and Objectives

1.11.1 Project rationale

B-cell receptor signalling is pivotal to CLL pathogenesis and disease progression. The use of BCR-kinase inhibitors for the treatment of CLL has demonstrated a high level of success, particularly in patients with progressive disease. However, resistance to BCR kinase inhibitors is already occurring. Whilst mutations within BTK and PLCγ2 explain some of this resistance, other patients progress or become resistant for unknown reasons.

We have shown that autophagy markers act as predictors of prognosis in CLL, with high autophagy levels corresponding to more progressive disease phenotypes (Smith *et al.*, 2020). In a tumour setting, autophagy has been widely reported to exert pro-tumour functions by increasing cell proliferation, survival skills and stress resistance (Yun and Lee, 2018). Within subsets of B cells, autophagy is crucial for metabolic processes and cell survival (Clarke *et al.*, 2018), and autophagy inhibition in primary CLL cells increases drug cytotoxicity (MacCallum *et al.*, 2013), illustrating a protective role for autophagy in CLL. Since autophagy has also been linked to treatment resistance in CLL (Mahoney, 2010), and autophagy markers have been shown to correlate to clinical outcome, autophagy inhibition may be an area of therapeutic interest. In addition to this, autophagy has been reported to have various roles in the immune response and regulation. In particular, roles have been demonstrated in antigen processing and presentation pathways, which subsequently leads to T cell recruitment, activation and proliferation of both B and T cells. In the context of CLL, this T cell help may support CLL cell survival and proliferation (Os *et al.*, 2013). Furthermore, T cells in CLL have been shown to display a distinctive phenotype with exhaustion features (Riches *et al.*, 2013), which could result from chronic antigenic stimulation following constitutive engagement with CLL cells. This is further supported by deficiency in immune synapse formation, which has been shown to become defective following engagement with tumour cells (Ramsay *et al.*, 2008). With increasing evidence suggesting the importance of T cells, and their interaction with CLL cells, in CLL disease progression, there is interest in exploration of therapies targeting these populations. Therefore, this project aims to explore the role of autophagy in CLL, and the potential biological relevance of this, including in antigen processing. The final chapter of this thesis will focus on CLL-T cell interactions, using BCR kinase and autophagy inhibitors to explore this pathway, with the aim of developing a better understanding of the role of BCR signal-dependant autophagy in CLL.

1.11.2 Project aim

This project will aim to define the autophagy pathways and biological relevance in CLL, particularly autophagy occurring downstream of BCR activation, since CLL is driven by BCR activation, and this is where autophagy is significantly upregulated. I will also examine phagocytosis in relation to antigen processing pathways, in response to particulate antigen internalisation by CLL cells, and how this related to antigen presentation. I will examine how efficiently CLL cells are able to process antigen and present to T cells, inducing a T cell activation and proliferation response, and the potential roles of autophagy and BCR signalling in this process.

1.11.3 Hypothesis

The central hypothesis of this project is that BCR-driven autophagy in CLL may be involved in antigen processing and presentation, downstream of a phagocytic response to anti-IgM coated beads, in order to remove antigen and present this to CD4+ T cells. This may enable a better understanding of CLL-T cell interactions in CLL.

1.11.4 Objectives

The objectives will be as follows:

1) To examine BCR driven autophagy in CLL.

2) To examine BCR driven phagocytosis in CLL

3) To determine functional relevance by testing the roles of each in antigen processing and presentation

Chapter 2 : Materials and Methods

2.1 Patient Samples collection and storage

2.1.1 Sample collection and storage

CLL Peripheral blood samples were collected from patients following informed consent. CLL was diagnosed according to IWCLL 2008 clinical criteria. Peripheral blood mononuclear cells (PBMCs) were collected from blood and extracted at room temperature. Lymphoprep (20ml) (Fisher Chemicals, P/7500/17) was added to a sterile container and overlaid with 20ml of blood, followed by centrifugation at 350g for 30 minutes. The concentrated PBMC layer was removed, and the cells re-suspended in 50ml of complete media (RPMI 1640 plus glutamine, penicillin and streptomycin, supplemented with 10% foetal bovine serum (FBS)). These were counted, resuspended in Freezing Medium (Foetal Bovine Serum (Decomplemented) 90% Dimethylsulfoxide (DMSO) 10%), placed in a Mr Frosty at room temperature and subsequently placed in an ultra-cold freezer (-70OC to -80OC) for a minimum of 4 hours. Samples are then cryopreserved in liquid nitrogen at concentrations between $5x10^7$ and $1x10^8$ cells/ml, as part of the South Coast Tissue Bank, according to standard operating procedure. A full table of all CLL samples used in this work can be found in (Appendix 1 : CLL samples used in this research).

2.1.2 Recovery of CLL samples

Following retrieval of samples from the liquid nitrogen store, samples were thawed and resuspended immediately in 10mL of complete medium, pre-warmed to 37°C. These were centrifuged and resuspended in 4mL of fresh medium, as a wash step to remove DMSO from freezing media. Cells were counted using a haemocytometer and cell viability was evaluated by trypan blue cell exclusion assay. Only samples with >90% viability were retained for further experimentation. (RPMI 1640 Sigma, ref: R0883-500ML - 500 mL, Foetal bovine serum (FBS) PAA, ref: A15-102, at 10%, Glutamine Sigma, ref: G7513 2 mM Penicillin/ streptomycin Sigma, ref: P4333 both at 10 ml/L)

2.2 CLL Sample selection, Culture and Cell Lines

CLL was diagnosed according to IWCLL 2008 clinical criteria (Hallek *et al.*, 2008). All isolates used contained more than 90% CD19/CD5-positive tumour cells. CLL cells (1 x10^7 mL−1) were routinely cultured in RPMI 1640 medium, with the addition of 10% foetal bovine serum, L-Glutamine, 1% penicillin and streptomycin. Cultures were incubated for the specified time according to experimental conditions at 37°C, 5% CO_2 ; where drugs were added these were pre-incubated with the cells for 60 minutes prior to addition of Anti-IgM/IgD or control antibody conjugated DynaBeads, which were prepared as previously described (Coelho *et al.*, 2013). Latex beads were supplied by PolySciences (Polybead Carboxylate Microspheres, PolySciences; 09850-5). Where latex beads were used, these were prepared using PolyLink protein coupling kit (PolySciences; 24350-1) as per manufacturer instructions and conjugated to anti-IgM/IgD or control antibodies at the same antibody concentration as dynabeads. A standard concentration of two beads per cell was used unless otherwise specified.

2.2.1 SKW3-T18 Cells

The SKW3-T18 cell line was kindly gifted for this project by Professor Ludvig Munthe, University of Oslo. SKW3-T18 cells were established by Geir Age Loset and Terje Frigstad (Nextera AS). The TCR from human T cell clone T18 (Schjetne *et al.*, 2002) was cloned and retrovirally reconstructed in the TCR negative mouse BW58 T cells, in order to verify the TCR construct. Following this functional verification in BW58 T cells, the TCR was subsequently introduced into the TCR-negative human SKW3 T-cell line (a derivative of the T-acute lymphoblastic leukaemia cell line KE-37 (Gacon *et al.*, 1983)) to generate SKW3-T18 cells, as described (Frick *et al.*, 2021). DR4 tetramer reagents were obtained from Benaroya Research Institute (Seattle, WA) and used according to the manufacturer's instructions. to express a TCR (in SKW3-T18 cells) which recognises a nonamer peptide derived from mouse kappa light chains (κLC) when presented on HLA-DRB1*04:01 (Schjetne *et al.*, 2002). Thus, when HLA-DRB1*04:01-expressing CLL cells are exposed to a mouse κLC-containing anti-human IgM F(ab')$_2$ antibody (Ms κ+ anti-IgM), the CLL cells can internalise and process the mouse antibody, and then present the κLC-derived peptide to SKW3-T18 cells. Resultant activation of SKW3-T18 cells can be monitored by analysing cell surface expression of CD69 or secretion of IL2

2.2.2 Co-Culture Antigen Presentation Assays

Cell line culture was performed routinely as part of the antigen presentation assays, with Boleth HLA typed control B cells (ECACC HLA-Typed Collection, BOLETH, Catalogue number 8805203, obtained from Public Health England Culture Collections) and SKW3-T18s cultured in RPMI 1640 medium, with the addition of 10% foetal bovine serum, L-Glutamine, 1% penicillin and streptomycin. Cultures were grown at 37°C, 5% CO_2, at densities between 0.5-1x10^6 cells/mL. Cell line identity was confirmed using short tandem repeat analysis (Powerplex 16 System, Promega, Southampton, UK) and absence of mycoplasma was confirmed using Mycoplasma PCR detection kit (Applied Biological Materials, Richmond, Canada).

CLL cells were HLA typed for co culture experiments. HLA-typing was performed by Molecular Pathology (Molecular Pathology, University Hospital Southampton), using the Olerup SSP HLA-DRB1-*04 HLA Typing Kit (CareDx). CLL cells were purified using MACS B-CLL cell negative selection isolation kits (B-CLL Cell Isolation Kit, human, Miltenyi Biotec, Catalogue number 130-103-466), leaving untouched B cells ready for downstream assays. CLL cells were then treated with inhibitor where applicable as per experimental conditions, prior to incubation with soluble antibody or antibody-coated beads (2:1 bead:cell ratio) for 15 or 60 minutes, respectively. SKW3-T18 and CLL cells were then incubated at a 1:4 SKW3-T18 : CLL cell ratio, at a final density of 100,000 SKW3-T18 and 400,000 CLL cells in a total volume of 200µL in 48 well plates. Supernatants were collected after 24 hours and IL-2 quantified using an enzyme-linked immunosorbent assay (ELISA; R&D Systems) according to the manufacturer's instructions.

2.2.3 Compound additions

Where specified for drug additions, the pan-caspase inhibitor Q-VD-Oph (Calbiochem InSolution Q-VD-OPh, Merck 551476) was added to cell culture medium prior to plating to inhibit caspase-dependent cell death. In starvation conditions, cells were incubated as per experimental procedure following to 5 x washes in Earl's Balanced Salt Solution (EBSS) (ThermoFisher, 24010043), which contains no glucose or amino acids. Cells were then plated in EBSS for specified time prior to collection. Hydroxychloroquine (HCQ) was either added at start of culture, or for the last hour of culture, as specified for each experimental procedure. Where used, chemical inhibitors were included in starvation media and all starvation washes. Where inhibitors were used, these were pre-incubated with cells for 60 minutes prior to stimulation or experimental conditions.

Table 1. Table of Inhibitors used and concentrations

Inhibitor Name	Inhibitor Protein Target	Concentrations Used (μM)	Supplier and Catalogue Number
Ibrutinib	BTK	0.5, 0.1, 0.025	Selleckchem S2680
Acalabrutinib	BTK	0.1, 0.025	Selleckchem S8116
Idelalisib, Cal101	Class I PI3Kδ	1	Selleckchem S2226
Entospletinib	SYK	1	Selleckchem S7523
R406	SYK	1	Selleckchem S2194
Saracatinib	Src/Abl	1	Selleckchem S1006
Cerdulatinib	JAK/SYK	1	Selleckchem S3566
SAR405	Class III PI3K (VPS34)	1-10	Selleckchem S7682
VPS34-IN1	Class III PI3K (VPS34)	1-10	Selleckchem S7980
MRT68921	ULK1/ULK2	1-10	Merck SML1644-5MG
SBI-0206965	ULK1/AMPK	1-30	Selleckchem S7885
Hydroxychloroquine	Sequesters protons in lysosome, raising pH	10-100	Selleckchem S4430
Bafilomycin-A1	vATPase	0.1-1	R&D 1334
MG101	Broad spectrum cysteine protease/cathepsin/calpain inhibitor	1-10	Selleckchem S7386
DYNGO-4A	Dynamin	1-10	Selleckchem S7163
Cytochalasin D	Actin filament polymerisation	1-10	Merck 504776

2.3 Antibodies and reagents

Table 2. Table of antibodies used in Immunoblotting and concentrations

Immunoblotting Protein	Supplier and Catalogue Number	Concentration used
LC3B	CST 3868S	1:1000
pATG13 (Ser318)	Rockland 600-401-C49S	1:2000
ATG13	Sigma SAB4200100-200UL	1:1000
p62	CST 5114S	1:1000
ATG3	CST 3415S	1:1000
ATG7	CST 8558S	1:1000
GABARAPL2	CST 14256S	1:1000
PINK1	CST 6946S	1:1000
Parkin	Santa Cruz SC-32282	1:1000
phospho-Akt (Ser473)	CST 4060L	1:1000
Akt	CST 9272S	1:1000
phospho-Erk (Thr202/Tyr204)	CST 9101S	1:1000
Erk	CST 9102S	1:1000
phospho-p70S6K (Thr389)	CST 9205S	1:1000
P70S6K	CST 9202S	1:1000
pSYK (Tyr525/526)	CST 2710S	1:1000
SYK	CST 2712S	1:1000
pAMPK (Thr172)	CST 2531S	1:1000
AMPKα	CST 5832S	1:1000
pS6 (Ser235/236)	CST 2211S	1:1000
S6	CST 2317S	1:1000

Table 3. Table of antibodies used in Immunostaining and concentrations

Immunostaining Target	Supplier and Catalogue Number	Concentration used
LC3B	Sigma L7543	1:500
LAMP1	Abcam 555798	1:50
LAMP2A	Abcam ab18528	5µg/ml (Batch concentration not stable)
HLA Class II	Abcam ab207376	1:500
WGA-Rhodamine	Vector Labs RL-1022	1:100
CellMask DeepRed	ThermoFisher C10046	1:100
Bead staining secondary antibody	Fisher 10246392	20µg/ml / 1:100

Table 4. Table of antibodies used in Flow Cytometry and concentrations

Flow Cytometry Protein	Supplier and Catalogue Number	Concentration used
LC3B	Novus NB100-2220AF647	1:50
CD5	BioLegend 364010	1:20
CD19	BioLegend 302232	1:20
CD69	BioLegend	
CD3 (Human)	BioLegend 317313	1:25
CD28 (Human)	BioLegend 302911	1:20
CD3 (Mouse)	BioLegend 100213	1:20
CD28 (Mouse)	BioLegend 102109	1:50
HLA DR	Biolegend 307624	1:20
Bead staining secondary antibody	Fisher 10246392	20µg/ml / 1:100

Table 5. Table of antibodies used in cell stimulation assays

Cell Stimulation Antibody	Supplier and Catalogue Number	Concentration used (µg/mL)
Goat F(ab')2 Anti-Human anti-IgM	Cambridge Biosciences 2022-01	20
Mouse F(ab')2 Anti-Human anti-IgM	Cambridge Biosciences 9023-01	20
Goat F(ab')2 IgG (Control)	Cambridge Biosciences 0110-01	20
Anti-CD3/CD28 Beads (Human)	ThermoFisher 11131D	-
Anti-CD3/CD28 Beads (Mouse)	ThermoFisher 11456D	-

2.4 Western blotting

2.4.1 Cell Lysis and Protein Extraction

Cells were centrifuged at 2500RPM for 5 minutes and pellets resuspended in whole cell lysis buffer (20mM Hepes-KOH, pH 7.4, 50mM NaCl, 2% Nonidet P-40 (or IGEPAL CA-630), 0.5% Na deoxycholate, 0.2% sodium dodecyl sulphate, 1mM sodium orthovanadate, 1 mM EGTA, pH 7, 10 mM sodium fluoride, 2.5 mM sodium pyrophosphate, 1 mM β-glycerophosphate). To each 1mL of Lysis buffer, 10µl Sigma protease inhibitor cocktail (P 8340) and 10µL 100 mM phenylmethylsulfonyl fluoride (PMSF) were added immediately before use. Cells were lysed in this solution at 4°C and centrifuged at 13000 RPM for 10 minutes.

2.4.2 Protein Gel Electrophoresis and Transfer

Supernatants were mixed with a loading dye mix (13µL cell lysate, 5µL Loading Dye Buffer (Invitrogen NP0007), 2µL 1M DTT) These were then either stored or immediately run on gels. Cell lysate- dye mixes were stored at -20°C for imminent use or -80°C for longer storage. These were then separated on 12% (ThermoFisher, NP0342BOX) or 10% (ThermoFisher, NP0302BOX) polyacrylamide SDS–PAGE gels. 500µL NuPage Antioxidant (ThermoFisher,NP0005) was added into the running buffer of the gel running compartment during protein gel electrophoresis, before transferring to nitrocellulose (Amersham Protran NC 0.45µm, GE healthcare, 15259794) or polyvinylidene difluoride (PVDF) (LC3B only) membranes (Amersham Hybond 0.2µm PVDF, GE healthcare, 15239814). Where PVDF membranes were used for LC3B, these were pre-activated in methanol for 20 seconds, rinsed in water and soaked in transfer buffer for 5 minutes prior to use.

Table 6. Table of gel percentages and membrane specifications for different protein targets

Protein	Polyacrylamide SDS-PAGE Gel	Transfer Membrane
LC3B	12%	PVDF 0.2 µm pore size
Signalling Proteins	10%	Nitrocellulose 0.45 µm pore size
Other Autophagy Proteins	12%	Nitrocellulose 0.45 µm pore size

Membranes were blocked in tris buffered saline containing 0.1% tween -20 (Sigma P1379) (TBST) supplemented with either 5% BSA or 5% Polyvinylpyrrolidone (Sigma P5288-500G) + 2.5% FBS for 1H at room temperature before incubation with primary antibodies diluted in blocking buffer overnight at room temperature, or at 4°C over 2 days. Following primary antibody incubation, membranes were washed 3 times before 1 hour incubation with horseradish peroxidase-

conjugated secondary antibody (DAKO polyclonal goat anti-rabbit immunoglobulins/HRP P0448 or polyclonal goat anti-mouse immunoglobulins/HRP P0447). Proteins were detected using enhanced chemiluminescence (Pierce ECL Western Blotting Substrate, 32106 or Amersham ECL Select, GE 12644055), and visualised with a UVP CDC imager. Densitometry analysis was performed using ImageJ software and statistical analysis carried out in GraphPad PRISM.

2.5 Immunofluorescence

Cells were collected following experimental conditions and fixed in 4% paraformaldehyde solution for 15 minutes on ice. Permeabilisation was carried out in 0.25% Triton/PBS for 10 minutes at room temperature where required for intracellular stains. Cells were then incubated in relevant primary antibody overnight at 4°C. Samples were subsequently washed and secondary antibody mix added to each condition for 45 minutes at room temperature. Cells were washed and cytospinning carried out. Slides were dried for 10 minutes at RT before mounting with Vectashield Hardset mountant with DAPI (Vector Laboratories, H-1500) to stain DNA.

2.6 Flow Cytometry Bead Internalisation Assay

Cells were collected following experimental conditions and placed on ice for 10 minutes. An anti-goat AlexaFluor488 conjugated antibody (ThermoFisher A-11055) was then incubated with cells on ice for 30 minutes at a concentration of 20µg/mL (1:100 dilution factor). Cells were then washed in media and flow cytometry performed. For flow cytometry analysis the BD FACSCanto II was used, and results analysed used FlowJo software (V10). Results were then graphed using GraphPad PRISM and statistical analysis performed.

2.7 ELISA for IL2

ELISA kits were obtained from R&D Systems (Human IL-2 Quantikine ELISA Kit, Catalogue number S2050) and ELISA manufacturer protocols followed. Assays were performed as required for experimental conditions, for CLL co-culture experiments cells were co-cultured for 24 Hours before supernatants were analysed for IL2 by ELISA. Photometric readings were taken at 450 and 540 nm and wavelength subtraction performed manually, according to manufacturer directions, for background removal (450-540nm). Standard curves from known IL2 protein standards were performed in a range from 2000 – 0 pg/mL and experimental results were plotted against the curves generated on Microsoft Excel. All ELISAs were performed in technical duplicate per plate and average results plotted.

2.8 RNA-Seq library preparation and data analysis

CLL samples (n=6) were incubated with goat F(ab')2 anti-human IgM or control antibody coated Dynabeads at a 2:1 bead to cell ratio for 6 or 24 hours. Total mRNA was isolated using the Promega reliaprep RNA extraction kit (Reliaprep RNA Cell Miniprep System, Catalogue Z6011, Promega, Southampton, UK) and quality control was performed on a fragment analyser (Fragment Analyzer, Advanced Analytical Technologies), with a RNA Integrity Number (RIN) cut-off of above 8.0 determined as acceptable quality. A table of all RNA samples sent for sequencing is provided in Appendix 2. RNA-seq was performed at the Oxford Genomics Centre (Oxford, UK) using Illumina TruSeq Library Prep kit V2 and Illumina Novaseq 6000 sequencing platform. Raw RNA-seq data(fastq files) were analysed by Dr Dean Bryant, an experienced bioinformatician, who aligned data against the hg19 reference genome using BWA, and initial data quality control was performed using FastQC. Counts matrices were produced using HTseq-count and exported for differential expression analysis in EdgeR. Transcriptomic data were fitted to multifactor GLM models and tested for differential expression using quasi-likelihood f-tests. Multiple testing correction was performed using the Benjamini-Hochberg procedure. Gene Pathway analysis was performed using Ingenuity Pathway Analysis software (IPA; Qiagen). Other statistical comparisons and heat maps were made using Prism 9 software (GraphPad Software, La Jolla, CA, USA).

Chapter 3 Effect of BCR stimulation on autophagy in CLL cells

3.1 Introduction and Aims

At the start of my PhD project, our group had previously demonstrated increased expression of various autophagy markers (LC3B-II, GABARAPL2, ATG3 and ATG7) in CLL cells compared to healthy donor B cells (HDB). LC3B-II expression was also higher in U-CLL compared to M-CLL samples and high LC3B-II expression was associated with a shorter time-to-first-treatment demonstrating that raised levels of autophagy markers was clinically significant. This work was published in (Smith *et al.*, 2020) during the course of my project and the key data is presented below to illustrate this effect (**Figure 17**). The majority of these experiments looking at basal levels of autophagy were performed by Dr Lindsay Smith, but I did contribute immunoblotting data characterising protein expression in a small number of CLL samples for this part of the study.

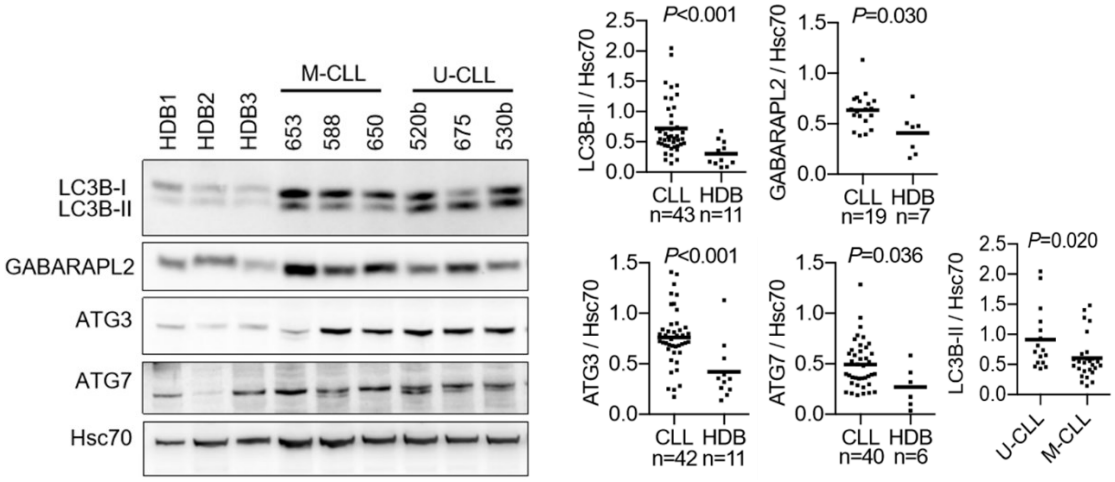

Figure 17. Characterization of autophagy-markers in unstimulated CLL cells and HDB.

(Left) Immunoblot analysis of LC3B-II, GABARAPL2, ATG3 and ATG7 expression in healthy donor B cells (HDB) and representative M-CLL and U-CLL samples. (Right) Quantitation for all samples comparing autophagy marker expression between CLL and HDB samples, and LC3B-II expression between U- and M-CLL. The statistical significance of the differences is shown (Mann-Whitney test). Figures taken from (Smith *et al.*, 2020).

Based on these initial data, I hypothesised that stimulation of the BCR of CLL cells could act as a driver of autophagy and explain the higher levels of autophagy detected in CLL cells compared to normal B cells. Thus, U-CLL tend to have higher sIgM signalling capacity than M-CLL (Mockridge *et al.*, 2007; D'Avola *et al.*, 2016) and previous studies have shown that activation of other BCR-regulated pathways can be detected at higher levels in unstimulated U-CLL cells compared to M-CLL cells (eg the unfolded protein response) (Krysov *et al.*, 2014). Therefore, the overall goal of the experiments described in this chapter was to determine whether stimulation of the BCR of CLL cells increased autophagy, using both immunoblotting and confocal imaging. I also analysed the effects of various chemical modulators (including BCR-associated kinases and autophagy inhibitors) on these responses and compared the BCR-induced autophagy response to that induced by a classical autophagy inducer, starvation.

The specific aims of the experiments were:

- To characterise the effect of anti-IgM or anti-IgD on expression of autophagy markers in CLL cells
- To investigate the effects of chemical modulators on autophagy in CLL cells
- To investigate the effects of BCR-associated kinase inhibitors on anti-IgM-induced autophagy
- To compare autophagy responses to anti-IgM and serum-starvation
- To analyse CLL cell autophagy using confocal imaging

3.2 Effect of anti-IgM or anti-IgD on expression of autophagy markers

3.2.1 Initial analysis of LC3B expression

I selected immunoblot analysis of LC3B isoform expression as my principal readout to quantify autophagy. This analysis focused on LC3B-II, the lipidated form of LC3B which is found in association with autophagosome membranes (or other autophagic structures) and therefore provides a direct measure of the number of autophagosomal structures within the cell (Mizushima and Yoshimori, 2007). LC3B-I isoform expression was also quantified in some experiments, as LC3B-I accumulation may indicate blockage of LC3B lipidation and thereby indicate suppression of active autophagy, especially in subsequent experiments investigating effects of inhibitors. Since LC3B antibodies may have different affinities for the LC3B-I and -II isoforms, it was not appropriate to draw any conclusions based on LC3B-I/LC3B-II ratios.

To test whether BCR stimulation of CLL cells resulted in activation of autophagy, I stimulated CLL samples with anti-IgM-coated beads and used immunoblotting to quantify expression of LC3B isoforms. Bead-bound antibodies were used for sIg stimulation as they induce stronger signalling in CLL cells compared to soluble antibodies (Krysov *et al.*, 2014). I tested effects of both anti-IgM- and anti-IgD- coated beads, as signalling pathways activated downstream of these two forms of the BCR can differ (Ten Hacken et al., 2016)(Lanham *et al.*, 2003) (Krysov *et al.*, 2012). Beads coated with a control F(ab_2)' antibody were used as a control (Krysov *et al.*, 2012). The experiment was performed as a time course to probe the kinetics of potential effects on LC3B and compare to activation of upstream signalling (phospho-ERK and AKT), and to define optimal time points for more detailed follow-on experiments with larger sample cohorts. Two samples were selected for this initial experiment (1 U-CLL and 1 M-CLL) both of which were considered as sIgM and sIgD signal responsive in terms of anti-IgM or anti-IgD-induced iCa^{2+} mobilisation (Mockridge *et al.*, 2007).

This analysis demonstrated that LC3B-II (and LC3B-I) expression was increased to a similar extent (maximum ~7-fold on average) by anti-IgM and anti-IgD, at 12 and 24 hours (**Figure 18)**. There was some indication that anti-IgD, but not anti-IgM, increased LC3B-I/II expression at earlier time points (4-6 hours) but at these times responses were very modest. Consistent with the signal competence of the selected samples, both ERK and AKT phosphorylation were strongly increased by anti-IgM and anti-IgD at the earliest time point analysed (15 minutes). Therefore, these results demonstrate that stimulation of sIgM or sIgD of CLL cells can induce autophagy.

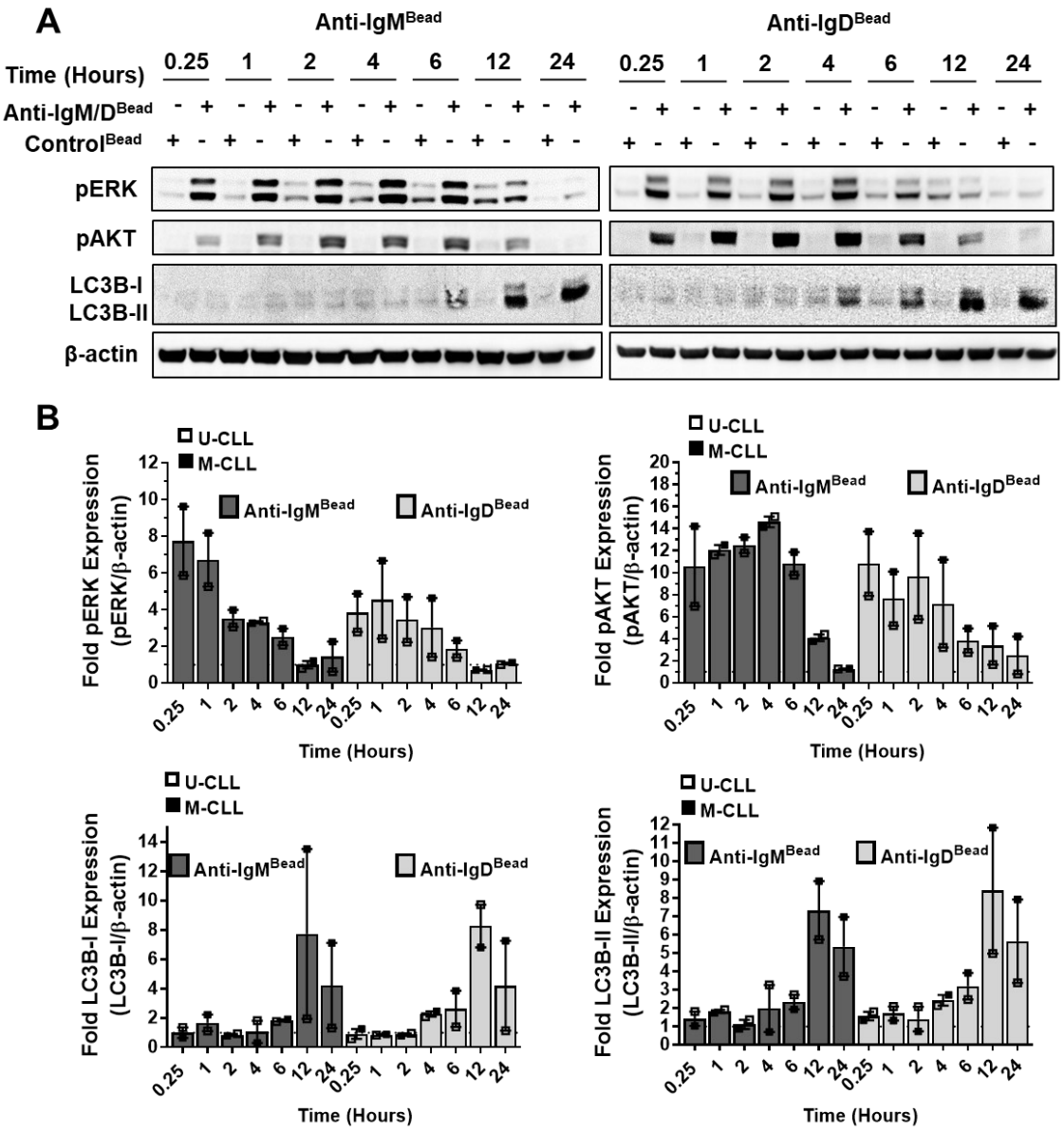

Figure 18. Expression LC3B and phosphorylation of AKT and ERK following sIgM and sIgD stimulation in CLL cells.

CLL samples (n=2) were incubated with anti-IgM-, anti-IgD- or control antibody-coated beads for the indicated times before analysis of phospho-AKT, phospho-ERK, LC3B and β-actin (loading control) by immunoblotting. (A) Example immunoblots and (B) summary of data for both samples. Graphs show fold change in expression for phospho-AKT, phospho-ERK, LC3B-I and LC3B-II (mean±range) with results for control antibody-coated beads set to 1.0 for each time point.

3.2.2 Analysis of LC3B, ATG3, ATG7 and GABARAPL2 expression in larger sample cohorts

Follow-on experiments were performed to investigate regulation of LC3B and additional autophagy markers in a larger number of samples. The additional markers analysed were ATG3, ATG7 and GABARAPL2; ATG3 and ATG7 are responsible for conjugation of PE to LC3B and GABARAPL2 prior to insertion into the membrane of forming autophagosomes (Taherbhoy *et al.*, 2011). The time points selected for analysis were 2-, 4- and 24-hours post-stimulation allowing analysis of both early and later events based on my preliminary study (section 3.2.1).

Figure 19 shows results for 8 samples that I analysed for LC3B expression. These samples comprised 3 U-CLL and 5 M-CLL samples, all of which were considered as sIgM and sIgD signal responsive and were part of a larger cohort reported in (Smith *et al.*, 2020). This confirmed that incubation with anti-IgM- or anti-IgD-coated beads significantly increased LC3B-II expression at 24 hours
The response to anti-IgD was weaker than anti-IgM at 24 hours (~5- versus 11-fold, respectively). This difference to previous results, where response to anti-IgM and anti-IgD were similar, (**Figure 19**) may reflect the smaller number of samples included in that analysis (n=2). Moreover, it was also evident from this experiment that LC3B-II expression was significantly increased by both anti-IgM and anti-IgD at 4 hours but to a more modest extent than at 24 hours (~3-4-fold). Increased phosphorylation of ERK and AKT confirmed activation of signalling by anti-IgM and anti-IgD in these experiments.

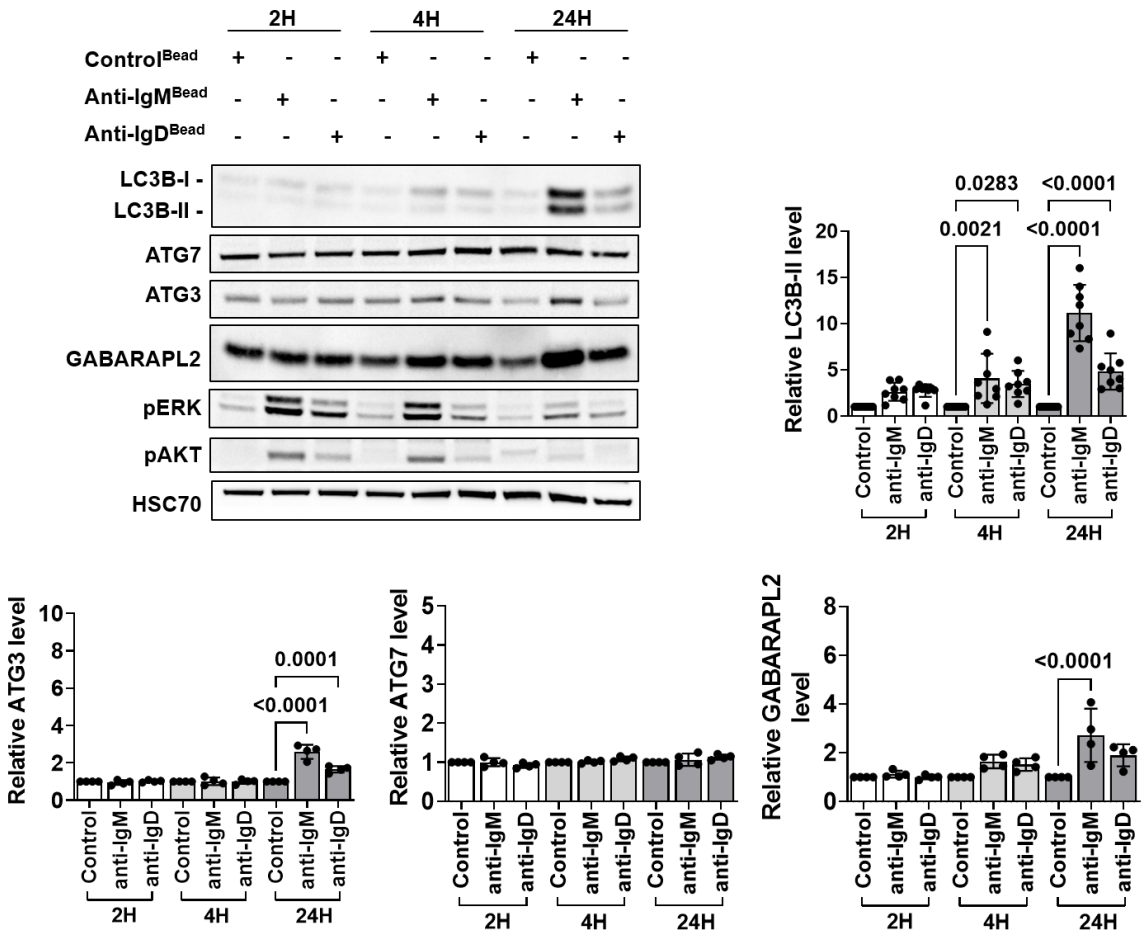

Figure 19. Effect of anti-IgM or anti-IgD on signalling and autophagy markers in CLL cells.
CLL samples were treated with anti-IgM- (anti-IgM^{bead}), anti-IgD- (anti-IgD^{bead}) or control antibody-coated beads (Control^{bead}) for 2-, 4- or 24-hours and expression of LC3B (n=8) GABARAPL2, ATG3 and ATG7, and phosphorylation of ERK and AKT (all n=4) were analysed by immunoblotting. HSC70 was analysed as a loading control. Figure shows representative immunoblots and quantitative summaries for all samples. Graphs show results for individual samples and mean (±SD) with values for control antibody-coated beads set to 1.0 for each time point. The results of statistical comparison (Wilcoxon matched-pairs signed rank tests) comparing values for control and anti-IgM/anti-IgD-coated beads at each time point are indicated (where not shown, *P*>0.05). These results were included in analysis of a larger cohort published in (Smith *et al.*, 2020).

I also analysed GABARAPL2, ATG3 and ATG7 expression in 4 samples (**Figure 19**). This demonstrated significant increased expression of ATG3 (anti-IgM and anti-IgD) and GABARAPL2 (anti-IgM only) at 24 hours. By contrast, expression of ATG7 was essentially unaltered in these samples. Similar patterns of regulation were observed when results from my analysis were integrated into a larger sample cohort (L. D. Smith et al., 2020).

Finally, LC3B-II levels were analysed following incubation with anti-IgM-coated beads for 24 hours in a large group of samples (n=45) allowing comparison of responses between U- and M-CLL (**Figure 20**). All samples were considered as sIgM and sIgD signal responsive. Anti-IgM significantly increased LC3B-II expression when the entire cohort was considered, and in both CLL subsets alone. However, the response of U-CLL samples was significantly greater than that of M-CLL samples. The greater response of U-CLL is consistent with the stronger sIgM signal capacity of this cohort (Mockridge *et al.*, 2007), even though all samples were selected for study based on competence for sIgM signalling.

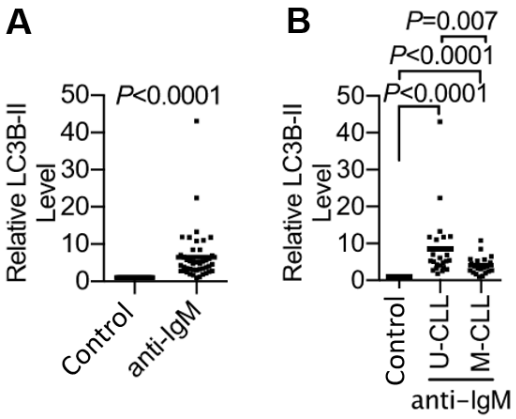

Figure 20. Effect of anti-IgM on LC3B expression in U and M-CLL.
CLL samples were treated with anti-IgM- or control antibody-coated beads for 24 hours and LC3B-II expression analysed by immunoblotting. (A) Total samples and (B) samples divided by IGHV mutational status are shown. The data shown is for a total of 45 samples and comprises results from the 8 samples shown in figure 19. Mean values are indicated. A Mann–Whitney test was used for statistical analysis

3.2.3 Analysis of p62 expression and ATG13 and P70S6K phosphorylation

I extended analysis of the response of CLL cells to sIgM or sIgD stimulation to additional markers at early (0.25 and 6 hours) and later (24 hours) times after sIg stimulation. This included expression of p62 and phosphorylation of ATG13. p62 is a selective autophagy cargo receptor that recognises ubiquitinylated proteins and targets these to forming canonical autophagosomes. Therefore, when canonical autophagy is activated p62 is typically degraded (Klionsky *et al.*, 2008). ATG13 is part of the canonical autophagy pathway initiation complex (Wallot-Hieke *et al.*, 2018) where it is critical in autophagosome complex assembly. ATG13 is phosphorylated at S318 by ULK1 in order to activate this complex. Therefore, ATG13 S318 phosphorylation is a readout of ULK activity (Petherick *et al.*, 2015a). I also analysed p70S6K phosphorylation as an additional signalling marker (with AKT and

ERK phosphorylation). P70S6K is activated downstream of mTORC1 via phosphorylation at T389 (Hornberger *et al.*, 2007). Analysis of this phosphorylation site provides a measure of mTORC1 activity which typically inhibits autophagy (Kim *et al.*, 2011).

Immunoblot analysis demonstrated significant increased expression of p62 (anti-IgM and anti-IgD) and increased phosphorylation of ATG13 (anti-IgM only) at 24 hours (**Figure 21,Figure 22**). Consistent with the results shown above (**Figure 20**), anti-IgM treatment did increase expression of LC3B-II expression at 6 and 24 hours, whereas responses to anti-IgD were more modest and did not reach statistical significance in this analysis.

Analysis of signalling responses demonstrated that similar to AKT and ERK, sIgM stimulation also significantly increased phosphorylation of P70S6K (**Figure 21,Figure 22**). This response was strongest in samples treated with anti-IgM at 6 hours and is therefore somewhat delayed compared to the AKT/ERK phosphorylation. This may reflect the position of P70S6K as a relatively distal marker of signalling, downstream of mTORC1. Increased phosphorylation of pP70S6K is consistent with the known signalling downstream of the BCR. However, co-occurrence of increased mTORC1 activity and increased autophagy is surprising as mTORC1 normally suppresses autophagy. As above, similar patterns of regulation were observed when results from my analysis were integrated into a larger sample cohort (L. D. Smith et al., 2020).

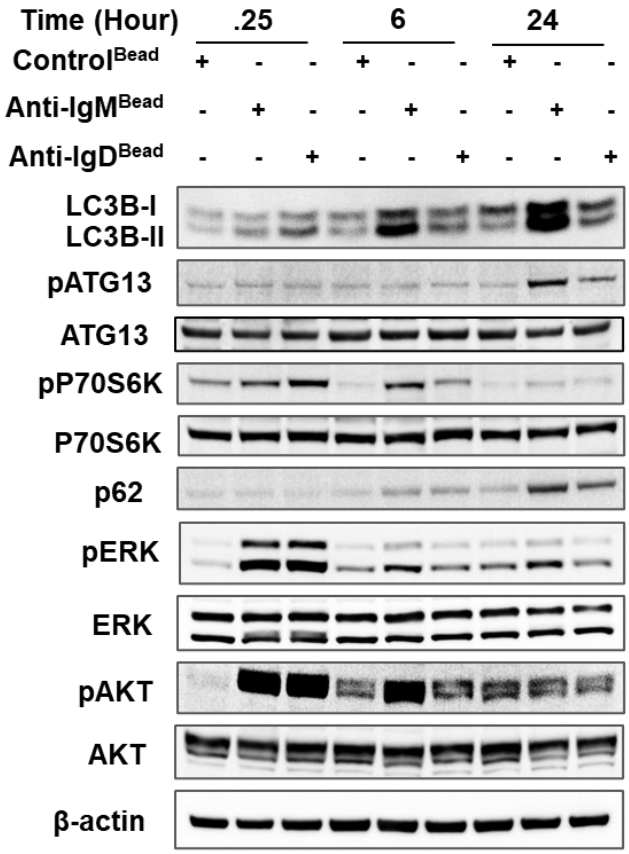

Figure 21. Effect of anti-IgM or anti-IgD on p62 expression and ATG13 and P70S6K phosphorylation in CLL cells – immunoblotting.
CLL samples (n=6) were incubated with anti-IgM-, anti-IgD- or control antibody-coated beads for 0.25-, 6- or 24-hours. Expression of LC3B, p62, ATG13, P70S6K, ERK, AKT and β-actin (loading control), and phosphorylation of P70S6K, ATG13, ERK and AKT, were analysed by immunoblotting. Representative blots are shown. Quantification for all samples is provided in **Figure 22**. Figure published in (Smith *et al.*, 2020).

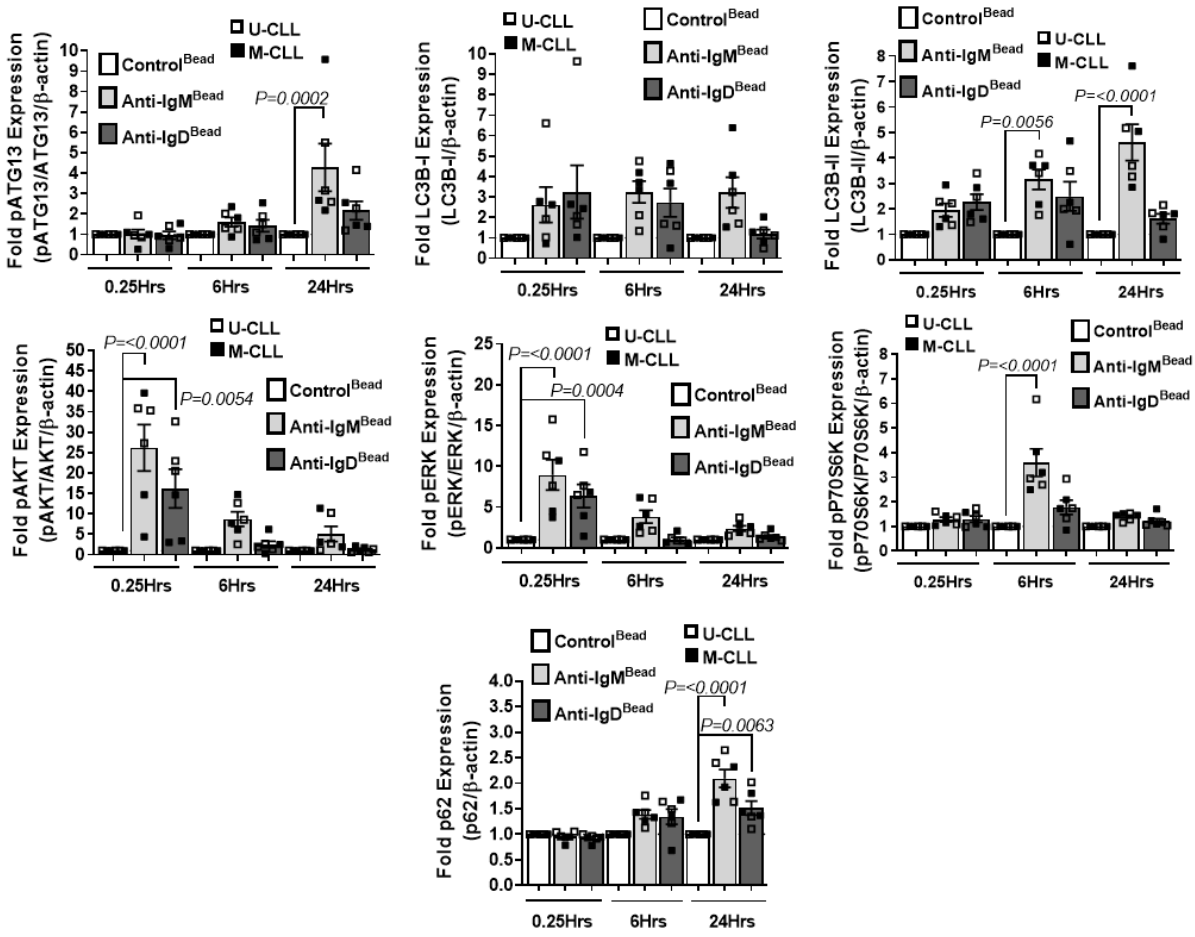

Figure 22. Effect of anti-IgM or anti-IgD on p62 expression and ATG13 and P70S6K phosphorylation in CLL cells – quantitation.
Quantitation of the experiments shown in **Figure 21** for all samples analysed (n=6). Graphs show results for individual samples and mean (±SD) with values for control antibody-coated beads set to 1.0 for each time point. The results of statistical comparison (Wilcoxon matched-pairs signed rank tests) comparing values for control and anti-IgM/anti-IgD-coated beads at each time point are indicated (where not shown, *P*>0.05).

Finally, I performed a preliminary experiment to analyse expression of PINK1 and Parkin, markers of mitophagy (Youle and Narendra, 2011; Wu *et al.*, 2015). Immunoblot analysis (Figure S1) demonstrated that these proteins were detectable in unstimulated CLL samples, but that expression was not increased by anti-IgM. Thus, whereas basal mitophagy may be a feature of CLL cells, it is not clearly linked to BCR signalling and was not studied in any further detail.

Overall, these results demonstrate that stimulation of the BCR of CLL cells using bead-bound antibodies increased autophagy. The response was characterised by increased expression of LC3B-I and -II isoforms, p62, ATG3 and GABARAPL2, and increased phosphorylation of ATG13. Increase in LC3B isoform expression appeared to precede changes in other markers and responses were generally stronger for anti-IgM compared to anti-IgD.

3.3 Effect of chemical modulators of autophagy on anti-IgM-induced on autophagy in CLL cells

3.3.1 Bafilomycin A1 and hydroxychloroquine

Having established that BCR stimulation induced autophagy in CLL cells, I next investigated the effects of various chemical compounds on this response. I first analysed the V-ATPase inhibitor bafilomycin A1 (Baf) and the lysosomotrophic compound hydroxychloroquine (HCQ), both of which have been shown to block autophagosome turnover by the lysosome in other cell types, resulting in an accumulation of autophagosomes (Yoshimori *et al.*, 1991; Mauthe *et al.*, 2018; Klionsky *et al.*, 2021). This can be used to indicate autophagic flux (or active autophagy) or enhance sensitivity of assays to detect autophagy. However, chloroquine and related compounds have also been characterised for their ability to induce non-canonical forms of autophagy that do not require the ULK-ATG13 initiation complex (Florey *et al.*, 2015; Jacquin *et al.*, 2017).

I first performed a pilot experiments to test effects of Baf and HCQ at various concentrations/lengths of time in a single sample **(Figure 23**). When CLL cells were treated for 2 hours with HCQ alone (at 100 μM), expression of LC3B-II was increased. LC3B-II was also increased by Baf (100nM) and HCQ (10 μM) in cells treated with anti-IgM for 24 hours (compared to anti-IgM alone at this time), indicating increased active autophagy. Other autophagy markers, including P62 and phospho-ATG13, were unaffected by baf (100 nM) or HCQ at 10 μM. However, when 100 μM HCQ is added for the last 2 hours of a 24 hour anti-IgM stimulation, there was a reduction in ATG13 phosphorylation and P62 expression. There is also an apparent reduction in LC3B-II, and these markers remain comparable whether anti-IgM was added for 24 hours, and then 100 μM HCQ added for 2 hours, or no anti-IgM stimulation was present and the 100 μM HCQ added in the last 2 hours of culture for cells alone. This shows that HCQ alone at 100 μM induces autophagy, possibly by a non-canonical pathway. However, at 10 μM, HCQ does not induce autophagy, but does promote accumulation of autophagosomes. Neither Baf (100 nM) or HCQ (10 μM) appeared to have a substantial effect on induction of AKT or ERK phosphorylation following anti-IgM stimulation (**Figure 23**).

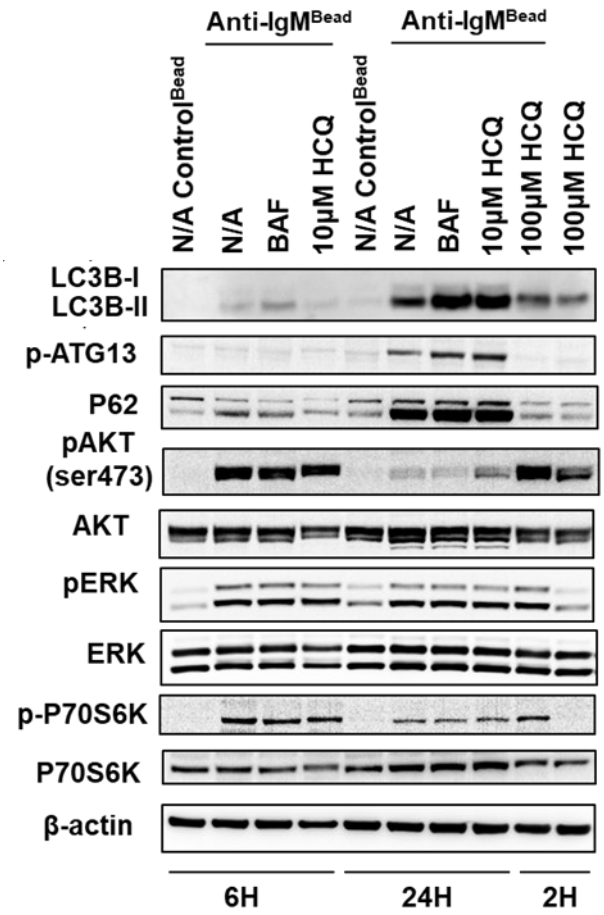

Figure 23. Effect of HCQ or BafA1 on autophagy marker expression and signalling in CLL cells.
A CLL sample was incubated with anti-IgM- or control antibody-coated beads for 6- or 24-hours, in the presence of HCQ (10 or 100 µM) or baf (100 nM) or with no addition (N/A) (lanes 1-8). Lanes 9 and 10 shows cells incubated with anti-IgM or no addition for 22 hours and then exposed to HCQ (100 µM) for 2 hours, respectively. Expression of LC3B-II, p62, AKT, ERK, P70S6K and β-actin (loading control), and phosphorylation of ATG13(S318), AKT and ERK were analysed by immunoblotting.

In longer term experiments (performed at 24 hours), lower concentrations of HCQ (5-10 µM) increased basal LC3B-II expression (ie, in cells treated with control antibody-coated beads) and strongly increased LC3B-II accumulation in cells stimulated via s-IgM (**Figure 24**), indicating active autophagy was occuring. Similar results were obtained with BafA1 which increased LC3B-II expression when tested alone at 100 nM for 2 hours, or at lower concentrations (≥50 nM) for 24 hours (revealing CLL cells basal capacity for autophagy), and increased LC3B-II expression in cells treated with anti-IgM. By comparing the NA (0) for each BafA1 and HCQ immunoblots and representative graphs below (**Figure 24**) with the HCQ and BafA1 treated conditions, clear increases in LC3B-II are observed, showing active autophagy is occurring both at a basal level in CLL cells (control) or when induced by anti-IgM. Baf (100 nM) or HCQ (10 µM) were included in some of the following experiments in this thesis to more clearly reveal active autophagy, particularly when basal lysosomal degradation, indicating active autophagy, is higher than the rate of LC3B-II synthesis or where differences are subtle and more easily observed when lysosomal fusion is inhibited.

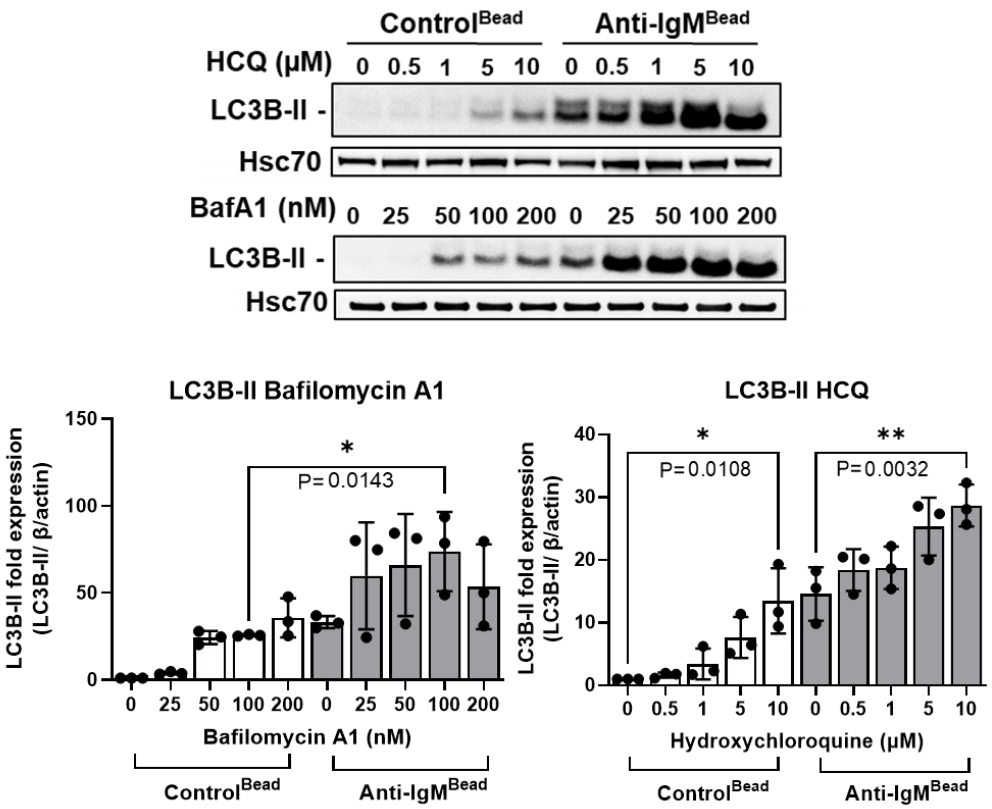

Figure 24. Effect of HCQ or BafA1 LC3B expression in CLL cells.

CLL samples (n=3) were pre-treated with the indicated concentrations of Baf or HCQ for 1 hour and then treated with anti-IgM- (anti-IgM^{bead}) or control antibody-coated beads (Control^{bead}) for 24 hours. Expression of LC3B and HSC70 (loading control) was analysed by immunoblotting. Figure shows (top) representative immunoblots and (bottom) quantitative summaries for all samples. Graphs show results for individual samples and mean (±SD) with values for control antibody-coated beads/no addition cells set to 1.0. The results of statistical comparison (Tukey's multiple comparisons test) comparing values for 100nM bafilomycin with and without anti-IgM stimulation (P=0.00143), and for hydroxychloroquine comparing values within control and anti-IgM stimulated are indicated (where not shown, *P*>0.05). The comparison between 10μM HCQ control bead treated and 10μM HCQ treated with anti-IgM bead had a P value of 0.0015(not shown on graph).

3.3.2 Vps34 inhibitor SAR405

Vps34 is a class-III PI3K, which, in complex with Beclin, ATG14L and Vps15, forms part of the initiation complex (Rostislavleva *et al.*, 2015). This initiation complex is involved in formation and elongation of the autophagosome resulting in insertion of lipidated LC3B-II into the autophagosome membrane. I used SAR405, a highly potent and selective inhibitor of Vps34 (Pasquier, 2015), to investigate the role of Vps34 in both basal (ie, in control antibody treated cells) and anti-IgM-induced autophagy in CLL cells (**Figure 25**).

In anti-IgM-treated cells, SAR405 induced a dose-dependent reduction in expression of LC3B-II, but not LC3B-I. These effects were seen at concentrations ≥1 μM. Therefore, Vps34 is required in CLL cells to mediate LC3B-II lipidation following sIgM stimulation as SAR405 results in accumulation of LC3B-I, the non-autophagosome-associated form (**Figure 25**). The effects of SAR405 in unstimulated CLL cells were somewhat distinct as SAR405 appeared to increase expression of LC3B-I, without reducing LC3B-II expression. This suggests that basal autophagy in CLL cells is also dependent on Vps34. The difference in effects between control antibody and anti-IgM treated cells may reflect that differing levels of autophagy under these conditions (ie, high following anti-IgM, low in control cells).

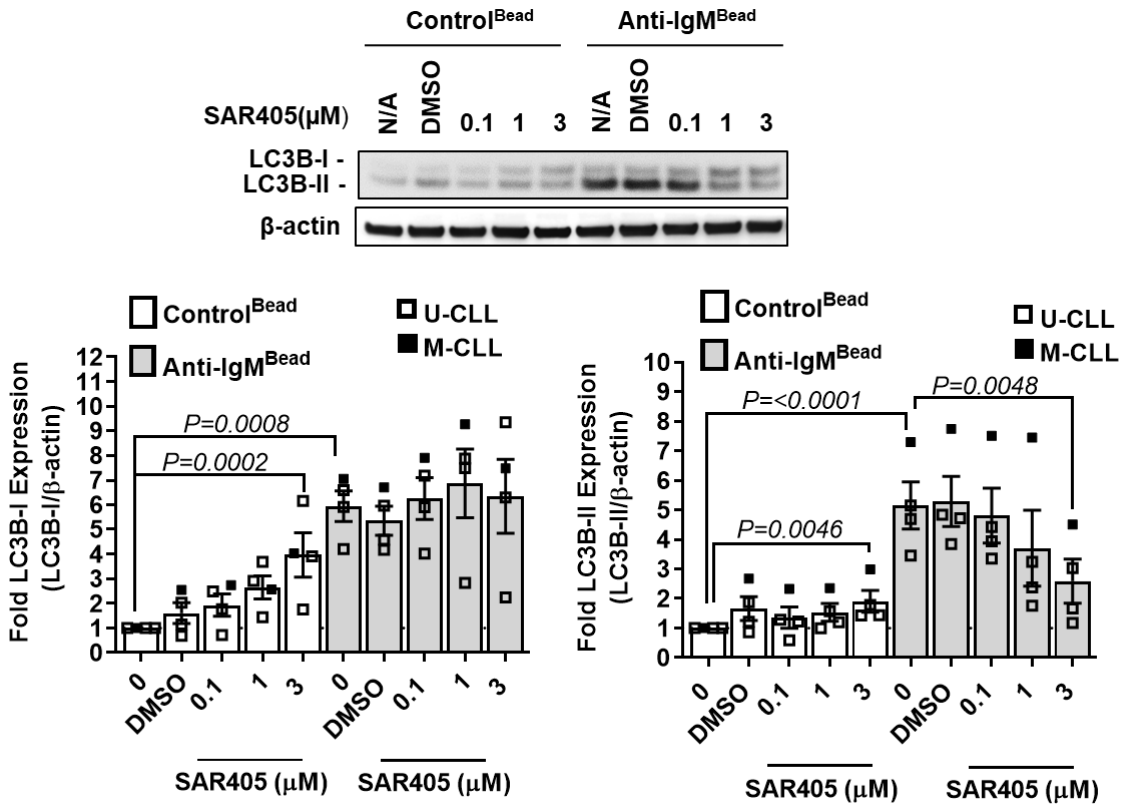

Figure 25. Effect of Vps34 inhibitor SAR405 on LC3B expression in CLL cells.
CLL samples (n=4) were pre-treated with SAR405 at the indicated concentration or DMSO, or left untreated (N/A) for 1 hour prior to treatment with anti-IgM- or control antibody-coated beads for 24 hours. HCQ (10 μM) was included throughout the incubation period. Expression of LC3B and β-actin was analysed by immunoblotting. Representative immunoblots and summary of results for all samples. Graphs show results for individual samples and mean (±SD) with values for control antibody-coated beads/no addition cells set to 1.0. The results of statistical comparison (Bonferroni's multiple comparisons test) comparing values for LC3B-I and –II, N/A and 3 μM control or anti-IgM beads, or for LC3B-II a comparison between control N/A and anti-IgM/NA is also indicated (where not shown, P>0.05).

3.3.3 ULK inhibitors SBI-0206965 and MRT68921

I next used an inhibitor of ULK1 (SBI-0206965)(Egan *et al.*, 2015) or ULK1/2 (MRT68921)(Petherick *et al.*, 2015a) to investigate the role of ULK isoforms in autophagy in CLL cells. Experiments were performed in the presence or absence of BafA1.

SBI-0206965 was used over a concentration range (0.1 - 30 μM) and LC3B-I/II expression was analysed at 24 hours following sIgM stimulation. SBI-0206965 reduced induction of LC3B-I/II expression following sIgM stimulation at concentrations ≥10 μM in the absence of BafA1 (**Figure 26**). However, SBI-0206965 had no clear effect in the presence of BafA1 (**Figure 27**), where overall levels of LC3B were higher. Moreover, it should be noted that significant changes were only observed for cells treated with 30 μM SBI-0206965, a concentration which is substantially higher

that that previously shown to inhibit phosphorylation of S249 on Vps34 (ULK phosphorylation site) in cells (5 µM) (Egan *et al.*, 2015). Thus, the rather modest effects of SBI-0206965 on LC3B expression may be due to off-target effects which would need to be probed in further experiments. Overall, inhibition of ULK1 using the compound SBI0206965 does not appear to be sufficient to inhibit basal or anti-IgM-induced autophagy in CLL cells.

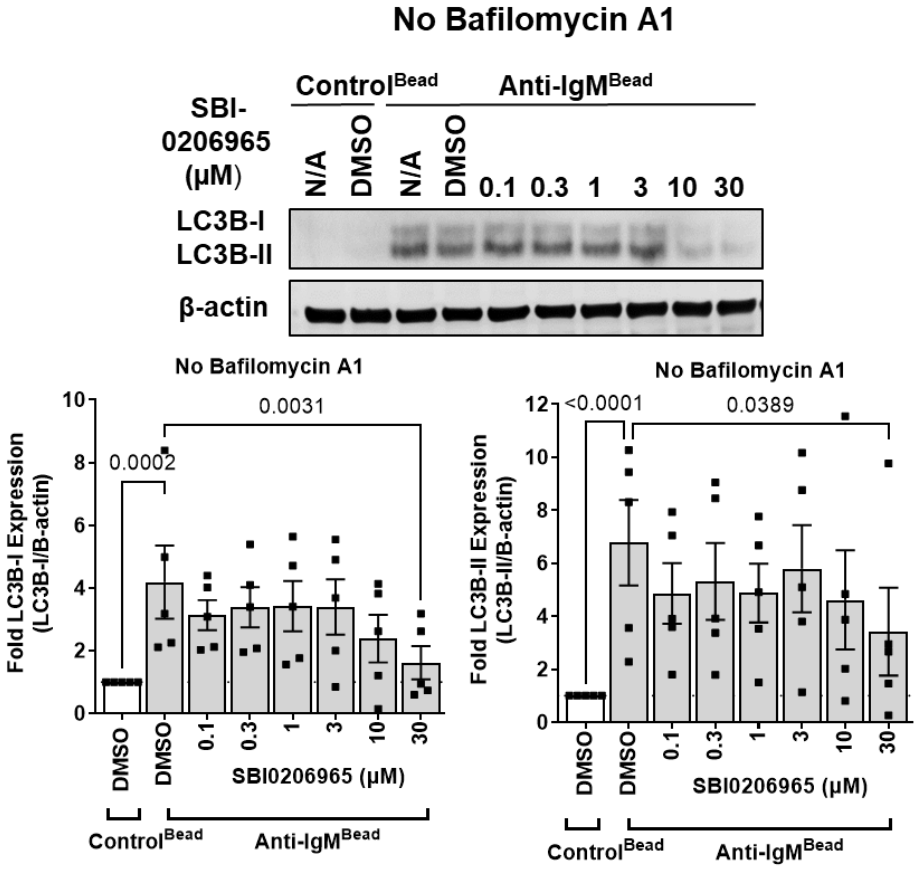

Figure 26. Effect of the ULK1 inhibitor SBI-0206965 on anti-IgM-induced LC3B expression.
CLL samples (n=5) were pre-treated with SBI-0206965 at the indicated concentrations or DMSO, or left untreated (N/A) for 1 hour prior to treatment with anti-IgM- or control antibody-coated beads for 24 hours. Expression of LC3B and β-actin was analysed by immunoblotting. Representative immunoblots and summary of results for all samples. Graphs show results for individual samples and mean (±SD) with values for control antibody-coated beads/DMSO-treated cells set to 1.0. The results of statistical comparison (two-way ANOVA) comparing values to anti-IgM-coated beads/DMSO-treated cells are indicated (where not shown, P>0.05).

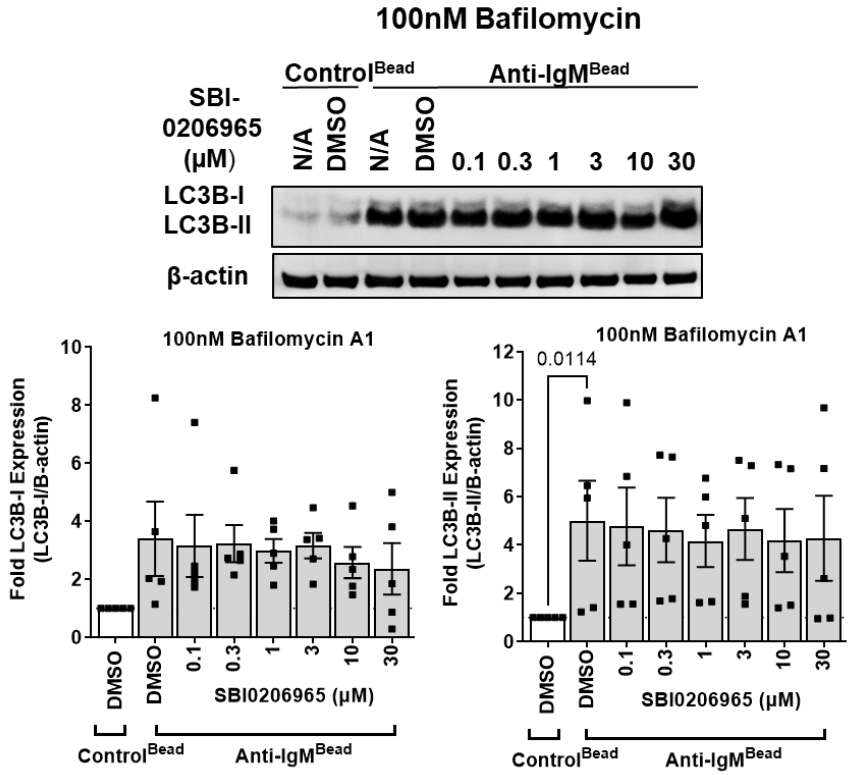

Figure 27. Effect of the ULK1 inhibitor SBI-0206965 on anti-IgM-induced LC3B expression in the presence of Baf

CLL samples (n=5) were pre-treated with SBI-0206965 at the indicated concentrations or DMSO, or left untreated (N/A) for 1 hour prior to treatment with anti-IgM- or control antibody-coated beads for 24 hours. Baf (100 nM) was included in all incubations. Expression of LC3B and β-actin was analysed by immunoblotting. Representative immunoblots and summary of results for all samples. Graphs show results for individual samples and mean (±SD) with values for control antibody-coated beads/DMSO-treated cells set to 1.0. The results of statistical comparison (two-way ANOVA) comparing values to anti-IgM-coated beads/DMSO-treated cells are indicated (where not shown, P>0.05).

Similar experiments were performed to investigate the effects of the dual ULK1/2 inhibitor MRT68921. Initial experiments showed a reduction in loading control in treatment of CLL cells with MRT68921, at concentrations ≥3 μM. Therefore, I examined PARP cleavage by immunoblotting as a marker of apoptosis induction. Concentrations of MRT68921 ≥3 μM induced PARP cleavage and reduced the levels of β-actin, analysed as a loading control (**Figure 28**). Therefore, more detailed experiments were performed in the presence of the caspase inhibitor Q-VD-Oph to minimise MRT68921-induced apoptosis (**Figure 29**). These experiments were also performed in the presence of HCQ (10 uM) for the last hour of incubation to more fully reveal the extent of active autophagy occurring after 23 hours of anti-IgM treatment in the presence of MRT68921.

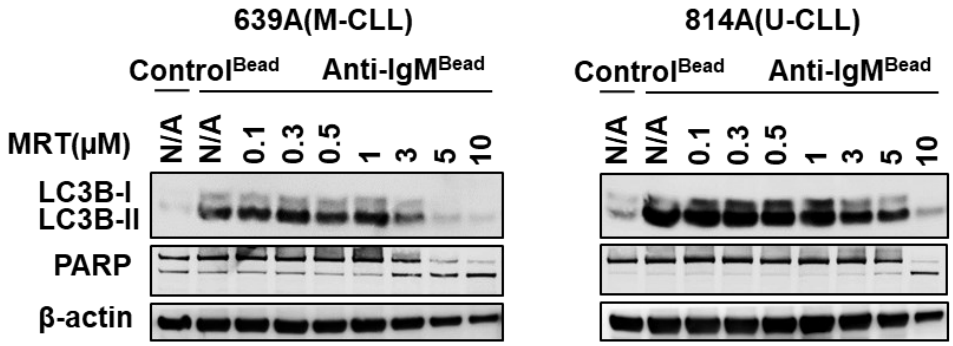

Figure 28. Effect of MRT68921 on PARP cleavage in CLL cells
CLL samples (n=2) were pre-incubated with MRT68921 at the indicated concentrations (or left untreated as a control, N/A) for 1 hour and then incubated with anti-IgM- or control antibody-coated beads for 24 hours. HCQ (10 μM) was added for the final hour of all incubations. Expression of PARP and β-actin was analysed by immunoblotting.

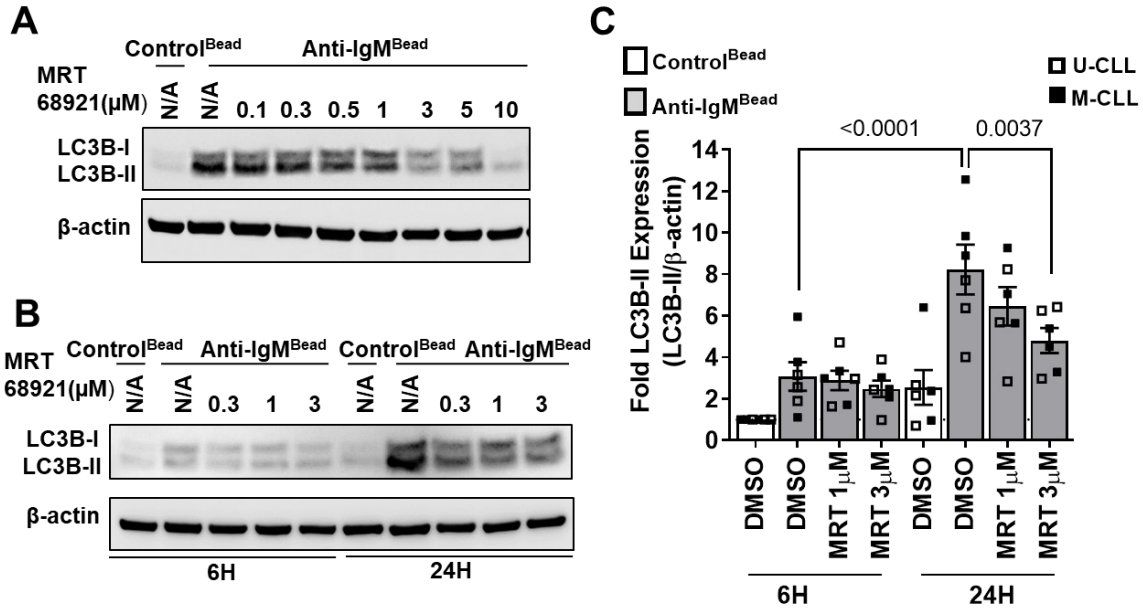

Figure 29.The effect of MRT68921 on anti-IgM induced autophagy.
CLL samples (n=6) were pre-treated with MRT68921 at the indicated concentrations or left untreated (N/A) for 1 hour prior to treatment with anti-IgM- or control antibody-coated beads for 6 or 24 hours. Q-VD-Oph (10 μM) was included throughout, and HCQ (10 μM) for the final hour of all incubations. Expression of LC3B and β-actin was analysed by immunoblotting. A+B show Representative immunoblots and (C) summary of results for all samples. Graphs show results for individual samples and mean (±SD) with values for control antibody-coated beads/DMSO-treated cells at 6 hours set to 1.0. The results of statistical comparison (two-way ANOVA) comparing values to anti-IgM-coated beads/DMSO-treated cells at 24 hours are indicated (where not shown, P>0.05).

In contrast to SBI-0206965, MRT68921 did significantly inhibit LC3B-II expression at 24 hours (**Figure 29**). Effects were observed at concentrations from 1 μM and were significant at 3 μM. This concentration is similar to that shown to block starvation-mediated autophagy of MEFs (1 μM) (Petherick *et al.*, 2015b). Thus, dual inhibition of ULK1 and 2 may be required in CLL to fully inhibit ULK mediated autophagy.

3.4 Effect of BCR-associated kinase inhibitors on anti-IgM-induced on autophagy in CLL cells

Similar experiments were performed to investigate the effects of inhibitors of kinases involved in BCR signal transduction on anti-IgM-induced autophagy. The inhibitors selected were entospletinib (SYK inhibitor), ibrutinib (BTK inhibitor), cerdulatinib (dual SYK/JAK inhibitor) and idelalisib (PI3Kδ inhibitor). The concentrations used were selected based on the literature (Currie *et al.*, 2014; de Rooij *et al.*, 2015). Entospletinib, ibrutinib and cerdulatinib significantly reduced anti-IgM-induced LC3B-II expression at 24 hours (**Figure 30,Figure 31**). Entospletinib was the most effective inhibitor, showing complete reversal of anti-IgM-induced LC3B-II expression. Cerdulatinib was also relatively effective. These compounds share the ability to inhibit SYK (cerdulatinib also inhibits JAKs), so the effect of cerdulatinib appears to be driven by its SYK-inhibiting activity. Ibrutinib partially reduced LC3B-II induction (by ~40%) indicating that BTK is not an essential component of the sIgM mediated LC3B signal pathway. In contrast to the other inhibitors, LC3B-II expression was only very modestly reduced by idelalisib and the effect of this drug was not significant. However, idelalisib was analysed in the smallest number of samples, so it is possible that analysis of additional samples could demonstrate a modest, but statistically significant difference- as for ibrutinib.

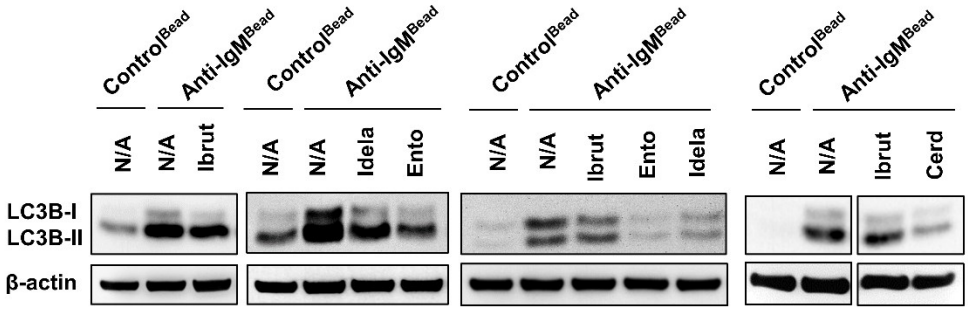

Figure 30. Effect of kinase inhibitors on anti-IgM-induced LC3B-II expression – immunoblotting. CLL samples were pre-treated with the indicated inhibitors (Ibrutinib 500nM , Idelalisib 1µM, Entospletinib 1 µM, Cerdulatinib 1 µM), or with no addition (N/A) as a control for 1 hour, and then incubated with anti-IgM- or control antibody-coated beads for 24 hours. Expression of LC3B-II and β-actin (loading control) was analysed by immunoblotting. Representative blots are shown. Quantification for all samples (8 for entospletinib (Ento), 13 for ibrutinib (Ibrut), 16 for cerdulatinib (Cerd) and 4 for idelalisib (Idela)) is provided in **Figure 31**.

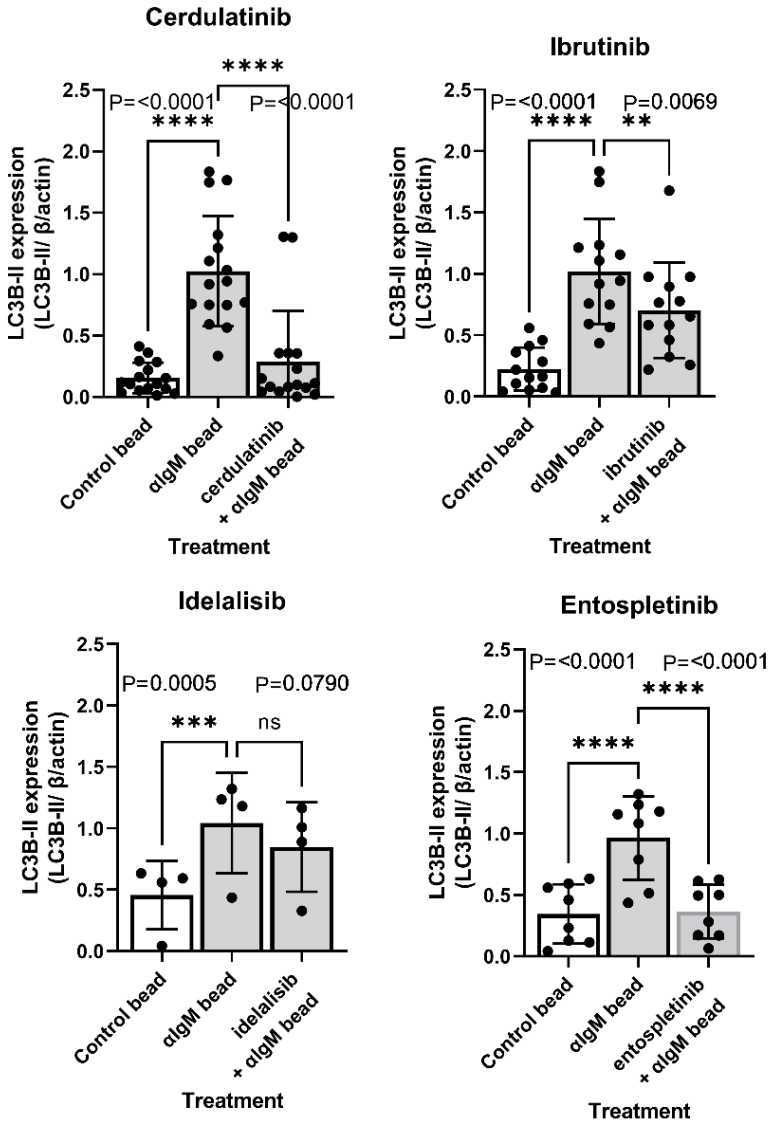

Figure 31. Effect of kinase inhibitors on anti-IgM-induced LC3B-II expression – quantitation. Quantitative analysis of experiment shown in **Figure 30**. Graphs show individual values and mean (±SD) LC3B-II expression with mean values for anti-IgM-coated beads only treated cells set to 1.0. The statistical significance of the differences is shown (Tukey's multiple comparisons test).

3.5 Comparison of anti-IgM- and starvation-induced autophagy in CLL cells

My results demonstrated that anti-IgM (and anti-IgD) induce autophagy in CLL cells, and that increased LC3B expression is dependent on the activity of Vps34 and ULK isoforms, as well as signalling through SYK. The next series of experiments was performed to compare the responses to anti-IgM with starvation, a classical inducer of autophagy (Kim *et al.*, 2011; Puente, Hendrickson and Jiang, 2016). Starvation was induced by incubating cells in EBSS medium which lacks glucose and amino-acids and responses were analysed in a time course up to 360 minutes.

Starvation of CLL cells resulted in a very clear accumulation of LC3B-II which was first detected within ~10 minutes and increased to a peak at ~4 hours (**Figure 32**). There was a rapid increase in P70S6K phosphorylation at T389, the mTORC1 phosphorylation site, indicating an initial surge in mTOR activity, a nutrient sensing autophagy inhibitor (Datan *et al.*, 2014), which rapidly declined. Over activation of P70S6K has also been proposed to reverse inhibition of autophagy (Klionsky, Meijer and Codogno, 2005). While phosphorylation was initiated rapidly, it then declined after 60 minutes, concurrent with the peak of LC3B-II induction. In contrast to P70S6K phosphorylation, p62 expression declined rapidly following transfer to EBSS medium, but then increased (again, concurrently with the peak response of LC3B-II expression). Finally, ATG13 phosphorylation declined steadily throughout the time course. Thus, induction of autophagy in response to starvation is more rapid than that induced by anti-IgM. Similar to anti-IgM, accumulation of LC3B-II expression is accompanied by increased p62 expression, but not ATG13 phosphorylation for the starvation conditions, which in itself is in conflict with traditional starvation-mediated pathways. In contrast to anti-IgM stimulation were there was a surprising increase in P70S6K phosphorylation despite induction of autophagy, starvation-induced autophagy was associated with reduced P70S6K phosphorylation. Thus, the apparently counterintuitive induction of P70S6K phosphorylation following anti-IgM stimulation is a specific feature of the response to anti-IgM and not a general feature of autophagy in CLL cells *per se*. Analysis of three further samples confirmed that the increase in LC3B-II expression following starvation was relatively rapid (detected at 30 minutes) compared to response to anti-IgM (**Figure 32**).

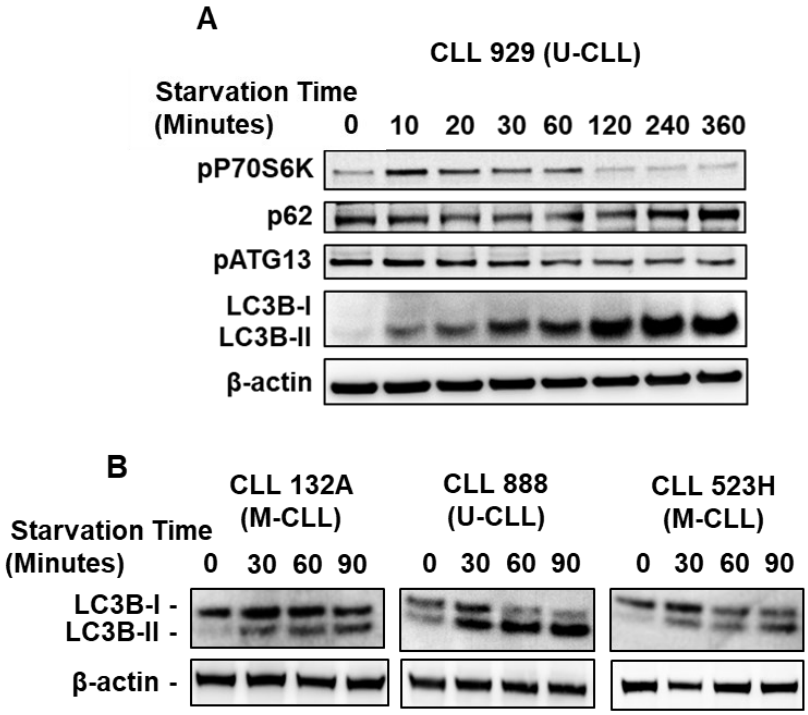

Figure 32. Effect of starvation on autophagy in CLL cells.
CLL samples were starved and expression of p62, LC3B and β-actin, and phosphorylation of P70S6K and pATG13, analysed by immunoblotting at the indicated times. Starvation protocols were as described in methods. (A) shows a starvation time course, used to examine kinetics of autophagy induction. (B) shows analysis of 3 more patients at selected time points.

I subsequently investigated the effects of autophagy inhibitors on the response to starvation. CLL cells are very sensitive to starvation-induced apoptosis, so to mitigate the potential apoptotic effect of starvation in cells treated with inhibitors, the experiment was performed in the presence of a caspase inhibitor. Analysis was performed at 30 minutes, as starvation mediated autophagy is a rapid event (**Figure 33**). The increase in LC3B-II expression in serum starved cells was significantly inhibited by the Vps34 inhibitor SAR405 and the ULK1/2 inhibitor MRT68921, but not by the ULK1 inhibitor SBI-0206965 (**Figure 33**). Thus, the ability of these inhibitors to suppress induction of LC3B-II expression is similar for both anti-IgM- and starvation-induced responses.

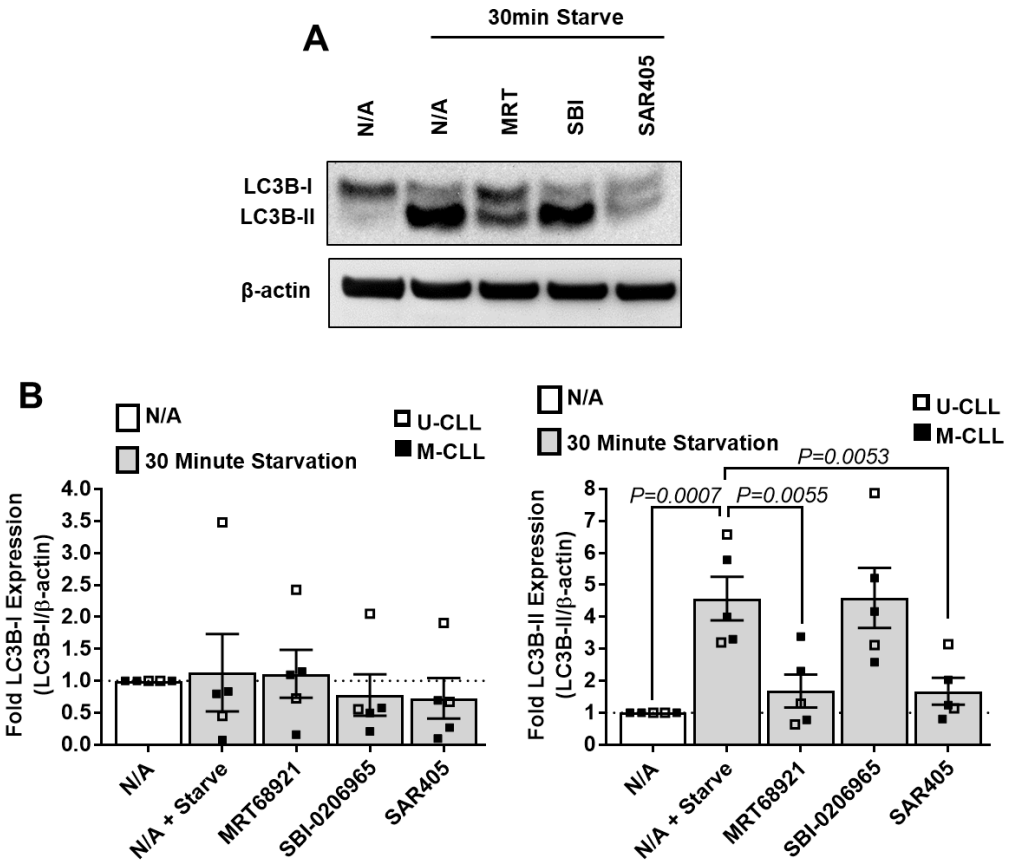

Figure 33. Effect of autophagy inhibitors on LC3B expression following starvation on CLL cells
CLL samples (n=5) were pre-incubated with SBI-0206965 (SBI), MRT68921 (MRT) or SAR405 (all at 1 μM), or left untreated (N/A) for 1 hour prior to starvation for 30 minutes. All incubations were performed in the presence of 10 μM Q-VD-Oph and 10 μM HCQ. Expression of LC3-B and β-actin was analysed by immunoblotting. (A) Representative immunoblots and (B) summary of data. Graphs show individual values and mean (±SD) LC3B-II expression with mean values for unstarved cells set to 1.0. The statistical significance of the differences to starved cells without any inhibitor is shown (two way ANOVA; where not shown P>0.05).

3.6 Analysis of CLL cell autophagy using confocal microscopy

My immunoblotting results clearly indicate that BCR stimulation increases autophagy in CLL cells (section 3.2). However, rather than simply relying on analysis of expression of LC3B (and other autophagy markers), it was important to analyse both the formation and, importantly, the localisation of autophagosomes and their proximity to lysosomes. Co-localisation of autophagosomes with lysosomes in microscopy shows active autophagy processes occurring. Formation of autophagosomes was therefore analysed using confocal microscopy and co-staining cells for LC3B and the lysosomal marker LAMP1, as co-localisation of LC3B and LAMP1 reveals autophagosomal and lysosomal association, a hallmark for active autophagy (Klionsky *et al.*, 2021). DAPI was used to stain nuclei. The experiment was performed using CLL cells that had been starved (as in section 3.5) or treated with anti-IgM-coated beads for 24 hours, with or without addition of HCQ for the final hour of this period (**Figure 35**).

Analysis of starved CLL cells demonstrated an increase in LC3B fluorescence (consistent with increased expression shown by immunoblotting, and also clear LC3B/LAMP1 co-localisation indicating autophagosome-lysosome fusion (**Figure 34**, **Figure 35**). Both the expression of LC3B and LC3B/LAMP1 co-localisation were increased in the presence of HCQ, as expected. Similar results were obtained for cells treated with anti-IgM- (but not control antibody-) coated beads, where there was a clear increase in LC3B/LAMP1 co-localisation, especially in the presence of HCQ (**Figure 35**). These results confirm that, like serum starvation, sIgM stimulation induces autophagy in CLL cells.

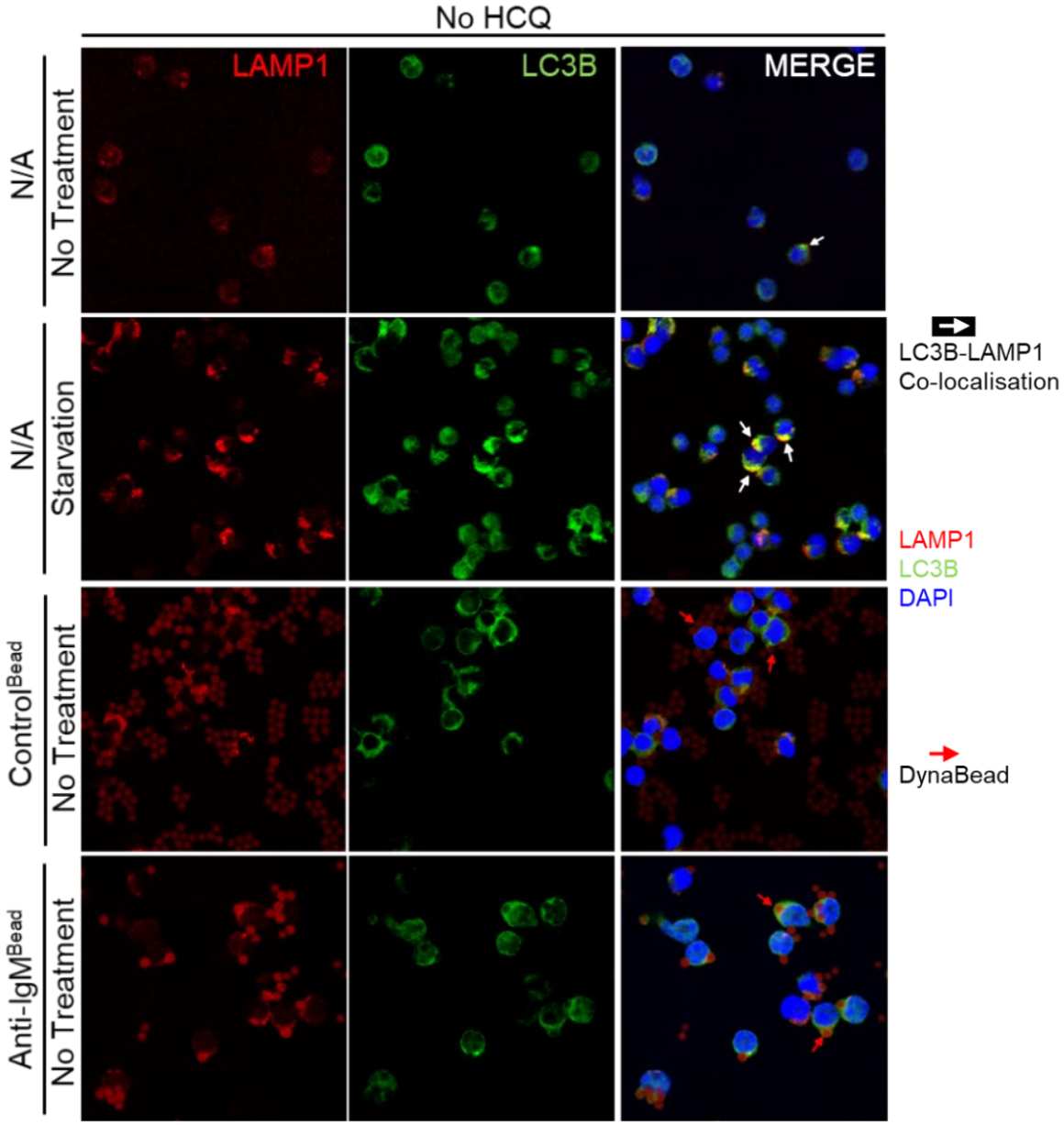

Figure 34. LAMP1/LC3B localisation in CLL cells following starvation or sIgM stimulation - No HCQ

CLL samples were treated with anti-IgM- or control antibody-coated beads, or incubated in standard or starvation culture conditions for 24 hours in the absence of HCQ. Cells were fixed and stained for LAMP1 (red), LC3B (green) and nuclei (blue) and analysed by confocal microscopy. Images show LAMP1 and LC3B staining alone and merged images with all three colours. LAMP1/LC3B co-localisation is shown in merged images as yellow. Results show representative fields from a single sample. White arrows show co-localisation of LAMP/LC3B, red arrows show Dynabeads.

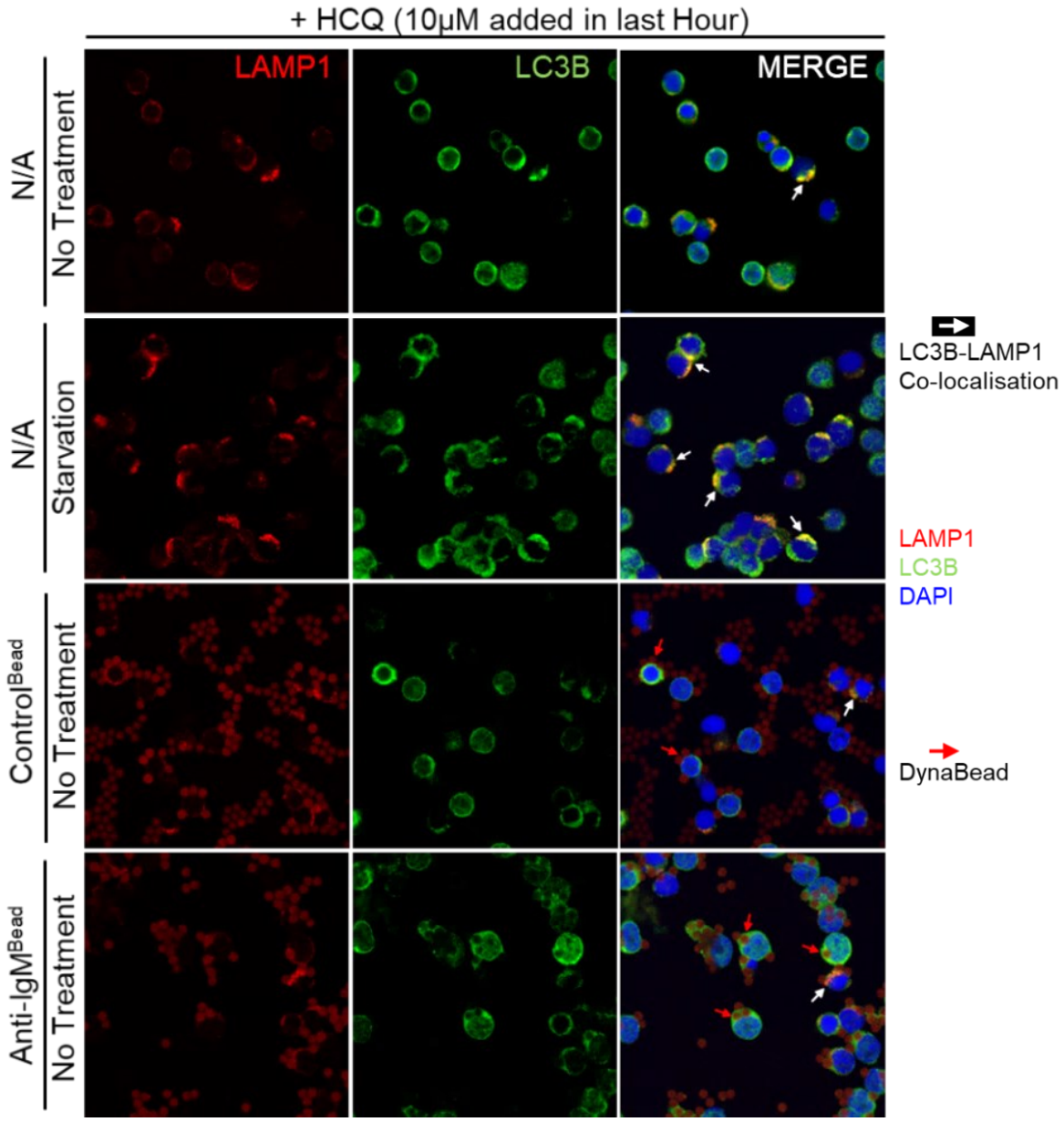

Figure 35. LAMP1/LC3B localisation in CLL cells following starvation or sIgM stimulation + HCQ

CLL samples were treated with anti-IgM- or control antibody-coated beads, or incubated in standard or starvation culture conditions for 24 hours in the presence of HCQ (10 µM) for the last hour of this incubation. Cells were fixed and stained for LAMP1 (red), LC3B (green) and nuclei (blue) and analysed by confocal microscopy. Images show LAMP1 and LC3B staining alone and merged images with all three colours. LAMP1/LC3B co-localisation is shown in merged images as yellow. Results show representative fields from a single sample. White arrows show co-localisation of LAMP/LC3B, red arrows show Dynabeads.

One unexpected finding from this analysis was that CLL cells appeared to be capable of internalising anti-IgM-coated beads. The Dynabeads auto-fluoresced strongly so it was straightforward to observe both control and anti-IgM-coated beads which appeared as red, spherical objects in the LAMP1 channel images. Although the majority of anti-IgM- and control antibody-coated beads were not associated with CLL cells, there was a small number of anti-IgM-coated beads (but not control beads) that appeared to have been endocytosed by CLL cells, indicated by red arrows in **Figure 35**, and shown at higher magnification in **Figure 36**. Interestingly, LC3B expression, and to a less easily visualised extent, LC3B-LAMP1 co-localisation, appeared to be stronger in cells containing anti-IgM-coated beads, suggesting that internalisation and induction of autophagy were linked (**Figure 35** and **Figure 36**). However, the DynaBead auto-fluorescence in the LAMP1 imaging channel made it more challenging to analyse LAMP1 staining. Overall, this study reveals the surprising finding that CLL cells can internalise anti-IgM-coated beads. This was dependent on sIgM engagement, as it was not observed for control beads.

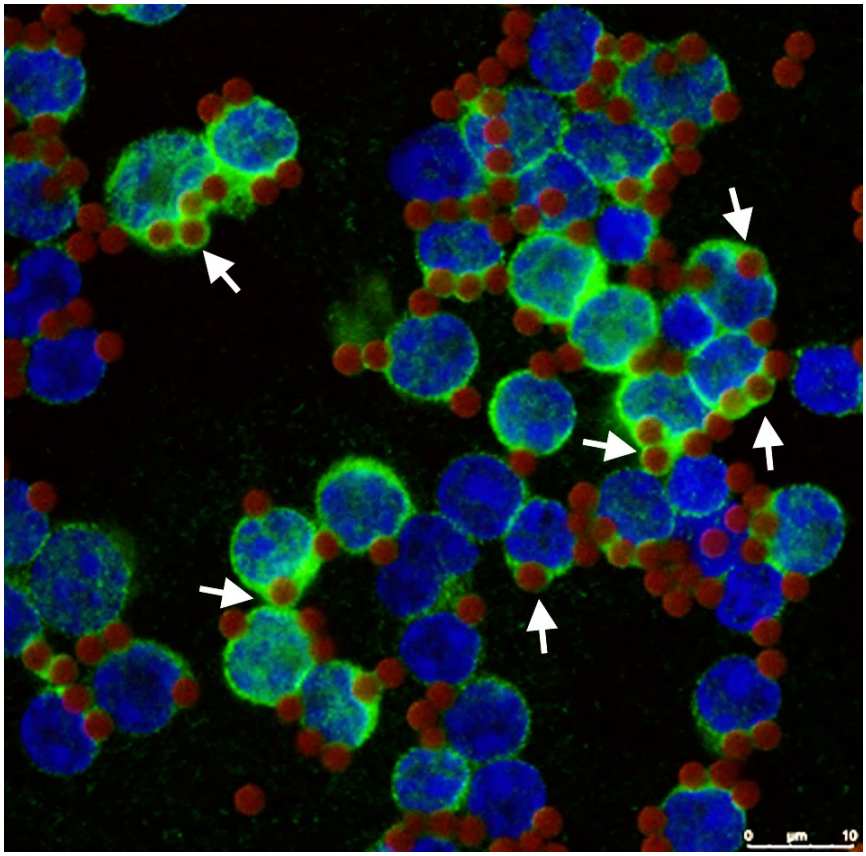

Figure 36. LC3B expression in CLL cells following incubation with anti-IgM coated Dynabeads.
CLL samples were treated with anti-IgM-coated bead for 24 hours (with HCQ (10 µM) added for the last hour of this incubation). Cells were fixed and stained for LC3B (green) and nuclei (blue) and analysed by confocal microscopy. Image shows a high magnification of merged images with all three colour channels for LC3B, DAPI and DynaBeads. Results show a representative field from two samples analysed. White arrows show apparent bead internalisation with LC3B in the cytoplasm surrounding the beads in some cases.

3.6 Summary of Results : Autophagy in CLL

- CLL cells increase autophagy marker expression following anti-IgM or anti-IgD stimulation
- Anti-IgM response induced the greatest increase in autophagy marker expression at 24 hours
- This autophagy is dependent on BCR kinases, particularly SYK, as well as VPS34 and ULK1/2
- While characterising autophagy by microscopy, internalisation of anti-IgM (but not control antibody) coated beads was observed

3.7 Discussion

The overall goal of the experiments described in this chapter was to characterise BCR driven autophagy. The results demonstrate that autophagy is induced in CLL cells following activation of the BCR. While BCR signalling occurs at early time points (along with P70S6K phosphorylation), the level of autophagy proteins, such as phospho-ATG13, LC3B-II and p62, are most robustly upregulated at later time points. Increased phosphorylation of ATG13 at S318 indicates that ULK1 is activated at 24 hours following BCR engagement, corresponding to the larger increase in LC3B-II at this time. This is consistent with activation of a canonical autophagosome biogenesis pathway. Stimulation with anti-IgM resulted in a more consistent and elevated autophagy signature at 24 hours compared to anti-IgD, consistent with previously characterised differences in signal transduction following anti-IgM or anti-IgD stimulation. Autophagy could be inhibited with MRT68921, a dual ULK1/2 inhibitor, but not SBI0206962, a ULK1 inhibitor, indicating a potential dual role of ULK1/2 in BCR driven autophagy. SAR405 and VPS34-IN1 both reduced LC3B-II expression and resulted in a slight accumulation of LC3B-I, indicating a blockage of insertion of LC3B-II into the forming autophagosome consistent with VPS34 inhibition. Therefore, BCR driven autophagy is also dependent on VPS34. Moreover, anti-IgM-induced autophagy was inhibited by SYK inhibitors, showing a requirement of downstream signalling for autophagy induction. BTK and Class I PI3Kδ inhibition also reduced LC3B-II expression, to a lower extent. A surprising result from confocal microscopy analysis was that CLL cells were capable of internalising anti-IgM coated Dynabeads, and this will be explored further in subsequent chapters.

3.7.1 BCR stimulation increases autophagy marker expression in CLL, and this is a signal dependant response

Following initial experiments to examine the kinetics of BCR-driven autophagy, experiments were performed utilising control antibody-, and anti-IgM- or anti-IgD-coated beads. The aim of these experiments was to further probe the signalling and autophagy pathways and the kinetics of these events. I demonstrated than anti-IgM and anti-IgD beads, but not the control beads, stimulated BCR signalling (ie, phosphorylation of signalling proteins, pAKT, pERK and pP70S6K). This signalling occurred between 15 minutes and, up to, ~4-6 hours post-stimulation. Once this response started to decline, autophagy marker expression gradually increased and peaked at 24, revealed most clearly by expression of LC3B-II and p62, and phosphorylation of ATG13 at a ULK phosphorylation site.

Interestingly, anti-IgM stimulation induced the strongest autophagy marker expression increases at 24 hours, compared to autophagy induction by anti-IgD coated beads. This is likely linked to the kinetics and strength of signalling through anti-IgM compared to anti-IgD forms of the BCR, as defined in other work. While only a proportion of healthy circulating peripheral B cells co express IgM and IgD, the majority of CLL cells express sIgM and IgD, although at lower levels than healthy B cells (Dighiero *et al.*, 1980). sIgM and sIgD isotypes have been shown to have similar binding specificities for antigen (Tisch, Roifman and Hozumi, 1988), although antigens with lower binding site numbers have been shown to activate IgM receptors but fail to trigger IgD signalling, whereas high binding antigens may elicit activation of both receptor types (Ubelhart *et al.*, 2015). In CLL, signalling through surface IgM results in a prolonged signal that supports downstream survival and chemokine responses, while signalling through IgD results in more rapid receptor internalisation and failure to induce these responses to the same extent (Ten Hacken *et al.*, 2016). These differences could explain the differences in signal transduction and strength of downstream autophagy responses in this work. While stimulation with anti-IgD appears to result in a comparable, or in some cases stronger response in terms of autophagy and signalling marker expression at time points including 15 minutes, 2 hours, and 4 hours, by 24 hours this response has greatly diminished, whereas for autophagy marker expression anti-IgM stimulation results in an apparently slower transduction of signal, but a greater autophagy response at 24 hours

While the results comparing anti-IgM/anti-IgD stimulation to control beads highlight a BCR driven mechanism, the BCR signalling dependence for autophagy induction was confirmed through use of BCR kinase inhibitors. These results show a greater dependence on SYK for downstream autophagy than for BTK or PI3Kδ. These results appeared to correspond to the level to which each of these

compounds is capable of inhibiting the full BCR signalling cascade. Thus, since SYK is upstream of BTK and other molecules in the BCR signalling pathway, it follows that direct inhibition higher in the pathway would result in a stronger signal inhibition. Previous work in B cell lines has also shown that SYK is a positive regulator of autophagy (Krisenko *et al.*, 2015). However, SYK can also be targeted to stress granules to increase autophagic clearance. This suggests that SYK has capacity to both negatively and positively regulate autophagy, but the dominant effect in sIgM activated CLL cells appears to be to drive autophagy.

3.7.2 Defining BCR driven autophagy in CLL

Autophagy can be broadly divided into several subcategories, which have different roles and outcomes in various cellular processes. Canonical autophagy can be characterised by a dependence on the ULK pre-initiation complex(Lee and Tournier, 2011; Zhao and Klionsky, 2011; Egan *et al.*, 2015; Petherick *et al.*, 2015b; Qi *et al.*, 2015), which can be measured by examining the site that ULK phosphorylates on ATG13 (ser318), in turn activating the initiation complex and inducing autophagosome formation through production of PI3P by VPS34. ATG phosphorylation at S318 can therefore be used as a readout for canonical, ULK-driven autophagy.

My results show a clear increase in phosphorylation of ATG13 at ser318, which indicates that ULK is activated at 24 hours following BCR engagement, corresponding to the larger increase in LC3B-II at this time. This is consistent with activation of a canonical autophagosome biogenesis. However, the increase in autophagy observed at 6 hours occurs despite phosphorylation at thr389 on P70S6K, which would typically indicate mTORC1 activation and canonical autophagy inhibition. This could suggest that LC3B-II expression at 6 hours may be occurring as a consequence of a non-canonical pathway, whereas at 24 hours this could be through activation of a canonical pathway. Such a switch between non-canonical to canonical autophagy pathways contrasts with results characterising autophagy pathways in normal B cells (Martinez-Martin *et al.*, 2017). However, this may be an overly simplistic view of several conflicting and complex pathways, and a distinction betwee basal and BCR driven autophagy in CLL cells. An alternative explanation is that the results shown could be a result of conflicting signals arising from BCR stimulation, with AKT phosphorylation driving downstream signalling that results in mTORC1 activity, while ERK phosphorylation activates signalling pathways that result in AMPK activation.

Since AMPK activation results in direct phosphorylation of mTORC1 and inhibition of the complex (Kim *et al.*, 2011; Alers *et al.*, 2012), mTORC1 activity should be inhibited by ERK signalling and

autophagy subsequently induced at early time points. However, P70S6K phosphorylation, indicative of mTORC1 activity, was increased most strongly at early time points and then decreased, at which point LC3B-II levels begin to increase, occurring most significantly at 24 hours, at which point phospho-P70S6K expression has returned to basal levels. Consequently, it is possible that BCR signalling activates the AKT/mTORC1 pathway to a much greater extent than the ERK/AMPK pathway, and in the conflicting signals mTORC1 is expressed highly enough to out-compete AMPK levels until signalling begins to decrease (shown in my results from 4 hours).

3.7.3 Canonical and Non-canonical autophagy in CLL

Previous work has suggested that BCR cross-linking stimulates non-canonical autophagy within the first 20 hours of engagement (Martinez-Martin *et al.*, 2017). In this study, peak phospho-P70S6K expression occurs between 2 and 5 hours, which gradually decreased to basal expression levels after 20 hours. Absence of phospho-P70S6K indicates that mTORC1 is inactivated. Autophagy levels, as indicated by LC3B-II expression, peak at 24 hours, with the authors suggesting that this subsequent autophagy peak is a result of canonical autophagy induction (Martinez-Martin *et al.*, 2017) . The same research showed that p62 levels increase initially following BCR stimulation with anti-IgM, and that treatment with bafA1 and chloroquine increased the relative expression further by western blot, suggesting that the p62 seen would be turned over by the autophagosome without use of end-point inhibitors. The authors also examine longer term results in culture and conclude a switch from canonical to non-canonical autophagy shapes B cell responses in the context of viral infection. However, there are many differences between healthy, murine B cells and tumour CLL cells, and we do not note any increases in autophagic markers after 24 hours. By 48 hours autophagy levels remain virtually the same, as tested in initial experiments (data not shown), and beyond that CLL cells lose viability in culture.

I show here that at 24 hours following stimulation, both p62 levels and LC3B-II levels are significantly increased. Treatment with bafA1 or HCQ do not appear to significantly increase p62 levels as they do with LC3B-II, indicating that p62 is not involved in the type of autophagy occurring at this time point, as it is not being turned over by the autophagosome. This is not consistent with findings in murine non-tumour B cells, showing that BCR engagement stimulated non-canonical autophagy initially, corresponding to high p62 turnover and mTORC1 activity, followed by a switch back to canonical autophagy (Martinez-Martin *et al.*, 2017). This research also showed that the autophagy observed while mTORC1 was active was dependent on SYK and downstream signalling proteins, but not on class III PI3K, required for canonical and non-canonical autophagy (Martinez *et al.*, 2015). However, our results differ from those seen in the Martinez-Martin study, as Vps34

inhibition in CLL cells prevented BCR-mediated increases in LC3B-II expression. CLL appears to differ from murine, non-malignant B cells in the autophagy pathways and responses initiated following BCR signalling

3.7.4 Using autophagy pathway inhibitors to define autophagy

My results with HCQ and bafA1 treatments show little difference in LC3B-II expression between the two inhibitors, and therefore I am unable to apply the same 'autophagy ratio' described in other work (Jacquin *et al.*, 2017; Martinez-Martin *et al.*, 2017). In line with their other findings however, SYK does seem to be required for anti-IgM bead induced autophagy, at least to a greater extent than downstream signalling proteins. The conclusions of the research by Martinez-martin et al were that, following BCR stimulation with soluble anti-IgM, a canonical autophagy pathway is activated which then switches to a non-canonical pathway. These conclusions do not align with the results that I show here, which indicate that the reverse may be occurring, with a switch from non-canonical to canonical. However, this may be due to differences between murine and human B cells, between CLL and healthy B cells, differences in cell of origin, the Vps34 inhibitor used or a difference in response between soluble and bead immobilised anti-IgM, but this requires further investigation. There may be an interplay of different types of autophagy, or parallel activation of other pathways involving p62 or autophagy related proteins, such as the UPR (Krysov *et al.*, 2014) or mitophagy.

In attempting to define whether treatment with bead bound anti-IgM induces canonical or non-canonical pathways, our results show that bafilomycin treatment results in greater LC3B-II accumulation than either 10 of 100 μM HCQ treatment following sIgM stimulation. The recently described autophagy index (Jacquin *et al.*, 2017; Martinez-Martin *et al.*, 2017) indicates that HCQ, and related lysosomotropic compounds, induce non-canonical autophagy at high concentrations (~50-100μM), as shown by the Florey group previously (Florey *et al.*, 2015; Jacquin *et al.*, 2017) whereas bafilomycin inhibits non-canonical autophagy, but does not affect LC3 lipidation during autophagosome formation; only affecting unconventional lipidation of LC3 in non-canonical processes such as LAP and entosis (Florey *et al.*, 2015). In B cells this index had been used to conclude that anti-IgM stimulation results in a shift from canonical to non-canonical autophagy (Martinez-Martin *et al.*, 2017). My results show higher levels of autophagy with bafilomycin than HCQ 100 μM treatment. Further clarification may be obtained through knockdown of specific proteins essential for non-canonical autophagy only, such as Rubicon and NOX2 (Martinez *et al.*, 2015; Simon and Clarke, 2016). Beclin1 phosphorylation at Serine14 by ULK1 is also a defining feature of canonical autophagy, but the antibodies available for this phosphorylation site currently

indicate that they are only suitable for use in cell lines due to poor binding efficiency. However, it may be worth exploring this option further to conform ATG13 phosphorylation results, if improved reagents become available. Defining the programming and role of BCR-dependent autophagy in CLL will identify whether this pathway is targetable in disease, whilst also illuminating its role in general BCR biology

ULK inhibitors

Following BCR stimulation, an increase in phospho-ATG13 at ser318 (corresponding to ULK activity) and the corresponding LC3B-II increase at 24 hours indicates that canonical autophagy is occurring at this time point, which was partially inhibited by ULK inhibitors. Starvation-mediated autophagy was also partially inhibited by the dual ULK1/2 inhibitor, MRT68921, at 1 μM, in line with concentrations used in other literature (Bryant et al., 2019; Follo, Cheng, Richards, Bueno, & Broaddus, 2018; Petherick et al., 2015a). However, with SBI-0206965 treatment I only observed partial inhibition of LC3B-II expression at concentrations above 10 μM. Other work utilised concentrations of SBI-0206965 up to 100 μM in some cell types for maximum effect (Tang et al., 2017). However, since SBI-0206965 has been shown to be effective for LC3B-II inhibition in a panel of PDAC cell lines from 2 μM (Bryant et al., 2019), NSCLC cell lines from 1 μM to 10μM (Tang et al., 2017) and 10 μM in HEK-293T cell lines (Egan et al., 2015). This is an area of interest, as other work has shown that both ULK inhibitors and chloroquine synergise with ERK and RAS inhibitors, to induce tumour cell apoptosis in pancreatic cancer (Bryant et al., 2019), and also with mTOR inhibitors (Egan et al., 2015). Examining signalling markers, the two inhibitors seem to have little in the way of off-target effects, but it is interesting that MRT68921-induced caspase dependant apoptosis from concentrations >3μM, while SBI-0206965 did not. However, this could be due to the fact that SBI-0206965 was ineffective at targeting ULK mediated autophagy in CLL, while MRT68921 was effective, illustrated by comparisons between the two compounds for both BCR- and starvation-induced autophagy. Interestingly, while SBI-0206965 was initially identified as a highly selective ULK1 inhibitor (Egan et al., 2015), recent findings have indicated that it can also inhibit AMPK (at 1 μM) (Dite et al., 2018). This might be expected to make it a more effective inhibitor of canonical autophagy, particularly for starvation mediated pathways.

SBI-0206965 treatment, which has been reported to inhibit both ULK1 and AMPK, shows little reduction in LC3B-II or pATG13 expression. I directly compared the effect of SBI-0206965, MRT68921 and SAR405, all at 1 μM, on starvation-mediated autophagy, which is known to utilise a canonical autophagosome biogenesis pathway. Since previous results indicate that SBI-0206965 is not as effective as MRT at inhibiting the autophagy induced at 24 hours following BCR stimulation

in CLL, and this drug has been previously reported to be effective from 1 μM, I wanted to confirm the effectiveness in CLL. However, although initial work reported effectiveness at 1 μM, subsequent work in other literature uses concentrations from 1 to 10 μM for maximum effectiveness in cell lines (Egan *et al.*, 2015; Tang *et al.*, 2017). Since partial inhibition of ATG13 phosphorylation and LC3B-II expression was demonstrated from 1 μM in cell lines, this concentration should show some inhibition of LC3B-II expression in CLL. Results indicate that MRT68921 and SAR405 both effectively inhibit starvation-mediated LC3B-II expression in CLL, although since starvation does not seem to induce ATG13 phosphorylation here, it is difficult to assess the effect on ULK activity

AMPK is a global nutrient sensor responsible for activating the ULK complex and inhibiting mTOR, which should then release inhibition of autophagy. P70S6K phosphorylation at Thr389, which occurs downstream of mTORC1 activation, increases following starvation. This indicates that mTORC1 is activated during starvation, and should be repressing autophagy, which is an abnormal response to cellular starvation. This remains unchanged following starvation treatment with SBI-0206965 and MRT68921, suggesting SBI-0206965 does not inhibit AMPK in CLL, or that AMPK is already being repressed during CLL starvation. If SBI-0206965 inhibited AMPK, mTORC1 activity and subsequent P70S6K phosphorylation should increase compared to starvation N/A. If AMPK was activated in CLL following starvation, mTORC1 should be inhibited, showing as a reduction in P70S6K phosphorylation by mTORC1. In conclusion, this suggests that SBI-0206965 may not effectively inhibit AMPK or ULK1 activity in CLL. Another difference worth considering is that SBI-0206965 selectively inhibits ULK1, and it has been reported that in some cases ULK2 may compensate for loss of ULK1 function, and that this ability is cell type specific (Lee and Tournier, 2011). MRT68921 appears to be the more effective ULK inhibitor in CLL, and this may be due to the dual ULK1/ULK2 inhibition. Assuming both inhibitors are generally effective in other cell types, as shown in the literature, this could indicate the requirement or increased dependence on ULK2 in BCR mediated and starvation mediated autophagy in CLL. Further work could examine relative basal expression of the two ULK forms between healthy donor B cells and CLL to unpick the mechanism of action.

VPS34 inhibitors

Pre-treatment of CLL cells with SAR405 to inhibit Vps34, followed by stimulation of CLL cells with anti-IgM coated beads, revealed a requirement for the Class III PI3K, Vps34, in BCR-mediated autophagy. Results comparing responses between control beads (no BCR stimulation and therefore reflecting basal autophagy), may demonstrate a requirement of Vps34 both basal and anti-IgM driven autophagy. Vps34 is responsible for PI3P production as part of the Beclin autophagosome

initiation complex. It has been previously reported that PI3P is crucial for autophagosome biogenesis (Burman and Ktistakis, 2010), and PI3P produced by Vps34 is essential in LC3B-I lipidation to LC3B-II and integration into the autophagosome membrane (Brier *et al.*, 2019), although PI5P can also be utilised in Vps34-independent pathways (Vicinanza *et al.*, 2015). Interestingly, an accumulation of LC3B-I was noted, with my results suggesting that by inhibiting Vps34, autophagosome elongation is halted, as expected by the mechanism of action, but also that insertion of LC3B-II into the membrane is halted, apparently causing an upstream inhibition of LC3B-1 to to LC3B-II conversion and accumulation of –I. Thus, SAR405 inhibits autophagosome completion. Since autophagy is still being driven upstream of this complex, this results in an accumulation of LC3B-I and a reduction in membrane-bound LC3B-II, as LC3B-I is only converted to LC3B-II for the purpose of membrane insertion during autophagosome biogenesis and elongation. A schematic illustration of this is shown in **Figure 37**.

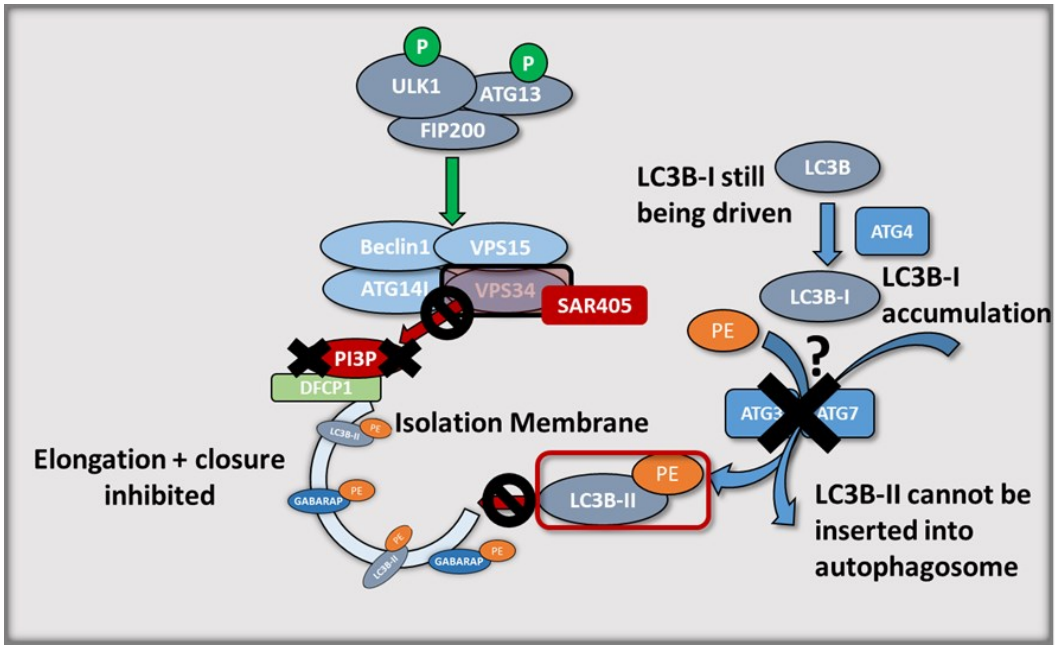

Figure 37. Vps34 in autophagosome elongation and formation

Vps34 inhibition results in reduction of LC3B-II and an apparent accumulation of LC3B-I, with potential mechanism of action illustrated above. Vps34 produces PI3P which primes formation and elongation of the autophagosome membrane. By inhibiting this, it also apparently inhibits lipidation of LC3B-I into LC3B-II catalysed by atg3 and z, since the autophagosomal membrane is no longer being initiated and elongating.

3.7.5 P62 in BCR driven autophagy

p62 is responsible for delivering cargo to the autophagosome prior to degradation- in canonical autophagy, where p62 is turned over, p62 protein levels should decrease corresponding to LC3B-II levels (Komatsu and Ichimura, 2010; Chang *et al.*, 2013), and increase with use of autophagosome turnover inhibitors. Therefore, assessment of p62 expression with HCQ will reveal whether p62 is being turned over during BCR-mediated autophagy induction. Results show that BCR driven p62 expression does increase marginally with both bafilomycin and HCQ treatment compared to N/A, but this is not significant. In addition to this, treatment with autophagosome biogenesis inhibitors such as SAR405, VPS34-IN1 and MRT68921 do not show any significant p62 accumulation. If p62 expression was being driven for involvement in autophagy following BCR stimulation, one or more of these inhibitors should show a clear increase in p62 levels. This indicates that the p62 increase shown following BCR stimulation could be involved in an alternative BCR-driven pathway, rather than in BCR-mediated autophagy.

Other work has shown an increase in p62 mRNA expression at 20 hours following anti-IgM bead stimulation in CLL cells, compared to unstimulated cells (Dal Bo *et al.*, 2015). In this work p62 and ATG7 mRNA increased following BCR engagement, while ATG5, ATG16L2, ATG9B and ATG12 all decreased significantly at 20 hours following BCR engagement, compared to unstimulated cells. ATG16 is required for correct localisation of ATG12 and ATG5 by forming an Atg12–5-16 complex, required for canonical autophagy, but also required for the unfolded protein response (UPR). However, the isoform ATG16L2 examined in this study, while able to form an ATG12-5-16 complex is not required for canonical autophagy in the same way that ATG16L1 is (Ishibashi *et al.*, 2011; Xiong *et al.*, 2018), so this may not aid in determination of the type of autophagy occurring. However, since this work did not look at other isoforms of ATG16, and since ATG5, 12 and 9B are also downregulated following BCR engagement, which could indicate a form of post-transcriptional regulation for these autophagy proteins. In the research showing p62 mRNA is elevated (Dal Bo *et al.*, 2015), no corresponding western blot for p62 is shown, so we are unable to draw any conclusions from this work regarding autophagic flux and corresponding p62 turnover. However, ATG7 is upregulated along with p62, and ATG7 has been shown to have additional roles opposing its canonical role in autophagosome biogenesis. In some circumstances, ATG7 can preferentially sequester p62 aggregates, through interaction with LC3-I, which may subsequently impair LC3-I conversion to LC3-II(Gao *et al.*, 2013).

The conclusions drawn by the authors being that cells may increase expression of ATG7 isoforms in excess to compensate for increases in p62 expression, to allow functional autophagy to continue

despite p62-ATG7 aggregation. ATG3, which is expressed at low levels, may also control the effects of p62 on the autophagosome formation machinery by binding to LC3-I before interacting directly with ATG7, with the binding of ATG3-ATG7 not impaired by p62. Therefore ATG3 may protecting from p62 aggregation, until interaction with LC3-I and conversion to LC3-II is complete, at which stage ATG3 releases and exposes the p62 interacting region of LC3-II, allowing LC3B-II-p62 binding and sequestration into autophagosomes (Gao *et al.*, 2013). This could indicate that, in the study by Dal Bo et al, CLL cells are increasing p62 expression as part of the UPR, which feeds into the autophagy pathway.

As part of the UPR, p62 expression can be increased following stimulation of ER stress , markers of which include phospho-ERK (Verfaillie *et al.*, 2010), which is involved in the BCR signalling pathway. p62 may subsequently activate the Keap1-Nrf2 pathway during selective autophagy induced by cellular stress (Ichimura *et al.*, 2013). It has been previously reported that BCR activation drives the unfolded protein response (UPR)(Skalet *et al.*, 2005; Krysov *et al.*, 2014), which requires p62, and that an interplay between the UPR and autophagy occurs as a survival mechanism in tumour cells(Yan *et al.*, 2015). So while the increases in p62 we see at 24 hours following stimulation with bead bound anti-IgM could indicate non-canonical autophagy, where p62 is accumulating because it is not being targeted to canonical autophagosomes, it could also be that the BCR is driving increased expression of p62 for another pathway. Recent work has identified cell cycle progression gene 1 (CCPG1) as a non-canonical autophagy cargo receptor protein (Smith *et al.*, 2018), involved in facilitating interactions between core autophagy proteins to initiate selective autophagy of the endoplasmic reticulum (ER-phagy), as well as demonstrating non-canonical binding directly to FIP200. This process may protect against UPR hyper-activation, with CCPG1 protein shown to co-localise with WIPI2, LC3B and FIP200, while also accumulating following treatment with bafA1, indicating involvement in autophagic flux (Smith *et al.*, 2018). The same work demonstrated that *CCPG1* is a UPR-regulated gene actively transcribed following UPR activation, linking the UPR to non-canonical forms of autophagy.

Overall, there is a high degree of complexity to BCR signalling and BCR mediated autophagy pathways, with BCR stimulated autophagy apparently occurring through a different pathway to basal elevated autophagy in CLL, confirmed by the observation that ATG13 is not basally phosphorylated in CLL. With the current methods utilised we are unable to conclusively define the type of autophagy occurring following BCR stimulation, only offer indications for further work and potential functional roles, which we aim to characterise in later chapters.

Chapter 4 Characterisation of anti-IgM-coated bead internalisation by CLL cells

4.1 Introduction and Aims

Results in Chapter 3 showed that BCR stimulation increases autophagy in CLL cells. However, a striking observation was that CLL cells appeared to be capable of internalising the anti-IgM-coated beads that were used to stimulate sIgM in these experiments. Internalisation was dependent on sIgM since control antibody-coated beads were not internalised.

Normal B cells are capable of using the BCR to internalise antigens in various forms, including soluble and particulate antigens. For example, normal B cells have been shown to internalise particulate antigen in the form of anti-IgM-coated beads (Martinez-Riano *et al.*, 2018). They can then present the processed antigen to T cells and this initiates a more potent immune response compared to soluble anti-IgM (Martinez-Riano *et al.*, 2018). Antigen encountered routinely by healthy B cells is also likely to be in particulate form, such as fungi and apoptotic bodies. CLL cells are known to be able to endocytose soluble anti-IgM (Os *et al.*, 2013) but internalisation of anti-IgM coated beads has not been observed before. Therefore, the overall goal of the experiments described in this chapter was to characterise the internalisation of anti-IgM-coated beads by CLL cells. This required development of a new assay to quantify bead internalisation. Autophagy has been linked to antigen removal and processing in other cell types, and I therefore also used this assay to investigate the role of autophagy (and kinases) in bead internalisation.

The specific aims of the experiments were:

- To develop a quantitative flow cytometry assay to quantify anti-IgM-coated bead internalisation
- To investigate effect of BCR-associated kinase inhibitors and autophagy inhibitors on anti-IgM-coated bead internalisation
- To investigate internalisation of different sized anti-IgM-coated beads

4.2 Development of a flow cytometry assay to quantify anti-IgM-coated bead internalisation

Confocal imaging analysis revealed the internalisation of anti-IgM-coated beads (**FiguresFigure 34, Figure 35, Figure 36**) but also identified several technical challenges. First, high auto-fluorescence of DynaBeads made parallel analysis of markers difficult. Second, analysis was time-consuming and it was challenging to discriminate between beads that had been internalised from those that may be attached to the CLL cell, but not internalised. The goal was therefore to develop a flow-based assay to allow quantitative analysis of bead internalisation.

4.2.1 Comparison of internalisation of anti-IgM-coated latex beads and DynaBeads

To address the issue of bead auto-fluorescence, I coupled the anti-IgM and anti-IgD antibodies to latex beads which have very low auto-fluorescence. I selected 3 micron latex beads for this analysis as these were closest in size to the 2.8 micron DynaBeads. The latex beads have a carboxylate-modified surface which (after activation) allows covalent coupling between carboxylate groups and primary amine groups. By contrast, DynaBeads are coated in epoxy residues which allows direct covalent coupling to primary amine or sulfhydryl groups. Flow cytometry confirmed that, compared to anti-IgM-coated DynaBeads, anti-IgM-coated latex beads exhibited very little auto-fluorescence after incubation with CLL cells (**Figure 38**).

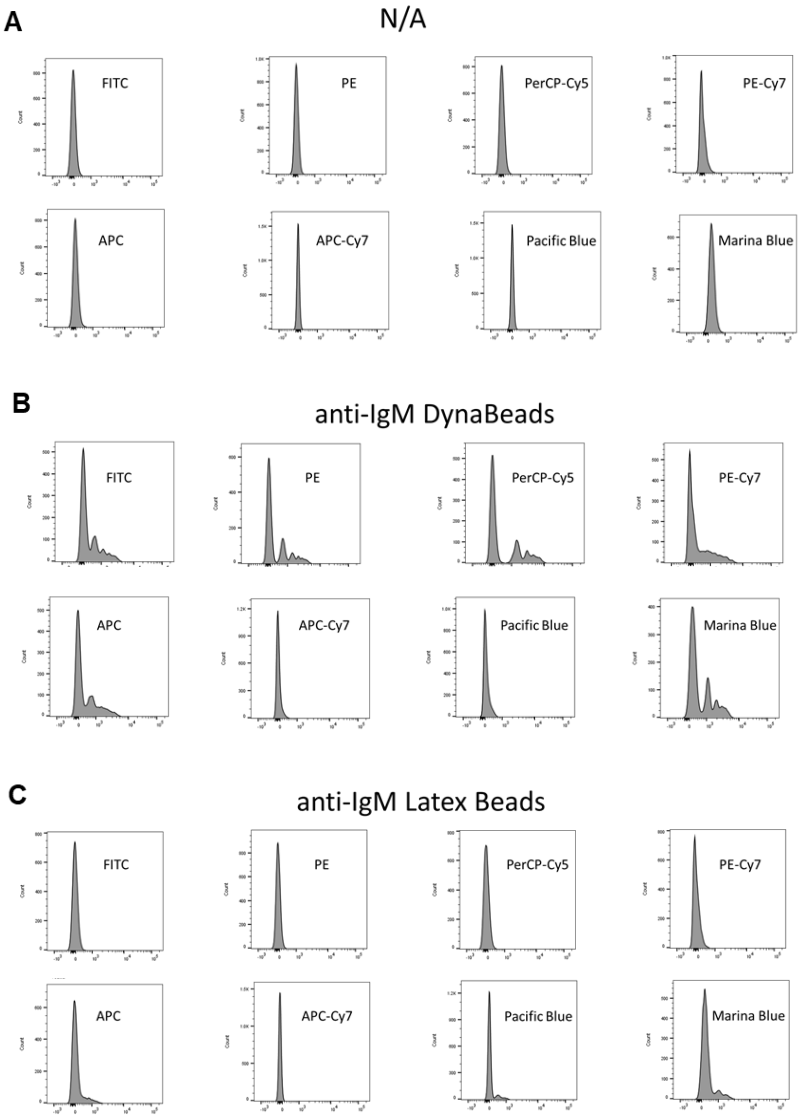

Figure 38. Comparison of autofluorescence of DynaBeads and latex beads.
Flow cytometry analysis of (A) CLL cells alone, (B) CLL cells incubated with anti-IgM-coated Dynabeads or (C) CLL cells incubated with anti-IgM-coated latex beads.

It was important to confirm that the anti-IgM-coated latex beads, like anti-IgM-coated DynaBeads, were capable of inducing signalling responses and autophagy in CLL cells. I therefore compared the responses of CLL cells following stimulation by anti-IgM or anti-IgD-coated latex beads or DynaBeads (all used at a two beads per cell ratio) (**Figure 39**). Kinase activation was analysed at 30 minutes and demonstrated that although all beads increased phosphorylation of all targets analysed (SYK, AKT, ERK, P70S6K), responses were somewhat greater for DynaBead-coupled antibodies (**Figure 39A**). Autophagy activation was measure by expression of LC3B and p62, and phosphorylation of ATG13, after 24 hours. In contrast to signal analysis (**Figure 39A**), autophagy responses appeared to be modestly stronger for the latex beads compared to Dynabeads, especially for anti-IgM which generally induced stronger autophagy responses than anti-IgD in this sample (**Figure 39B**).

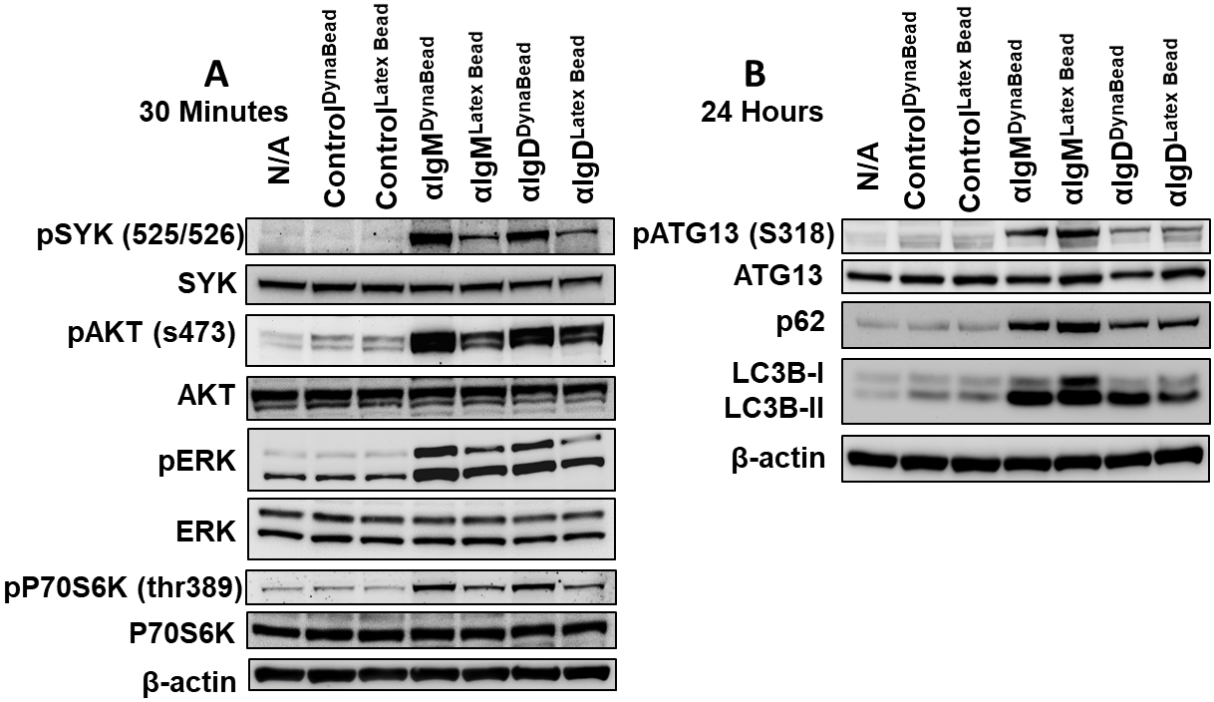

Figure 39 Comparison of effects of anti-Ig-coated latex beads or DynaBeads on signalling and autophagy markers in CLL cells.
CLL cells were incubated with anti-IgM-, anti-IgD- or control antibody-coated Dynabeads or latex beads (or left untreated, N/A) for (A) 30 minutes or (B) 24 hours, before analysis of the indicated proteins by immunoblotting.

One possible explanation for the different extent of response to anti-IgM-coated latex and Dynabeads, especially for earlier kinase activation, may relate to the differing chemistries which could result in different amounts of antibody being coupled. Another possible explanation could be the physical properties of the beads themselves as Dynabeads are more dense. This could affect

the speed at which they encounter cells and therefore engage sIgM after mixing. Some pilot experiments were performed to determine whether increasing the bead/cell ratio for the latex beads would increase the signalling response (data not shown). However, the results were not consistent between samples and I therefore continued to use a 2 bead:1 cell ratio for both latex and DynaBeads as, overall, the differences in the effects of these reagents on signalling (and later induction of autophagy markers) were relatively modest.

4.2.2 Development of a quantitative method to analyse anti-IgM-coated bead internalisation

Development of a quantitative flow cytometry method to quantify internalisation was based on the study of normal B cells by (Martinez-Riano *et al.*, 2018). Thus, CLL cells were incubated with anti-IgM-coated latex beads and, after a set time, were placed at 4°C and stained with an anti-goat AlexaFluor488 antibody, which can bind the goat anti-IgM antibody that is coupled to the beads. Thus, extracellular anti-IgM-coated beads are labelled with the AlexaFluor488 antibody. By contrast, internalised anti-IgM-coated beads are not labelled with the AlexaFluor488 antibody as they are protected by the plasma membrane. The anti-goat AlexaFluor488 antibody will also recognise the control antibody couple to the beads, so the behaviour of the control beads without anti-IgM can also be tracked in this way.

I first validated the assay using microscopy. After examining several time points, a 3 hour time point was selected for high degree of bead internalisation without the complications of longer time points affecting CLL cell viability with compound treatments.. In addition to the anti-goat AlexaFluor488 antibody, I stained the cell membrane using CellMask Deep Red, to identify the plasma membrane, and the nucleus using DAPI. The basis for the assay is illustrated below (
Figure 40) using colours for the stains which match those shown in the subsequent analyses.

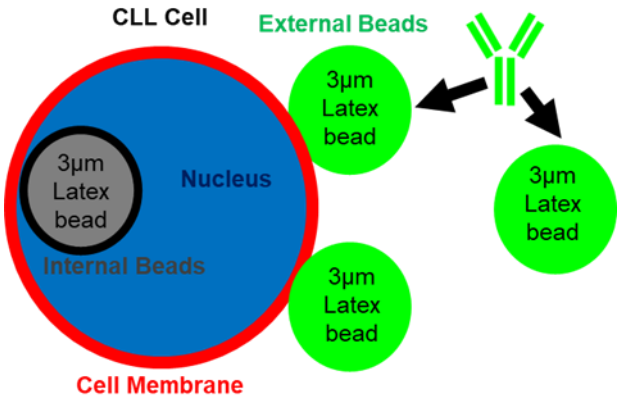

Figure 40. Diagram of methodology used to quantify bead internalisation.
Illustration of the staining technique used to analyse bead internalisation. Cells are incubated with anti-IgM-coated latex beads for 3 hours before being placed on ice to halt internalisation, stained with the AlexaFluor488-labeled anti-goat antibody and then fixed before analysis.

Confocal microscopy demonstrated that the assay performed as expected (**Figure 41**). Non-internalised anti-IgM-coated beads were readily identifiable due to their intense green staining, whereas internalised beads did not stain with the anti-goat AlexaFluor488 antibody but were identifiable as grey “ghosts” within the CLL cells. Control beads were not internalised. Higher power

images confirmed that at least a proportion of anti-IgM-coated beads were internalised as unlabelled, but not labelled (ie extracellular) beads, were enveloped by plasma membrane (**Figure 42**).

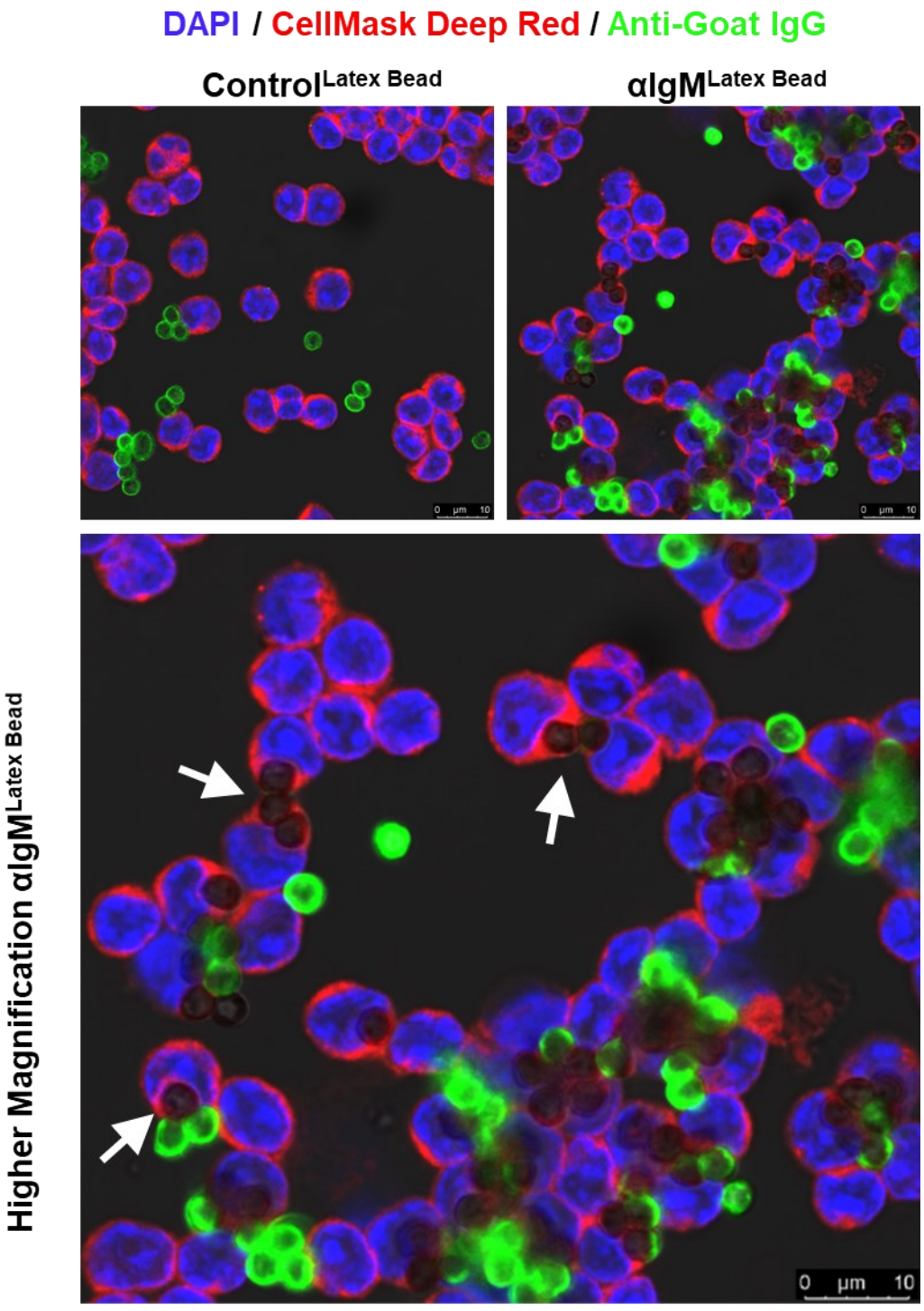

Figure 41. Confocal microscopy to analyse bead internalisation.
CLL cells were incubated with anti-IgM- or control-antibody-coated latex beads for 3 hoursbefore being placed on ice and stained with an AlexaFluor488-labeled anti-goat antibody, fixed and then analysed by confocal microscopy. CellMask Deep Red and DAPI were used to stain the plasma membrane and nucleus, respectively. Merged images are shown. Top panels show comparison of with anti-IgM- or control-antibody-coated latex beads. Bottom panel is a high magnification image for anti-IgM-coated latex beads with internalised beads (ie, negative for AlexaFluor488) indicated by arrows.

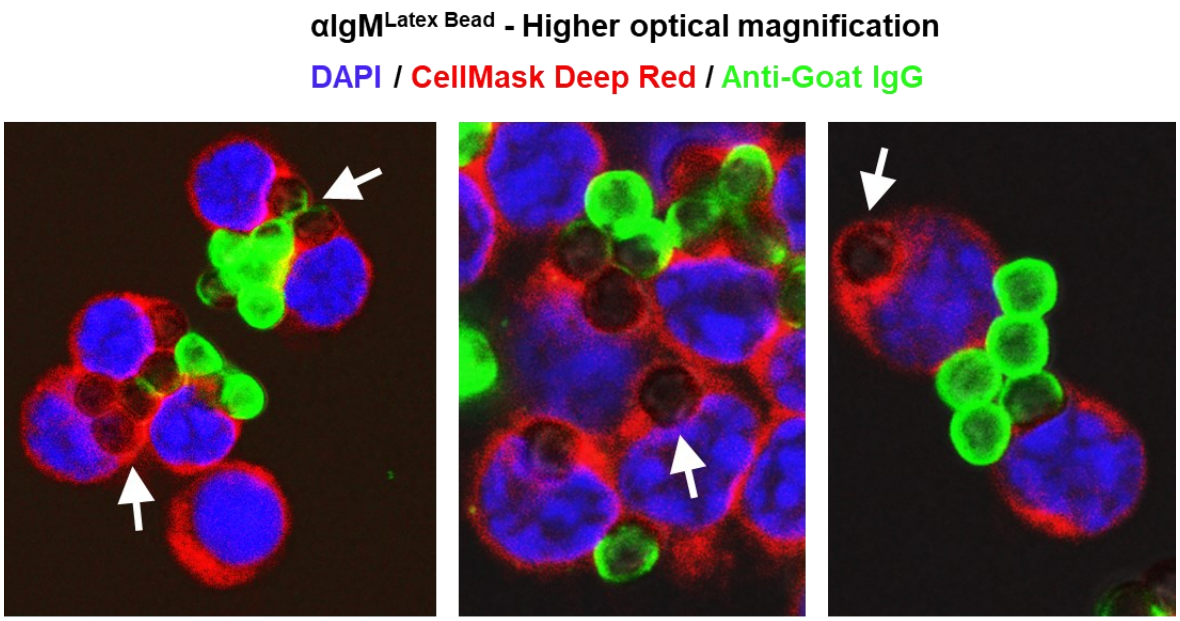

Figure 42. Higher magnification confocal images of internalised anti-IgM-coated latex beads. See legend to **Figure 41** . Arrows indicate internalised beads surrounded by plasma membrane.

The final step was to modify the assay for use by flow cytometry (**Figure 43**). FSC/SSC analysis of CLL cells incubated with anti-IgM-coated latex beads for 3 hours, fixed and then stained with the AlexaFluor488-labeled anti-goat antibody identified three major populations; (i) beads only, (ii) cells only and (iii) cells+beads (**Figure 43A**). Staining with anti-CD19 and anti-CD5 antibodies in a subset of samples confirmed that the cells+beads population comprised CLL cells (and not normal B cells that maybe present in the PBMC sample; data not shown) and doublet exclusion was performed to ensure that the studied population comprised single cells (**Figure 43B**). Analysis of FITC fluorescence confirmed that unbound beads had very high fluorescence (consistent with being available for AlexaFluor488-labelling) whereas the fluorescence of free cells was very low. The histogram of the cells+beads showed a distribution of fluorescence consistent with the idea that at least a proportion of the beads had been internalised and therefore protected from AlexaFluor488-staining (as fluorescence was not different from free cells). For quantification, I calculated the MFI of the cells+beads population for the various conditions. CLL cells incubated with anti-IgM-coated beads at 4°C (where internalisation is inhibited) were used as a control (ie, no internalisation). This initial analysis demonstrated that incubation at 37 °C strongly reduced the fluorescence of the cells+beads compared to cells incubated at 4 °C, consistent with internalisation (**Figure 43C**). Interestingly, internalisation appeared to be prevented by SYK inhibition using pre-incubation with entospletinib.

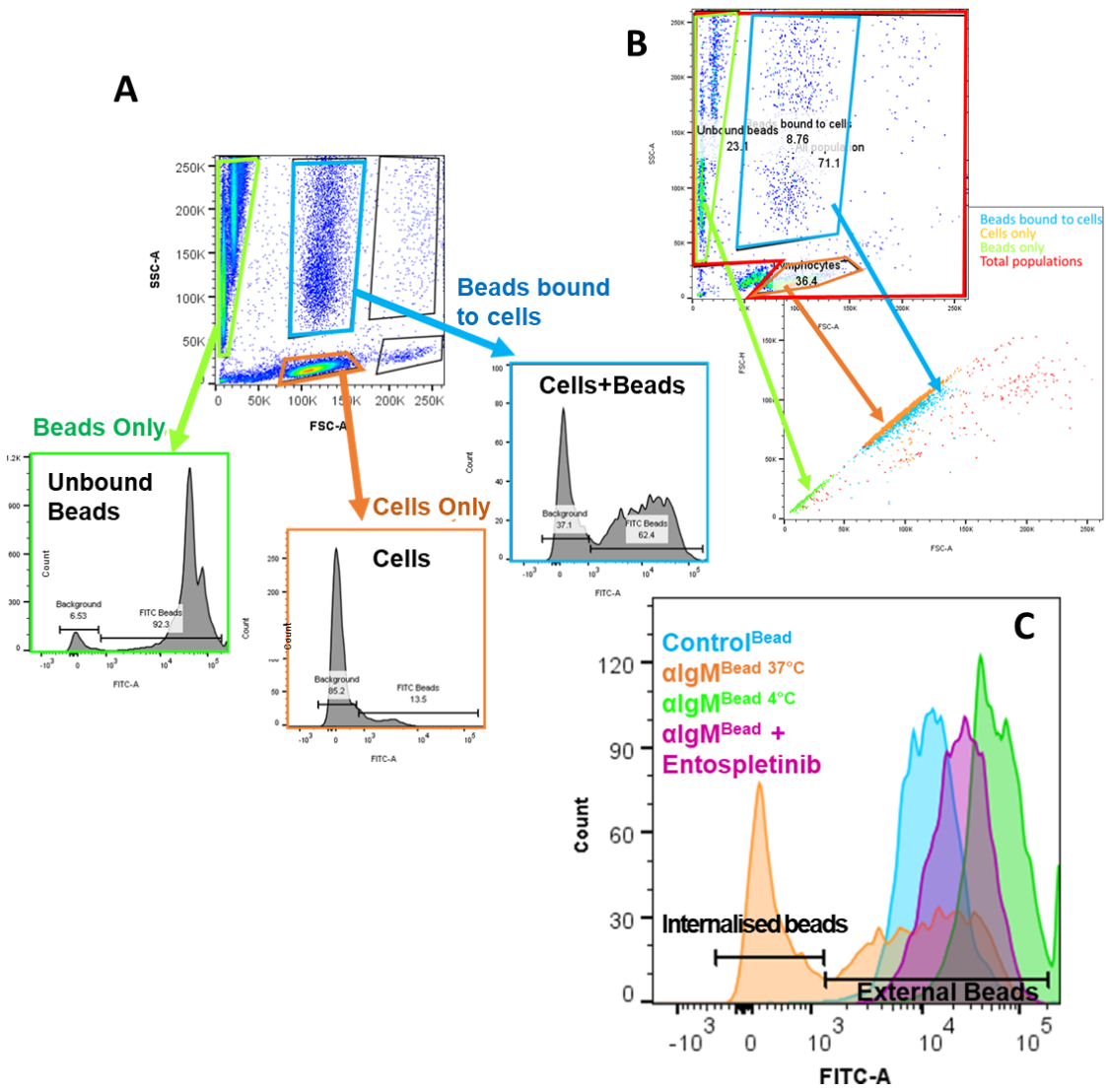

Figure 43. Development of a flow cytometry assay to quantify anti-IgM-coated bead internalisation by CLL cells.

(A) Gating based on FSC/SSC to identify bead only, cell only and cell+bead populations. (B) Doublet exclusion to ensure the cell+beads population consisted of single cells bound to beads. (C) Histograms showing FITC MFI of the indicated cell+bead populations.

4.3 Effect of inhibitors on anti-IgM-coated bead internalisation

4.3.1 Kinase and autophagy inhibitors

The quantitative flow cytometry assay was then used to analyse the effect of inhibitors on anti-IgM-coated bead internalisation in 10 samples (**Figure 44**). The inhibitors used were entospletinib (SYKi), idelalisib (PI3Kδi), ibrutinib (BTKi) and two Vps34 inhibitors, VPS34-IN1 and SAR405. Concentrations tested were as described in Chapter 3. VPS34-IN1 was included as an additional VPS34 inhibitor in these experiments. Entospletinib was the most effective inhibitor of anti-IgM-coated bead internalisation (~80% inhibition on average relative to cells incubated at 4 °C). Ibrutinib and idelalisib appeared to modestly inhibit bead internalisation but, overall, these difference were not statistically significant. VPS34 inhibition using either SAR405 or VPS34-IN1 had no effect on bead internalisation.

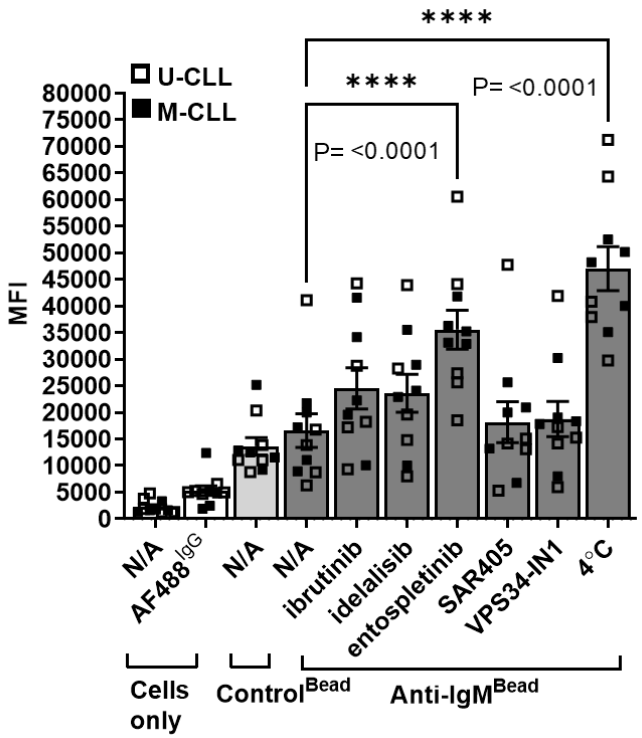

Figure 44. Effect of kinase and autophagy inhibitors on internalisation of anti-IgM-coated beads. CLL samples (n=10) were pre-treated for 1 hour with the indicated compounds, ibrutinib (500nM), entospletinib, idelalisib, SAR405 and VPS34-IN1 (all at 1μM), or left untreated (N/A) before analysis of internalisation of anti-IgM- or control antibody-coated latex beads for 3 hours at 37 °C or 4 °C. The other controls performed (columns 1 and 2) were cells only and cells stained with the anti-goat antibody ($AF488^{IgG}$). Graph shows MFI for individual samples with mean (±SD) and the results of statistical analysis (Bonferroni's multiple comparisons test) in comparison to anti-IgM/N/A-treated cells (where not shown P>0.05).

Overall, these results show that internalisation of anti-IgM beads is dependent on kinases acting downstream of the BCR (especially SYK), but not the autophagy regulator VPS34. The predominant role of SYK may reflect its role as a key, proximal initiator of the BCR signalling cascade, upstream of signal bifurcation leading to activation of PI3K and BTK.

4.3.2 Endocytosis and phagocytosis inhibitors

Cells can internalise molecules via several different pathways, including caveolin-mediated endocytosis, clathrin-mediated endocytosis and phagocytosis (Kumari, Mg and Mayor, 2010). Some key features of these pathways are shown in **Table 7**. To probe what pathway was used by CLL cells for internalisation of anti-IgM-coated beads, I used the flow assay to examine the effects of dyngo-4a (a dynamin inhibitor) or cytochalasin D (an inhibitor of actin filament polymerisation). These compounds have been frequently used to define phagocytic or endocytic events and the concentrations selected for analysis were in line with these studies (Tse *et al.*, 2003; Le Roux *et al.*, 2007; Basquin *et al.*, 2013). Entospletinib was used as a positive control for inhibition. This analysis demonstrated that anti-IgM-coated bead internalisation was effectively blocked by cytochalasin D (at 1 or 10 µM) and, as expected entospletinib, but was unaffected by dyngo-4a (**Figure 45**). Therefore, internalisation of anti-IgM-coated beads appears to dependent on a phagocytic process.

	Caveolin-mediated Endocytosis	Clathrin-mediated Endocytosis	Phagocytosis
Size of molecule internalised	Can internalise molecules over 200 nm and up to 500 nm	Can internalise molecules up to 200 nm	Can internalise large, particulate/aggregated antigen Size requirements reported from 1 µm to 6 µm
Signalling required	Does not require signalling	Does not require signalling	Requires signalling (SYK-dependent in macrophages)
Dynamin requirement	Requires dynamin	Requires dynamin	Does not require dynamin
Actin filament remodelling	-	Does not require actin remodelling	Requires actin filament polymerisation

Table 7. Table of requirements for caveolin and clathrin-mediated endocytosis versus phagocytosis.

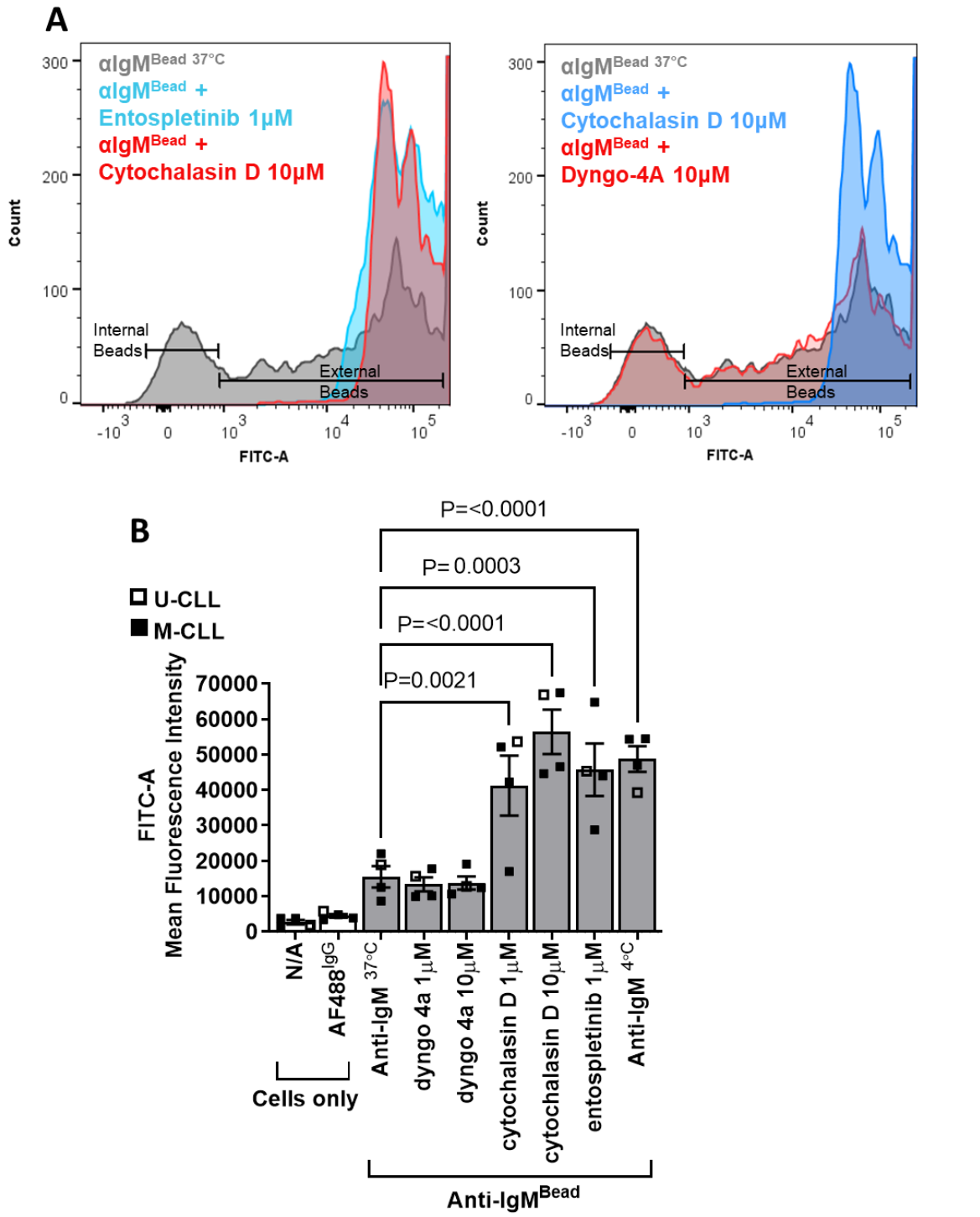

Figure 45. Effect of actin polymerisation and dynamin inhibition on internalisation of anti-IgM-coated beads.

CLL samples (n=4) were pre-treated for 1 hour with the indicated compounds or left untreated (N/A) before analysis of internalisation of anti-IgM-coated latex beads for 3 hours at 37 °C or 4 °C. The other controls performed (columns 1 and 2) were cells only with no addition (N/A) and cells stained with the anti-goat antibody ($AF488^{IgG}$). (A) Representative histograms and (B) quantitation for all samples. Graph shows MFI for individual samples with mean (±SD) and the results of statistical analysis (Bonferroni's multiple comparisons test) in comparison to anti-IgM only-treated cells (where not shown P>0.05).

Taken together, these results demonstrate the internalisation of 3 micron anti-IgM-coated beads by CLL cells is dependent on the activity of SYK and actin polymerisation, but not VPS34 or dynamin. Therefore, internalisation is dependent on BCR-mediated signalling, but not autophagy, and appears to be mediated by a phagocytosis-like pathway.

4.4 Comparison of signalling capacity and internalisation of different size anti-IgM-coated latex beads

In the final series of experiments aimed at characterising bead internalisation, I investigated the signalling/internalisation responses of CLL cells when they were exposed to anti-IgM-coated latex beads of various sizes (0.5, 1 and 3 micron). Soluble anti-IgM and control antibody was also analysed as a control. Rather than using beads and cells at a fixed ratio as in previous experiments, I used a fixed concentration of beads these experiments (10 mg/ml; equivalent to 30 μg beads and 1 $x10^6$ cells). This was performed to ensure approximately equivalent sIgM engagement by the different sized beads (which therefore have different antibody binding capacities).

I first tested the effect of the various anti-IgM-coated beads on signalling (ERK and AKT phosphorylation) and autophagy (LC3B expression). All of the anti-IgM-coated beads induced ERK/AKT phosphorylation to an approximately similar extent demonstrating that all of the beads have the capacity to induce signalling in CLL cells (**Figure 46**). Importantly, LC3B expression was also increased in CLL cells exposed to any of the anti-IgM-coated beads. By contrast, increased ERK/AKT phosphorylation and LC3B expression was not apparent in cells treated with soluble anti-IgM, consistent with the relatively weak and transient nature of signals induced by soluble anti-IgM in CLL cells.

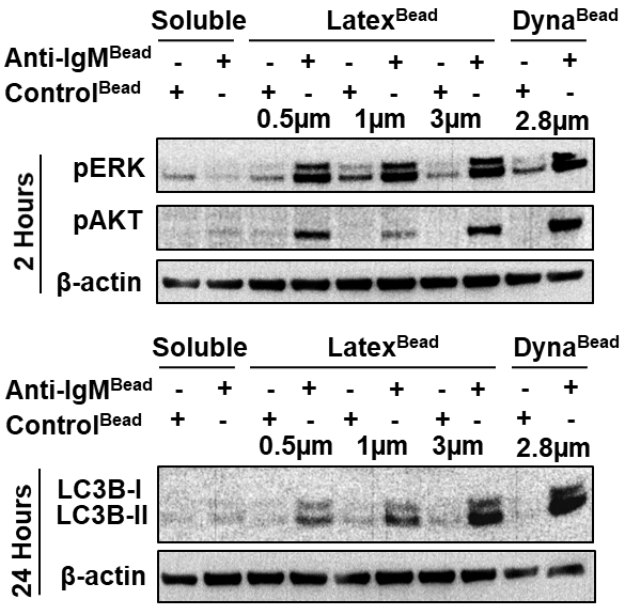

Figure 46. Effect of different size anti-IgM-coated beads on signalling and LC3B expression in CLL cells

CLL samples were incubated with soluble anti-IgM or control antibody, or anti-IgM- or control antibody-coated latex beads (0.5, 1 or 3 micron) or DynaBeads (2.8 micron) using a fixed weight or beads per cell. Expression of phospho-ERK and AKT, and LC3B-II was analysed using immunoblotting after 2- or 24-hours, respectively. Figure shows representative immunoblots from a total of four samples analysed.

Next, I used the flow cytometry assay to compare the internalisation of the 0.5 and 3 micron anti-IgM-coated latex beads, and the effects of dyngo-4a, cytochalasin D and entospletinib. Interestingly, whereas both beads were internalised efficiently by CLL cells, the sensitivity to inhibitors varied between the different sized beads. A shown above (section 4.3.2), internalisation of 3 micron anti-IgM-coated latex beads was inhibited by entospletinib, and also cytochalasin D, but not dyngo-4a (**Figure 47, Figure 48**). By contrast, internalisation of 0.5 micron anti-IgM-coated latex beads was inhibited by all compounds tested, demonstrating a role for dynamin in addition to actin polymerisation in internalisation of 0.5 micron (but not 3 micron) beads.

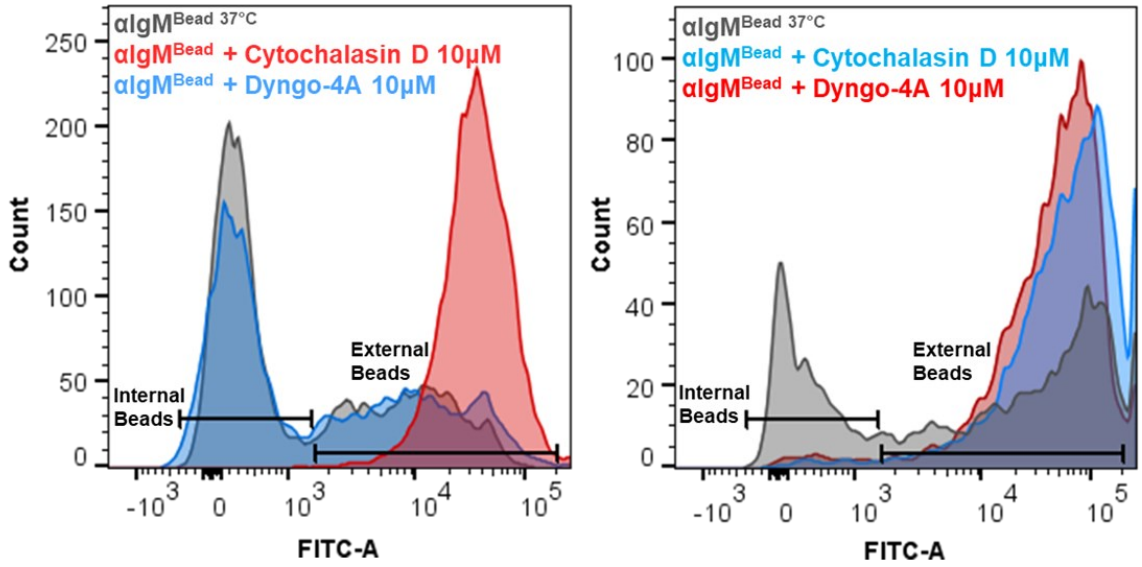

Figure 47. Effect of inhibitors on internalisation of 0.5 and 3 micron anti-IgM coated beads – flow cytometry.

CLL samples (n=5) were pre-treated for 1 hour with dyngo-4A, cytochalasin D or entospletinib, or left untreated (N/A) before analysis of internalisation of either 0.5 or 3 micron anti-IgM-coated latex beads for 3 hours at 37 °C or 4 °C. Representative histograms are shown (3 and 0.5 micron beads on left and right, respectively). Quantitation is shown in **Figure 48**

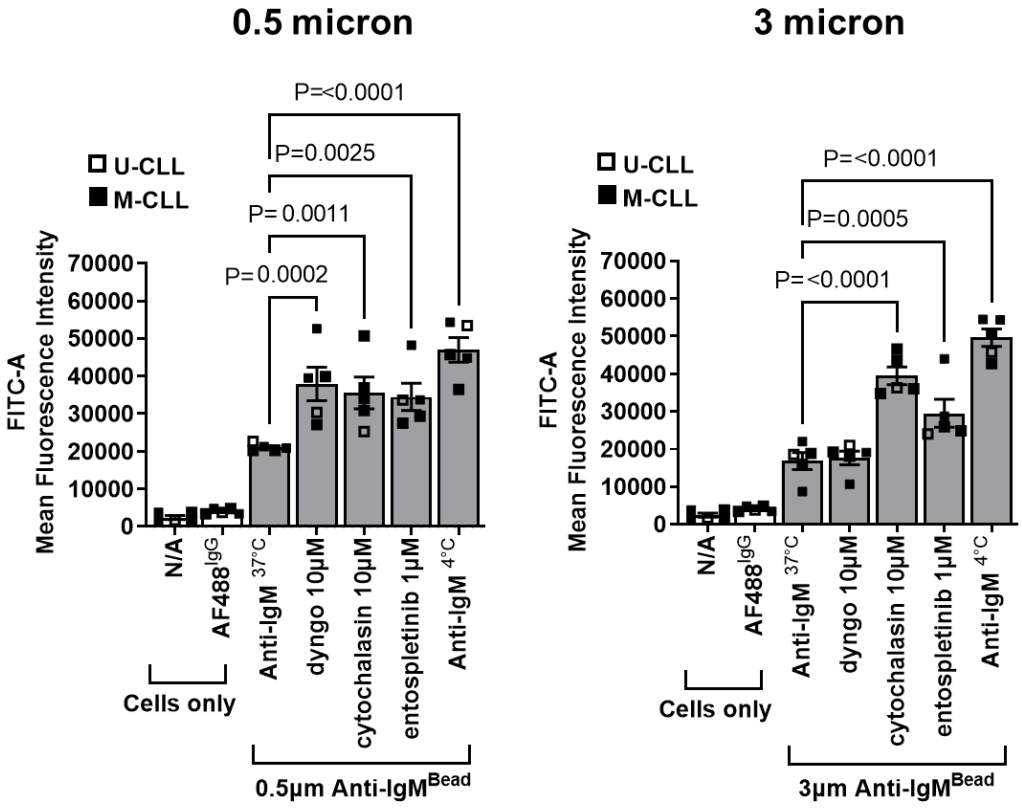

Figure 48. Effect of inhibitors on internalisation of 0.5 and 3 micron anti-IgM coated beads – flow cytometry - quantitation.

Quantitation of the experiments shown in **Figure 39** for all samples analysed (n=5). Graphs shows MFI for individual samples with mean (±SD) and the results of statistical analysis (Bonferroni's multiple comparisons test) in comparison to anti-IgM only-treated cells (where not shown P>0.05). The other controls shown (columns 1 and 2) are MFI of cells only with no addition (N/A) and cells stained with the anti-goat antibody (AF488^{IgG}).

4.5 Summary of Results :

- CLL cells are able to internalise 3 micron anti-IgM-coated latex beads (but not control antibody-coated beads). This occurs from 3 hours of incubation, as revealed by flow cytometry assays and microscopy
- Anti-IgM-coated bead internalisation can be inhibited most effectively using cytochalasin D and entospletinib, showing the major requirement being signalling through SYK and remodelling of actin filaments, indicating a pathway resembling phagocytosis
- By comparison, 0.5 micron anti-IgM coated beads are internalised through a different pathway that requires actin remodelling and SYK, but also dynamin, indicating a potential involvement of a clathrin-mediated endocytosis
- Autophagy inhibitors did not affect the internalisation response

4.6 Discussion

The goal of the experiments outlined in this chapter was to characterise BCR-mediated internalisation of anti-IgM coated beads. In order to do this in a reliable and high throughput way, a flow-based assay was required using a different bead type with low autofluorescence. I successfully characterised and implemented use of 3 micron latex beads for this purpose and implemented an effective flow based assay, validated via confocal microscopy. Using chemical modulators of various aspects of traditionally defined endo- and phagocytosis pathways, I probed the internalisation mechanisms and defined two apparently distinct pathways for internalisation of 0.5 micron and 3 micron anti-IgM-coated beads.

Other work has shown that antigen/bead internalisation generates stronger GC responses in B cells compared soluble antigen. (Martinez-Riano *et al.*, 2018). Since successful immune responses to antigen, including in the context of infection or vaccination, rely on activation of a functional humoral immune response following from a GC reaction, the investigation of strength of response derived from different antigen particle sizes is of interest. In the context of CLL, a deeper understanding of antigen responses may help to inform on some of the hallmarks of CLL, which appear to imply constitutive engagement with common or autoantigen, and the reliance on microenvironmental signals for survival, such a T-cell help. The strength of GC response generated by the form of antigen encountered will correlate to the strength of T-cell recruitment and responses, which may have implications in CLL proliferation. In the process of a strong GC reaction, activation of follicular B cells is essential, which acquire and present antigen, displayed on MHC molecules at the cell surface, to cognate $CD4^+$ T cells.

Here, I show that CLL cells can phagocytose large antigen-coated particles, in the form of 3 micron anti-IgM coated beads. Until relatively recently, this kind of phagocytic process was thought to be an exclusive function of professional antigen-presenting cells, such as macrophages and dendritic cells. I show that larger (3 micron), particulate antigen phagocytosis by CLL cells is BCR-driven and dependent on this signalling response, particularly through SYK, in addition to actin filament remodelling. However, smaller 0.5 micron beads appeared to be internalised through a dynamin dependant pathway. Other work has shown that this is of particular relevance in vaccination approaches. The commonly used alum adjuvants in vaccinations owe their increased success to stronger GC responses, as a result of direct phagocytosis of alum–antigen complexes by B cells (Martinez-Riano *et al.*, 2018), reflecting research characterising the response of other specialized phagocytic cells previously (Romero Mendez *et al.*, 2007; Ghimire, 2015; Danielsson and Eriksson, 2021). Information on how the strength of GC response, and high affinity antibody generation, relates to antigen form and structure has many applications, informing vaccination approaches, but also ability to recruit T cell help required for survival in the tumour microenvironment.

4.6.1 Internalisation pathways differ based on bead size

Through use of signalling and actin filament formation inhibitors, I showed that actin rearrangement was crucial for internalisation of both 3 and 0.5 micron beads. However, the bead internalisation pathway seems to differ between 0.5 micron beads and 3 micron beads, with the smaller beads utilising a dynamin-dependent, SYK dependent, actin dependent pathway, while the larger beads do not require dynamin and therefore are being internalised in a clathrin-independent phagocytic pathway. This demonstrates the different requirement for internalisation pathways utilised by B cells in response to smaller and larger particulate antigen, which aligns with other findings in the B cell response to particulate antigen (Martinez-Riano *et al.*, 2018). The role of particulate antigen internalisation and antigen presentation is beginning to be defined in B cells (Adler *et al.*, 2017), and is an area of increasing interest. Antigen acquisition by B cells following removal initiates cross-linking and endocytosis of the BCR into clathrin coated pits (Tolar and Spillane, 2014; Hoogeboom and Tolar, 2016; Roberts *et al.*, 2020), rather than full internalisation of both antigen and the bound particle in a phagocytic event. In this work, we show that while anti-IgM beads are internalised, control antibody coated beads fail to be taken up by the cells, indicating a BCR driven pathway. This is confirmed by the use of the BCR signalling inhibitors, ibrutinib, idelalisib, and entospletinib, which reduced bead internalisation, with the most significant reduction observed for entospletinib treated cells, showing a greater dependence on SYK for phagocytosis of 3 micron anti-IgM coated latex beads. Previous work has indicated that SYK

signalling is required for actin rearrangement (Jaumouille *et al.*, 2014) and phagocytosis pathways (Crowley *et al.*, 1997; Huang *et al.*, 2006; Tabata *et al.*, 2020). Ibrutinib and idelalisib were less efficient at inhibiting bead internalisation, corresponding to reduced signalling marker and BCR-mediated autophagy-marker induction compared to entospletinib in previous sections.

4.6.2 LC3 Associated Phagocytosis, Autophagy and Immunity

LC3 Associated Phagocytosis (LAP) has been widely reported in macrophages (Heckmann *et al.*, 2017) as part of the phagocytic response to antigen. LAP is one example of a non-canonical form of autophagy, a broad description of processes that lipidate LC3 onto single membrane or non-autophagosomal structures. LAP describes the process of lipidation of LC3 onto phagosome membranes, enhancing phagosome clearance (Simon and Clarke, 2016; Heckmann *et al.*, 2017). There are a number of non-canonical functions for various autophagy proteins, which are distinct from canonical autophagy, with canonical autophagy involving the ULK complex and insertion of lipidated LC3 onto double membrane bound autophagosomes. LAP contributes to immune regulation and the inflammatory responses across various cell types, with roles including aiding of clearance of pathogen and apoptotic cells (Codogno, Mehrpour and Proikas-Cezanne, 2011; Simon and Clarke, 2016; Dupont *et al.*, 2017). Characterized by the conjugation of LC3 family proteins to phagosome membranes (Sanjuan *et al.*, 2007), LAP utilises part of the canonical autophagosome formation pathways and machinery, but by-passes the ULK–FIP200-AT101-ATG13 complex (Martinez *et al.*, 2011) and upstream AMPK-mTORC regulators (Kim *et al.*, 2013). LAP however does require rubicon and the beclin/Vps34-Vps15 complex involved in canonical autophagy (Martinez *et al.*, 2015). Some pathogens attempt to modify the LAP pathway for pathogenicity, and removal of the LAP pathway in mouse models has been shown to inhibit effective clearance of *Aspergillus fumigatus* following infection (Sprenkeler, Gresnigt and van de Veerdonk, 2016).

Reactive oxygen species (ROS) produced by NADPH oxidase 2 (NOX2) has been shown to enhance stability of LAPosomes, through inactivation of the protease ATG4B, which is involved in recycling of LC3 from LAPosomes. When ROS production is inhibited in macrophages, MHC class II presentation of Candida albicans antigen is also reduced. Similarly, where ATG4B is overexpressed in these macrophages, MHCII presentation is reduced(Ligeon *et al.*, 2021). LAP is distinct from the, arguably artificial, forms of non-canonical autophagy induced by osmotic imbalances using lysosomotropic compounds (Florey *et al.*, 2015; Jacquin *et al.*, 2017). While LAP is certainly involved in pathogen clearance and antigen processing, particularly for MHC-II pathways, (Munz, 2012), it is unclear of the involvement in the internalisation component of the phagocytic event, and is more likely to be involved in downstream antigen processing. Here I show that Vps34 inhibition fails to

affect bead internalisation, indicating that autophagy is not required for internalisation of 3 micron beads. However, our results showing that the autophagy inhibitors, SAR405 and VPS34-IN1, have no effect on internalisation, does not necessarily enable us to define the role of autophagy in this process. Further functional studies on antigen processing and presentation are required for elucidation of this mechanism, and the role of autophagy in potential downstream antigen processing steps.

4.6.3 Autophagy in BCR driven phagocytosis

Recent work has demonstrated the requirement of autophagy, specifically of ATG5, in B cell response and presentation of particulate antigen in MHC-II/LAMP1 positive intracellular compartments, and that, following BCR stimulation, ATG5 is important in recruiting MHCII-containing vesicles by mobilizing the actin cytoskeleton (Arbogast *et al.*, 2018). This work also indicated that this was important in GC formation following particulate antigen stimulation, and that ATG5 was involved in regulating synapse formation between B cells and antigen presenting cells (Arbogast *et al.*, 2018). Taken together, these emerging results indicate a link between antigen internalisation and processing, autophagy and B cell immune responses, including antigen presentation. Inhibition of BCR signalling by entospletinib prevents increases in p62, LC3B-II and phosphorylation of ATG13, confirming that signalling through the BCR is driving ATG13 phosphorylation at 24 hours, in addition to p62 and LC3B expression.

Interestingly, cells with beads bound or internalised appeared to display higher LC3B levels in results shown in section 3.6. We have shown that autophagosome turnover inhibition does not inhibit internalisation, but this does not disprove the possibility that autophagy is involved in a later stage following internalisation, such as antigen processing and presentation (Arbogast *et al.*, 2018). Results show that anti-IgM beads are internalised at an early time point (within 3 hours), while autophagy markers are not elevated until 12-24 hours. This could support that autophagy is not involved in the internalisation process itself, which is confirmed by the findings that autophagy inhibitors do not halt bead internalisation. As previously shown, other work investigating the non-canonical process of LAP indicates that LAP is more likely to be involved in subsequent stages following antigen internalisation, linking autophagy to the antigen-processing and presentation stages downstream of the phagocytic events (Dooley *et al.*, 2014; Florey *et al.*, 2015; Martinez *et al.*, 2015). While I have shown that phagocytosis of the anti-IgM-coated beads occurs within 3 hours, autophagy marker expression levels are very low at this time point. Antigen processing and presentation has been previously shown to occur in B cells at 2 hours following BCR stimulation (Martinez-Riano *et al.*, 2018). In addition, a role for non-canonical autophagy in maintaining B cell homeostasis during germinal centre formation has been indicated in other work (Martinez-Martin *et al.*, 2017), with the GC microenvironment being important in generation of B cell memory

Chapter 5 : Antigen presentation from anti-IgM-coated beads in CLL cells

5.1 Introduction and Aims

Results described to this point have demonstrated that anti-IgM-coated beads can (i) induce signalling leading to increased autophagy and (ii) be internalised via a signalling and actin-polymerisation-dependent pathway in CLL cells. However, the functional consequences of BCR-induced autophagy in CLL cells remain unclear. Therefore, the goal of the first series of experiments described in this chapter was to perform an RNA-Seq experiment to examine and characterise the effects of autophagy inhibition on gene expression in CLL cells, in the presence or absence of sIgM stimulation. RNA-seq was selected as an approach since it is unbiased, and therefore has potential to identify responses without an *a priori* rationale. Results were analysed using bioinformatical tools to identify pathways that were regulated in response to sIgM stimulation and/or autophagy inhibition.

A striking finding from this RNA-Seq experiment was that sIgM stimulation strongly engaged pathways linked to antigen presentation in CLL cells, including upregulation of MHC-II and CIITA, calreticulin and calnexin. Whilst previous studies have demonstrated that the tumour microenvironment can support CLL cell survival through induction of anti-apoptotic signals (Burger *et al.*, 2009), it is unclear which molecular mechanisms support the proliferation of CLL cells *in vivo*. Thus, presentation of antigen to helper T cells via MHC-II may be one mechanism by which CLL cells can receive T-cell help and, via cell surface receptors such as IL4R and CD40, this can promote CLL cell proliferation and survival (Aguilar-Hernandez *et al.*, 2016; van Attekum *et al.*, 2017). CLL cells are capable of presenting antigens internalised via the BCR and other cell surface receptors to helper T cells and CLL patients contain cognate T-helper cell clones (Os *et al.*, 2013). Engagement of T-cell help results in increased CLL cell proliferation *in vitro* and *in vivo* where CD4+ (but not CD8+) T-cells are required for CLL cell proliferation in patient-derived xenografts (PDX) (Os et al., 2013; Bagnara et al., 2011). Therefore, antigen presentation via MHC-II and subsequent T-cell help may be an important driver of CLL cell accumulation and a potential therapeutic target.

Importantly, various canonical and non-canonical forms of autophagy, including LAP, contribute to MHC-II antigen presentation (Strawbridge and Blum, 2007; Crotzer and Blum, 2009), including in normal B cells (Zhou *et al.*, 2005) (

Figure 49). LAP, or other forms of non-canonical autophagy, may be especially important as routes for the processing and presentation of particulate antigens. Although it is not known whether CLL cells have the capacity to present particulate antigens, as previous experiments were restricted to

soluble BCR ligands (Os *et al.*, 2013), other work in B cells has shown antigen extraction at the immune synapse utilising phagocytosis of particulate antigen to be essential in producing a strong GC response, and high affinity antibody generation (Martinez-Riano *et al.*, 2018). Autophagy has also been suggested to contribute to cross-presentation of endogenous antigen (Li *et al.*, 2008; Martinez *et al.*, 2011; Heckmann *et al.*, 2017; Koster *et al.*, 2017; Lamprinaki *et al.*, 2017). Where internalisation does not occur, other mechanisms for antigen extraction can be utilised by B cells (Spillane and Tolar, 2017), including release of lysosomal contents into the extracellular milieu, allowing liberation of "free" antigen which can then be internalised or loaded directly into surface MHC-II molecules (Yuseff *et al.*, 2011). Therefore, the goal of the second series of experiments presented in this chapter was to determine whether CLL cells were capable of obtaining antigen from anti-IgM-coated beads for presentation via MHC-II, and the effect of inhibition of autophagy (as well as BCR-associated kinases) on CLL cell antigen presentation.

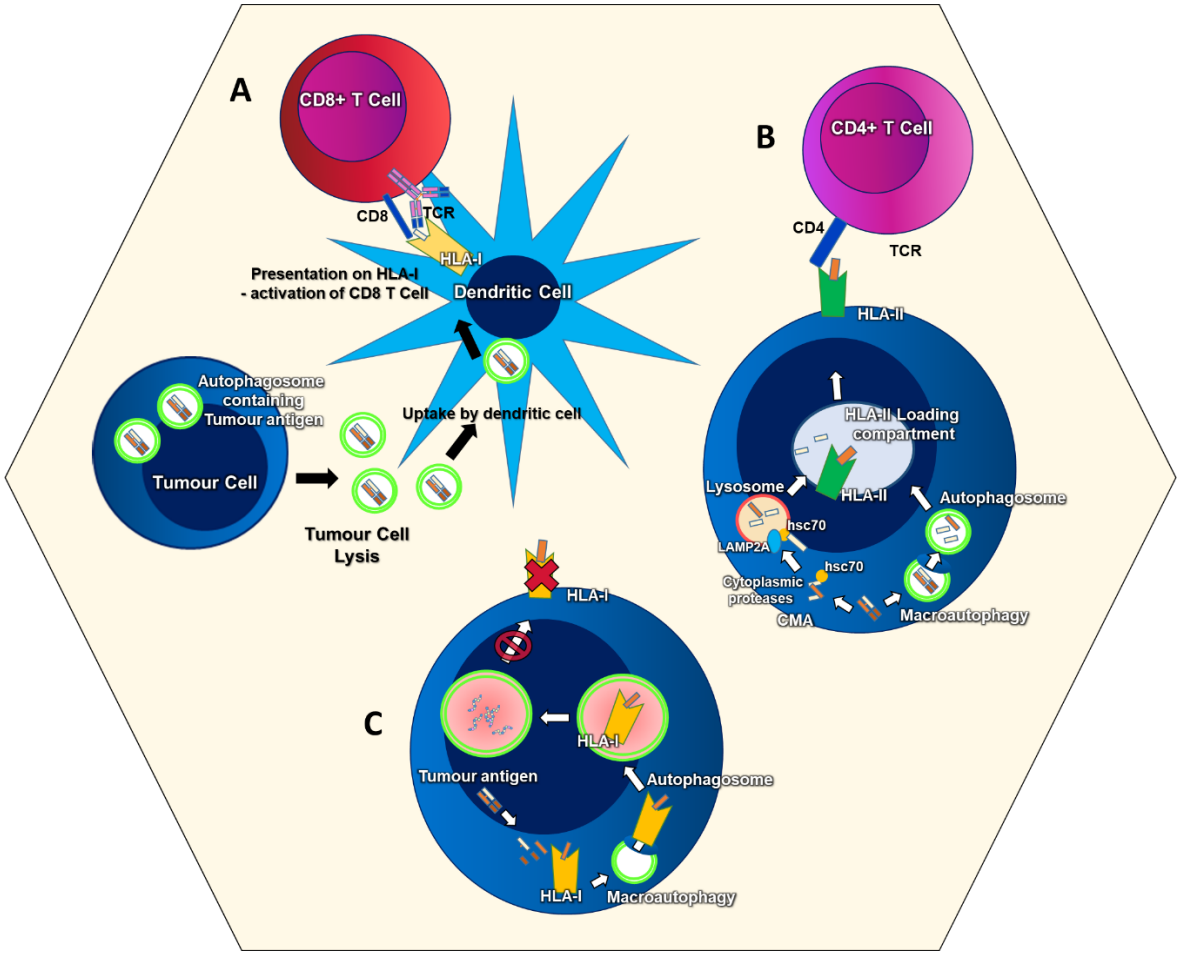

Figure 49. Example of three proposed mechanisms of autophagy involvement in class I and II antigen presentation

(A) Autophagy is often upregulated in tumour cells, and extracellular autophagosomes containing endogenous antigen have a proposed to have a roll in MHCI mediated antigen processing by dendritic cells. (B) Both macroautophagy and chaperone mediated autophagy can play a role in mediating antigen processing and delivery to the HLA loading compartment. (C) Autophagy may also negatively regulate antigen processing and presentation via MHCI by degrading tumour antigen following lysosomal fusion, preventing processing and loading.

.

The specific aims of the experiments were:

- To perform and analyse an RNA-Seq experiment to characterise effects of anti-IgM (±VPS34-IN1) on CLL cell gene expression
- To determine whether CLL cells are capable of presenting particulate antigen
- To investigate effects of inhibitors of autophagy and signalling kinases on CLL cell MHC-II antigen presentation

5.2 RNA-seq analysis of anti-IgM and VPS34-IN1-regulated gene expression in CLL cells

5.2.1 Experimental overview and initial bioinformatic analysis

RNA-seq was performed using 6 CLL samples (**Table 8**). These samples included both U-CLL and M-CLL, but all were classified as anti-IgM-responsive based on analysis of calcium flux. Each sample was treated with the VPS34 inhibitor, VPS34-IN1, or DMSO for 1 hour, and then with anti-IgM- or control antibody-coated beads. The experiment was performed using the VPS34 inhibitor VPS34-IN1 (at 3 μM) as this compound appeared to be a more potent VPS34 inhibitor than SAR405, since at comparable concentrations it showed slightly better inhibition of LC3B-II (data not shown) and was highly effective at inhibiting both basal and BCR driven LC3B-II expression at this concentration without any clear effects on cell viability or BCR signalling *per se* (Section 3.3.2*)*. RNA was isolated at two time points to allow analysis of relatively early (6 hr) and later (24 hr) events. The analysis was performed using PBMCs to minimise potential artefacts associated with the isolation of CLL cells and the samples were therefore selected to contain a relatively high proportion of CLL cells based on analysis of CD5 and CD19.

Table 8. Details of samples used for RNA-Seq

Sample	*IGHV* mutation status[a]	*IGHV* gene and allele	Tumour population (%)[b]	sIgM (MFI)	sIgM iCa^{2+} Signalling Capacity (%)[c]
87B	M	IGHV2-5*02 F	95	12	36
132A	M	IGHV4-4*07 F	88	25	18
523G	M	IGHV3-72*01 F	96	23	13
1384	M	IGHV3-33*01 F, or IGHV3-33*06 F	84	82	21
1427	U	IGHV1-8*01 F	95	1268	83
1431	U	IGHV3-21*01 F, or IGHV3-21*02	97	50	76

[a]M, mutated; U, unmutated. [b]Percentage of CD5/CD19 positive cells amongst lymphocytes. [c]Percent responding cells by iCa^{2+} analysis (Mockridge *et al.*, 2007). Data was provided by the Southampton Tumour Bank.

RNA-Seq was performed by the Oxford Genomics Centre using an Illumina platform and data quality control, mapping of reads and identification of differentially expressed genes was performed by Dr Dean Bryant, a highly experienced bioinformatician. Bryant also performed multidimensional scaling (MDS) analysis and prepared volcano plots and heat maps for initial visualisation of the data. I interpreted the data and performed Ingenuity Pathway Analysis (IPA) to identify regulated pathways.

MDS was performed to analyse effects of the different variables on gene expression. Consistent with the known heterogeneity of CLL, the gene expression profiles clustered strongly according to the individual patient sample (**Figure 50**), but not time point (6 versus 24 hours), drug treatment (DMSO versus VPS34-IN1) or stimulation (anti-IgM coated beads versus control beads) (data not shown). Due to the predominant influence of sample, data was first processed to calculate fold changes in expression for each gene between conditions separately for each sample. These fold changes were then compared to identify regulated genes.

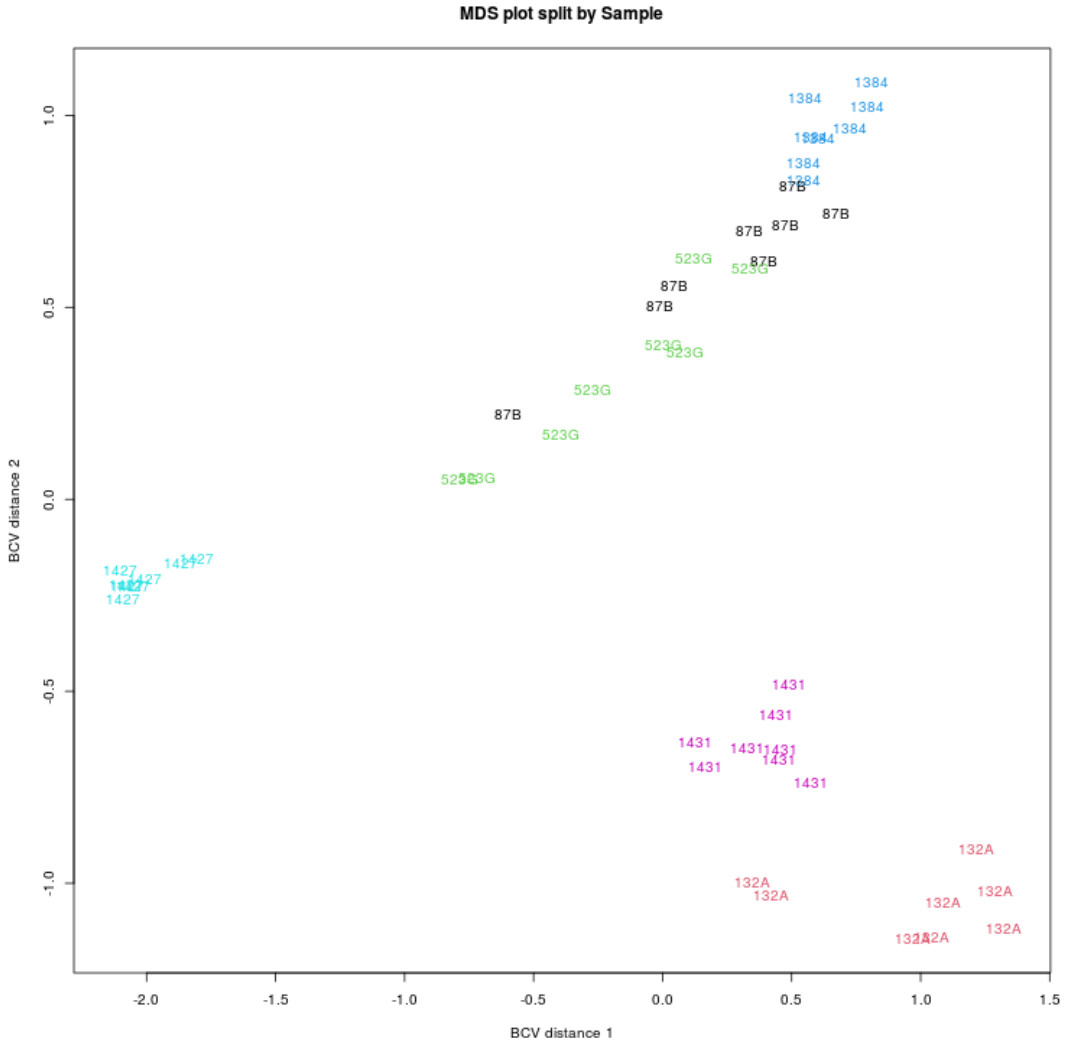

Figure 50. MDS analysis of gene expression profiles by sample.
Figure shows results of MDS analysis of the 48 RNA-seq profiles obtained from 6 CLL samples, each treated with bead-immobilised anti-IgM or control antibody in the presence of VPS34-IN1 (3 μM) or DMSO, for 6 or 24 hours. Profiles are annotated by sample identification and show close clustering. MDS plots were provided by Dr DJ Bryant.

A heat map was generated to visualise the overall effects of the different conditions on gene expression. This suggested that the predominant regulator in this experiment was anti-IgM with evidence for substantial induction and repression of gene expression (**Figure 51**).

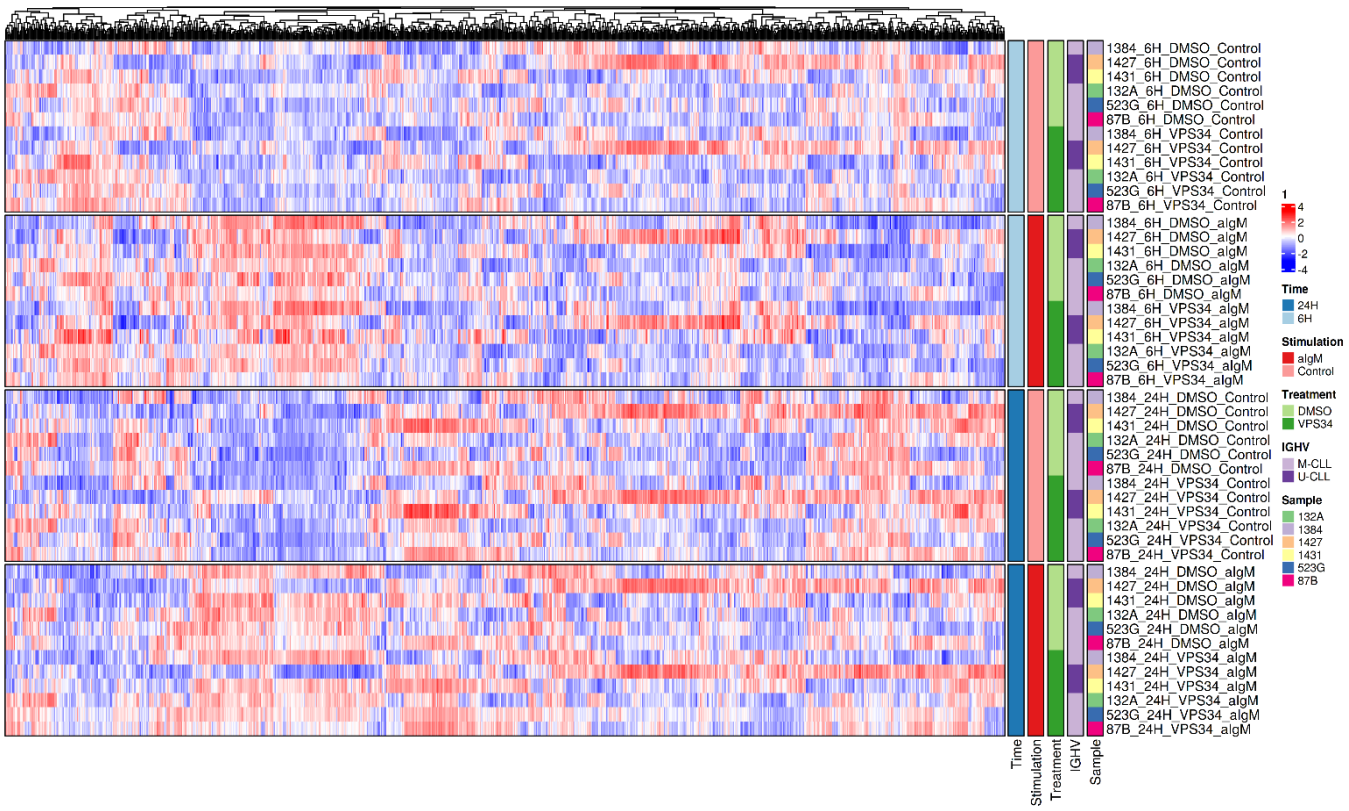

Figure 51. Heat map showing effect of various conditions on gene expression
The heatmap (provided by Dr DJ Bryant) shows supervised hierarchical clustering for the 1,000 most differentially expressed genes across all samples.

5.2.2 Anti-IgM-regulated gene expression

I next investigated the effect of anti-IgM on gene expression by analysing genes that were differentially expressed between samples treated with control antibody/DMSO and anti-IgM/DMSO, at both the 6- and 24-hour time points (**Figure 52**). Using cut-offs of $\log_2$FC >1.0 and FDR <0.05, there were 995 and 1,085 genes that were significantly upregulated in anti-IgM-treated cells at 6 and 24 hours, respectively. Using cut-offs of $\log_2$FC <-1.0 and FDR <0.05, there were 2,473 and 2,052 genes that were significantly down-regulated in anti-IgM-treated cells at 6 and 24 hours, respectively. Therefore, anti-IgM has a substantial effect on the gene expression profile of CLL cells. A full list of significantly regulated genes is provided in the Appendix.

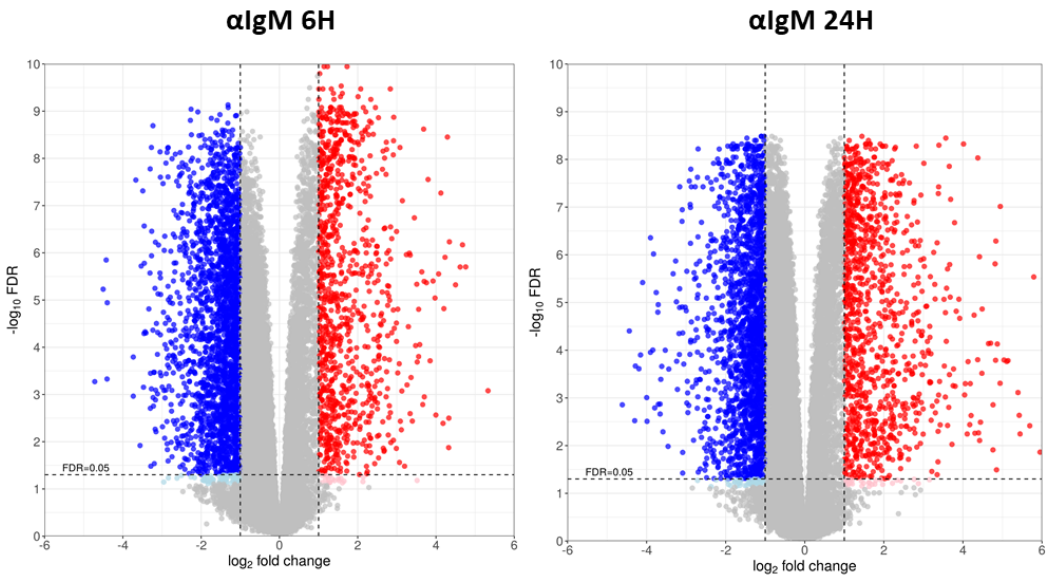

Figure 52. Volcano plots showing effect of anti-IgM on gene expression at 6 and 24 hours. Each data point represents an individual gene and is coloured red if significantly upregulated (log_2FC >1.0; FDR <0.05) or blue if significantly downregulated (log_2FC <-1.0; FDR <0.05) by anti-IgM. All other genes are coloured grey.

I used the canonical pathway function within IPA to probe the nature of the genes/pathways that were regulated by anti-IgM. In this analysis, significantly regulated (query) genes are compared against curated gene lists to identify pathways which have a greater than expected overlap (ie, enrichment). The software reports a Benjamini-Hochberg method corrected p-value for each pathway. This is a measure of the statistical significance of the overlap of query genes within the pathway and is typically provided as a -log value so high values reflect greater statistical significance. The software also reports a ratio (the number of query genes in a given pathway divided by the total number of genes that make up that pathway) and an activation z-score which indicates the activation state of the canonical pathway (positive for activated, negative for inhibited). Finally, RNAs present in the query gene list that overlap with the canonical pathway are provided ("molecules").

At 6 hours, the top canonical pathway identified for the anti-IgM-induced genes was the "Antigen Presentation Pathway" (**Table 9**). Enrichment of this pathway was driven by regulation of expression of MHC-II molecules, as well as other key regulators of antigen presentation, including CIITA. Other enriched pathways of note were "PD-1, PD-L1 Cancer immunotherapy pathway", "B cell development" and "Th1 and Th2 Activation Pathway". However, it should be noted that enrichment within these pathways was also largely driven by regulation of MHC-II molecules which are shared members of these pathways. Analysis also identified the "tRNA Charging" pathway, consistent with the observation that anti-IgM drives mRNA translation in CLL cells (Yeomans *et al.*, 2016).

Table 9. Top-10 IPA canonical pathways enriched in the anti-IgM-induced transcriptional response at 6 hours.

Rank	Ingenuity Canonical Pathway[a]	-log p-value	Ratio	z-score[b]	Molecules
1	Antigen Presentation Pathway	10.7	0.359	NaN	CALR, CANX, CIITA, HLA-DOA, HLA-DPA1, HLA-DPB1, HLA-DQA1, HLA-DQA2, HLA-DQB1, HLA-DQB2, HLA-DRA, HLA-DRB1, HLA-DRB5, PDIA3
2	PD-1, PD-L1 Cancer Immunotherapy	8.47	0.179	-1.604	BCL2L1, CD274, CD80, HLA-DOA, HLA-DPA1, HLA-DPB1, HLA-DQA1, HLA-DQA2, HLA-DQB1, HLA-DQB2, HLA-DRA, HLA-DRB1, HLA-DRB5, IL2RB, PDCD1, STAT5A, TGFB2, TNF, TNFRSF1B
3	MSP-RON Signalling in Macrophages	7.73	0.162	-1.886	CIITA, CREB5, HLA-DOA, HLA-DPA1, HLA-DPB1, HLA-DQA1, HLA-DQA2, HLA-DQB1, HLA-DQB2, HLA-DRA, HLA-DRB1, HLA-DRB5, KLK1, KLK2, NFKB1, REL, SOCS3, STAT3, TNF
4	Sirtuin Signalling Pathway	7.51	0.106	0.447	DOT1L, ESRRA, GADD45A, GADD45B, GADD45G, LDHA, MAPK12, MAPK6, MYC, MYCN, NAMPT, NFKB1, PCK2, PGAM1, POLR1A, POLR1B, POLR1C, PPIF, REL, RRP9, STAT3, TIMM13, TIMM23, TIMM8A, TIMM9, TNF, TOMM20L, TOMM40, TUBA1B, TUBA1C, VDAC1
5	tRNA Charging	7.28	0.282	3.317	AARS1, EARS2, FARSB, GARS1, IARS1, NARS2, SARS1, TARS1, VARS1, WARS1, YARS1
6	Th1 and Th2 Activation Pathway	6.91	0.128	NaN	BHLHE41, CD274, CD80, GFI1, HLA-DOA, HLA-DPA1, HLA-DPB1, HLA-DQA1, HLA-DQA2, HLA-DQB1, HLA-DQB2, HLA-DRA, HLA-DRB1, HLA-DRB5, IL2RB, IL6R, NFIL3, NFKB1, SOCS3, STAT3, STAT5A, TNFRSF4
7	B cell Development	6.8	0.256	NaN	CD80, HLA-DOA, HLA-DPA1, HLA-DPB1, HLA-DQA1, HLA-DQA2, HLA-DQB1, HLA-DQB2, HLA-DRA, HLA-DRB1, HLA-DRB5
8	Purine Nucleotides De Novo Biosynthesis II	6.19	0.545	2.449	ADSL, ATIC, GART, PAICS, PFAS, PPAT
9	Th1 Pathway	6.01	0.139	3.051	CD274, CD80, HLA-DOA, HLA-DPA1, HLA-DPB1, HLA-DQA1, HLA-DQA2, HLA-DQB1, HLA-DQB2,

					HLA-DRA, HLA-DRB1, HLA-DRB5, IL6R, NFIL3, NFKB1, SOCS3, STAT3
10	Role of PKR in Interferon Induction and Antiviral Response	5.99	0.132	-0.500	CYCS, DNAJC3, HSP90AA1, HSP90AB1, HSP90B1, HSPA5, HSPA8, HSPA9, MAP2K3, MAPK12, NFKB1, NFKBIE, NLRP6, NPM1, PDGFA, REL, STAT3, TNF

[a]IPA canonical pathway analysis was performed using genes that were significantly up-regulated ($log_2FC > 1.0$; FDR<0.05) at 6 hours in anti-IgM-treated cells. [b]NaN, no activity pattern predicted. Full analysis is provided in the Appendix.

At 24 hours, the "Antigen Presentation Pathway" was retained amongst the top-10 canonical pathways but was ranked less highly (at 5) compared to the 6-hour data (**Table 10**). Interestingly, 2 of the top 3 ranked enrichments at this time (with the "BAG2 Signaling Pathway" and "Inhibition of ARE-Mediated mRNA Degradation Pathway") were largely driven by regulation of proteosome subunits (eg, PSMB2, PSMB3) and may therefore also relate to antigen presentation as the proteosome is important for generation of peptides for MHC-I presentation (and cross-presentation to MHC-II). Pathway analysis at 24 hours identified strong regulation of cholesterol biosynthesis (4 of the top-10 canonical pathways), consistent with the observation that anti-IgM stimulation of CLL cells drives metabolic reprogramming, including expression of genes encoding cholesterol biosynthetic enzymes (Lemm, E et. al, Submitted 2021).

Table 10. Top-10 IPA canonical pathways enriched in the anti-IgM-induced transcriptional response at 24 hours.

Rank	Ingenuity Canonical Pathway[a]	-log p-value	Ratio	z-score[b]	Molecules
1	BAG2 Signaling Pathway	11.2	0.25	1.667	CASP3, CDKN1A, HSP90AA1, HSPA2, HSPA5, HSPA8, HSPA9, MYC, NFKB1, PSMB2, PSMB3, PSMB5, PSMB6, PSMB7, PSMC1, PSMC2, PSMC3, PSMD1, PSMD11, PSMD14, REL
2	Superpathway of Cholesterol Biosynthesis	10.8	0.448	3.606	ACAT2, CYP51A1, DHCR24, DHCR7, FDFT1, HMGCR, HMGCS1, IDI1, MSMO1, MVD, MVK, NSDHL, SQLE
3	Inhibition of ARE-Mediated mRNA Degradation Pathway	8.5	0.155	2.673	EXOSC4, EXOSC5, LTA, MAPK12, MAPK6, PRKAR1B, PRKAR2B, PSMB2, PSMB3, PSMB5, PSMB6, PSMB7, PSMC1, PSMC2, PSMC3, PSMD1, PSMD11, PSMD14, TNF, TNFRSF1B, TNFSF14, TNFSF15, TNFSF4, YWHAE, YWHAG
4	Sirtuin Signaling Pathway	8.48	0.12	0	ATP5F1B, ATP5MC1, ATP5PF, GADD45B, GADD45G, LDHA, MAPK12, MAPK6, MYC, MYCN, NAMPT, NDUFA4L2, NDUFAB1, NDUFB3, NFKB1, NQO1, PCK2, PGAM1, PGK1, PPIF, REL, RRP9, SLC25A5, SOD1, SREBF1, TIMM13, TIMM23, TNF, TOMM22, TOMM40, TOMM40L, TP73, TUBA1B, TUBA1C, VDAC1
5	Antigen Presentation Pathway	7.81	0.308	NaN	CALR, CANX, CD74, HLA-DPA1, HLA-DQA1, HLA-DQB1, HLA-DRA, HLA-DRB1, HLA-DRB5, PDIA3, PSMB5, PSMB6
6	Crosstalk between Dendritic Cells and Natural Killer Cells	7.18	0.187	3.464	ACTB, ACTG1, CAMK2B, CCR7, CD80, CD83, CSF2, FSCN1, HLA-DRA, HLA-DRB1, HLA-DRB5, IL2RB, LTA, NFKB1, REL, TNF, TNFRSF1B
7	FAT10 Signaling Pathway	6.79	0.232	NaN	PSMB2, PSMB3, PSMB5, PSMB6, PSMB7, PSMC1, PSMC2, PSMC3, PSMD1, PSMD11, PSMD14, SQSTM1, TNF
8	Cholesterol Biosynthesis I	6.75	0.538	2.646	CYP51A1, DHCR24, DHCR7, FDFT1, MSMO1, NSDHL, SQLE
9	Cholesterol Biosynthesis II (via 24,25-dihydrolanosterol)	6.75	0.538	2.646	CYP51A1, DHCR24, DHCR7, FDFT1, MSMO1, NSDHL, SQLE
10	Cholesterol Biosynthesis III (via Desmosterol)	6.75	0.538	2.646	CYP51A1, DHCR24, DHCR7, FDFT1, MSMO1, NSDHL, SQLE

[a]IPA canonical pathway analysis was performed using genes that were significantly up-regulated ($log_2FC>1.0$; FDR<0.05) at 24 hours in anti-IgM-treated cells. [b]NaN, no activity pattern predicted. Full analysis is provided in the Appendix.

A similar analysis was performed to probe the pathways associated with the genes that were downregulated by anti-IgM at 6 and 24 hours (**Table 11** and **Table 12**). Overall, the downregulated gene expression signature was less strongly associated with any of the canonical pathways as the -log (p-values) for even the top-10 pathways were very modest compared to the pathways associated with anti-IgM-induced genes. Moreover, the relevance of the identified pathways was not obvious as they often related to non-B cell pathways (eg, "Cardiac Hypertrophy Signalling", "Axonal Guidance Signaling" and "Hepatic Fibrosis Signaling Pathway"). One possible exception to this was the "Phagosome Formation" pathway which was predicted to be downregulated (negative z-score) at 6 hours.

Table 11. Top-10 IPA canonical pathways enriched in the anti-IgM-down-regulated transcriptional response at 6 hours.

Rank	Ingenuity Canonical Pathway[a]	-log p-value	Ratio	z-score[b]	Molecules
1	Leukotriene Biosynthesis	3.7	0.429	-2.236	ALOX5, DPEP2, DPEP3, GSTM4, LTC4S, MGST2
2	Cardiac Hypertrophy Signaling (Enhanced)	3.5	0.11	-5.642	ACVR1C, ADCY4, AKT3, ATP2A3, BMPR2, CACNA1C, CACNA1F, CACNA2D2, CACNB4, CTF1, EDN1, FGF17, FGF22, FZD2, GDPD1, GDPD3, GNB5, GNG7, HDAC11, HDAC5, HDAC7, IL10RA, IL10RB, IL15, ITGA10, ITGA2, ITGAM, ITGB4, ITGB7, ITPR2, LTB, MAP2K6, MAP3K1, MAP3K3, MAPK3, MPPE1, PDE4A, PDE6C, PDE6G, PDE7B, PIK3CD, PLCB2, PLCD1, PLCD3, PLCG2, PLCH2, PRKCE, RASD1, RPS6KA5, RRAS, SMO, TG, TNFSF10, TNFSF12, TNFSF13, TNFSF13B, WNT10A, WNT2B, WNT3
3	Axonal Guidance Signaling	3.46	0.111	NaN	ABLIM2, ADAM19, ADAM28, ADAM29, ADAM8, ADAMTS4, ADAMTS6, ADAMTS7, AKT3, ARHGEF6, CXCR4, EPHA4, EPHB2, EPHB6, ERAP2, FZD2, GDF7, GNAZ, GNB5, GNG7, HERC2, ITGA10, ITGA2, ITGAM, ITGB4, ITGB7, LIMK2, MAPK3, NTN5, PGF, PIK3CD, PLCB2, PLCD1, PLCD3, PLCG2, PLCH2, PLXNA2, PLXND1, PRKCE, PTCH1, RASD1, RND1, ROBO3, RRAS, SEMA3B, SEMA4B, SEMA4F, SLIT1, SMO,

					SRGAP1, SRGAP2, STK36, TUBB4A, WNT10A, WNT2B, WNT3
4	Hepatic Fibrosis Signaling Pathway	3.12	0.112	-5.191	ACVR1C, AKT3, BMPR2, CACNA1C, CACNA1F, CACNA2D2, CACNB4, CCDC88A, CDKN1B, COL11A2, COL18A1, COL1A1, CREB3L4, CSNK1G2, EDN1, FOXO4, FZD2, IL1RAP, ITGA10, ITGA2, ITGAM, ITGB4, ITGB7, LEPR, MAP2K6, MAPK3, MYLK, MYLK3, NCF1, PGF, PIK3CD, PLCG2, PRKCE, PTCH1, RASD1, RHOH, RND1, RND2, RRAS, SMO, TCF7L1, TF, TIRAP, TLR4, WNT10A, WNT2B, WNT3
5	Senescence Pathway	3.12	0.121	-3.536	ACVR1C, AKT3, ATM, BMPR2, CACNA1C, CACNA1F, CACNA2D2, CACNB4, CAPN3, CAPN5, CAT, CBX7, CBX8, CCNE2, CDC25B, CDKN1B, ELF2, ELK3, FOXO4, ITPR2, MAP2K6, MAPK3, PCGF2, PDK2, PDK4, PHF1, PIK3CD, PPP2R3B, PPP2R5B, RASD1, RBL2, RPS6KA5, RRAS, SMAD6, SMAD9, YPEL3
6	Phagosome Formation	3.09	0.102	-8.367	ACKR3, AKT3, AP1G2, CCR2, CD14, CELSR2, CNR2, CYSLTR1, FCAR, FCGR2B, FCGR2C, FPR1, FPR3, FZD2, GAB2, GABBR1, GPLD1, GPR137C, GPR152, GPR155, GPR174, GPR18, GPR34, GPR63, IGHA1, IGHG1, IGHG2, IGHG4, ITGA10, ITGA2, ITGAM, ITGB4, ITGB7, ITPR2, LIMK2, LPAR3, LPAR5, MAP2K6, MAPK3, MYH11, MYH7B, MYLK, MYLK3, MYO5C, OPRD1, OPRL1, OXTR, PIK3CD, PIP5KL1, PLA2G4B, PLA2G6, PLCG2, PLD2, PLD3, PRKCE, PTK2B, RAPGEF3, RASD1, RRAS, S1PR1, S1PR4, SLC52A1, SMO, TBXA2R, TLN2, TLR1, TLR4, TLR6, TLR9, VIPR1
7	Molecular Mechanisms of Cancer	3.05	0.11	NaN	ADCY4, AKT3, APAF1, APH1B, ARHGEF3, ARHGEF6, ATM, BMPR2, CASP10, CCNE2, CDC25B, CDK19, CDKN1B, CDKN2D, FZD2, GAB1, GAB2, GNAZ, GNB5, GNG7, HDAC11, HDAC5, HDAC7, ITGA10, ITGA2, ITGAM, ITGB4, ITGB7, MAP2K6, MAPK3, PIK3CD, PLCB2, PRKCE, PTCH1, RAPGEF3, RASD1, RASGRF1, RBL2, RHOH, RND1, RND2, RRAS, SMAD6, SMAD9, SMO, STK36, WNT10A, WNT2B, WNT3
8	UVA-Induced MAPK Signaling	2.96	0.163	-3	ATM, MAPK3, PARP10, PARP3, PARP4, PARP8, PIK3CD, PLCB2, PLCD1, PLCD3, PLCG2, PLCH2, RASD1, RPS6KA5, RRAS, SMPD3

9	Sphingosine-1-phosphate Signaling	2.9	0.153	-3	ACER2, ADCY4, AKT3, CASP10, MAPK3, PIK3CD, PLCB2, PLCD1, PLCD3, PLCG2, PLCH2, PTK2B, RHOH, RND1, RND2, S1PR1, S1PR4, SMPD3
10	Cellular Effects of Sildenafil (Viagra)	2.84	0.141	NaN	ADCY4, CACNA1C, CACNA1F, CACNA2D2, CACNB4, GUCY2C, ITPR2, KCNH2, KCNN4, MYH11, MYH7B, MYLK, MYO5C, PDE4A, PLCB2, PLCD1, PLCD3, PLCG2, PLCH2, PPP1R12B, PRKG2

[a]IPA canonical pathway analysis was performed using genes that were significantly down-regulated ($log_2FC<-1.0$; FDR<0.05) at 6 hours in anti-IgM-treated cells. [b]NaN, no activity pattern predicted. Full analysis is provided in the Appendix.

Table 12. Top-10 IPA canonical pathways enriched in the anti-IgM-down-regulated transcriptional response at 24 hours.

Rank	Ingenuity Canonical Pathway[a]	-log p-value	Ratio	z-score[b]	Molecules
1	Sperm Motility	5.49	0.126	-3.606	AATK, CACNA1I, CLK1, CLK4, CNGA4, EPHA4, FER, FGFR4, FLT1, FLT3LG, GNAL, GNAO1, GNAZ, GNB5, GNG7, INSR, LMTK3, MAP2K6, PDE2A, PDE4B, PDE4D, PLA2G4B, PLA2G6, PLAAT4, PLCD3, PLCG2, PLCH1, PLCH2, PRKCE, PRKCH, PRKG2, SLC16A10
2	Hepatic Fibrosis / Hepatic Stellate Cell Activation	4.6	0.129	NaN	COL11A2, COL18A1, COL28A1, COL4A3, COL4A4, COL5A2, COL6A2, COL6A3, COL6A6, COL9A3, CXCR3, EDN1, FLT1, IFNAR2, IGFBP3, IL10, IL10RA, IL18RAP, IL1RAP, MYH7B, MYO5C, SMAD3, TGFA, TIMP2, TLR4
3	cAMP-mediated signaling	4.23	0.118	-3.138	ADCY4, ADORA2A, ADORA2B, CNGA4, CREM, DRD4, DUSP1, GDPD1, GDPD3, GNAL, GNAO1, MPPE1, OPRL1, PDE2A, PDE3B, PDE4B, PDE4D, PDE6C, PDE7B, PDE9A, PTGDR, PTGER2, RAPGEF3, RGS14, RGS2, S1PR1, VIPR1
4	tRNA Splicing	4.18	0.227	-3	GDPD1, GDPD3, MPPE1, PDE2A, PDE3B, PDE4B, PDE4D, PDE6C, PDE7B, PDE9A
5	Cardiac Hypertrophy Signaling (Enhanced)	4.02	0.0911	-5.864	ADCY4, ATP2A3, CACNA1F, CACNA2D2, CTF1, EDN1, FGFR4, FGFRL1, FZD4, GDPD1, GDPD3, GNB5, GNG7, HDAC10, HDAC7, IL10RA, IL10RB, IL11RA, IL18RAP, IL2RA, IL7R, ITGA2, ITGA4, LTB, MAP2K6, MAP3K1, MEF2B, MPPE1, PDE2A,

					PDE3B, PDE4B, PDE4D, PDE6C, PDE7B, PDE9A, PIK3R5, PLCD3, PLCG2, PLCH1, PLCH2, PRKCE, PRKCH, RASD1, TG, TNFSF8, WNT2B, WNT3, WNT7B, WNT9A
6	GP6 Signaling Pathway	4.01	0.142	-4	COL11A2, COL18A1, COL28A1, COL4A3, COL4A4, COL5A2, COL6A2, COL6A3, COL6A6, COL9A3, FYB1, GRAP2, LAMA5, PIK3R5, PLCG2, PRKCE, PRKCH, RASGRP2
7	CREB Signaling in Neurons	3.65	0.0864	-6.782	ACKR3, ADCY4, ADGRG1, ADORA2A, ADORA2B, BMP6, C5AR2, CACNA1F, CACNA1I, CACNA2D2, CCR6, CELSR2, CMKLR1, CX3CR1, DRD4, F2R, FGFR4, FLT1, FZD4, GNAL, GNAO1, GNAZ, GNB5, GNG7, GPR135, GPR152, GPR155, GPR171, GPR18, GPR183, GRIN2C, HCRTR1, INSR, LGR4, OPRL1, P2RY2, PIK3R5, PLCD3, PLCG2, PLCH1, PLCH2, PRKCE, PRKCH, PTGDR, PTGER2, RASD1, S1PR1, S1PR5, SHC3, SLC52A1, TGFA, VIPR1
8	Cardiac β-adrenergic Signaling	3.56	0.121	-2.496	ADCY4, ATP2A3, CACNA1F, CACNA2D2, GDPD1, GDPD3, GNAL, GNAO1, GNAZ, GNB5, GNG7, MPPE1, PDE2A, PDE3B, PDE4B, PDE4D, PDE6C, PDE7B, PDE9A, PPM1L, PPP2R3B
9	Human Embryonic Stem Cell Pluripotency	3.41	0.12	NaN	BMP6, FGFR4, FGFRL1, FZD4, GNAL, GNAO1, GNAZ, GNB5, GNG7, NOG, PIK3R5, S1PR1, S1PR5, SMAD3, SMAD6, TCF7L2, WNT2B, WNT3, WNT7B, WNT9A
10	Leukotriene Biosynthesis	3.3	0.357	-2	ALOX5, DPEP2, DPEP3, GSTM4, LTC4S

[a]IPA canonical pathway analysis was performed using genes that were significantly down-regulated ($log_2FC<-1.0$; FDR<0.05) at 24 hours in anti-IgM-treated cells. [b]NaN, no activity pattern predicted. Full analysis is provided in the Appendix.

Overall, this analysis demonstrated that anti-IgM had a profound effect on gene expression as it regulated expression of 1,000s of genes. More genes were down-regulated by anti-IgM than up-regulated but it was hard to discern a clear biological signature amongst the down-regulated response. By contrast, the induced signature was characterised by pathways related to both protein synthesis and metabolism, consistent with previous studies in CLL cells showing sIgM-mediated metabolic reprogramming (Vangapandu *et al.*, 2017)and induction of mRNA translation (Yeomans *et al.*, 2016). In addition, there was a striking regulation of the antigen presentation pathway.

Further probing of the effect of anti-IgM on antigen presentation was performed by generating heatmaps showing fold changes in expression induced by anti-IgM for selected genes based on KEGG pathways, with additional HLA groups added (**Figure 53**). This confirmed that anti-IgM increased expression of many RNAs encoding proteins in this pathway, including HLA-II molecules, CALR, CANX and CIITA, at both 6 and 24 hours. Interestingly, expression of MHC-I molecules was generally relatively unaffected, or modestly downregulated by anti-IgM.

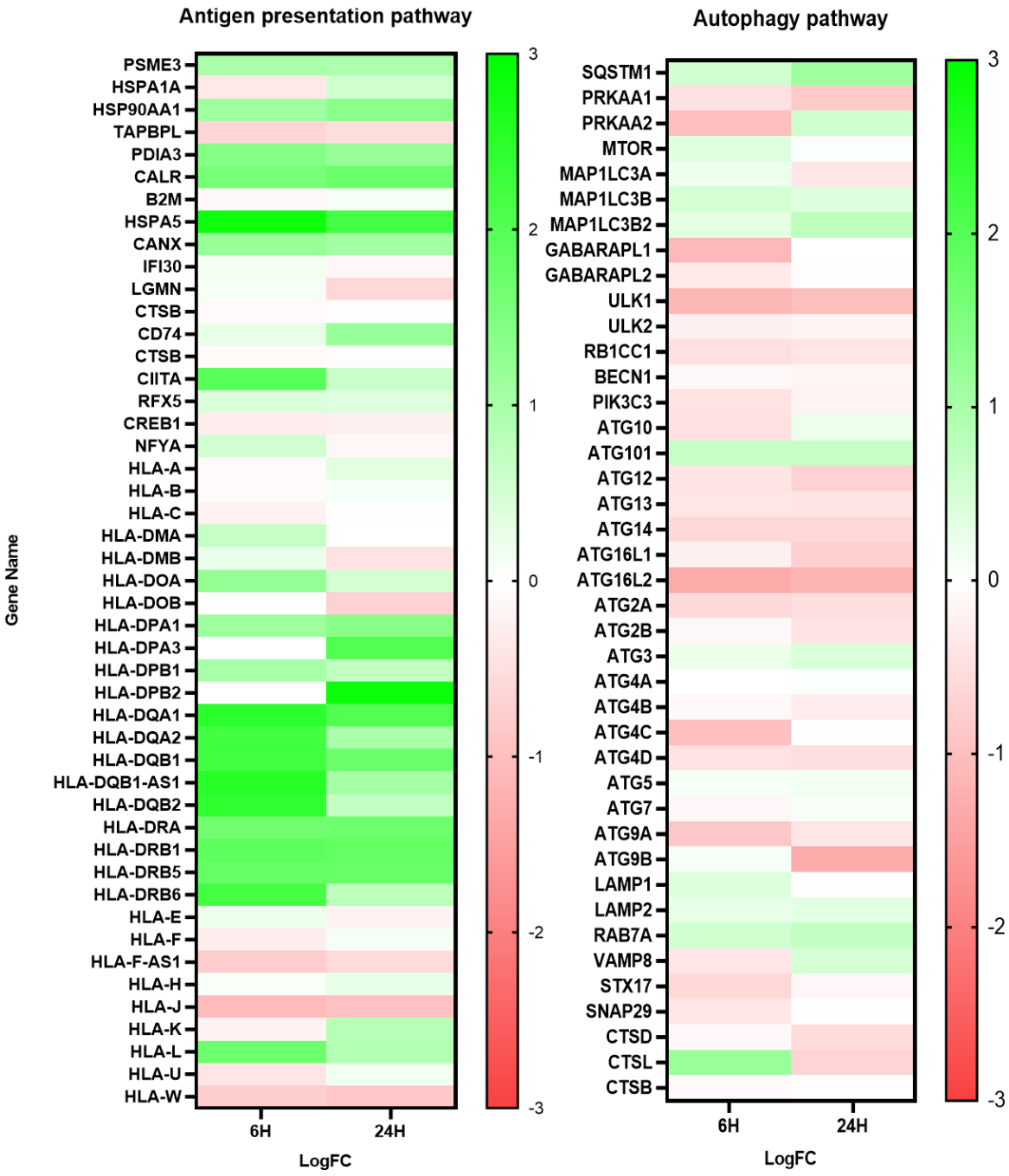

Figure 53. Effect of anti-IgM on antigen presentation and autophagy related genes

Heat-maps show log_2 fold changes induced by anti-IgM at 6 or 24 hours for the indicated genes (with scale bar on right). Genes are from the KEGG pathways Autophagy (hsa04140) and Antigen Processing and Presentation (hsa04612), with some additional HLA gene types included.

Although not identified as a regulated pathway by IPA, I also investigated effects of anti-IgM on the autophagy pathway (KEGG pathway hsa04140), since anti-IgM increased expression of autophagy-related proteins, including GABARAPL2, LC3B, and several ATG proteins (Section 3.2.2). However, there was very little evidence for induction of autophagy-related RNAs in this analysis, and several RNAs were actually modestly down-regulated at either time point (**Figure 53**). Therefore, anti-IgM-induced expression of autophagy-related proteins appears to be due to post-transcriptional regulation, at least at these time points.

5.2.3 Effect of VPS34-IN1 on gene expression

The effect of VPS34 inhibition in the absence of sIgM stimulation was analysed by comparing gene expression in control antibody/DMSO and control antibody/VPS34-IN1 treated samples. This demonstrated that, in contrast to anti-IgM, VSP34-IN1 had very modest effects on gene expression in CLL cells. VPS34-IN1 significantly up-regulated expression of 81 and 78 genes at 6 and 24 hours, respectively. VPS34-IN1 also significantly down-regulated expression of 61 and 97 genes at these time points (**Figure 54**). A full list of significantly regulated genes is provided in the Appendix.

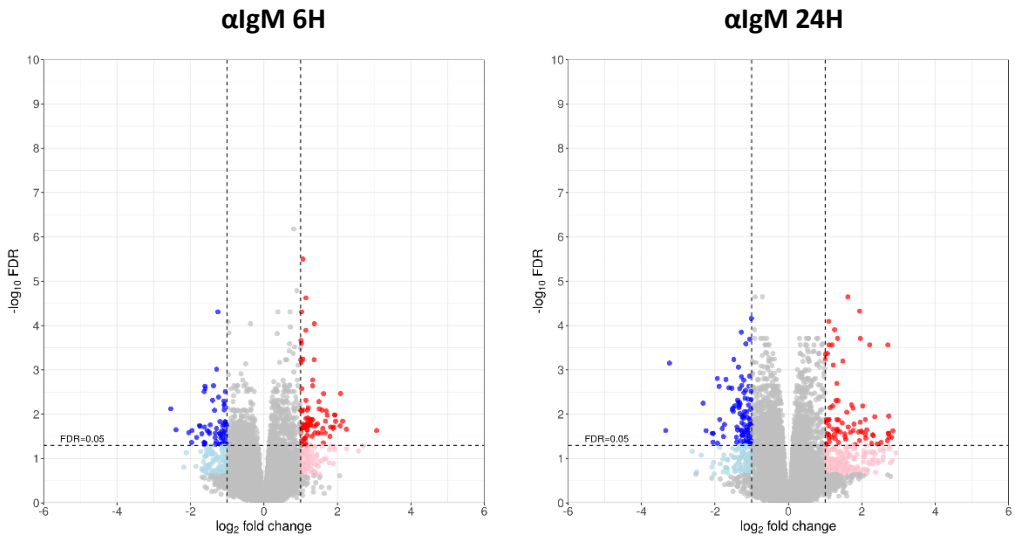

Figure 54. Volcano plots showing effect of VPS34-IN1 on gene expression at 6 and 24 hours
Each data point represents an individual gene and is coloured red if significantly upregulated (log_2FC >1.0; FDR <0.05) or blue if significantly downregulated (log_2FC <-1.0; FDR <0.05) by anti-IgM. All other genes are coloured grey.

Because of the relatively small number of regulated genes, IPA analysis of effects of VPS34-IN1 was performed, using genes which were significantly regulated at 6 or 24 hours independently of whether they were induced or repressed. Overall, evidence for pathway enrichment was modest, as the -log (p-values) and ratios obtained were low, especially at 24 hours (**Tables 13** and **14**).

Although the pathway "Phagosome formation" was enriched at 6 hours, the overlap between the VPS34-IN1 regulated signature and this pathway (indicated by the ratio) was very low (just 11 of the 689 total molecules in pathway were significantly regulated by VPS34-IN1). It was interesting to note, however, that regulation of a subset of chemokines/cytokines (CXCL2, CXCL3, CXCL8, CCL7) appeared as common drivers of the stronger enrichments observed at 6 hours ("Granulocyte Adhesion and Diapedesis", "Role of Hypercytokinemia/hyperchemokinemia in the Pathogenesis of Influenza", "Agranulocyte Adhesion and Diapedesis").

Table 13. Top-10 IPA canonical pathways enriched in the VPS34-IN1 regulated transcriptional response at 6 hours.

Rank	Ingenuity Canonical Pathway[a]	-log p-value	Ratio	z-score[b]	Molecules
1	Granulocyte Adhesion and Diapedesis	6.55	0.0476	NaN	ACKR3, C5AR1, CCL7, CSF3R, CXCL2, CXCL3, CXCL8, IL1R1, MMP11
2	Role of Hypercytokinemia/hyperchemokinemia in the Pathogenesis of Influenza	5.49	0.0698	1.633	CXCL3, CXCL8, IFIT3, MX1, PYCARD, RSAD2
3	Agranulocyte Adhesion and Diapedesis	5.1	0.0374	NaN	ACKR3, C5AR1, CCL7, CXCL2, CXCL3, CXCL8, IL1R1, MMP11
4	Role of Pattern Recognition Receptors in Recognition of Bacteria and Viruses	4.01	0.0385	NaN	C3AR1, C5AR1, CXCL8, PTX3, TLR5, TNFSF10
5	Role of IL-17A in Arthritis	3.82	0.0702	NaN	CCL7, CXCL3, CXCL8, MAP2K6
6	Hepatic Fibrosis / Hepatic Stellate Cell Activation	3.5	0.0309	NaN	COL19A1, COL5A2, CXCL3, CXCL8, IL1R1, MET
7	Phagosome Formation	3.39	0.016	0.905	ACKR3, C3AR1, C5AR1, CMKLR1, CX3CR1, FCER1G, HCAR3, ITGB8, MAP2K6, PLA2G7, TLR5
8	TREM1 Signaling	3.32	0.0519	2	CCL7, CXCL3, CXCL8, TLR5
9	Role of IL-17A in Psoriasis	2.72	0.143	NaN	CXCL3, CXCL8
10	HIF1α Signaling	2.52	0.024	-1.342	MAP2K6, MET, mir-135, MMP11, SLC2A5

[a]IPA canonical pathway analysis was performed using genes that were significantly regulated (log_2FC <-1.0/>1.0; FDR<0.05) at 6 hours in VPS34-IN1-treated cells. [b]NaN, no activity pattern predicted. Full analysis is provided in the Appendix.

Table 14. Top-10 IPA canonical pathways enriched in the VPS34-IN1 regulated transcriptional response at 24 hours.

Rank	Ingenuity Canonical Pathway[a]	-log p-value	Ratio	z-score[b]	Molecules
1	Crosstalk between Dendritic Cells and Natural Killer Cells	2.05	0.033	NaN	FSCN2, LTB, NCR3
2	Alanine Degradation III	2.03	0.5	NaN	GPT
3	Alanine Biosynthesis II	2.03	0.5	NaN	GPT
4	Apelin Muscle Signaling Pathway	1.68	0.0417	NaN	GNAI1, PPARGC1A
5	Reelin Signaling in Neurons	1.67	0.0238	NaN	ARHGEF10, MAP2K6, PDK4
6	Citrulline-Nitric Oxide Cycle	1.64	0.2	NaN	NOS1
7	GABA Receptor Signaling	1.63	0.0229	NaN	GABRB3, GNAI1, KCNH2
8	AMPK Signaling	1.57	0.0165	NaN	GNAI1, PFKFB1, PPARGC1A, PPM1J
9	Endocannabinoid Cancer Inhibition Pathway	1.53	0.021	NaN	GNAI1, MAP2K6, NOS1
10	Melatonin Signaling	1.35	0.0278	NaN	GNAI1, MAP2K6

[a]IPA canonical pathway analysis was performed using genes that were significantly regulated (log_2FC <-1.0/>1.0; FDR<0.05) at 24 hours in VPS34-IN1-treated cells. [b]NaN, no activity pattern predicted. Full analysis is provided in the Appendix.

Overall, RNA-seq and IPA demonstrated that, in contrast to anti-IgM, VPS34-IN1 has relatively little effect on gene expression in CLL cells. Importantly, there was no evidence for activation of transcriptional response pathways that are commonly associated with "off-target" effects of compounds, including production of reactive oxygen species (ROS) or NRF2 activation, ATP depletion (eg AMPK activation) and/or activation of stress responses (eg unfolded protein response), consistent with the idea that VPS34-IN1 is a relatively selective inhibitor.

It was interesting to note that several cytokines/chemokines were regulated by VPS34-IN1, as this is consistent with previous work showing that VPS34 inhibition (using chemical inhibitors of genetic ablation) increases pro-inflammatory chemokine/cytokine expression in melanoma cells, and that this leads to improved responses to immunotherapy *in vivo* (Noman *et al.*, 2020). VPS34-mediated cytokine regulation has also been described in dendritic cells (Parekh *et al.*, 2017), T cells (McLeod *et al.*, 2011),(Yang *et al.*, 2021) and macrophages (G.Yang et al., 2020). Since I used PBMCs in my analysis, this raised the question of what cells might increase expression of these chemokines/cytokines in response to VPS34-IN1. In contrast to anti-IgM, which can only target sIgM-expressing B cells, responses to VPS34-IN1 could be a consequence of effects on non-CLL cells in the samples.

To address this possibility, I correlated the logFC in gene expression induced by VSP34-IN1 with the proportion of CLL cells in the sample, corresponding to the percentage of CD5/CD19 co-expressing cells (**Figure 55**). This was performed for CCL7, CXCL2 and CXCL3, and also IL1R1, which were all strongly induced in VPS34-IN1-treated samples. Although the number of samples was too small for statistical analysis, regulation of these genes was either unrelated to (CXCL2, IL1R1) or seemed to be positively correlated with the proportion of CLL cells in the sample (CCL7, CXCL3)(**Figure 55**). This suggests that VPS34-IN1-regulated cytokine/chemokine expression is not due to an effect of drug on non-CLL cells within the sample.

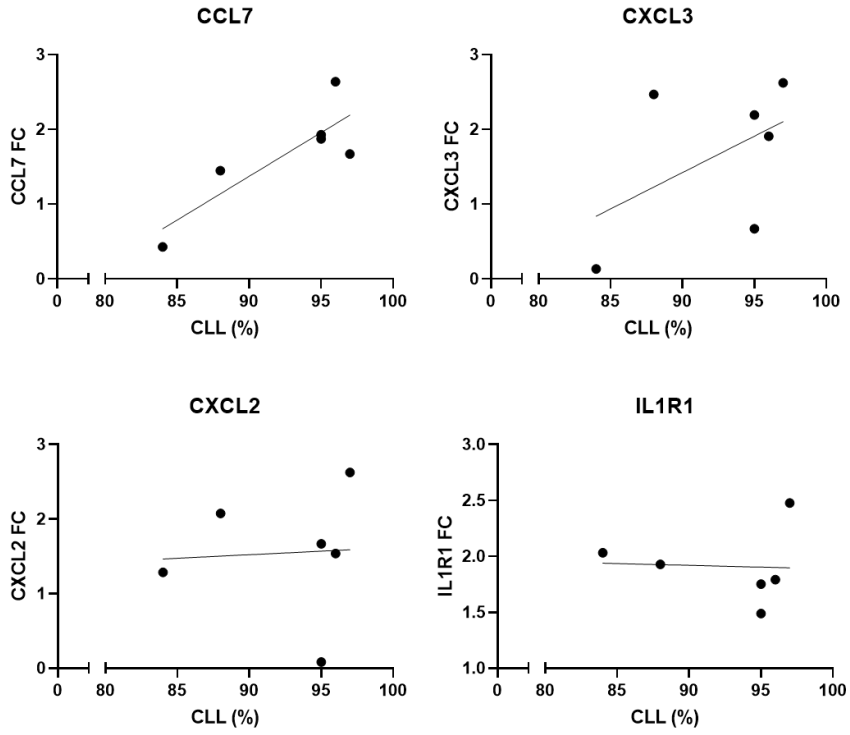

Figure 55. Relationship between VPS34-IN1 regulated gene expression and proportion of CLL cells in each sample at 6 Hours
Graphs show proportion of CLL cells (CLL (%)) and effect of VPS34-IN1 (fold change, FC) on expression of CCL7, CXCL3, CXCL2 and IL1R1 RNAs for the 6 samples analysed by RNA-Seq (with results of linear regression shown).

5.2.4 Effect of VPS34-IN1 on anti-IgM-regulated gene expression

Finally, I investigated the effect of VSP34-IN1 on the transcriptional response to anti-IgM. Comparison between control antibody/DMSO and anti-IgM/VPS34-IN1 treated samples identified 872 and 806 genes that were significantly up-regulated at 6 and 24 hours, respectively, and 2251 and 934 genes that were significantly down-regulated at 6 and 24 hours, respectively (see Appendix for full list of these genes). Thus, compared to the analysis of control antibody/DMSO versus anti-

IgM/DMSO treated samples to identify anti-IgM-regulated genes (section 5.2.1), VPS34-IN1 slightly reduced the number of genes that were significantly induced by anti-IgM at 6 and 24 hours (by 13 and 25%, respectively), or were significantly down-regulated by anti-IgM at 6 hours (by 9%). However, the effect of VPS34-IN1 on anti-IgM down-regulated gene expression at 24 hours was more dramatic (ie, 55% reduction in the number of significantly regulated genes in the presence of VPS34-IN1).

To illustrate these effects, gene expression changes in samples treated with anti-IgM and VPS34-IN1 (relative to control antibody/DMSO-treated samples) were shown as volcano plots (**Figure 56**). However, in contrast to the previous plots, individual genes were coloured according to their regulation by anti-IgM alone (ie, in the absence of VPS34-IN1). In this way, it is possible to more clearly track the effect of VPS34-IN1 on expression of anti-IgM-regulated genes.

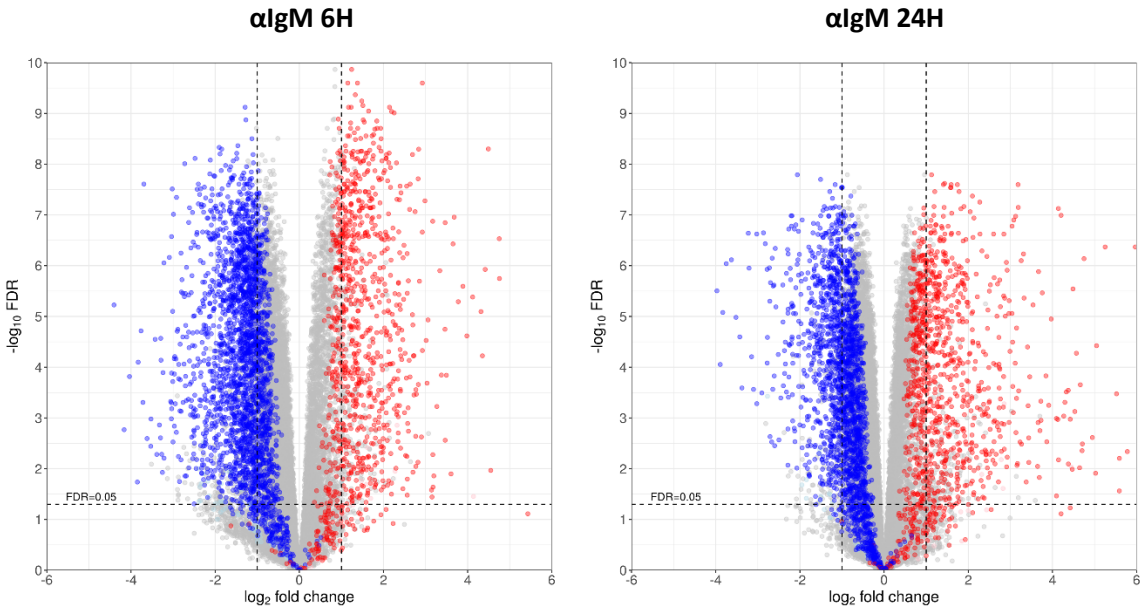

Figure 56. Volcano plots showing effect of anti-IgM on gene expression in the presence of VPS34-IN1 at 6 and 24 hours
Each data point represents an individual gene and is coloured red if significantly upregulated by anti-IgM (log_2FC >1.0; FDR <0.05) or blue if significantly downregulated by anti-IgM (log_2FC <-1.0; FDR <0.05). All other data points are coloured grey.

These volcano plots suggested that the effect of VPS34-IN1 on anti-IgM-regulated gene expression was to reduce the extent of, but not completely block, regulation. For example, for anti-IgM down-regulated genes at 24 hours (where VPS34-IN1 had the strongest effect on the number of significantly regulated genes) the majority of these genes were still differently expressed in response to anti-IgM (ie, FDR <0.05), however the fold change did not reach the <-1.0 value, so they were no longer included in the gene lists based on cut-offs. Consistent with this, IPA confirmed that the pathways which were enriched in the anti-IgM-induced signature at hours were remarkably similar in the presence or absence of VPS34-IN1 (**Table 15**). Thus, the "Antigen presentation

pathway" was retained as the top ranked pathway in the presence of VPS34-IN1 and, overall, 9/10 pathways were present in the top-10 ranked list regardless of the presence of VPS34-IN1.

Table 15. Top-10 IPA canonical pathways enriched in the anti-IgM-induced transcriptional response in the presence of VPS34-IN1 at 6 hours.

Rank	Ingenuity Canonical Pathway[a]	-log p-value	Ratio	z-score[b]	Molecules
1	Antigen Presentation Pathway	10.4	0.333	NaN	CALR, CANX, CIITA, HLA-DOA, HLA-DPA1, HLA-DQA1, HLA-DQA2, HLA-DQB1, HLA-DQB2, HLA-DRA, HLA-DRB1, HLA-DRB5, PDIA3
2	Th1 and Th2 Activation Pathway	8.2	0.128	NaN	CCR5, CD274, CD80, GFI1, HLA-DOA, HLA-DPA1, HLA-DQA1, HLA-DQA2, HLA-DQB1, HLA-DQB2, HLA-DRA, HLA-DRB1, HLA-DRB5, IL2RB, IL6, IL6R, NFIL3, NFKB1, SOCS3, STAT3, STAT5A, TNFRSF4
3	Th1 Pathway	7.8	0.148	3.207	CCR5, CD274, CD80, HLA-DOA, HLA-DPA1, HLA-DQA1, HLA-DQA2, HLA-DQB1, HLA-DQB2, HLA-DRA, HLA-DRB1, HLA-DRB5, IL6, IL6R, NFIL3, NFKB1, SOCS3, STAT3
4	MSP-RON Signaling In Macrophages Pathway	7.3	0.145	-2	CIITA, HLA-DOA, HLA-DPA1, HLA-DQA1, HLA-DQA2, HLA-DQB1, HLA-DQB2, HLA-DRA, HLA-DRB1, HLA-DRB5, KLK1, KLK4, NFKB1, PTGS2, REL, SOCS3, STAT3
5	PD-1, PD-L1 cancer immunotherapy pathway	7.15	0.151	-1.387	CD274, CD80, HLA-DOA, HLA-DPA1, HLA-DQA1, HLA-DQA2, HLA-DQB1, HLA-DQB2, HLA-DRA, HLA-DRB1, HLA-DRB5, IL2RB, NGFR, PDCD1, STAT5A, TNFRSF1B
6	tRNA Charging	6.92	0.256	3.162	AARS1, EARS2, FARSB, GARS1, IARS1, SARS1, TARS1, VARS1, WARS1, YARS1
7	Purine Nucleotides De Novo Biosynthesis II	6.62	0.545	2.449	ADSL, ATIC, GART, PAICS, PFAS, PPAT
8	TREM1 Signaling	6.5	0.169	3.464	CD83, CIITA, CSF2, CXCL8, IL6, IRAK1, ITGAX, NFKB1, NLRP6, REL, STAT3, STAT5A, TREM1
9	B cell Development	6.49	0.233	NaN	CD80, HLA-DOA, HLA-DPA1, HLA-DQA1, HLA-DQA2, HLA-DQB1, HLA-DQB2, HLA-DRA, HLA-DRB1, HLA-DRB5
10	Sirtuin Signaling Pathway	6.31	0.089	1.213	CXCL8, DOT1L, GADD45A, GADD45B, GADD45G, H1-0, LDHA, MAPK12, MAPK6,

					MYC, MYCN, NAMPT, NFKB1, PCK2, POLR1A, POLR1B, POLR1C, REL, RRP9, SOD2, STAT3, TIMM8A, TOMM20L, TOMM40, TUBA1C, VDAC1

[a]IPA canonical pathway analysis was performed using genes that were significantly induced (log_2FC >1.0; FDR<0.05) at 6 hours in anti-IgM/VPS34-IN1-treated cells. [b]NaN, no activity pattern predicted. Full analysis is provided in the Appendix.

Overall, RNA-seq analysis demonstrated that anti-IgM induces extensive transcriptional reprogramming in CLL cells. This response encompassed many biological pathways, and notably, these changed at 6 versus 24 hours. Little data exists comparing the two time points, so this was a discovery of interest. There was a striking and sustained increase in expression of RNAs related to antigen presentation, particularly via MHC-II pathways. By contrast, VPS34 inhibition had only very modest effects on gene expression. Induction of chemokine/cytokine expression (potentially from CLL cells) was confirmed, but there was no evidence for selective modulation of the anti-IgM response (beyond a general down-modulation of the overall extent of gene regulation, especially at 24 hours), or any evidence of activation of pathways which may have indicate substantial off-target effects.

5.3 Antigen Processing and Presentation by CLL cells

5.3.1 Background

The identification of antigen presentation as a major regulated pathway following sIgM stimulation of CLL cells in the RNA-seq experiment was significant as it highlighted the dual function of the BCR as (i) an initiator of signalling leading to B cell survival/proliferation, and (ii) a mediator of antigen internalisation leading to T-cell help. Since CLL cells can internalise anti-IgM-coated beads (Chapter 4), I next performed a series of experiments to investigate whether CLL cells were capable of presenting antigen from anti-IgM-coated beads via MHC-II.

We used SKW3-T18 cells, derived from a human T-cell leukaemia (Vangapandu *et al.*, 2017), to investigate MHC-II-mediated antigen presentation by CLL cells. Parental SKW3 cells lack TCR expression and were modified by our collaborator (Prof Munthe, University of Oslo). Such a model was used previously to demonstrate that CLL cells were efficient antigen-presenting cells as they could endocytose and process soluble antigens via the BCR cell receptor, and present processed antigen on HLA-II to recruit T-cell help. **Figure 57** illustrates the basis of the assay.
Since previous experiments performed by Professor Munthe were restricted to soluble anti-IgM, the initial aim of these experiments was to investigate whether CLL cells were also able to present particulate antigen in the form of the anti-IgM-coated beads. I then used this system to probe the role of autophagy and BCR-associated kinase inhibitors in these antigen presentation pathways.

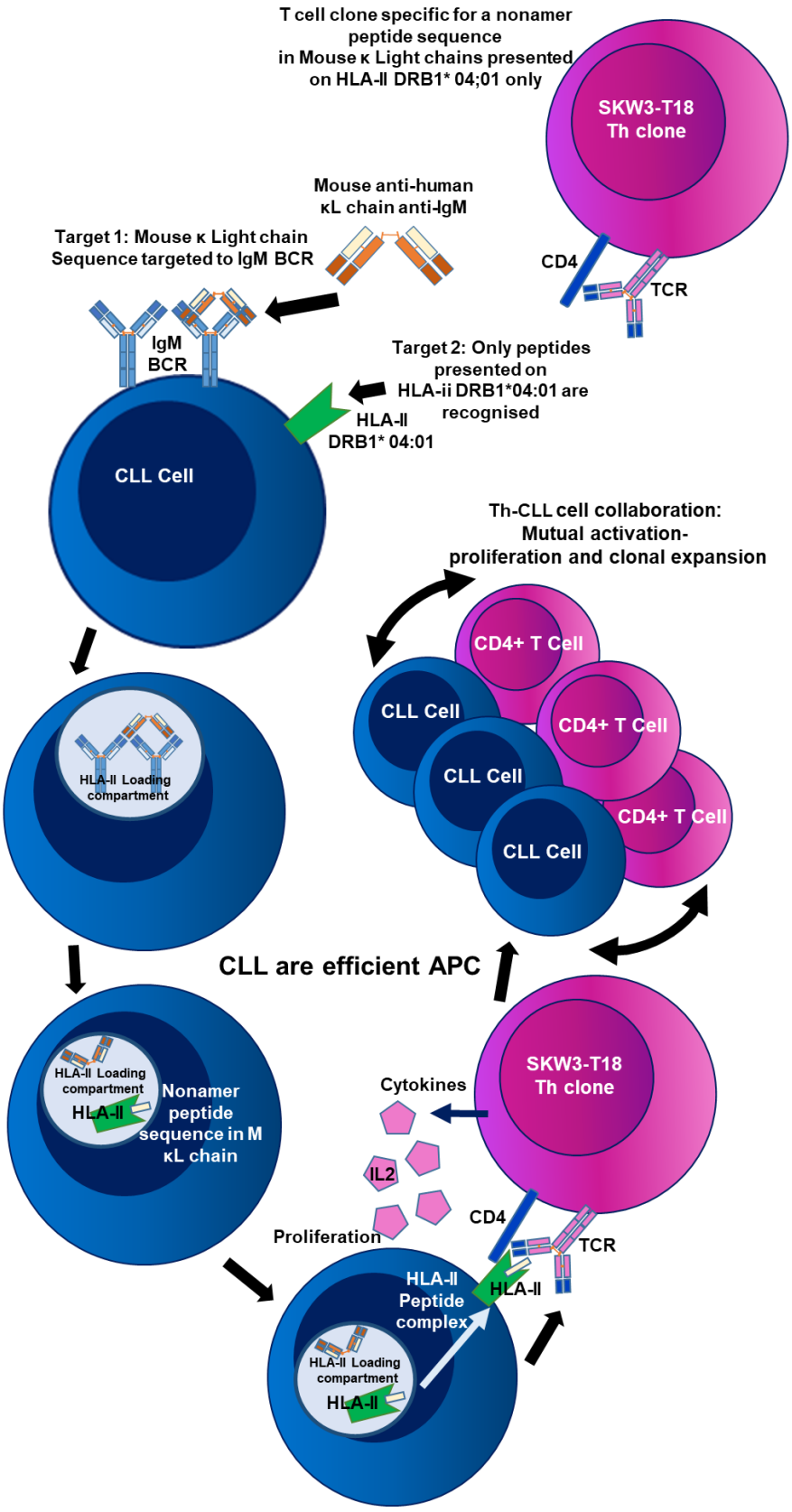

Figure 57. Illustration of T cell CLL cell collaboration assay.
SKW3-T18 cell line was modified by our collaborators at the University of Olso. A mouse TCR has been added specific to a nonamer peptide sequence in mouse kappa light chains, presented on HLA-II DRB1* 04:01. Following binding of mouse kappa anti-IgM to IgM BCR on CLL, the BCR with anti-IgM is internalised and the antibody trafficked to HLA loading compartments, where peptides are loaded onto HLA-II and presented in an antibody-HLA complex at the cell surface. This can then recruit the cognate TCR on SKW3-T18s and initiate binding, and activation, resulting in cytokine secretion including IL2. Mutual activation and proliferation can then occur.

5.3.2 Implementing an assay for detection of SKW3-T18 activation

Initial experiments were performed to compare the relative effectiveness of analysis of CD69 expression (by flow cytometry) and IL2 production (by ELISA) to quantify SKW3-T18 activation. Cells were treated with PMA/ionomycin which typically leads to strong T-cell activation. CD69 analysis was performed after 6 hours whereas IL2 was analysed at 24 hours as this cytokine is secreted into supernatant and therefore accumulates over time. Although PMA/ionomycin did increase CD69 expression (by ~7-fold), CD69 expression on control cells was relatively high (compared to unstained cells) (**Figure 58A**). By contrast, basal secretion of IL2 from SKW3-T18 cells was very low and the extent of the increase in IL2 secretion in response to PMA/ionomycin was therefore much larger (**Figure 58B**). Based on this superior dynamic range, analysis of IL2 was selected as the assay to monitor SWK3-T18 activation.

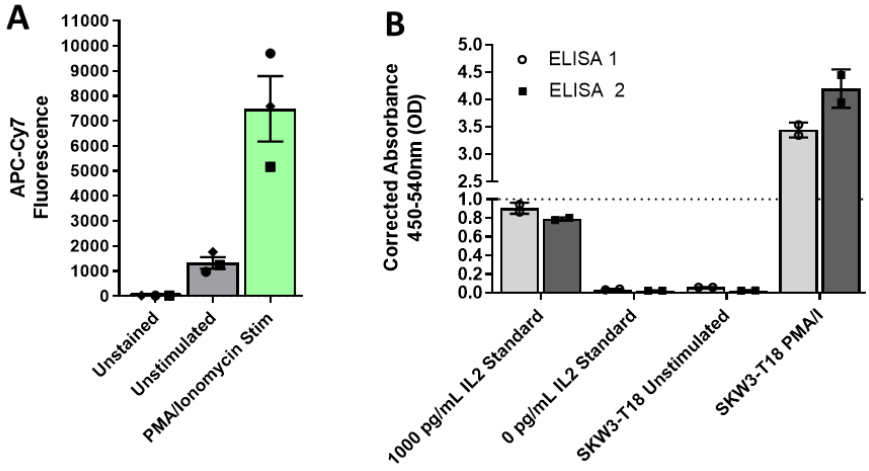

Figure 58 Implementing an assay for detection of SKW3-T18 activation:
(A) SKW3-T18 cells were stimulated with PMA/ionomycin for 6 hours, or left untreated as a control (unstimulated), and CD69 was the quantified by flow cytometry. Graph shows mean (±SD) expression with values obtained from 3 independent experimental repeats. (B) SKW3-T18 cells were stimulated with PMA/ionomycin of left untreated as a control (NA). After 24 hrs, supernatants were collected and analysed for IL2 content using an ELISA. IL2 standards (1000 and 0 pg/ml) were included as additional controls. Graph shows individual data points and mean (±SD) for two independent experiments, each performed in duplicate.

The next step was to test the response of SKW3-T18 cells using an appropriate HLA-II matched B cell line as the amount of suitable CLL material (ie HLA-DRB1*04:01 positive samples) was very limited. BOLETH cells (ECACC 88052031) were treated with Ms κ+ anti-IgM for 15 minutes, prior to coculture with SKW3-T18 cells and analysis of IL2 secretion by ELISA. I first examined the effect of different SKW3-T18/BOLETH co-culture cell densities on cell growth at up to 48 hours (at a fixed SKW3-T18/BOLETH cell ratio of 1:4). This was performed to determine optimal cell densities for these co-culture experiments and, in particular, to ensure T-cell overgrowth did not dominate the co-cultures. At 24 hours, very little cell accumulation was observed in co-culture conditions (**Figure 59A**) and this time point was therefore selected for subsequent analyses. Notably, cell numbers did increase at 48 hours demonstrating that the “pause” in proliferation of T cells associated with

plating into wells is transient, and not due to a substantial loss of viability. Based on this experiment, I also selected a cell density of 100,000 SKW3-T18 and 400,000 B cells (BOLETH) in a total culture volume of 0.2 ml for follow-on experiments for CLL cells. Using these conditions, IL2 secretion was only observed when BOLETH cells were exposed to Ms κ+ anti-IgM (**Figure 59B**). This confirmed the validity of analysis of IL2 secretion as an assay to detect antigen presentation on MHC-II from Ms κ+ anti-IgM-treated B cells

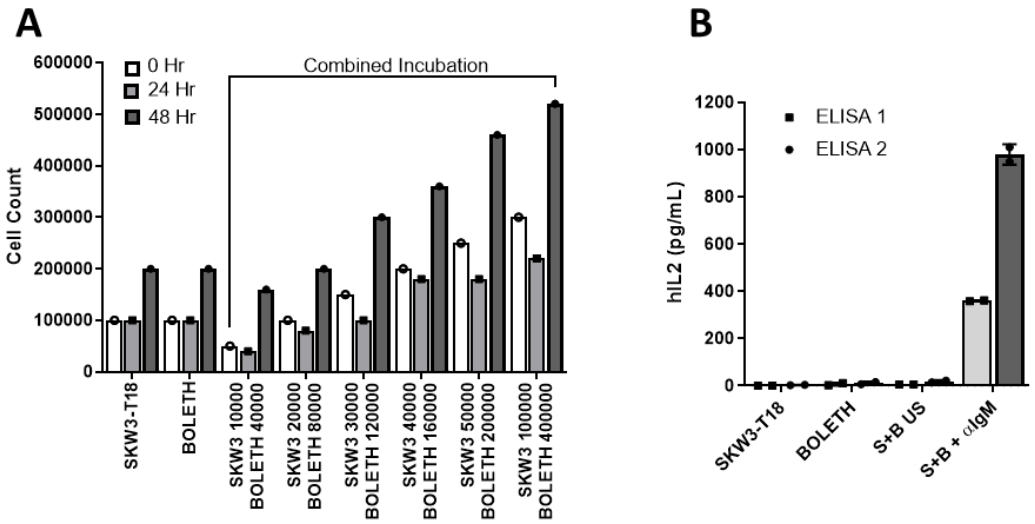

Figure 59. Implementing an assay for detection of SKW3-T18 activation:
(A) BOLETH cells were co-cultured with SKW3-T18 at various densities (all at a ratio of 1:4 SKW3-T18 to BOLETH cells) in 200 µL volumes. Densities spanned a range from 10,000 SKW3-T18 + 40,000 BOLETH cells to a 100,000 SKW3-T18 + 400,000 BOLETH . Total live cells counts (ie, Boleth and SKW3-T18 cells) were determined at 24 or 48 hours, and at the start of the experiment (0 hr). As additional controls, parallel cell counts were obtained from BOLETH or SKW3-T18 cells cultured alone. (B) SKW3-T18 or BOLETH were co-cultured in the presence (+αIgM) or absence (US) of mouse anti-IgM. For anti-IgM-treatment, BOLETH cells were pre-incubated with antibody for 15 minutes before mixing with SKW3-T18 cells. After 24 hours, IL2 secretion was quantified using an ELISA. The graph shows IL2 concentration for each ELISA, with the individual data points showing the ELISA technical duplicates for the two experiments, which are shown as side-by-side bars.

5.3.3 Identification of HLA DRB1* 04:01 positive CLL samples

As the next stage, it was necessary to identify CLL samples that were HLA DRB1* 04:01 positive as they would be able to present the target-peptide on MHC-II to the TCR of SKW3-T18 cells. Sixteen CLL samples were submitted for HLA typing and four were HLA DRB1* 04:01 positive. Two of these four were M-CLL, and two U-CLL. The CLL samples used in subsequent assays include these four samples, as well as three negative controls that were HLA DRB1* 04:01 negative. An example of one HLA DRB1* 04:01 positive and one negative control are shown in **Figure 60**, with a table of the characteristics of all the CLL samples used in this study shown in **Table 16**.

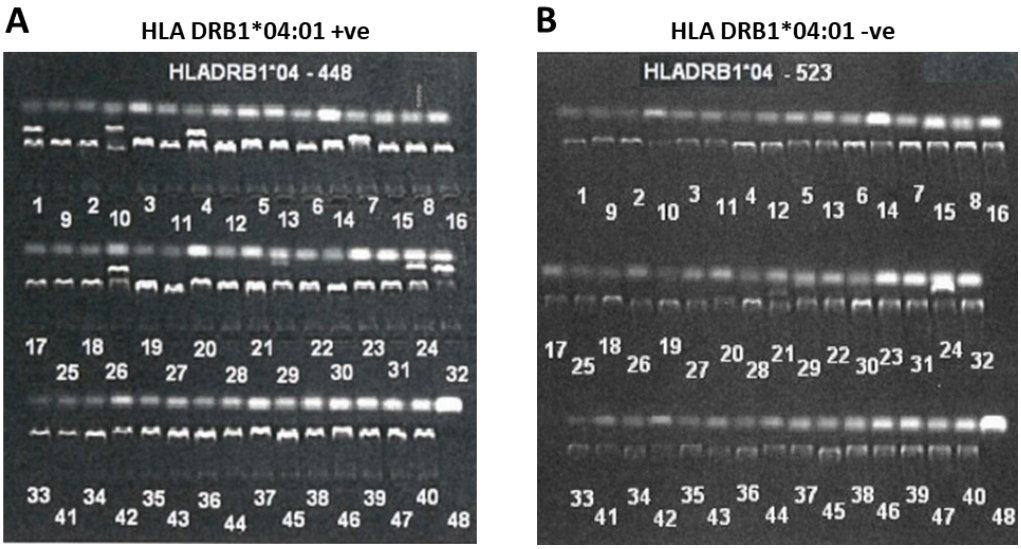

Figure 60. HLA typing of two representative CLL samples, one DRB1* 04:01 positive and one negative
Sixteen CLL patient samples were HLA typed and four HLA DRB1* 04:01 positive samples identified. (A) illustrates a HLA DRB1* 04:01 positive sample, with positive bands present in wells 1, 4, 7, 10, 24, 26 and 32 of the Olerup SSP DRB1*04 HLA Typing Kit (sample 448). (B) Shows a HLA DRB1* 04:01 negative sample (sample 523).

Table 16. CLL samples used in this research.

Sample ID	*IGHV* mutation status[a]	sIgM (MFI)	sIgM iCa^{2+} Signalling Capacity (%)[b]	HLA DRB1* 04:01 Status
496F	M	32	14	Positive
511A	U	32	39	Positive
348C	M	35	21	Positive
448B	U	115	73	Positive
87B	M	12	36	Negative
684B	M	28	14	Negative
523F	M	31	25	Negative

[a]M, mutated; U, unmutated. [b]Percent responding cells by iCa^{2+} analysis (Mockridge et al., 2014). Data was provided by the Southampton Tumour Bank.

5.3.4 CLL cell response pathways to mouse anti-IgM and compounds

Before analysis of antigen presentation activity, it was important to confirm that the Ms κ+ anti-IgM was able to induce signalling and increase autophagy, and to compare the responses to those obtained with the polyclonal goat $F(ab')_2$ anti-human IgM antibody used in previous experiments in this thesis (Chapter 3).

Results shown in **Figure 61** show representative immunoblots and graphed results for LC3B-II induction following stimulation with Ms κ+ anti-IgM or the goat polyclonal anti-IgM antibody (soluble or coated beads), using both HLA DRB1* 04:01 positive and negative samples (as signalling induction will not be affected by HLA-II type). Importantly, the induction of LC3B-II expression was very similar for the two bead-bound antibodies (5-7-fold average increase in expression) (**Figure 61B**). Similar to results shown previously for the goat antibody (Chapter 3), induction of LC3B-II expression in cells treated with Ms κ+ anti-IgM-coated beads was effectively inhibited by entosplentinib, but not MRT68921 or VPS34-IN1. The response to soluble Ms κ+ anti-IgM was modest (~3-fold increase on average) but did appear to be somewhat stronger compared to soluble goat polyclonal anti-IgM (which had little effect on LC3B-II expression, consistent with results shown in 4.4). Induction of LC3B-II expression by soluble Ms κ+ anti-IgM was inhibited by entosplentinib, but not autophagy inhibitors, and was strongly increased by HCQ, but not Baf (**Figure 61A**).

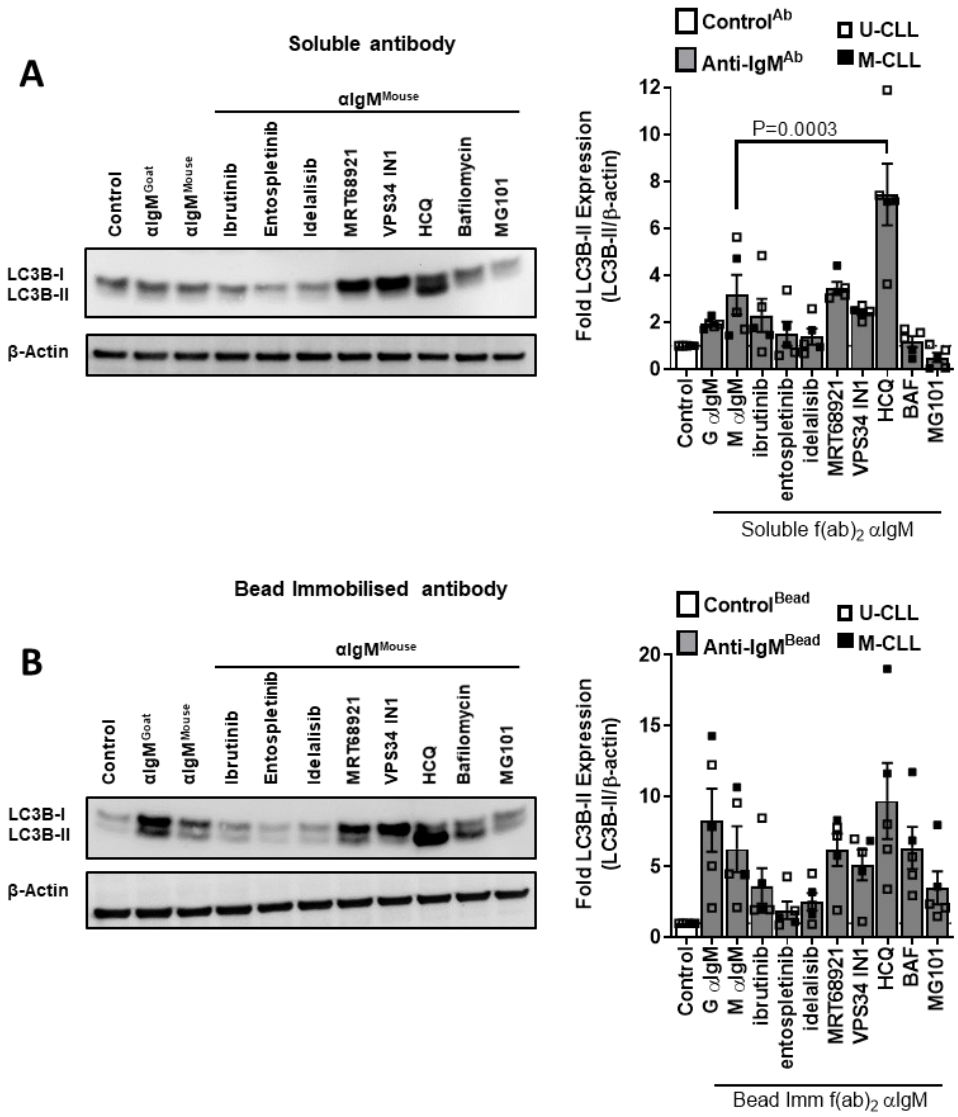

Figure 61. Comparison of the effect of anti-IgM antibodies on LC3B-II expression.
CLL samples (n=5) were pre-treated with the indicated compounds or left untreated as a control for 1 hour and then incubated with goat polyclonal anti-IgM (anti-IgM^{Goat}/G) or Ms κ+ anti-IgM (anti-IgM^{Mouse}/M) ((A) soluble or (B) coated beads) for 24 hours before analysis of LC3B and β-actin by immunoblotting. Figure shows representative immunoblots and quantitative summaries for all samples. Graphs show results for individual samples and mean (±SD) with values for control antibody-coated beads set to 1.0.

Further experiments were performed to investigate the effects of Ms κ+ anti-IgM-coated beads on upstream signalling (**Figure 62**). This confirmed that this antibody induced increased phosphorylation of both ERK and AKT and was therefore competent for signalling activation. These responses were effectively blocked by entospletinib, but unaffected by autophagy inhibitors, HCQ or Baf. BTK inhibition using acalabrutinib also did not inhibit these responses, whereas PI3Kδ inhibition using idelalisib partly reduced ERK phosphorylation, and more completely inhibited AKT phosphorylation.

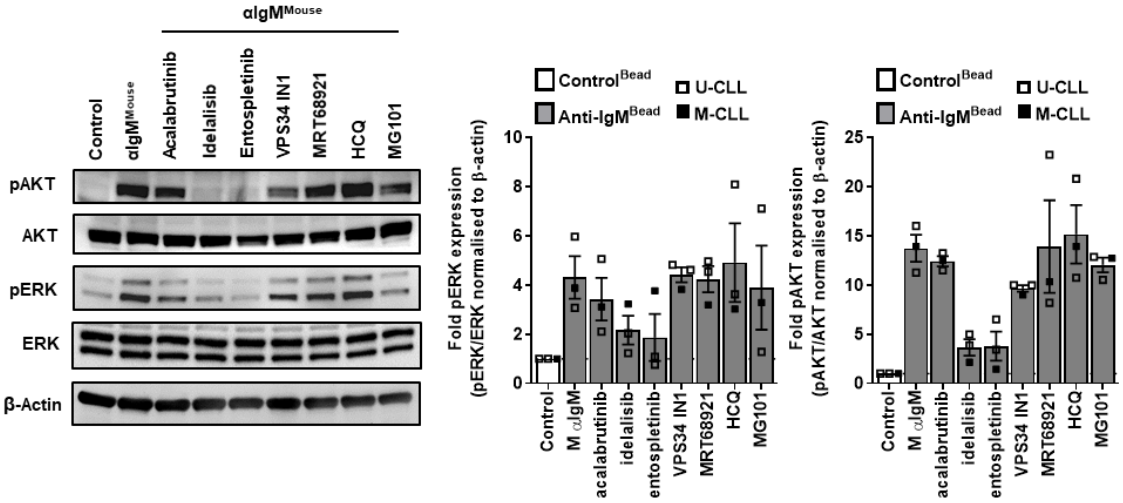

Figure 62. Effect of Ms κ+ anti-IgM-coated beads on AKT and ERK phosphorylation.
CLL samples (n=3) were pre-treated with the indicated compounds (acalabrutinib 100nM, Idelalisib,entospletinib, VPS34-IN1, MRT68921 and MG101 at 1μM, HCQ at 10μM) or left untreated as a control for 1 hour and then incubated with Ms κ+ anti-IgM- (anti-IgM^{Mouse}/M) or control antibody-coated beads for 30 minutes. Expression of AKT and ERK (total and phosphorylated), and β-actin, was analysed by immunoblotting. Figure shows representative immunoblots and quantitative summaries for all samples. Graphs show results for individual samples and mean (±SD) with values for control antibody-coated beads set to 1.0.

5.3.5 Screening HLA DRB1*0401 positive and negative CLL samples in T-cell collaboration assays

The next stage was to perform initial coculture tests with the SKW3-T18 cells and HLA DRB1*04:01 positive CLL samples to confirm responses to soluble anti-IgM. The first experiment assessed the four HLA DRB1*04:01 positive and three negative samples shown in **Table 7**. CLL cells were pre-incubated with soluble Ms κ+ anti-IgM or goat polyclonal anti-IgM for 15 minutes (a time point previously shown to initiate strong signalling responses and internalisation of soluble antibody). SKW3-T18s were then added and co-cultures incubated for 24 hours before ELISAs for IL2 were performed. Additional control incubations tested were no addition of antibody, and individually cultured CLL cells or SKW3-T18s. Results shown in **Figure 63** demonstrate clearly that IL2 secretion is only detected when HLA DRB1*04:01 positive (and not negative) CLL samples are treated with the Ms κ+ anti-IgM (and not the goat polyclonal anti-IgM).

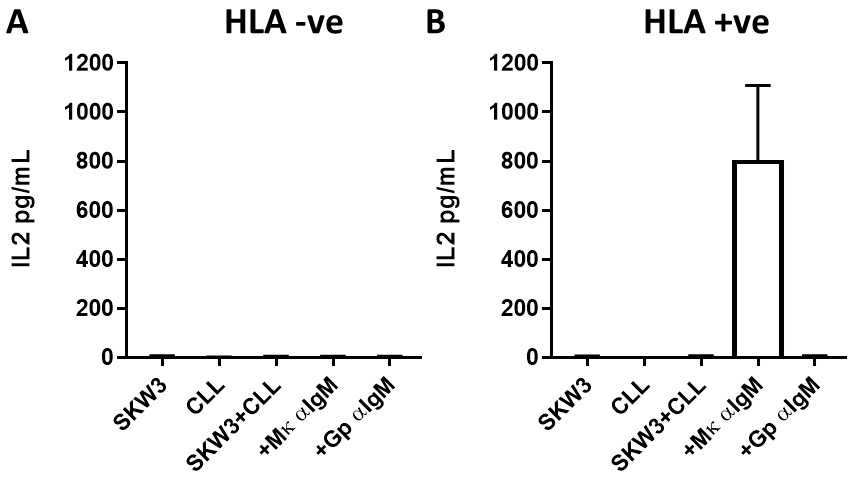

Figure 63. CLL patient – T cell co-culture tests.
(A) Shows 3 HLA DRB1*04:01 negative control samples incubated with Ms κ+ anti-IgM or goat polyclonal (Gp) anti-IgM, then cocultured with SKW3-T18 cells for 24 hours. ELISAs were performed on supernatant for IL2 expression. (B) Shows results for the 4 HLA DRB1*04:01 positive samples in the same experimental conditions. Graphs show mean (±SD).

5.4 CLL:SKW3-T18 cell co-culture assays

After establishing that the CLL samples selected respond to Ms κ+ anti-IgM and that they are able to present antigen to SKW3-T18 cells, I examined this response in more detail. I first compared the response to soluble Ms κ+ anti-IgM and Ms κ+ anti-IgM-coated beads to determine if CLL cells were capable of presenting from particulate antigens. Interestingly, the IL2 response of SKW3-T18 cells was similar for both forms of anti-IgM (**Figure 64**). The response was similar in the four CLL samples used in this experiment and the increase in IL2 secretion was statistically significant for both soluble Ms κ+ anti-IgM and Ms κ+ anti-IgM-coated beads. No response was detected using the goat polyclonal control anti-IgM (as soluble or bead-bound). These data demonstrate for the first time that CLL cells are capable of presenting particulate antigens via sIgM.

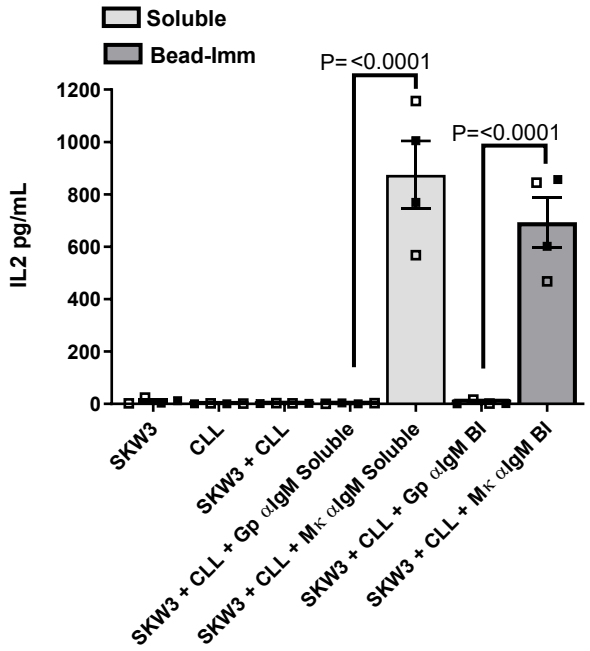

Figure 64. Comparison of effects of soluble Ms κ+ anti-IgM and Ms κ+ anti-IgM-coated beads on SKW3-T18 cells.
CLL samples (n=4, all HLA DRB*1 04:01 positive) were incubated with the indicated antibodies (Mk, Ms κ+ anti-IgM ; Gp, goat polyclonal anti-IgM) in Soluble or Bead Immobilised form (BI), for 15 or 60 minutes, respectively, and then co-cultured with SWK3-T18 cells for 24 hours. IL2 secretion was quantified by ELISA. SKW3-18 and CLL cells (and co-cultured cells without any added antibody) were analysed as additional controls. Graph shows results for individual samples and mean (±SD) with the results of statistical analysis (two-way Anova, multiple comparisons with Bonferroni's Multiple comparisons test) shown.

Next, I characterised the effects of BCR signalling and autophagy inhibitors on antigen presentation using this system. These experiments used ibrutinib and acalabrutinib (BTK inhibitors), entospletinib (a SYK inhibitor shown previously to completely inhibit internalisation of 3-micron anti-IgM-coated beads), idelalisib (a class I PI3Kdelta inhibitor). For autophagy analysis, the compounds used were VPS34-IN1 (Vps34 inhibitor), MRT68921 (dual ULK1/2 inhibitor). HCQ and Baf were used to inhibit lysosomal turnover. MG101, a cysteine protease, calpain and cathepsin inhibitor, was also used as a positive control to inhibit antigen processing. The CLL cells were pre-treated with these compounds for 1 hour prior to addition of soluble Ms κ+ anti-IgM or Ms κ+ anti-IgM-coated beads, and analysis of IL2 secretion after 24-hour co-culture with SKW3-T18 cells

The results (**Figure 65**) demonstrated that the positive control, MG101, significantly reduced IL2 secretion when SKW3-T18 cells were co-cultured with CLL cells treated with either soluble Ms κ+ anti-IgM or Ms κ+ anti-IgM-coated beads (by ~60%, on average). None of the BCR kinase inhibitors, or HCQ or Baf, had any substantial effect on antigen presentation from Ms κ+ anti-IgM-coated beads. Interestingly, IL2 secretion was increased following treatment of CLL cells with the autophagy inhibitors VPS3434-IN1 and MRT68921 (for Ms κ+ anti-IgM-coated beads), and MRT68921 for soluble antibody, although this was only statistically significant for the ULK1/2 inhibitor MRT68921 for both soluble and bead-immobilised antibody. The effect of these upstream autophagy inhibitors, and the lack of effect with the end point autophagosome turnover inhibitors HCQ/Baf, was very similar in experiments using soluble Ms κ+ anti-IgM. However, in contrast to experiments using antibody-coated beads, entospletinib did significantly reduce antigen presentation from soluble Ms κ+ anti-IgM, to a similar extent as MG-101. Idelalisib also appeared to reduce IL2 secretion (although this difference was not statistically significant), whereas BTK inhibition had no clear effect.

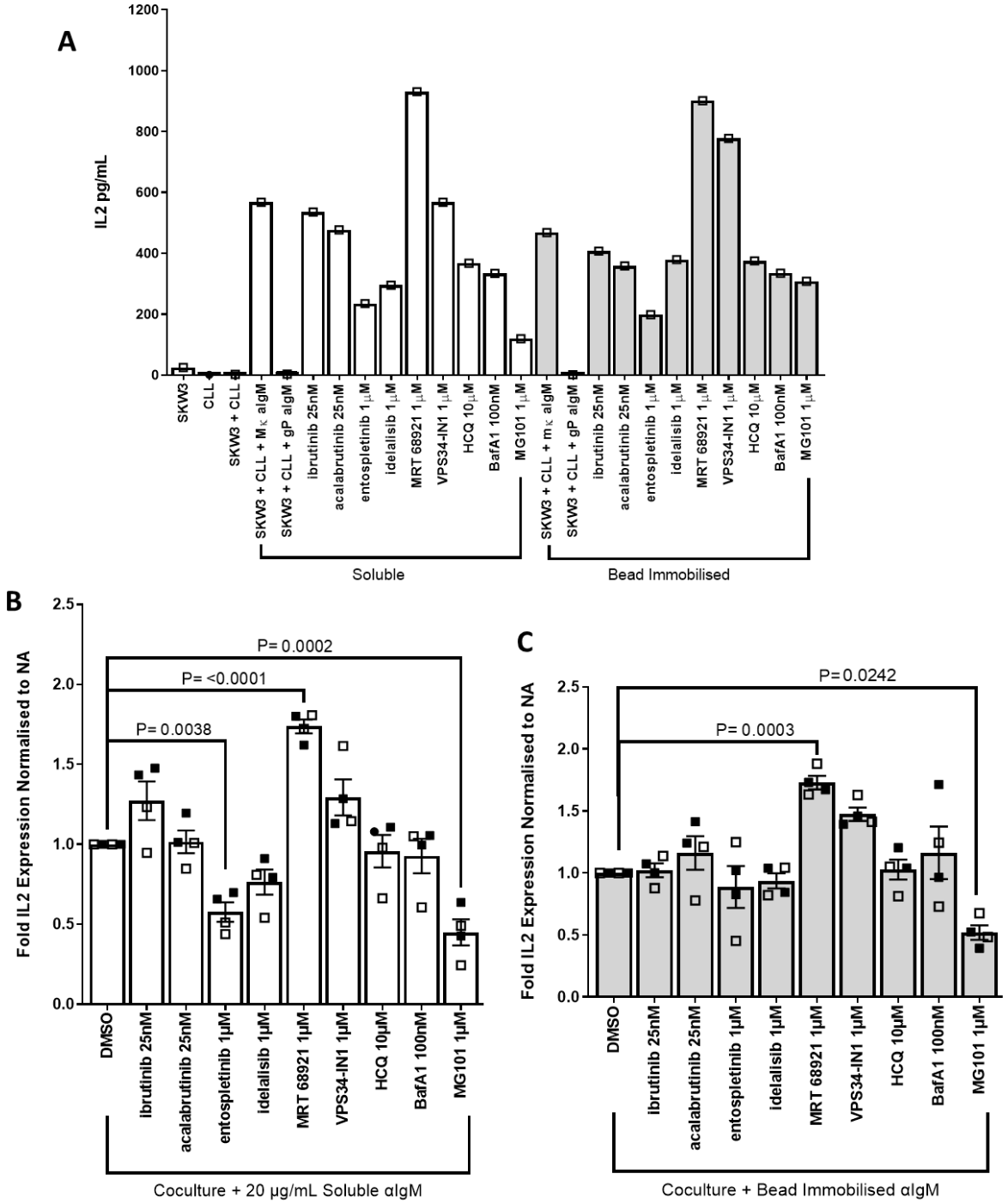

Figure 65. CLL:T-cell collaboration assays with BCR kinase and autophagy inhibitors.
CLL samples (n=4) were pre-treated with the indicated compounds for 1 hour before treatment with soluble Ms κ+ anti-IgM or Ms κ+ anti-IgM-coated beads for 15 or 60 minutes, respectively, and co-culture with CLL samples for 24 hours. IL2 secretion was quantified by ELISA. Graph A shows results (IL2 secretion) for a representative sample (mean of duplicate determinations). Graphs below show results for the 4 samples analysed with values for individual samples and mean (±SD) with values for DMSO-treated cells set to 1.0 for soluble (B) or bead-bound Ms κ+ anti-IgM (C). The statistical significance (two-way Anova, multiple comparisons with Bonferroni's Multiple comparisons test) of the differences compared to DMSO-treated cells is shown (if not shown P>0.05).

It was surprising that autophagy inhibition increased IL2 secretion, as autophagy has been shown to be important for antigen presentation in some situations (**Figure 65**). One possibility was that this outcome was due a direct effect of the inhibitors on SKW3-T18 cells as all cells in the assay were exposed to compounds. I therefore investigated the effects of VPS34-IN1 and MRT68921 on IL2 secretion from SKW-T18 cells alone and compared this effect to that obtained in the SKW-T18/CLL cell co-culture system. The results confirmed that both autophagy inhibitors increased IL2 secretion when SKW3-T18 cells were co-cultured with CLL cells with soluble Ms κ+ anti-IgM or Ms κ+ anti-IgM-coated beads (**Figure 66**). As shown above, the effect was greatest with MRT68921. However, VPS34-IN1 and MRT68921 also increased IL2 secretion from SWK3-T18 cells in the absence of CLL cells demonstrating that these compounds can directly increase IL2 production from SKW3-T18 cells. However, the increase in IL2 secretion from SWK3-T18 cells alone (~100 pg/ml) did not account for the increased in IL2 secretion from SWK3-T18 cells with CLL cells (and soluble or bead-bound Ms κ+ anti-IgM) (~500 pg/ml). These results suggest that increased IL2 secretion with autophagy inhibitors in experiments with SKW3-T18 and CLL cells (with soluble Ms κ+ anti-IgM/Ms κ+ anti-IgM-coated beads), is at least in part, a consequence of effects of autophagy inhibition in CLL cells.

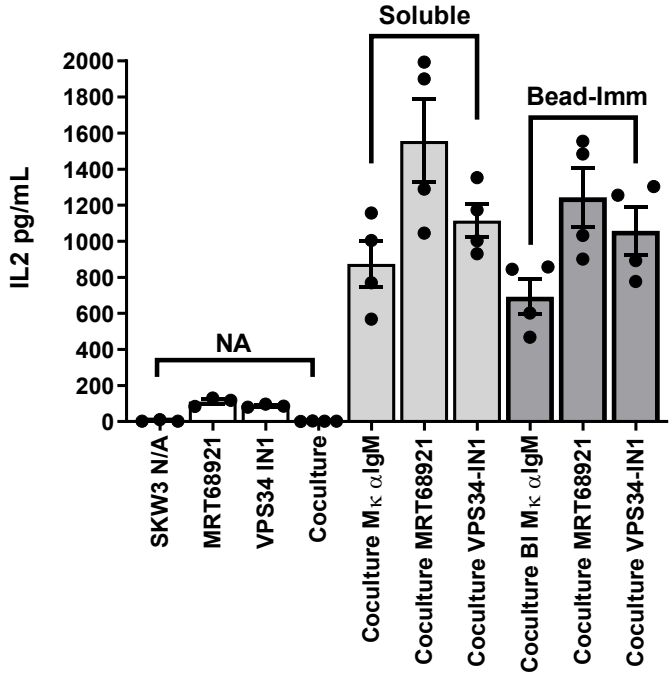

Figure 66. Effect of autophagy inhibitors on IL2 secretion from SKW-T18 cells with and without CLL cells.

Effects of MRT68921 or VPS34-IN1 (or no addition, N/A) for 24 hours on IL2 secretion from SKW-T18 cells alone (bars 1-4), or when used to pre-treated CLL cells for 1 hour before treatment with soluble Ms κ+ anti-IgM (bars 5-7) or Ms κ+ anti-IgM-coated beads (bars 8-10) for 15 or 60 minutes, respectively, and co-culture with CLL samples for 24 hours. IL2 secretion was quantified by ELISA. Graph shows results for 4 samples analysed with values for individual samples and mean (±SD).

5.5 Examining the role of bead phagocytosis in antigen removal

It was interesting to find that SYK inhibition had no effect on antigen presentation from anti-IgM-coated beads (**Figure 65**) but did very effectively inhibit their internalisation (Chapter 4). Thus, while these results demonstrate CLL cells can present antigen from the coated bead, this seemed to be uncoupled from their internalisation. An alternate mechanism of antigen presentation by B cells has been demonstrated by which cells release lysosomal contents into the extracellular milieu, allowing liberation of "free" antigen by proteolysis (Yuseff *et al.*, 2011; Reversat *et al.*, 2015). Released antigen can then be internalised or loaded directly into surface MHC-II molecules.

To test whether this pathway could be operating in my experiments on antigen presentation using anti-IgM-coated beads, I re-evaluated the data obtained from the flow cytometry assay used to quantify bead internalisation in Chapter 4 by analysing the fluorescence intensity of the unbound beads. At least some of these beads are likely to have engaged CLL cells via sIgM, but have not been internalised, and could therefore be subject to the proteolytic mechanism described above and therefore have lower levels of anti-IgM. Interestingly, the results showed a clear difference in levels of anti-IgM remaining on "free" beads incubated with cells for 3 hours at 37 ^{o}C versus control incubations performed at 4 ^{o}C (~40% reduction, **Figure 67**). This apparent removal of antigen (anti-IgM) from the bead was relatively unaffected by entospletinib. The loss of anti-IgM from the beads was also unaffected by autophagy inhibitors (VPS34-IN1 and MRT68921), Dyngo-4A and cytochalasin D (data not shown).

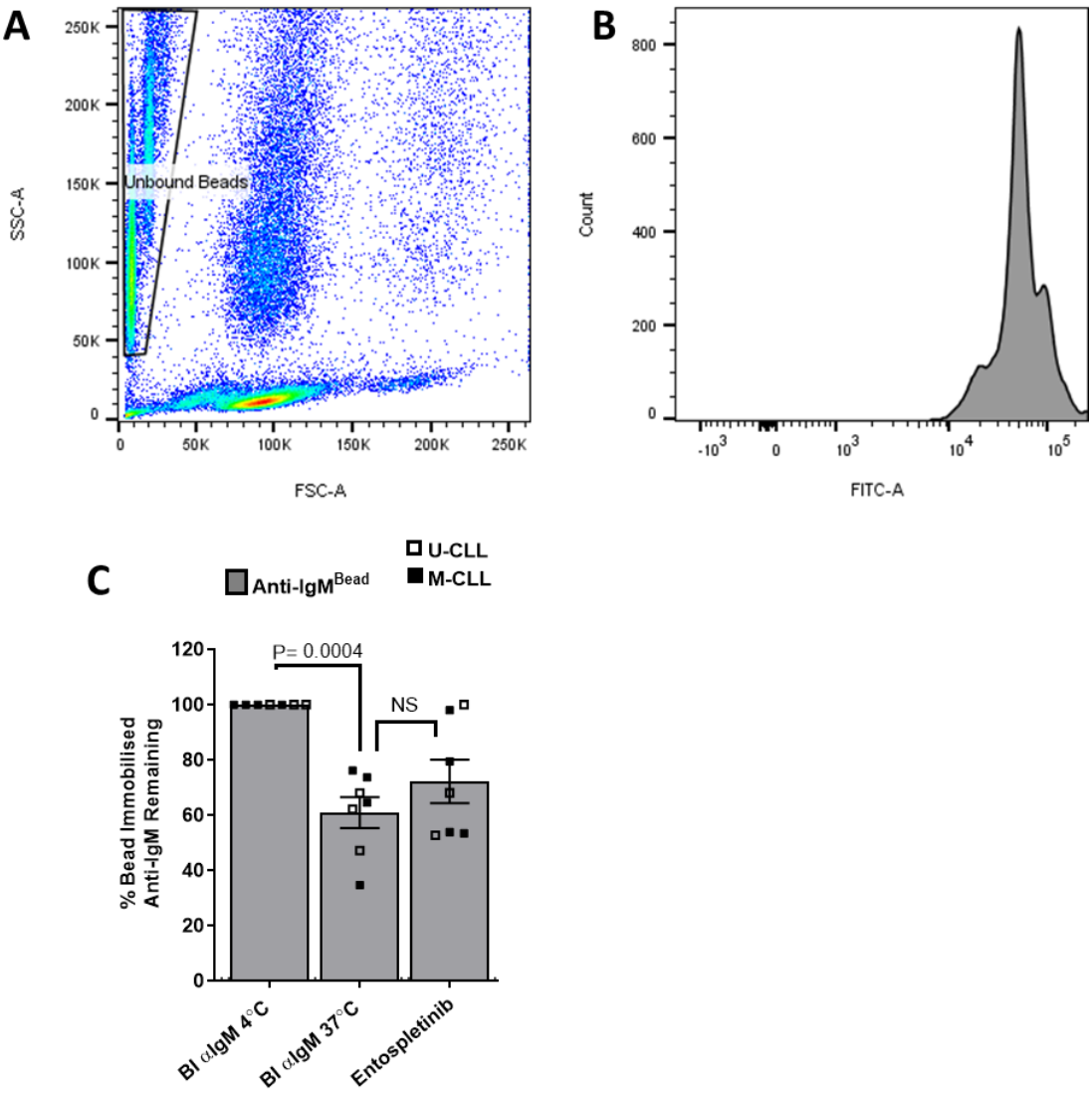

Figure 67. Re-analysis of flow cytometry data to quantify anti-IgM levels on unbound beads.
The data shown are from the experiment presented in **Figure 44**, but with gating on unbound beads. (A) Gate for unbound beads. (B) Representative histogram of FITC fluorescence of unbound beads. (C) Quantitiation for all samples analysed (n=7). Graph shows results for individual samples and mean (±SD) with values for control (4 °C) set to 100%. The statistical significance of the indicated differences is shown (NS, not significant).

5.6 Effect of inhibitors on antigen presentation with lower amounts of soluble anti-IgM

The ability of MG101 to reduce antigen presentation in CLL cells (**Figure 65**) was consistent with the known role of proteases for generation of peptides for loading to MHC-II. However, it was notable that MG101 did not completely block IL2 secretion but reduced it by ~60%. One possibility for the partial effects of MG101 was that the antigen presentation assay for soluble anti-IgM used (super)-saturating amounts of antibody, and was therefore relatively insensitive to the effects of inhibitors. Therefore, I decided to re-evaluate the effects of inhibitors, using a lower amount of soluble anti-

IgM in the assay. Titration experiments confirmed that anti-IgM was saturating when used at 20 µg/ml as in the initial experiments (**Figure 65**), as the level of IL2 secretion was unaffected until it was used at 6 ng/ml (**Figure 68**). Thus, antigen presentation can still be quantified even when using ~3,000-fold less soluble anti-IgM than was used in the initial experiments.

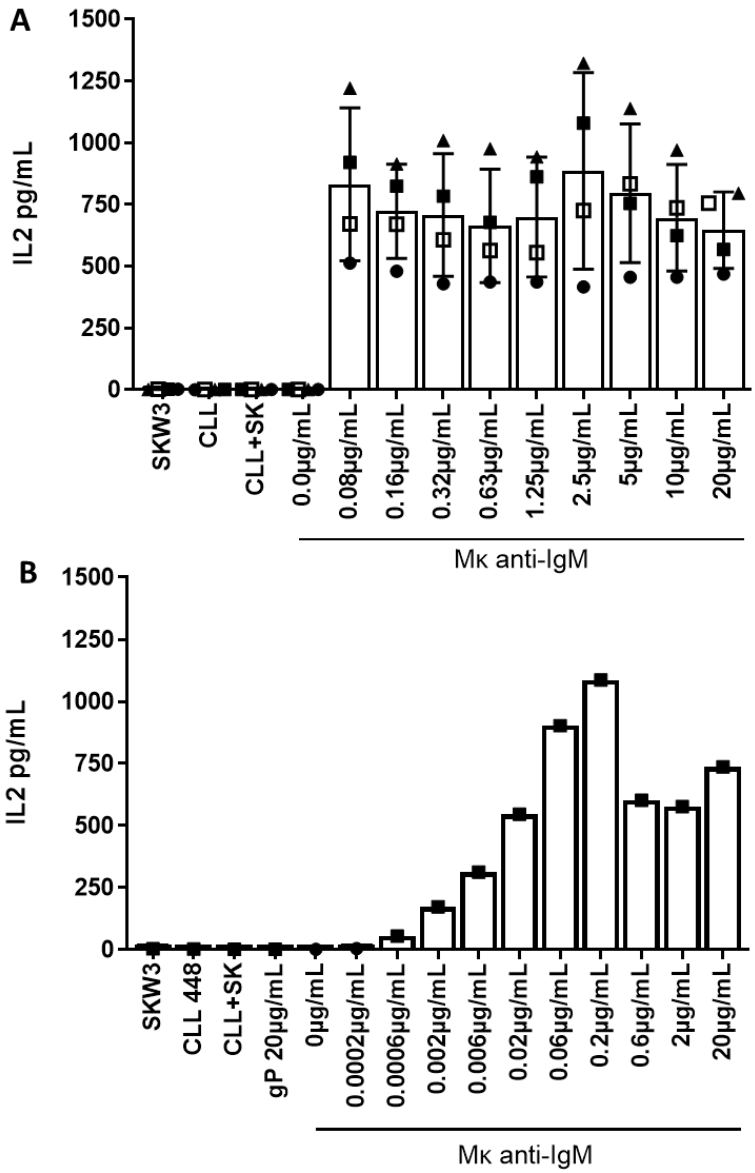

Figure 68. Effect of reducing anti-IgM concentrations on IL2 secretion.
CLL samples were treated with the indicated concentrations of soluble Ms κ+ anti-IgM (Mk) for 15 minutes and then co-cultured with SKW3-T18 cells for 24 hours before quantitation of IL2 secretion by ELISA. Controls were SKW3-T18 or CLL cells alone (A and B), or with the inclusion of CLL cells treated with goat polyclonal anti-IgM (gP) (B). Results show two experiments (A) soluble Ms κ+ anti-IgM concentration ranges from 0-20µg/mL for 4 samples. Different symbols were used for each patient sample and bars represent mean with error bars +/-SD. (B) 1 sample was used to further lower concentrations of soluble Ms κ+ anti-IgM to non-saturating levels.

Based on these titrations, the antigen presentation assay was repeated, but using the soluble Ms κ+ anti-IgM at lower concentrations (20 and 2 ng/ml). As expected, the amount of IL2 released differed between these two concentrations, so data were normalised to allow comparison of the effects of compounds. The experiment was performed using only 3 of the HLA DRB1*04:01 positive CLL samples, due to limited material available for the fourth.

The results demonstrated that the overall pattern of effects of inhibitors on IL2 secretion was similar to that described above (**Figure 65**). Thus, IL2 secretion was increased by MRT68921 and VPS34-IN1 (although only significantly for MRT68921), and effectively inhibited by entosplentinib and MG101 (**Figure 69**). However, the size of these effects was greater in these experiments, especially at the lower concentration of anti-IgM. Thus, with 2 ng/ml anti-IgM, both MG101 and entosplentinib reduced IL2 secretion by ~70-80%. Interestingly the reduction in IL2 secretion seen when CLL cells were pre-treated with idelalisib was significant in experiment using 20 ng/ml anti-IgM.

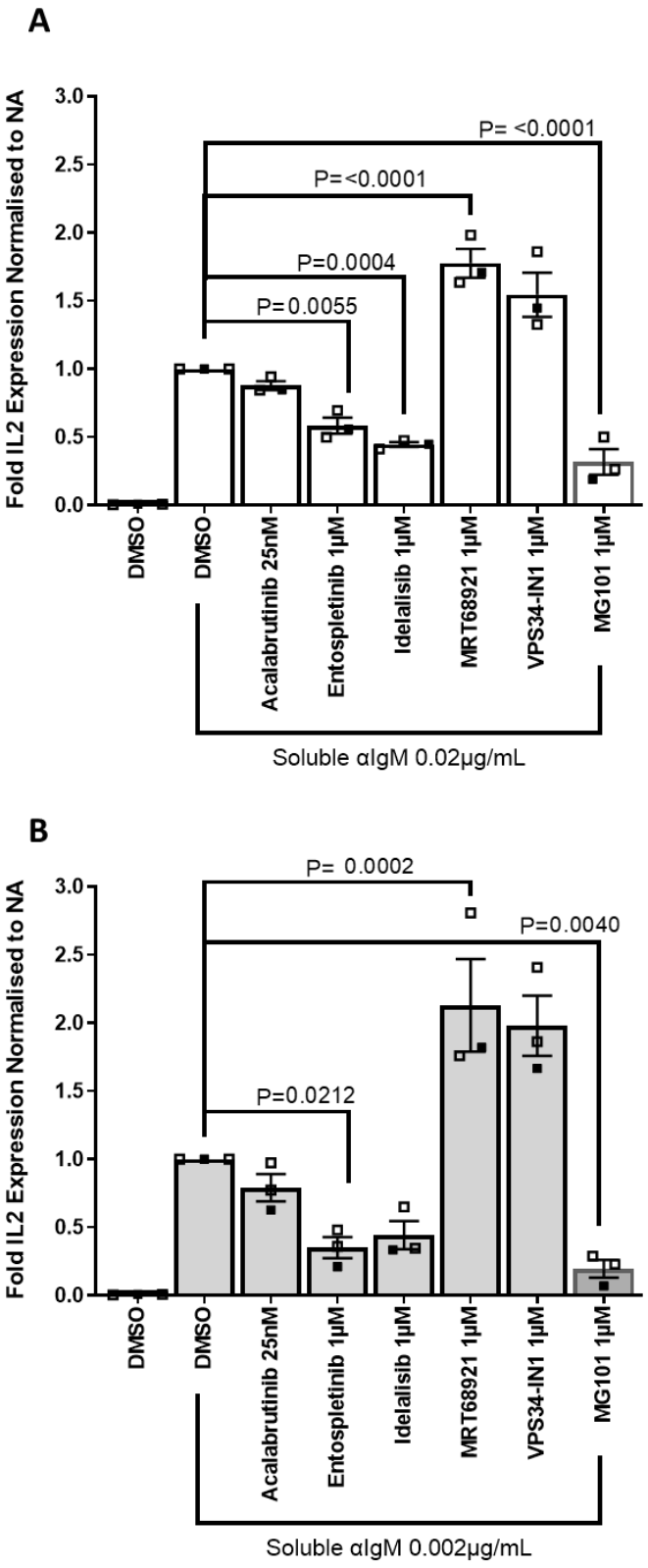

Figure 69. Effect of inhibitors on antigen presentation by CLL cells at sub-saturating concentrations of anti-IgM.

CLL samples (n=3) were pre-treated with the indicated compounds for 1 hour before treatment with soluble Ms κ+ anti-IgM at (A) 20 ng/ml or (B) 2 ng/ml for 15 minutes, and co-culture with SKW3-T18 cells for 24 hours. IL2 secretion was quantified by ELISA. Graphs show results for individual samples and mean (±SD) with values for DMSO-treated cells set to 1.0. The statistical significance (two-way Anova, multiple comparisons with Bonferroni's Multiple comparisons test) of the differences compared to anti-IgM/DMSO-treated cells is shown (if not shown P>0.05).

5.7 Summary of Results :

- CLL cells upregulate antigen presentation genes following anti-IgM treatment
- VPS34 inhibition has little effect on gene expression in the presence or absence of anti-IgM, but does appear to alter the cytokine signature modestly
- Mouse kappa light chain anti-IgM activates a BCR signalling and autophagy response
- CLL cells can present both soluble and solid-phase antigen via sIgM
- SYK-dependency differs for presentation of soluble and solid-phase antigen
- CLL cells are capable of removing antigen from beads without internalisation

5.8 Discussion

The aims of the experiments described in this chapter were to examine antigen processing and presentation in CLL. Initially, an unbiased approach was performed using RNA-seq, with antigen presentation pathways emerging as among the top pathways regulated by stimulation with anti-IgM coated beads, both at 6 and 24 hour time points. Autophagy was less clearly regulated at the RNA level, indicating potential post-transcriptional regulation, since I have shown strong regulation at the protein level (Chapter 3). Subsequent approaches to examine this antigen presentation response, and upstream regulatory pathways, used HLA-typed CLL samples and the SKW3-T18 CLL compatible cell line, engineered by the Munthe group at the University of Oslo (Os *et al.*, 2013) Results confirmed that CLL cells are able to efficiently present soluble antigen via MHC-II, and showed for the first time that CLL cells can efficiently obtain antigen from antibody-coated beads for processing and presentation. This antigen removal from beads does not seem to be dependent on SYK, whereas the processing and presentation pathway for soluble antigen in CLL seems to rely more heavily on SYK, as shown by the significant decrease in IL2 response by the T cells in the SYK-inhibited CLL cells. Reanalysis of earlier phagocytosis assay flow cytometry data showed that beads that may have engaged with CLL cells in culture, but not been phagocytosed, showed significant antibody removal from the bead surfaces. This did not seem to be significantly affected by SYK inhibitor treatment, indicating this potential antigen release pathway occurs independently of SYK.

5.8.1 RNA-seq data highlights antigen processing and presentation

IPA predicted the antigen processing response to be the number one regulated pathway by stimulation with bead immobilised anti-IgM at 6 hours. Many of the other top-ten regulated pathways were also related to antigen processing and presentation pathways and were identified

up by the IPA software due to upregulation of shared genes. Examples include Th cell activation markers, of which several are upregulated, including CD80, which can occur on B cells, where upregulation activates Th cells independently of CD86. CD134 is involved in B cell/T cell interactions. So although IPA identifies these apparently Th cell-related pathways, anti-IgM stimulation at 6 hours is actually affecting molecules on B cells that interact with a few increased T-cell molecules. STAT3 is also increased as part of this pathway and constitutively activated STAT3 plays an important role in CLL biology. CIITA is an MHC class II transactivator, involved in the MHCII- AP pathway. Macrophage pathways transcriptionally activated include SOCS3, which is repressed in CLL compared to HDB, with inhibition of this repression shown to supress signalling responses through AKT and cell proliferation (Chen *et al.*, 2016).

Overall, while VPS34-IN1 had little overall effect on the transcritiptional profile, it did seem to regulate CCL7, CXCL2 and CXCL3, and also IL1R1 in CLL cells. CCL7 is a potent chemoattractant expressed to attract a variety of cells in the immune and inflammatory responses, influencing cell migration and localisation (Balkwill, 2004). It acts as a chemotactic factor for cells including monocytes, dendritic cells, NK cells and activated T cells. This response recruits the required lymphocyte/cell subtype to infected tissues, to combat infection and coordinate the immune response. CCL7 has also been shown to promote tumour progression by supporting formation of a protective tumour microenvironment and increasing tumour metastasis (Cho *et al.*, 2012). B cells have been shown to secrete CCL7 in response to acute infection in vivo, and in response to CpG stimulation/BCR crosslinking *in vitro* (Inaba *et al.*, 2020).

CXCL3 and CXCL2 are both inflammatory chemokines capable of strong chemoattraction of neutrophils to specific areas following infection (Rudack *et al.*, 2003). They are ligands for receptors that control cell migration along concentration gradients of their ligands. CXCL3 and CXCL2 are both ligands for the receptor CXCR2(Ahuja and Murphy, 1996; Al-Alwan *et al.*, 2013) These chemokine receptors are expressed on B cells at different stages of differentiation to control migration and localisation of B cell responses (Muehlinghaus *et al.*, 2005). IL1R1 (Interleukin-1 receptor type 1) is a receptor for IL1, a key cytokine in the immune response that is predominantly secreted by macrophages and neutrophils and is characterised extensively in the context of TLR activation. It is also a key molecule in regulation of T-cell help for B cells, by inducing secretion of key proliferative cytokines that support B cell activation and differentiation (Ritvo and Klatzmann, 2019). This is potentially important as other work has shown that inhibiting Vps34, either through pharmacological inhibitors (including SAR405) or genetic knockout, resulted in inhibition of tumour growth by allowing increased NK and T cell infiltration into the tumour microenvironment. The inhibition of Vps34 in this tumour setting allowed upregulation of pro-inflammatory chemokines and cytokines, which included CCL5, CXCL10, and IFNγ, and Vps34 inhibitors improved treatment

efficacy (Janji *et al.*, 2020; Noman *et al.*, 2020). This suggests a role of Vps34 in tumour progression and protection of the tumour by microenvironmental signals which has been linked to the autophagy pathway. This protection is regulated by repression of chemokines and cytokines that would allow inflammatory responses and infiltration by anti-tumour cellular responses.

5.8.2 CLL cells can efficiently process and present soluble antigen

Results here confirm a previous study (Os *et al.*, 2013) which showed that CLL cells have the capacity to internalise, process and present soluble antigen through the BCR to activate a T cell response via MHC-II. However, the role for BCR kinases in this process, in particular SYK, has not previously been investigated. While B cells can indeed interact with soluble antigen and initiate a signalling response, the presentation of membrane-bound antigen may affect B cell activation capacity and responses, which may be particularly important during affinity-maturation, where high affinity antigen binding BCR expressing B cells are selected for and proliferation/ differentiation responses induced (Heesters *et al.*, 2016), with membrane bound antigens initiating stronger responses in vivo than soluble antigen (Carrasco and Batista, 2006).(Batista, Iber and Neuberger, 2001). On antigen binding to the BCR, receptor clustering is induced at the cell membrane and endocytosis occurs via clathrin-coated pits. Through this endocytic process, B cells are able to capture a diverse repertoire of different forms of antigen with affinity to the individual BCR, and the context and concentration of antigen may determine the resulting internalisation response. In this process, B cells capture diverse antigens in various contexts and concentrations. Recent evidence has shown that BCR cluster size increases with $F(ab')_2$ concentration (Roberts *et al.*, 2020), indicating concentration dependant mechanisms that may finetune responses in different immune contexts/ antigen availability. Furthermore, a switch of endocytosis pathways occurs dependant on these concentration dependant cluster sizes. Low concentrations of antigen, corresponding to smaller antigen-BCR cluster sizes, are internalised through a classical clathrin-mediated endocytic pathway, while higher concentrations induced a switch to larger membrane invaginations capped with dynamin, requiring recruitment of actin and the actin polymerizing protein FCHSD2 (Roberts *et al.*, 2020). Therefore, even in the context of soluble $F(ab')_2$, concentration dependant internalisation changes can occur. This, in particular makes the last titration experiment I described, and the use of inhibitors at these lower levels of anti-IgM, of interest. It could also explain why idelalisib becomes significant for reduction of antigen presentation at lower antibody concentrations.

One striking finding with the soluble antigen response results I present here is the requirement for SYK, which is not seemingly required in the bead-immobilised antigen response pathway (or to a lesser extent at least). This indicates different pathways operating between soluble and particulate

antigen, which is perhaps not surprising. What is a surprising observation is that SYK inhibition prevents soluble antigen downstream processing and presentation to T cells. Significant antigen processing inhibition can be noted at both high and low antibody concentrations, suggesting this is not dependent on different size receptor-antibody aggregates that could be induced at high antigen concentrations. There are some conflicting reports in B cells about whether signalling inhibition inhibits receptor endocytosis. Unpublished work by the Southampton CLL group, utilising quenching assays in addition to microscopy, indicates that inhibiting SYK does not inhibit BCR endocytosis. Literature reports that BCR endocytosis through lipid rafts is inhibited when early signalling molecules, such as LYN, are inhibited (Stoddart *et al.*, 2002; Niiro *et al.*, 2004), however, other literature indicates that SYK inhibition does not affect BCR-antigen internalisation (Caballero *et al.*, 2006). The role of actin has also been proposed in BCR internalisation and trafficking to endosomes (Brown and Song, 2001). Overall there is some conflict in literature, but data from our group, working on CLL with the same inhibitors and antibodies, has indicated that signalling inhibition does not block endocytosis of soluble antibody in CLL. Thus, it appears that SYK may be required in the downstream antigen processing response, eg to allow trafficking to MHC-II loading compartments. In dendritic cells, SYK has been shown to be required for internalisation of antigen complexes (plate immobilised antibody) and antigen presentation to T cells (measured by antibody conjugation to OVA) (Sedlik *et al.*, 2003). In B cells, SYK has been shown to regulate actin filament dynamics involved in BCR-antigen endocytosis, trafficking and processing of antigen captured by the BCR (Le Roux *et al.*, 2007). Therefore it could be that SYK is involved in the downstream trafficking and processing of antigen following endocytosis of soluble mouse kappa anti-IgM.

5.8.3 CLL cells are efficiently able to remove and process antigen from beads, potentially through a distinct pathway

Results here show that CLL cells are able to efficiently able to process and present soluble antigen to activate T cells, but surprisingly, they are also able to process antigen from beads, and even where phagocytosis does not occur, or is blocked with inhibitors, are able to remove antigen from these beads. B cells rely on antigen capture mechanisms to gather immobilised antigen, and transport these to the immune synapse. Engagement of the BCR by antigens tethered to a surface, such as a cell membrane (which we are effectively using beads to model a form of) induces immune synapse formation that results in BCR driven antigen uptake, for the purpose of processing and presentation onto HLA/MHC-II molecules. There are two predominant mechanisms proposed for the initial B cell mechanism of antigen capture. One mechanism involves enzymatic degradation of antigen from its source through localised lysosome secretion, a mechanism thought to be more useful in capture of antigens with lower affinity for the BCR (Yuseff *et al.*, 2011; Ibanez-Vega *et al.*,

2019). MHC-II-containing lysosomes have been shown to be recruited to the B cell –antigen synapse, where they subsequently undergo exocytosis. This causes localised acidification of the synapse and release of hydrolases. The combination of these events leads to chemical extraction of the immobilized antigen.(Yuseff *et al.*, 2011). These mechanisms could potentially be involved in removal of antigen from beads where signalling and phagocytosis is blocked, switching instead to an alternative pathway.

However, these extracellular protease/ lysosomal secretion mechanisms for antigen capture have also been linked to signalling requirements. Following BCR engagement, atypical protein kinase C (aPKCζ) is activated through phosphorylation, inducing lysosome recruitment, trafficking and secretion at the formed synapse. These pathways couple BCR signalling with antigen extraction at the synapse, and downstream processing and presentation (Yuseff *et al.*, 2011) Microtubule stabilization, triggered by engagement of the BCR, has been shown to prompt release of centrosome-associated Exo70 into the immune synapse. Thus, B cells deficient in Exo70 are unable to effectively process and present antigen. Centrosome repositioning and corresponding changes in microtubule stability has been shown to promote lysosome secretion at the immune synapse (Ibanez-Vega *et al.*, 2019; Ibanez-Vega *et al.*, 2021), indicating a role for cytoskeleton remodelling in endocytic events and lysosomal secretion to retrieve antigen. Interestingly, ERK1/2 have been shown to regulate exocytosis through phosphorylation of Exo70 (Le Roux *et al.*, 2007), further suggesting that BCR signalling may be required for this process. This fails to explain how antigen removal from beads is unaffected by signal inhibition or use of phagocytosis inhibitors in the results shown in this chapter. A summary of results, and the requirement of each signalling or autophagy pathway found for the responses measured, is shown in **Table 17**.

Compound	Effect	Soluble anti-IgM IL2 response	Bead anti-IgM IL2 response	Effect on internalisation	Effect on BCR driven Autophagy
ibrutinib 25 nM	BTK inhibitor	No effect	No effect	Little effect	Partial Inhibition
acalabrutinib 25nM	BTK inhibitor	No effect	No effect	Not tested	Partial inhibition
Entospletinib 1µM	SYK inhibitor	~50% reduction	¾ patients no effect- 1 patient strong effect	Complete inhibition of bead phagocytosis, no effect on soluble	Strong inhibition
Idelalisib 1µM	PI3K delta inhibitor	~20% reduction	Little effect	Little effect	More inhibition than ibrutinib, less than entospletinib
MRT68921 1µM	ULK1/2 inhibitor (pre-initiation)	~40% increase	~40% increase	Not tested	~30% LC3B-II inhibition
VPS34-IN1 1µM	VPS34 inhibitor (initiation)	~20% increase	~30% increase	No effect	~30% LC3B-II inhibition
HCQ 10µM/ Bafilomycin 100nM	Inhibit autophagosome /lysosome turnover	No effect	No effect	No effect	Inhibit turnover- increase accumulated autophagosomes
MG101	Proteasome inhibitor	~50% reduction	~50% reduction	Not tested	Decreases LC3B-II ?

Table 17. CLL Sample Response to Inhibitors

Actin-myosin mediated pulling forces have also been proposed as a second mechanism for antigen extraction by B cells, and since this relies on physical forces, requires strong binding of the BCR to the cognate antigen in order for antigen removal through force. Therefore, this physical mechanism of antigen removal also allows discrimination of high and low binding affinity antigens. These antigens are then internalised into clathrin-coated pits, implicating dynamin in this process (Natkanski *et al.*, 2013; Tolar and Spillane, 2014; Hoogeboom *et al.*, 2018). It is likely that a dual approach is taken by B cells to capture antigen, utilising both localised protease/lysosomal secretion and mechanical forces at the B cell immune synapse, acting in coordination to promote antigen extraction. The exact sequence of events and molecular mechanisms utilised for different sizes and forms of antigen, or antigen affinity dependency, remains to be elucidated however. Mechanistically, it is possible that myosin regulated pulling forces are more important for high affinity antigen, whereas lysosomal secretion mechanisms could be more important for lower affinity antigen (Yuseff and Lennon-Dumenil, 2015). Research using flexible membrane substrates, to better imitate the antigen bound surface provided in the context of antigen presented on antigen presenting cells, B cells have been shown to acquire antigen using myosin IIa mediated contractions, resulting in pulling and invagination of the membranes on which the antigen is presented on. The forces generated at the membranes by these myosin contractions were shown to rupture and break most BCR-antigen bonds, promoting the endocytosis of higher -affinity, multivalent BCR clusters, and not those with low affinity or valency. This further supports the role for physical, contractile based antigen removal in discrimination of high affinity antigen and retrieval from the immune synapse.(Natkanski *et al.*, 2013). Dynein recruitment has also been shown to be required for antigen extraction and organisation of MHC-II at synapses, as well as lysosomal secretion in enzymatic removal mechanisms.(Reversat *et al.*, 2015). In the experiments in this chapter where I examined anti-IgM removal from beads in an analysis of the flow-based phagocytosis assay, the only compound that seemed to have a slight effect on antibody removal from the beads was cytochalasin D, the actin filament polymerisation inhibitor. However, these results did not achieve statistical significance. It remains unclear the mechanism that CLL cells are utilising to extract bead immobilised antigen where phagocytosis and signalling is inhibited.

Alternatively, another mechanism for direct swapping of antigen from the BCR to surface MHC/HLA molecules has been proposed. Endocytosed antigens are proteolytically processed and small amounts of peptides captured by class II MHC molecules. However, when antigen is bound to the B cell antigen receptor (BCR), processing can trigger a concerted ‘hand-over' reaction whereby BCR-associated processed antigen is captured by neighbouring class II MHC molecules on the cell surface (Moss, Tree and Watts, 2007).

Chapter 6 : Final Discussion

This thesis tests the central hypothesis that BCR driven autophagy is involved in antigen processing and presentation in CLL. However, a surprising observation during testing of this hypothesis was that CLL cells were able to phagocytose anti-IgM coated beads. Therefore, a second hypothesis was tested, that BCR-driven autophagy and phagocytosis were involved in antigen processing and presentation in CLL.

In order to test this hypothesis, I first needed to characterise the autophagy pathway driven by the B-cell receptor, before moving onto functional studies. The three main aims of this thesis were:
1) To examine BCR driven autophagy in CLL.
2) To examine BCR driven phagocytosis in CLL
3) To determine functional relevance by testing the roles of each in antigen processing

The main findings were:

(1) Autophagy is induced following BCR activation using anti-IgM- or anti-IgD-coated beads. This response peaked at 24 hours post-stimulation and was strongest for anti-IgM coated beads. It is dependent on BCR signalling, especially SYK, as it was most strongly inhibited by entospletinib.

(2) At 24 hours, anti-Ig-induced autophagy appears to occur through a canonical autophagosome formation pathway. The machinery involved includes ULK1/2 (activation demonstrated through increased S318-phosphorylation of ATG13, and inhibition of anti-IgM-induced LC3B-II expression by MRT68921) and Vps34 (demonstrated through inhibition of anti-IgM-induced LC3B-II expression by SAR405 and VPS34-IN1). Experiments with Baf and HCQ confirmed induction of active autophagy.

(3) CLL cells are able to internalise anti-IgM-coated beads. Internalisation was detected within 3 hours and was, for 3 micron beads,mediated via a phagocytosis-like pathway as it was dependent on actin remodelling and signalling (SYK), but not dynamin. Autophagy inhibition did not affect bead internalisation.

(4) Stimulation of the BCR using bead-bound anti-IgM resulted in strong induction of the antigen presentation pathway. In comparison, autophagy inhibition (VPS34-IN1) had relatively little effect on gene expression but did appear to increase expression of RNAs encoding several cytokines/chemokines shown to aid in clearance of tumour cells.

(5) As previously demonstrated for soluble antigen (Os *et al.*, 2013), CLL cells are able to efficiently present solid-phase antigen (from anti-IgM-coated beads) via MHC-II. Antigen presentation was independent of autophagy, whereas SYK appeared to play an important role in presentation of soluble, but not solid-phase antigen. For soluble antigen, inhibitory effects of SYK inhibition increased as the amount of antigen used in the experiment was reduced.

(6) CLL cells are able to remove antigen (anti-IgM) from non-internalised beads in a SYK-independent manner.

Taken together, these results support the hypothesis that BCR signalling can induce autophagy in CLL cells, and may therefore explain the increased basal autophagy that is detected in CLL cells compared to normal B cells (Smith *et al.*, 2020).

The findings presented in this thesis strongly support the role of BCR signalling in autophagy induction in CLL. They also strongly support a role for BCR signalling in phagocytosis of anti-IgM coated beads in CLL. I also display the novel result that CLL cells are efficiently able to remove antigen from a particulate source, and present this on HLA II, to initiate T cell responses. The role for autophagy in these events, and the type of autophagy, remains unclear, and was not able to be fully answered during the course of this thesis.

6.1 Key questions

6.1.1 What is the biological and clinical significance of BCR-induced ATG in CLL cells?

Autophagy is an active cellular process involving the sequestration of cytoplasmic components, such as excess or damaged/ misfolded proteins and organelles, inside double membrane bound compartments called autophagosomes, followed by enzymatic degradation upon fusion with lysosomes. This recycles essential components, such as glucose and amino acids, for redistribution to required areas of the cell. Among the most well studied forms of autophagy are those induced by cellular starvation or stress, which induces signalling through AMPK, inhibition of negative regulation by mTORC1, and activation of the ULK pre-initiation and the downstream VPS34 containing initiation complexes. This triggers formation and elongation of the autophagosome membrane, a process involving insertion of lipidated LC3B-II and GABARAPL2 via ATG protein regulation. These are termed canonical autophagy pathways as they involve the initiation and pre-initiation complexes and formation of a double membrane bound autophagosome. However, LC3 can also be lipidated onto single-membrane, non autophagosomal structures, in a process that may bypass the ULK complex and upstream regulation. These are termed non-canonical autophagic processes and include LAP and entosis. Emerging roles for forms of autophagy, or combinations of several types, are becoming apparent in development, ageing, pathogenesis of infections, immune regulation and cancer- both in tumour prevention and progression.

In CLL, high basal expression of the autophagy genes, BECN1, PIK3C3, and PIK3R4, have been significantly associated with a shorter time to first treatment. They also correlated to poorer survival outcomes (Kristensen *et al.*, 2015), while BECN1 and ATG5 RNA expression correlate with poorer clinical outcome (Kong *et al.*, 2018). We previously illustrated expression of autophagy markers also correlated to shorter time to first treatment, more progressive disease, and poorer survival (Smith *et al.*, 2020) This was correlated to BCR signalling capacity, linking BCR driven autophagy to clinical outcome. LC3B-II, GABARAPL2, ATG3 and ATG7 are all upregulated in CLL compared to healthy donor B cells, and further upregulated in U-CLL compared to M-CLL. In other work, a small study in patient settings, two U-CLL patients with more progressive disease showed increased expression of LC3B, in addition to positive expression of CD38 and ZAP70, and autophagy correlates with CLL progression (Arroyo *et al.*, 2020). These findings all clearly link autophagy to CLL clinical outcome and progression, and our findings link this to BCR signalling capacity. However, the functional role of this autophagy remains unclear. My results show that autophagy doesn't appear

to contribute to Ag presentation, as autophagy inhibition using VPS34 and ULK inhibitors did not inhibit or reduce antigen processing of either soluble or particulate anti-IgM. IL2 production by the T cell line utilised was not decreased, (as shown in Chapter 5). Autophagy inhibition had no effect on bead internalisation either(Chapter 4) or removal of antigen from beads (Chapter 5), two possible routes of antigen capture. These results show that Autophagy does not play a role in antigen capture or processing in CLL. RNA seq analysis following anti-IgM treatment and subsequent IPA displayed that anti-IgM strongly regulated antigen processing pathways, showing the BCR as a dual signal transducer and antigen capture receptor. Since anti-IgM is well known to provide survival signals for CLL cells(Krysov *et al.*, 2014; Ten Hacken *et al.*, 2016), one hypothesis for the function of autophagy in CLL could be that autophagy may be involved in part of these pro-survival mechanisms. Autophagy has well established roles in aiding in survival under cellular stress, and in the context of cancers this can translate to treatment resistance mechanisms. This is supported by the evidence from this thesis that autophagy occurring following anti-IgM stimulation is occurring through a canonical pathway.

In support of this hypothesis, autophagy has also been linked to treatment resistance in CLL. Fludarabine or flavopiridol treatment have been shown to promote autophagy, with cell based assays showing that while chloroquine treatment showed no effect on fludarabine-mediated cell death, it enhanced cytotoxicity of flavopiridol consistently, and induction of autophagy appears to contribute to flavopiridol resistance in CLL (Mahoney, 2010; Mahoney *et al.*, 2012). Autophagy inhibition has also been shown to sensitise CLL cells to venetoclax induced apoptosis, with venetoclax treatment inducing autophagy as a survival response (Smith *et al.*, 2020; Avsec *et al.*, 2021). Based on these findings, it is possible that autophagy inhibitors have the potential for use in the clinical setting to improve treatment outcomes, in combination with other compounds. However, in CML and other forms of cancer, clinical trials show Chloroquine and hydroxychloroquine to be suboptimal at autophagy inhibition in the patient setting (Helgason *et al.*, 2013; Baquero *et al.*, 2019), with better second-generation autophagy inhibitors required.

Autophagy has been demonstrated as a pro-survival function in CLL in treatment resistance and the role in the protective stromal environment, with results demonstrating that CLL cells display high basal levels of oxidative stress. This oxidative stress is subsequently increased further by vorinostat treatment. As a consequence, CLL cells released hydrogen peroxide, which triggered autophagy, mitophagy and glycolysis in surrounding stromal cells. This resulted in CLL cells driving higher ATP production and enabled them to better resist treatment. A key finding of this work was that by targeting autophagy in this protective stromal cell environment, stromal protection against vorinostat treatment was markedly decreased in CLL cells. The conclusions from this work were that CLL stromal cells and the surrounding tumour microenvironment undergoes abnormal

autophagy to cope with treatment induced stress, and targeting this autophagy could help provide more effective treatment in CLL where stromal cells are providing protection. (Ding *et al.*, 2018). Similarly, insensitivity of Chronic Myeloid Leukaemia (CML) stem cells to Tyrosine Kinase Inhibitor (TKI) treatment may be driven by autophagy, and, autophagy inhibition using HCQ sensitised CML cells, and CML stem cells, to TKI treatment (Helgason *et al.*, 2013)

RNA seq data following inhibition of VPS34 using VPS34-IN1 did not alter BCR-induced gene expression (Chapter 5), although RNAseq did reveal impact of VPS34 on regulation of the chemokines CCL7, CXCL2 and CXCL3, and also IL1R1 in CLL cells. Interestingly, other work in CLL has shown that a subset of CLL patients with a form of rapidly progressive CLL showed loss of the expression of the costimulatory molecule SLAMF1, and that this correlates with significantly shorter time to first treatment and reduced survival outcomes. SLAMF1 deficiency associated with increased expression of CXCR4, CD38, and CD44, and positively affected chemotaxis response to CXCL12. Loss of SLAMF1 expression in CLL modulates genetic pathways that regulate chemotaxis and autophagy, with targeting of SLAMF1 through antibodies causing Beclin1 to associate with an autophagosomal complex containing SLAMF1, beclin1, and Vps34 (Bologna *et al.*, 2016; Bologna and Deaglio, 2018). Vps34 inhibition decreases melanoma cell growth and, in vivo, improved mice survival. In the tumour setting, inhibition of Vps34 increases infiltration of NK and T cells through cytokine regulation (Noman *et al.*, 2020), so targeting autophagy may be of therapeutic relevance in this context. Taken together, this indicates a role for Vps34 and the autophagy machinery in regulation of cytokine and chemokine associated regulation and responses, which may be of relevance in the tumour microenvironment and T cell infiltration.

One surprising result demonstrated in Chapter 5 was that the autophagy inhibitors ULK1/2 and VPS34-IN1 increased IL2 secretion in response to either soluble, or bead immobilised anti-IgM, rather than reduced the antigen processing and presentation response at all. This was surprising as autophagy has been demonstrated to contribute to Ag presentation via MHC-II by B cells in some settings. For example, there was a slight increase in IL2 secretion for SKW3-T18 when incubated with autophagy inhibitors without CLL cells (Shown in supplemental Figure S5) This is supported by literature showing cytokine regulation by autophagy in T cells (Hubbard *et al.*, 2010; Botbol, Guerrero-Ros and Macian, 2016). However, the T cell IL2 response to autophagy inhibitors alone failed to account for the magnitude of effect on IL2 production when cocultured with CLL cells that had been pre-incubated with autophagy inhibitors and then stimulated with anti-IgM. One possible explanation for autophagy inhibitors increasing the T cell IL2 response further when activated through MHC-II presentation of antigen by CLL cells, could be a role for autophagy in cross-presentation of intracellular antigen to MHC-II , which has been described in B cells (Li *et al.*, 2008; Van Kaer *et al.*, 2019). Reducing such cross-presentation of endogenous antigen may subsequently increase the CLL cells capacity for canonical MHCII presentation, therefore increasing T-cell activation responses to presented antigen. Autophagy may also be involved in negative regulation by decreasing the available peptide/antigen pool available for loading to MHCII, or decreasing available cell surface levels of MHCII, mechanisms described for autophagy regulation in MHCI pathways (Wenger *et al.*, 2012; Loi *et al.*, 2016; Yamamoto *et al.*, 2020).

6.1.2 What is the clinical significance of Ag presentation to Th cells in CLL?

There is increasing interest in the chronic lymphocytic leukaemia (CLL) microenvironment and the mechanisms that may promote CLL cell survival and proliferation. Healthy B cells need to gain help through T cell selection as part of the differentiation and proliferation response that gives rise to high affinity antibody producing plasma cells. A role for T helper cells has been suggested in CLL, but current evidence is circumstantial. T cells may aid CLL cell survival by preventing apoptosis and increasing CLL cell proliferation responses (Burger, Ghia, Rosenwald, & Caligaris-Cappio, 2009; Ferrer et al., 2014; Os et al., 2013; Panayiotidis, Ganeshaguru, Jabbar, & Hoffbrand, 1993). CLL patients have been shown to have increased numbers of CD8+ and CD4+ T-cells compared to healthy donors (Gonzalez-Rodriguez et al., 2010), with more of these T cell subsets present in more progressive CLL subtypes (Palma et al., 2017) .

In order for T cells to play a role in aiding CLL cell survival in vivo, the CLL cells must be capable of presenting antigen and eliciting cognate T cell help, which they are capable of with soluble anti-IgM(Os *et al.*, 2013). However, while T-cell numbers are increased in CLL lymph nodes, they display a dysfunctional phenotype. CLL patient T cells showed impaired actin filament reorganisation, preventing robust immune synapse formation with antigen presenting cells (Ramsay *et al.*, 2008), and this appears to be a process driven by the CLL cells themselves, which is induced when CLL cells engage with healthy T cells. This process induces a T cell exhaustion phenotype, driven by CLL cells, likely through utilising antigen presentation pathways to recruit T cells- frequently engaging in subsequent synapse formation and signalling, without subsequent differentiation responses. (Arruga *et al.*, 2020).

CLL is frequently associated with autoimmune diseases directed against constituents of the blood, including haemolytic anaemia (AIHA), with the suggestion that this predisposition to autoimmunity is due to CLL cells acting as aberrant antigen-presenting cells. CLL cells have been shown to be effective at inducing T cell responses to Rh autoantigen, with purified CLL cells being shown as responsible for this autoimmunity, driving autoimmune responses by acting as aberrant APCs. (Hall *et al.*, 2005). This ability of CLL cells to engage autoantigen and present to T cells, effectively activating and engaging Th cell proliferation responses, could contribute to the anergic CLL phenotype and exhausted T cell phenotypes characteristic of CLL. Repeated T cell engagement could also induce a protective or proliferative response, and increase CLL cell survival. Therefore the examination of CLL cells capacity to process and present antigen, inducing T cell responses and the pathways involved in these, is of clinical relevance in CLL. Previous work has suggested that CLL is driven by ongoing immune responses related to Th cell-CLL cell interaction following antigen presentation(Os *et al.*, 2013), therefore Th cells could support malignant B cells and targeting these

could be of clinical relevance in CLL treatment. Particulate antigen creates a stronger GC response than soluble (Martinez-Riano *et al.*, 2018), so the observations presented in this thesis may be particularly relevant for CLL pathogenesis

6.1.3 What is the pathway of presentation of particulate Ag?

B cells are able to extract antigen from a number of pathways via the BCR, as discussed in 5.8.3. Here I demonstrated that not only could CLL cells efficiently process and present soluble antigen, but that two potential pathways could contribute to the ability of CLL cells to gain antigen from beads. CLL cells internalised anti-IgM, but not control antibody-coated beads. The pathway for this resembles phagocytosis, as I have demonstrated it was dependent on actin remodelling, but not dynamin, and was inhibited by entospletinib. This is consistent with the requirement for BCR-mediated signalling in phagocytosis of anti-IgM-coated beads, by normal B cells (Batista and Neuberger, 2000). CLL cells are also able to efficiently remove antigen from anti-IgM coated beads and present to T cells, initiating T cell cytokine production and proliferation responses. Surprisingly, the processing of bead immobilised antigen does not appear to require SYK or phagocytosis, or can occur when these pathways are inhibited through a switch to an alternative processing pathway, not initiated for soluble antigen. This occurs efficiently when SYK is inhibited, or when phagocytosis is inhibited through actin filament polymerisation inhibition.

One potential explanation for this could be the switch to extracellular processing pathways, where antigen internalisation or traditional capture mechanisms are inhibited. Two pathways have been outlined previously, which include the physical pulling mechanisms of antigen extraction and the secretion of lysosomal proteases at the synapse. Enzymatic secretion pathways can be utilised where physical capture mechanisms fail, such as where antigen affinity is weaker or where phagocytosis is inhibited. Below I will outline the four potential scenarios presented in this thesis for extraction of either soluble or bead immobilised anti-IgM in the presence and absence of SYK inhibition.

Soluble antigen (anti-IgM) binds to the BCR and initiates a weak signalling response compared to bead immobilised antigen, corresponding to the ability of particulate antigen to produce stronger GC responses than soluble. These result in receptor clustering and internalisation of the BCR-antigen complex. Antigen is processed and loaded onto HLA-II, and presented on the cell surface to initiate a T cell response (Figure 70)

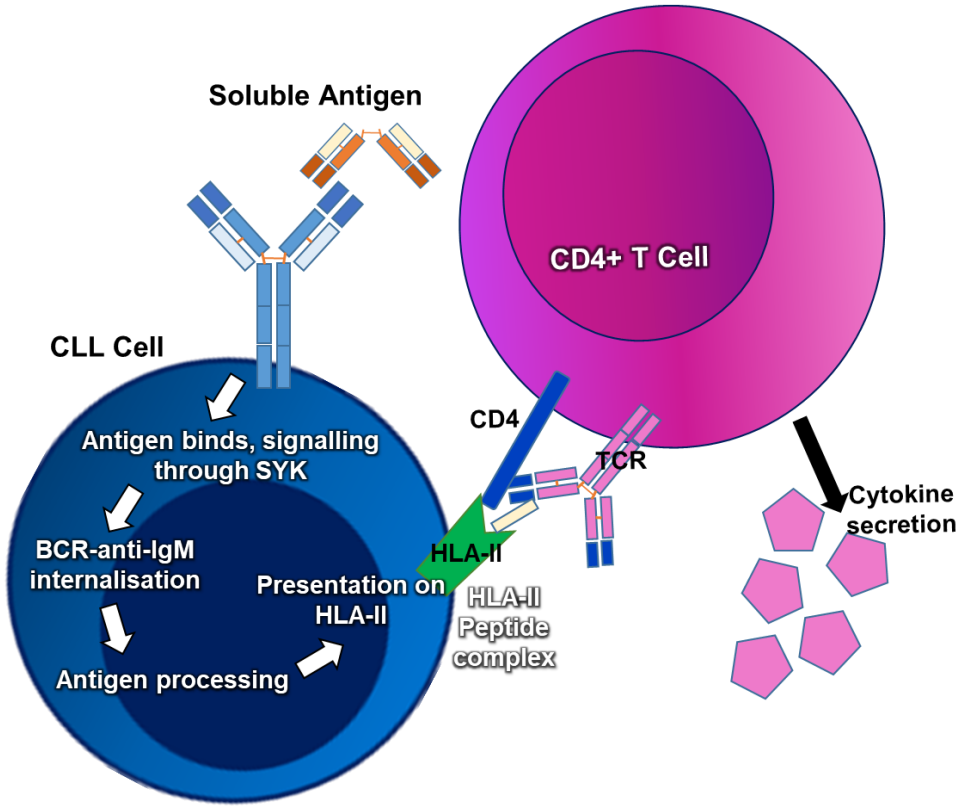

Figure 70. Illustration of potential mechanism of soluble antigen extraction

Soluble antigen (anti-IgM) binds to the BCR, resulting in receptor clustering and internalisation of the BCR-antigen complex. Antigen is processed and loaded onto HLA-II, and presented on the cell surface to initiate a T cell response when the cognate TCR is encountered, inducing cytokine secretion and proliferation/differentiation.

In the presence of a SYK inhibitor, such as entospletinib, soluble anti-IgM binds to the BCR and attempts to initiate a signalling response, which is blockaded by inhibition of SYK. Receptor internalisation may be inhibited, but previous results examining soluble antibody internalisation pathways indicate internalisation of the BCR antigen complex is still likely. However, blocking SYK and signalling .inhibits antigen processing and loading onto HLA-II, and subsequent presentation is inhibited. Therefore no T cell response can be actioned and no cytokine secretion occurs(Figure 71)

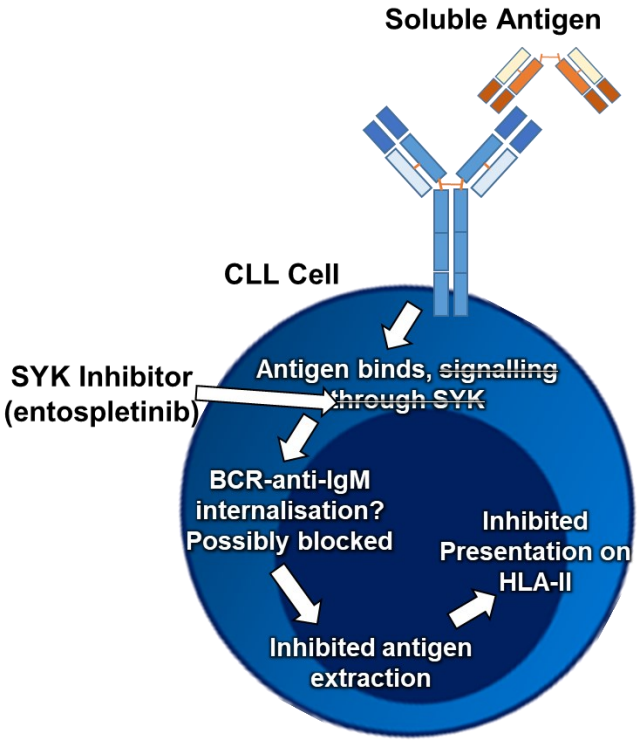

Figure 71. Illustration of potential mechanism of soluble antigen extraction where SYK is inhibited

In the presence of a SYK inhibitor, such as entospletinib, soluble anti-IgM binds to the BCR and attempts to initiate a signalling response, which is bloackaded by inhibition of SYK. Antigen processing and presentation is inhibited, but possibly not BCR internalisation. No T cell response is initiated.

In the context of bead immobilised antigen (anti-IgM), Binding of antigen to the BCR initiates receptor clustering and phagocytosis of the entire BCR-antigen-bead complex. Antigen is then subsequently removed from the beads and loaded onto HLA-II, where it is shuttled to the cell surface and presented. This initiates activation of the cognate T helper cell and cytokine secretion (Figure 72). This likely occurs by a physical attempt at pulling of antigen following binding, and subsequent phagocytosis pathway activation when antigen removal doesn't occur at the cell surface. Autophagy is unlikely to be involved in this process, as inhibition does not inhibit this processing, and this phagocytosis occurs within <3 hours of incubation with bead immobilised anti-IgM.

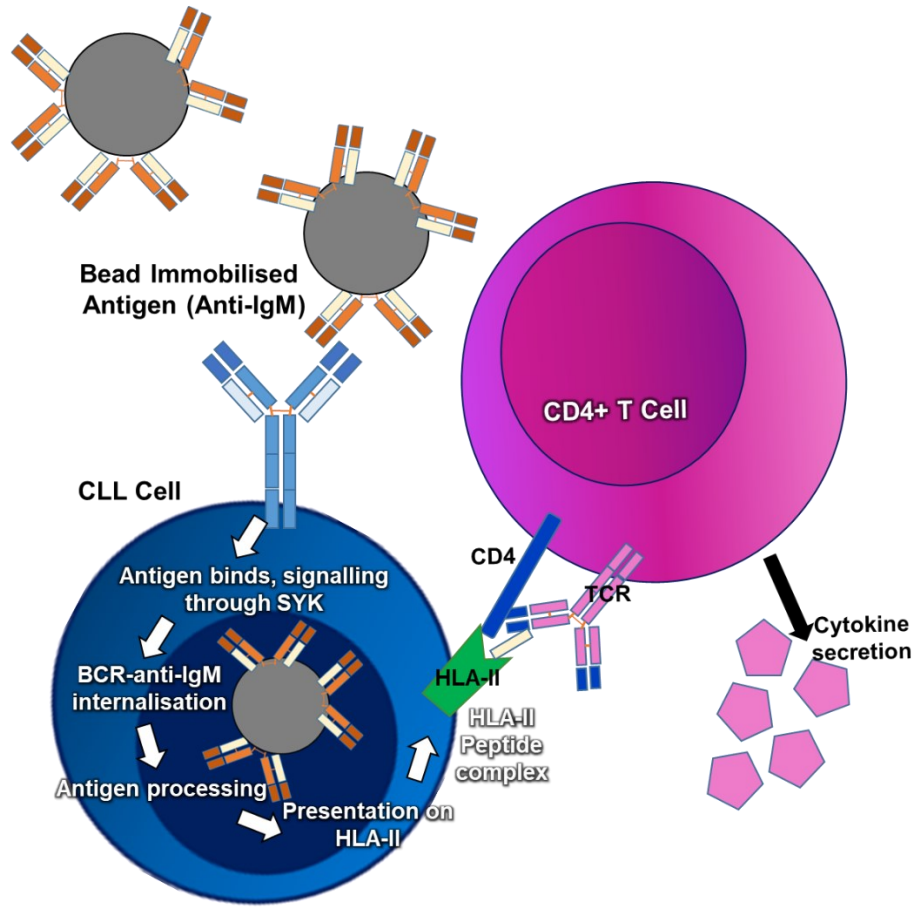

Figure 72. Illustration of potential mechanism of antigen from removal from beads.
Binding of bead-immobilised anti-IgM to the BCR initiates receptor clustering and phagocytosis of the entire BCR-antigen-bead complex. Antigen is subsequently removed from beads and loaded onto HLA-II, where it is presented on the cell surface. This initiates activation of the cognate T helper cell and cytokine secretion

Where CLL cells are pre-incubated with entospletinib, a SYK inhibitor, binding of bead immobilised anti-IgM to the BCR initiates receptor clustering and attempted phagocytosis of the entire BCR-antigen-bead complex. However, I have shown in chapter 4 that this phagocytic pathway is inhibited, and in chapter 5 that the CLL cells still find a way to remove antigen from the bead, which is unaffected by any inhibitor used in the assay. Therefore phagocytosis of the BCR-anti-IgM-bead complex is inhibited. In these circumstances, B cells may switch to lysosomal secretion at the synapse to remove antigen enzymatically (Yuseff *et al.*, 2011). Furthermore, direct handover of antigen processed at the synapse to HLA-II on the cell surface has also been documented in B cells (Moss, Tree and Watts, 2007). These mechanisms point to CLL cells utilising enzymatic pathways to remove anti-IgM from beads where phagocytosis fails, as documented in healthy B cells (Spillane and Tolar, 2018). Illustrated below is one hypothesis for how CLL cells may be able to switch to lysosomal secretion mechanisms, and utilise BCR-HLA-II handover approaches to present the processed antigen (Figure 73).

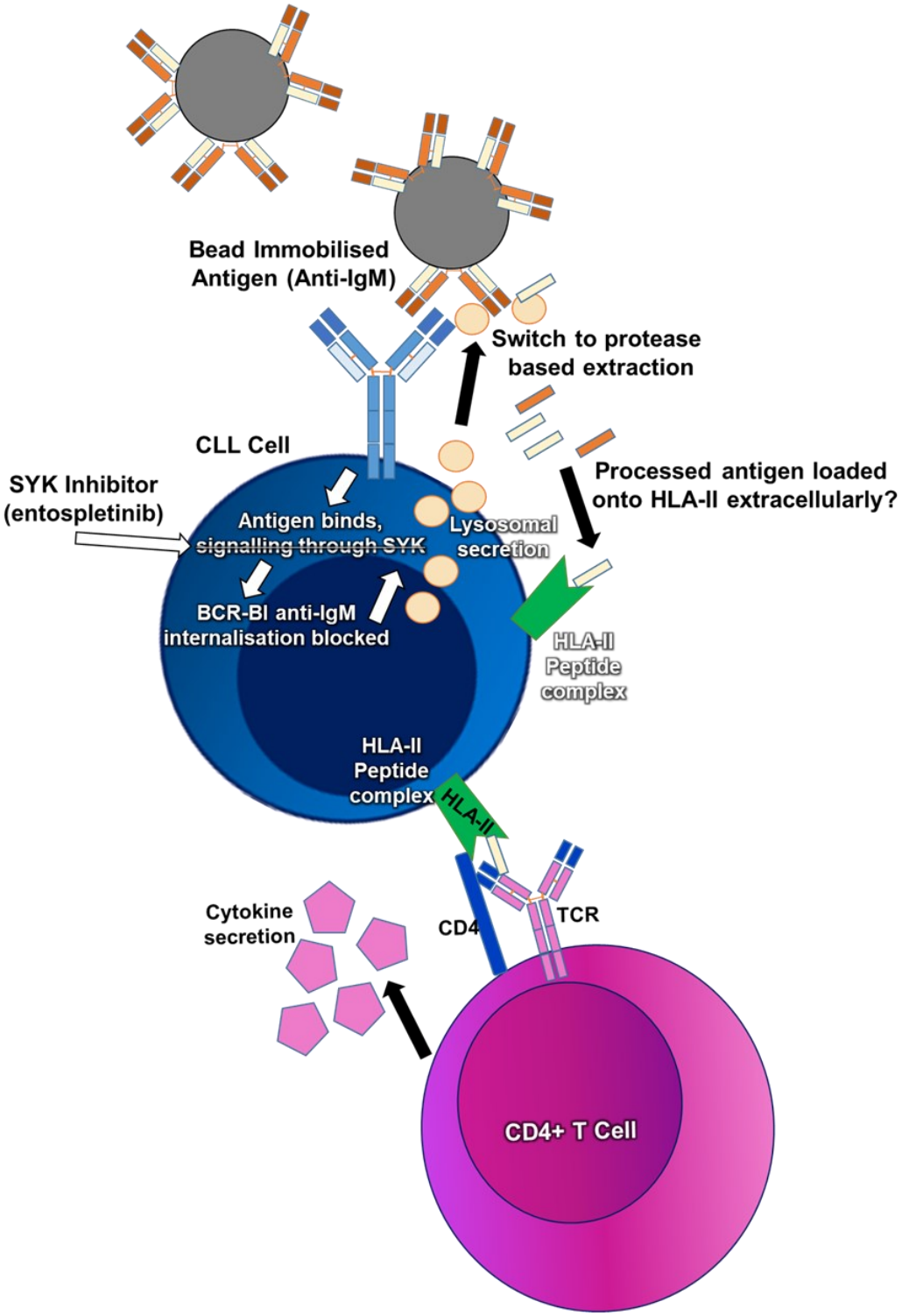

Figure 73. Illustration of potential mechanism of antigen from removal from beads where SYK is inhibited.

Where SYK is inhibited through use of a compound such as entospletinib, CLL cells bind bead immobilised anti-IgM but fail to phagocytose the BCR-anti-IgM-bead complex. In these circumstances, CLL cells may switch to proteolytic antigen removal and processing mechanisms through secretion of lysosomes. The antigen processed at the synapse may then undergo a handover reaction to complex to HLA-II already present on the CLL cell surface.

6.1.4 What is the clinical significance of kinase inhibition on Ag presentation?

The BCR plays a critical role in the pathogenesis of CLL and inhibitors targeted against these pathways, including ibrutinib, have revolutionised treatment for CLL. Multiple findings suggest that Th cells can support the accumulation of CLL cells in vivo, with one study demonstrating the capacity for CLL cells to utilise the BCR to internalise soluble antigen, and subsequently present this antigen for T-cell help (Os *et al.*, 2013). In this thesis I have demonstrated that CLL cells are capable of presenting antigen from particulate source to elicit T cell help, and this is of clinical relevance as particulate antigen elicits a stronger GC response than soluble (Batista and Neuberger, 2000; Martinez-Riano *et al.*, 2018). I displayed that these antigen processing responses in CLL are dependent on SYK, and are affected by the physical characteristics of antigen, including size and concentration.

An interesting finding was that while entospletinib effectively inhibited BCR driven autophagy, phagocytosis and antigen processing and presentation responses, at least for soluble antibody, ibrutinib, acalabrutinib and idelalisib were less effective at inhibiting BCR driven autophagy, also being less effective at inhibiting bead phagocytosis and antigen presentation in CLL. The results with relation to autophagy may provide better treatment insights in progressive CLL with elevated autophagy and increased treatment resistance, where microenvironmental signals or T cell help provide tumour cell protection. However, the finding that BTK inhibitors do not affect either soluble or particulate antigen processing or presentation is interesting. It raises the question as to the role of T cell help in CLL, as BTK inhibitors are among the most commonly used treatment options for CLL currently, which indicates that in the patient setting, for those receiving BTK inhibitors antigen processing by CLL cells is likely unaffected

Phagocytic capacity of normal B cells differs between B cell populations, likely influenced by stage of differentiation and activation. Initially, a specific subset of B1 B cells demonstrated phagocytic capacity,(Gao *et al.*, 2012; Parra *et al.*, 2012), which has since been expanded upon to include the capacity for naïve B cells to phagocytose particulate antigen through their BCR (Martinez-Riano *et al.*, 2018).I have shown here that both M-CLL and U-CLL samples are capable of phagocytosing bead immobilised antigen and recruiting a T cell response, as well as soluble antigen. Although sample numbers were small, due to limitations in patient material for HLA typing on a large scale, 2 M-CLL and 2 U-CLL samples were used in this work, and both appeared to have similar capacity to process and present antigen, when measured by the degree of T cell response induced by the CLL cells. This indicates that cell of origin in CLL does not greatly affect their capacity to engage with antigen or initiate efficient processing and presentation responses. This is interesting, as while all CLL cells demonstrate some evidence of antigen encounter, U-CLL are thought to arrive from pre-GC B cells,

and M-CLL from post GC. Theoretically, these should have different capacities or kinetics for antigen responses.

Overall, I demonstrate here that both U-CLL and M-CLL cells are capable of efficient particulate antigen capture and presentation through their BCRs. This may be particularly important for CLL pathogenesis, as particulate antigen initiates stronger GC responses and therefore engages T-cell help more effectively than soluble antigen. Antigen encountered on a day to day basis is more likely to resemble particulate antigen, as it is often membrane bound, and so this may be more biologically relevant. Presentation from either soluble or particulate anti-IgM was independent of BTK, indicating these processing responses may be unaffected in patients treated with ibrutinib. However, the soluble antigen response may be affected in patients treated with SYK inhibitors. CLL cells can internalise particulate antigen targeted to the BCR and appear to be able remove antigen through extracellular mechanisms; therefore it remains unclear which of these pathways are utilised by CLL cells for particulate antigen processing, or the requirements for phagocytosis in this response. Future studies of these pathways may reveal potential targets for therapies aimed at blocked antigen presentation, therefore depriving CLL cells of T-cell help.

6.2 Future studies

6.3.1 Development of a flow cytometry based autophagy assay

Immunoblot analysis for LC3B-II is the most reliable way currently of determining active autophagy, since immunostaining or flow cytometry staining techniques will detect pro-LC3B, LC3B-I and LC3B-II, with only LC3B-II being associated with autophagic structures and providing a reliable readout for active autophagy. Following on from the work shown in this thesis, it is clear that for further work, in the context of clinical trial samples for example, a quantitative assay would be required for measuring LC3B-II expression in a high-throughput manner. This would allow measurement of LC3B-II expression following different treatment conditions or patients. Ultimately, this could work towards combining LC3B-II expression quantification into a flow cytometry based assay to compare between CLL and healthy donor B cells, to observe differences between naïve and memory B cell subsets within the healthy donor samples, or for use with large patient sample datasets in clinical trial samples.

Preliminary work on setting up this assay yielded positive results but requires further optimisation. The first step in this process is to remove cytoplasmic LC3B-I from the sample, as LC3B antibodies are not selective between the lipidated and non-lipidated forms of LC3B. We can then measure LC3B-II by flow cytometry without results being skewed by the non-autophagosomal associated protein. By permeabilising cells with digitonin, a method widely used for permeabilising the outer cell membrane only (Kaminskyy, Abdi and Zhivotovsky, 2011), endosomal membranes remain intact and we are able to isolate membrane associated LC3B-II from cytoplasmic LC3B-I. An illustration of this method is shown in Figure 74. The cytoplasmic form is washed out, while the membrane associated LC3B-II remains in the cell pellet (shown in a concentration range for digitonin in Figure 75). The concentration of 0.04% digitonin was selected for a FACS experiment, and cells were stained with CD5 and CD19 to identify the $CD5^+$ $CD19^+$ tumour population, which would then be assessed for LC3B-II expression. A pilot experiment was performed using soluble anti-IgM, where the differences can be difficult to observe by western blot for low signalling patients. Initial results on one patient are shown in Figure 76. Further optimisation stages are required for this assay, including selection of a better FACS antibody. Commercially available LC3B FACS antibodies are quite 'dirty', with non-specific bands present, so the next stage in optimisation was to conjugate a fluorophore to the established CST antibody I routinely used for immunoblotting for LC3B, which is extremely specific with no background. This requires more time and further optimisation, but appears to be promising in terms of initial results, and could expand upon the findings of this thesis to address new questions raised as part of this work,

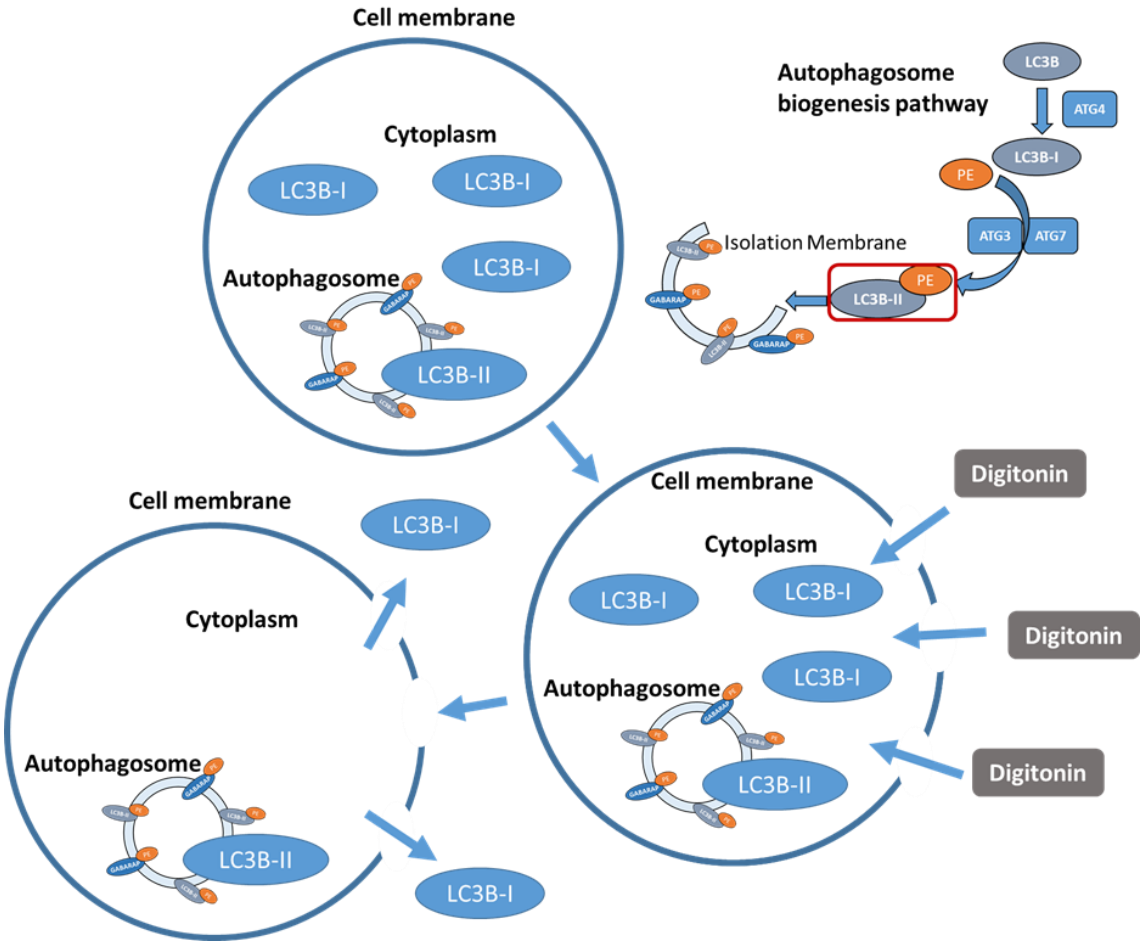

Figure 74. Illustration of selective permeabilisation assay for separation of cytoplasmic LC3B-I from autophagosomal LC3B-II.

Active autophagy occurs through autophagosome membrane initiation and elongation initiated by upstream complexes, which results in conjugation of LC3B-I to PE and insertion into the autophagosomal membrane as lipidated LC3B-II. Since antibodies stain all LC3B forms nonselectively, for assays where separation of isoforms is not possible visually, as in immunoblotting where the size difference between 16kDa LC3B-I and 14kDa LC3B-II is possible, removal of non active forms of LC3B residing in the cytoplasm is required. This can be performed using 'soft permeabilisation reagents', that permeabilise only outer cell mambranes, leaving endomembrane systems in tact. Digitonin is one such reagent, and wash steps following outer membrane permeabilisation can then remove cytoplasmic proteins, leaving the cell in tact for downstream assays.

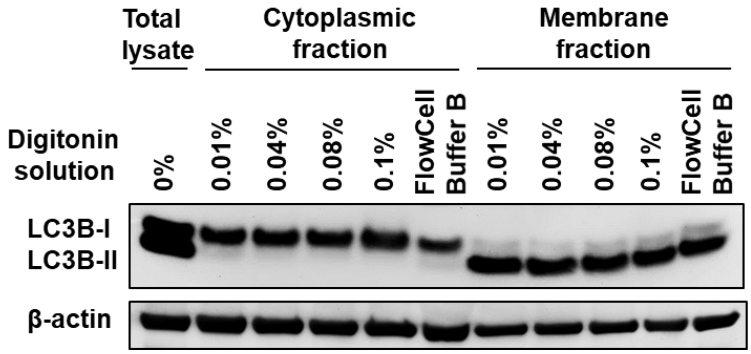

Figure 75. Selective permeabilization of the outer cell membrane yields separation of LC3B-I from LC3B-II.

Cells were incubated with bead-immobilised anti-IgM for 24 hours, with HCQ 10µM, to generate a positive signal for LC3B. Cells were then incubated with a concentration range of digitonin from 0.01% to 0.1% on ice for 5 minutes to Permeabilise outer membranes. Cells were then centrifuged at 2500RPM for 5minutes, the supernatant removed and mixed with an equal quantity of loading dye mix (Cytoplasmic fraction). The remaining cell pellets were lysed as per protocol in WCL, containing ipegal which also permeabilises endomembranes. The lysate was then mixed with the standard loading dye amount and loaded according to standard SDS-PAGE protocol (Membrane fraction), with immunoblotting subsequently carried out. FlowCellect buffer B was used as a control for successful selective permeablisation (FlowCellect Kit, Merck, product number FCCH100171).

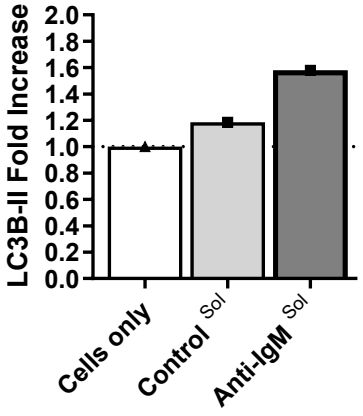

Figure 76. Initial test using soluble anti-IgM versus control antibody

Cells were incubated with soluble anti-IgM for 24 hours, with HCQ 10µM, to generate a positive signal for LC3B. Cells were then incubated with a concentration 0.04% digitonin on ice for 5 minutes to permeabilise outer membranes. Cells were then washed and stained for flow cytometry analysis with LC3B, as well as surface markers CD5 and CD19 to gate on CLL cells.

6.3.2 Examining the response to inhibitors in the context of soluble antigen endocytosis

While the majority of the work in this thesis has focused on the CLL response to bead-immobilised anti-IgM, this is predominantly due to the strength of response in terms of signalling and autophagy compared to soluble anti-IgM. While neither are fully biologically representative, each provides information on the context of response to antigen depending on the physical properties and availability. The autophagy response to soluble anti-IgM is elevated compared to control antibody, but can be hard to distinguish by immunoblotting compared to the strong signal induced by bead immobilised anti-IgM. However, a quantitative flow based assay for autophagy would unpick some of the subtle differences that immunoblotting may miss. Therefore, a quantitative antibody internalisation assay for soluble anti-IgM to provide matched data, would allow further exploration of these areas. The soluble anti-IgM quenching assay has been previously utilised by the Southampton CLL group, as illustrated below in Figure 77. This would enable more extensive pathway analysis by utilising different compounds

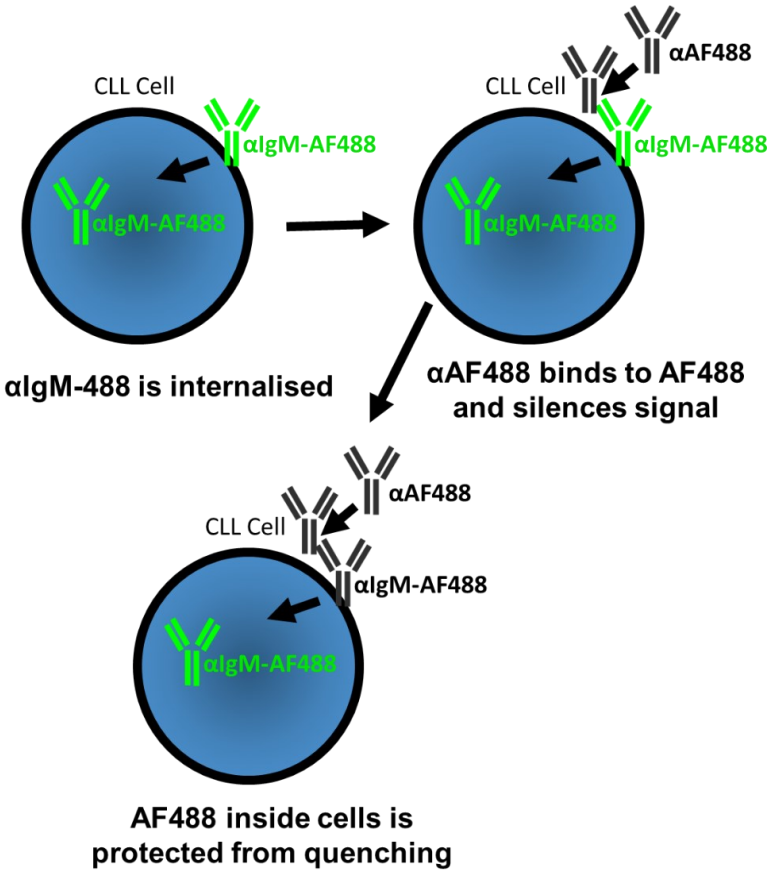

Figure 77. Illustration of quenching assay
Soluble anti-IgM is labelled with alexa fluor 488 (AF488) and incubated with CLL cells. An anti AF488 antibody is then used to silence the signal on any anti-IgM remaining on the cell surface. Any AF488-anti-IgM that has been endocytosed following BCR engagement will be protected by the anti-AF488 'quenching' stage, so provides a method to measure BCR driven endocytosis. This could be performed In the presence of BCR kinase inhibitors, as has been previously performed by the Southampton CLL group, to determine endocytosis responses.

6.3.3 Further exploring the role of autophagy in the CLL antigen processing and presentation pathway

One striking observation in the CLL cell- SKW3-T18 Th cell collaboration assays was the induction of IL2 following use of the autophagy inhibitors MRT68921 (ULK1/2i) and VPS34-IN1(Vps34i). Interestingly this did not occur with Bafilomycin or hydroxychloroquine controls. This could tell us that higher components of the autophagy machinery, the ULK and Vps34 complexes, are directly involved in the CLL antigen processing response in some positive regulatory way, or in the T cell cytokine secretion pathway, which has also been suggested in literature. Unpicking the effect of the drug on T or B cells could be done by isolating each of those variables in individual cultures with artificial stimulation. Initial pilot experiments examining the effect of the compounds on the T cells using PMA/Ionomycin stimulations showed no real or consistent difference in IL2 secretion following inhibitor treatment and stimulation. However, PMA/Ionomycin is a potent and artificial stimulation, and induced very high IL2 responses (Shown in supplementary data, Figure S7A), so this could have induced a maximal signal that made viewing differences induced by inhibitors difficult. Instead, I switched to use of anti-CD3/CD28 beads. Which provide a more physiologically relevant signal. I attempted use of both human and mouse beads (Shown in supplementary data, Figure S7B and C), as some mouse responsive components were engineered into this cell line, such as the TCR. However, neither elicited much IL2 response. I profiled the SKW3-T18s by flow cytometry to assess for species origin for CD3 and CD28 and observed that human origin surface receptors were present for both (supplementary data, Figure S8). Therefore, it is unclear why CD3/CD28 stimulation with anti CD3/CD28 beads failed to induce an IL2 response, although as with cells alone conditions (supplementary data, Figure S5A), the IL2 induction by autophagy inhibitors was present, indicating a T cell response pathway. The magnitude of this IL2 response through the autophagy inhibitors was significantly less than in the CLL-antigen coculture experiments however, with an average IL2 induction of ~60-80pg/mL, compared to coculture experiments showing IL2 levels following MRT68921 or VPS34IN1 of CLL cells, followed by coculture incubation of around ~800-1000pg/mL.

Since it appears that separating the T cell response to autophagy inhibitors may be challenging from the SKW3-T18 side of the pathway, an alternative approach could be to examine surface HLA-II expression in response to inhibitors for CLL cells. I attempted this at an equivalent time point to the coculture assays for IL2, selecting a 24 hour incubation with soluble mouse kappa anti-IgM, following pretreatment with inhibitors, and subsequently measuring HLA DR (HLA-DR clone L243, biolegend, 307623) present on the CLL cell surface at this point (Supplementary data, Figure S9).

However, no notable differences in surface HLA expression between inhibitor conditions or anti-IgM stimulation were present. This could be due to selection of a late time point, by which point surface HLA may have been recycled. The next step would be to perform a time course ,with anti-IgM stimulation to select a time point, at which point I could perform a full inhibitor screen with both soluble and latex bead immobilised anti-IgM. This could assess 1) the level of surface HLA induced by soluble vs bead immobilised antigen, and 2) the effect of inhibitors on the CLL side of this coculture experiment.

The results presented in this thesis addressed the initial hypothesis and aims, with new questions raised throughout the course of the thesis with regard to antigen removal mechanisms utilised by CLL cells, particularly where phagocytosis was blocked by SYK inhibition. A set of experiments to further explore these new questions could utilise coupling of bead immobilised anti-IgM to a pH dependant dye, to signify when anti-IgM removed from beads encounters the low pH present in lysosomes. This would explore where the antigen removed from beads is being sequestered and processed. Alternatively, a cysteine protease inhibitor that doesn't permeate cells, such as DCG04, could be used to identify antigen processing through lysosomal secretion at the synapse (Yuseff *et al.*, 2011). Both approaches would elucidate the antigen removal mechanisms that CLL cells utilise for bead immobilised anti-IgM, where phagocytosis does not occur.

.

Supplementary Data

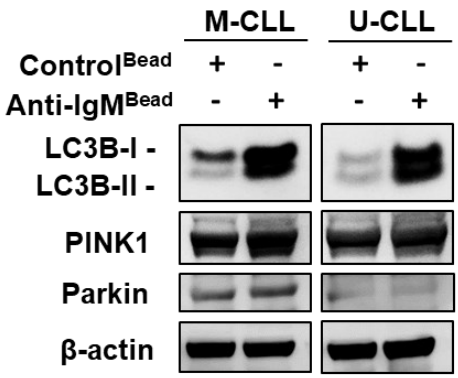

Figure S1 Analysis of PINK1 and Parkin in two CLL patients

CLL cells were stimulated with anti-IgM or control antibody coated beads for 24 hours, with HCQ added for the last hour of the experiment. Immunoblotting was performed and expression of LC3B, PINK1 and Parkin examined, along with the loading control.

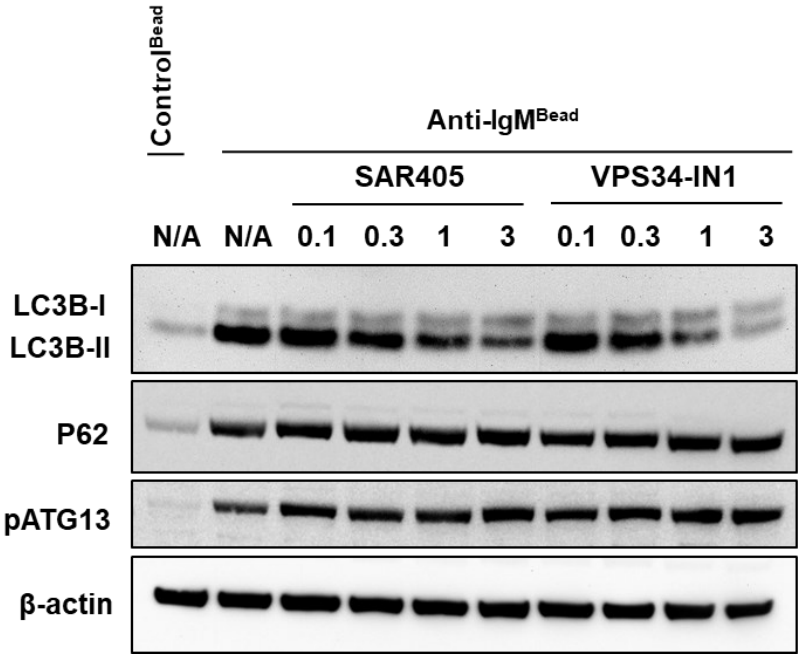

Figure S2 Comparison of SAR405 and VPS34-IN1

CLL cells were pre-incubated with either SAR405 or VPS34-IN1 for 1 hour priot to being stimulated with anti-IgM or control antibody coated beads for 24 hours, with HCQ added for the last hour of the experiment. Immunoblotting was performed and expression of LC3B, P62 and phosphorylation of ATG13 examined, along with the loading control.

1)

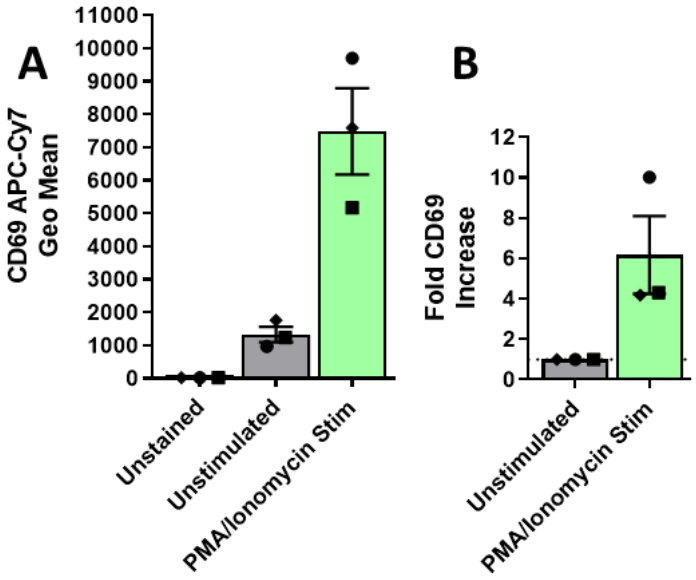

Figure S3 . Testing CD69 as a marker of activation for SKW3-T18

(A) SKW3-T18 cells were left untreated (unstimulated) or stimulated with PMA/Ionomycin for 6 hours, with CD69 measured by flow cytometry following experimental conditions. Results shown for 3 experimental repeats as geometric mean of fluorescence (A) or normalised to the unstimulated control (B).

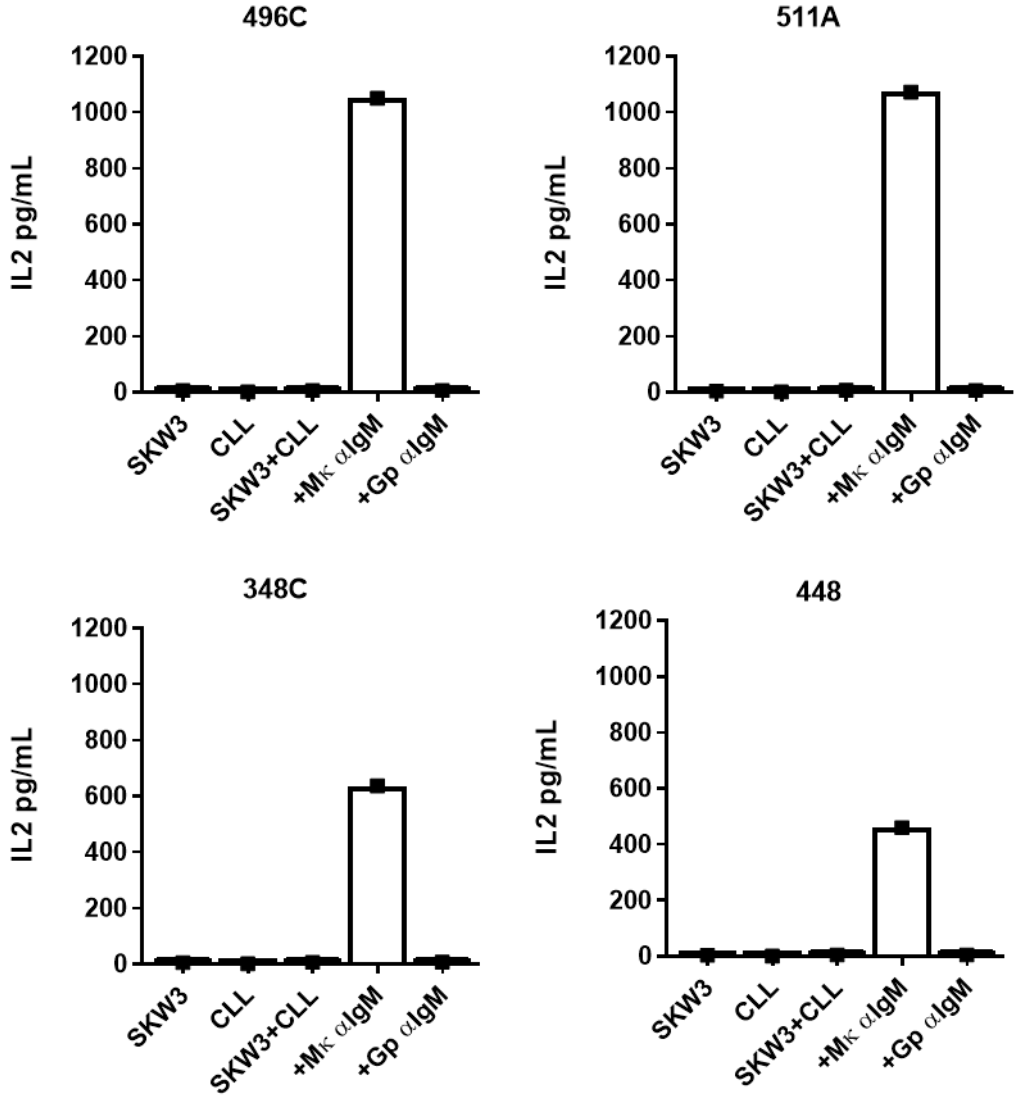

Figure S4 CLL patient – T cell co-culture responses for each CLL patient. 4 HLA DRB1*04:01 +ve patients were used in this research. CLL patient samples were incubated with mouse kappa light chain or goat polyclonal anti-IgM, then cocultured with SKW3-T18 T cells for 24 hours. ELISAs were performed on supernatant for IL2 expression. All were capable of inducing a T-cell activation IL2 response with the mouse kappa light chain anti-IgM condition, but not with the goat origin polyclonal anti-IgM.

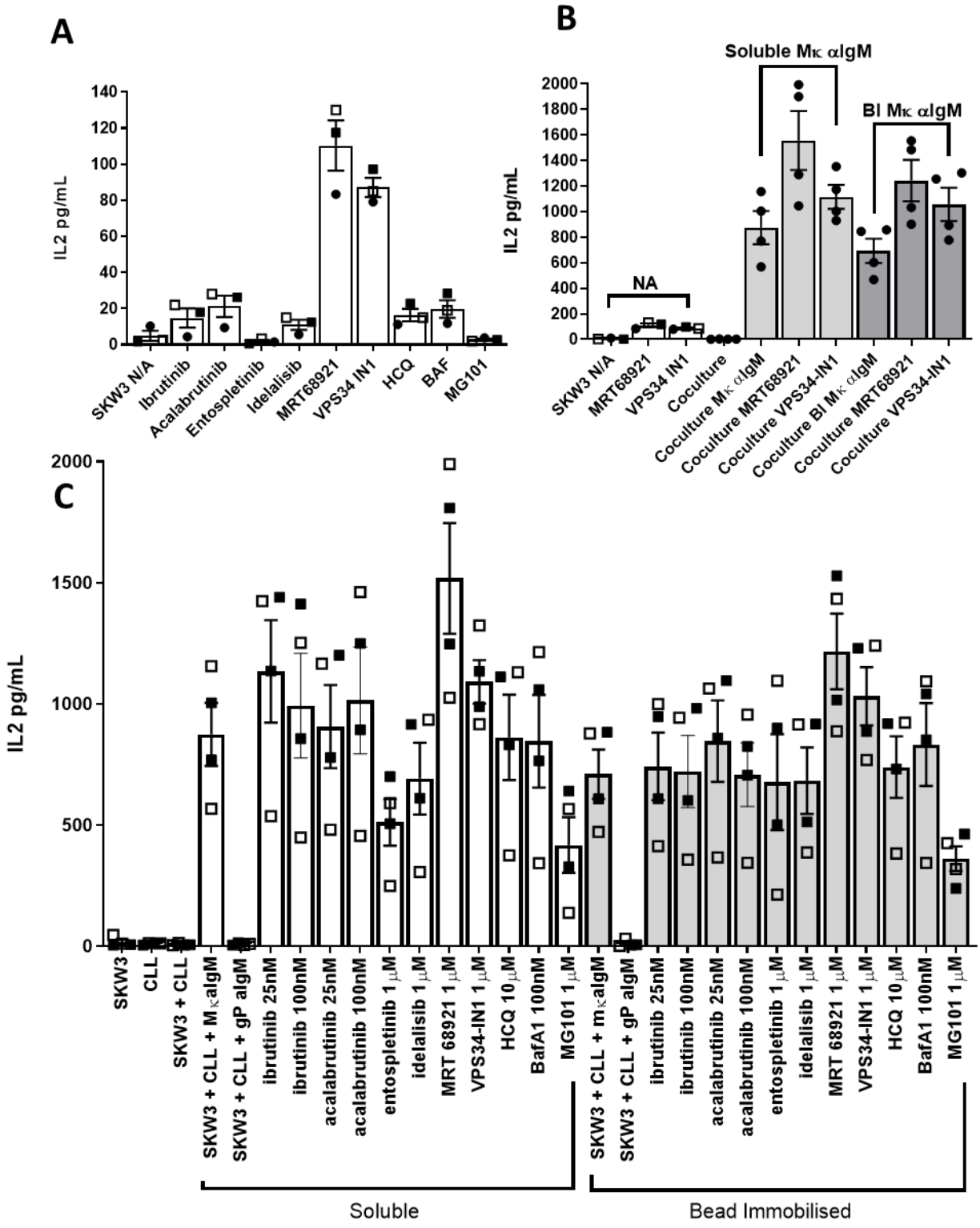

Figure S5 Comparison of SKW3-T18 clells response to inhibitors alone or in coculture assays (A) SKW3-T18 cells were incubated with each of the inhibitors for 24H with no stimulation and IL2 levels examined by ELISA. (B) Shows this data compared to the coculture data for IL2 induction levels. (C) Shows IL2 levels for the co-culture experiments without normalisation.

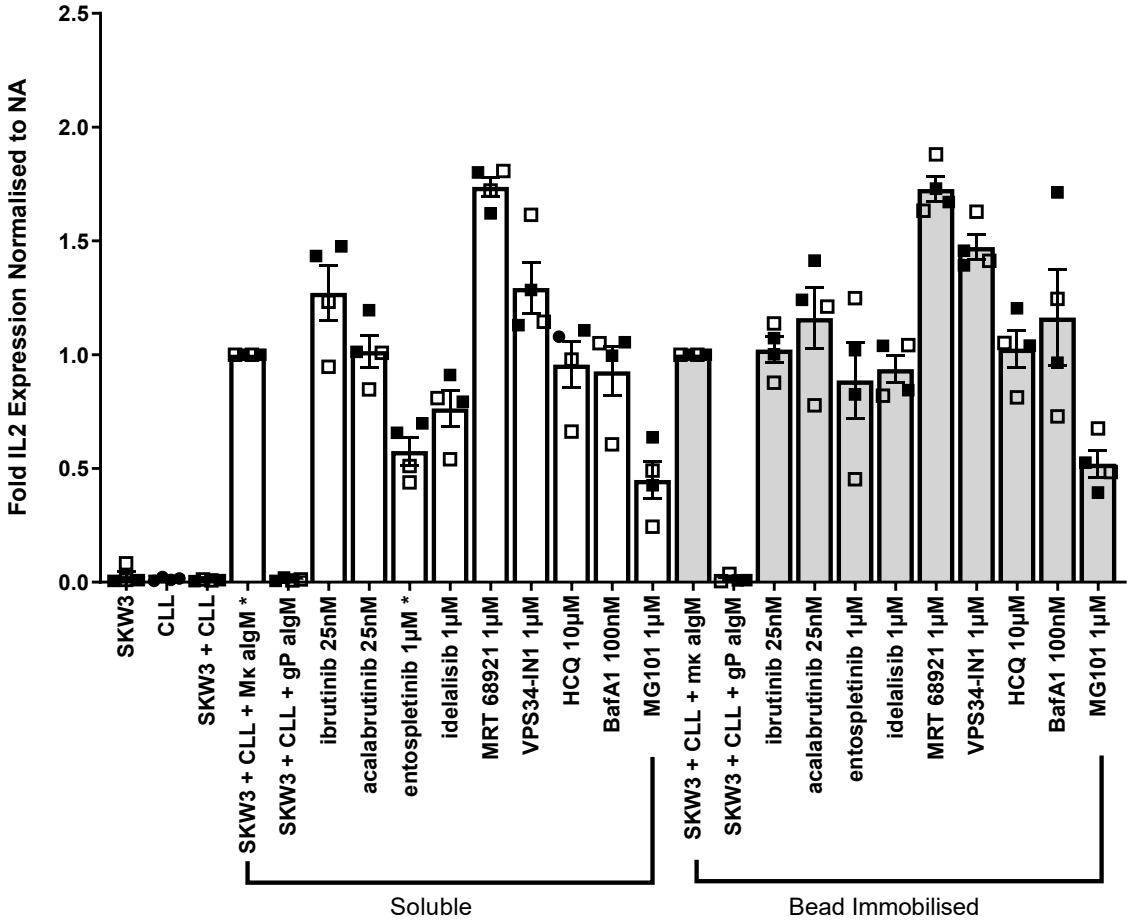

Figure S6 Coculture experiment normalised to individual antigen conditions. CLL samples (n=4) were pre-treated with the indicated compounds for 1 hour before treatment with soluble Ms κ+ anti-IgM or Ms κ+ anti-IgM-coated beads for 15 or 60 minutes, respectively, and co-culture with CLL samples for 24 hours. IL2 secretion was quantified by ELISA. Graph shows IL2 levels for the co-culture experiments with normalisation to each individual NA, for the soluble conditions normalised to SKW3+mK anti-IgM NA, and the bead condition normalised to the equivalent condition with bead bound anti-IgM.

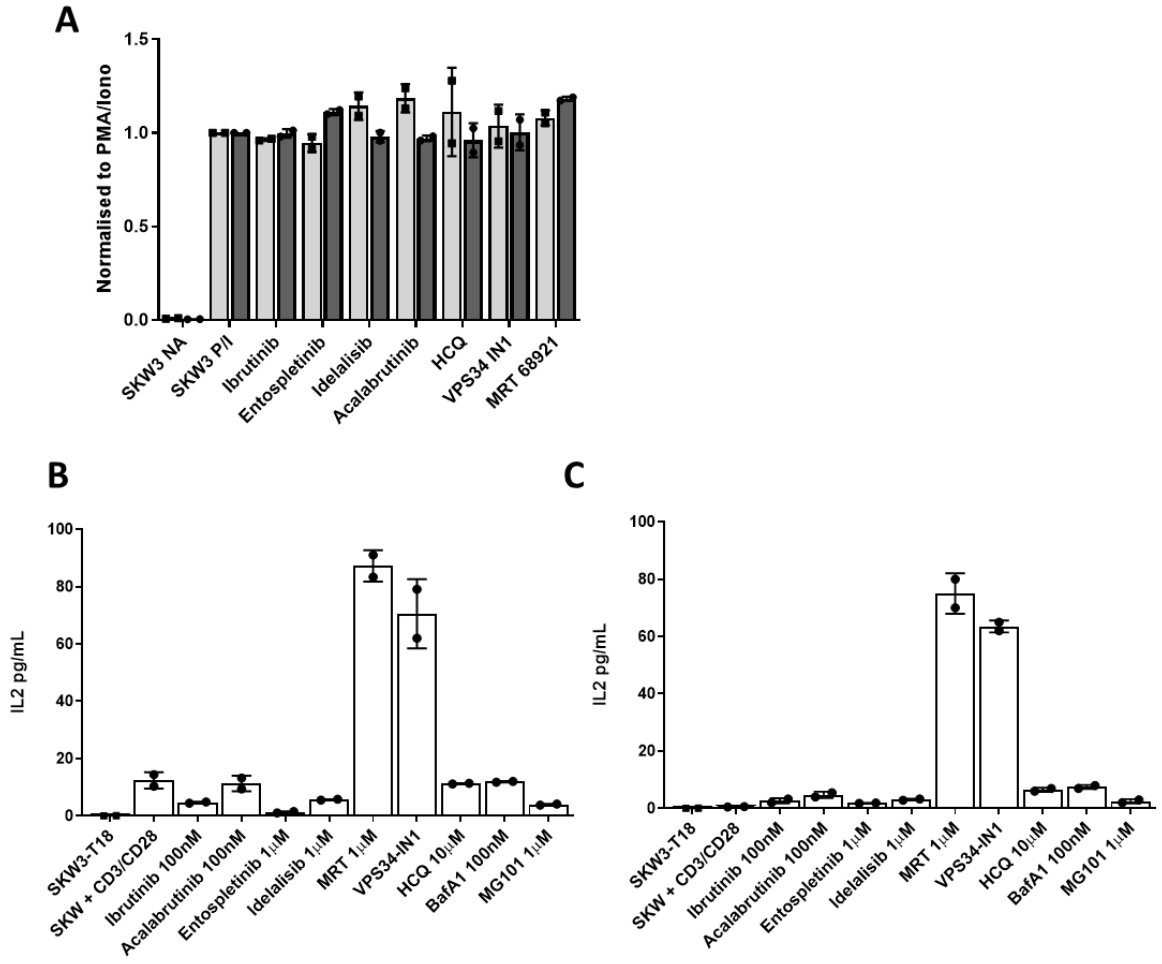

Figure S7 Effect of compounds on SKW3-T18 Th Cells (A) SKW3-T18 cells were pre incubated with inhibitors for 1H prior to PMA Ionomycin stimulation. (B) SKW3-T18s were pre-incubated with inhibitors for 1H prior to addition of anti-Human anti-CD3/CD28 dynabeads. Anti-human anti-CD3/CD28 Dynabeads failed to induce an IL2 response compared to NA conditions. (C) Anti-Mouse anti-CD3/28 Dynabeads were instead incubated with the SKW3 T18 cell line in place of the previous beads following inhibitor treatment. Less response appeared to be induced.

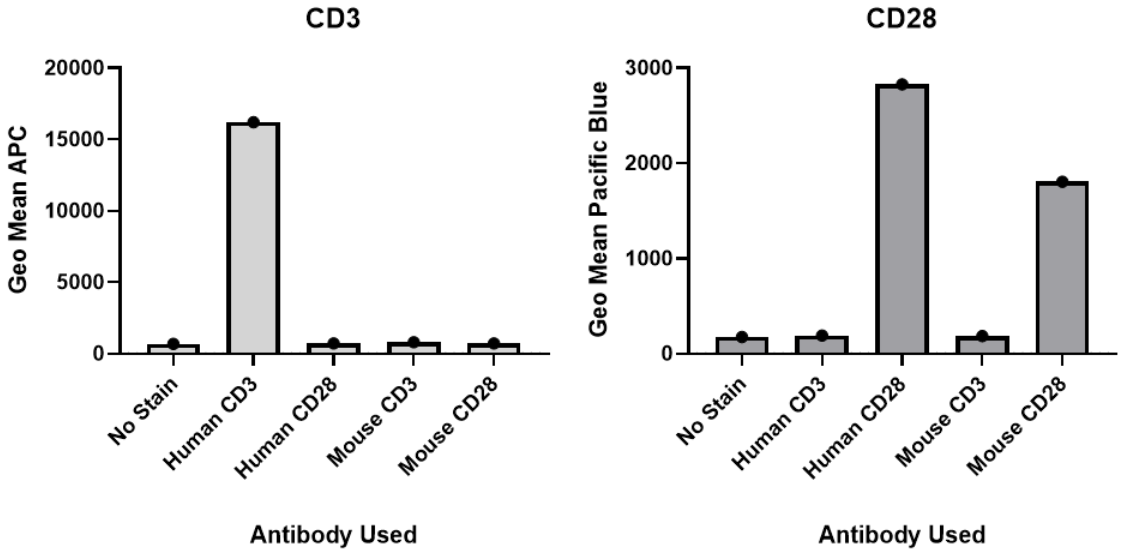

Figure S8 SKW3-T18s were analysed for presence of human and mouse CD3 and CD28. Results show human CD3 is expressed, but both human and mouse species CD28 appear to be present. Most importantly, both human CD3 and CD28 are expressed at high levels, so stimulation with anti-human anti-CD3/28 beads should induce an IL2 response. Mouse positive staining could be due to antibody species cross reactivity rather than actual mouse origin CD28.

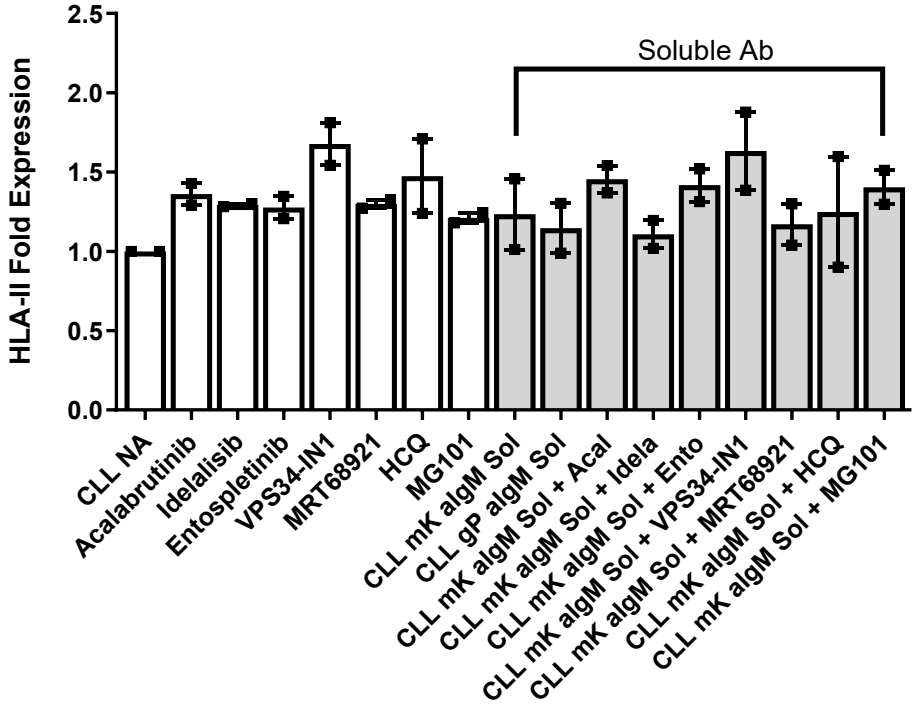

Figure S9 FACS HLA II Surface levels on CLL cells at 24H. CLL cells were pre-incubated with the compounds indicated and either incubated for 24 hours, or subsequently stimulated with soluble anti-IgM for 24 hours, and HLA-DR expression analysed by Flow cytometry.Results were normalised to the CLL N/A set as 1m and examine the HLA response to compound treatment in the presence and absence of antigen encounter.

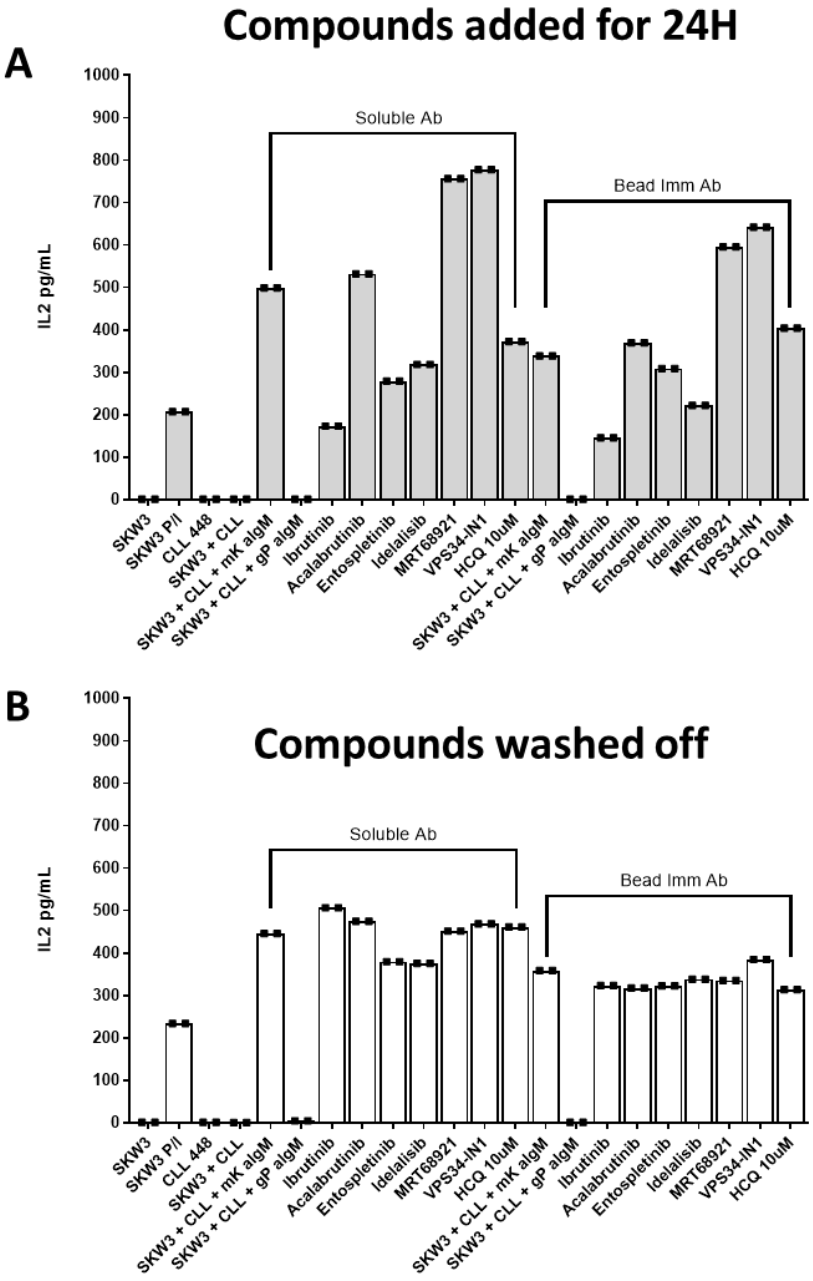

Figure S10 Compound wash off experiments for co-culture assay. CLL samples (n=2) were pre-treated with the indicated compounds for 1 hour. These were then either washed off to remove compounds from solution, or left on before treatment with soluble Ms κ+ anti-IgM or Ms κ+ anti-IgM-coated beads for 15 or 60 minutes, respectively, and co-culture with SKW3-T18s for 24 hours. IL2 secretion was quantified by ELISA

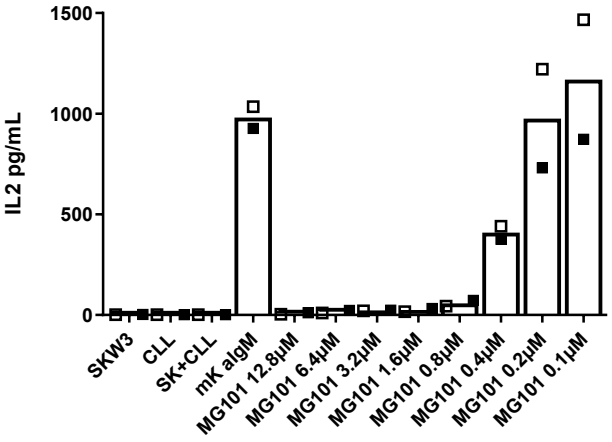

Figure S11 MG101 titrations CLL samples (n=2) were pre-treated with the indicated concentrations of MG101 for 1 hour before treatment with soluble Ms κ+ anti-IgM, and co-cultured with SKW3-T18s for 24 hours. IL2 secretion was quantified by ELISA. Full inhibition of antigen processing can be achieved at higher MG101 concentrations

Appendices

Appendix 1 : CLL samples used in this research

Sample ID	Clinical_Diagnosis	Tumour_population (%)	sIgM	sIgM iCa(%)	IGHV	VGENEandallele
87A	CLL	82	13	33		
87B	CLL	95	12	36	M-IGHV	IGHV2-5*02 F
87C	CLL	91	25			
106	CLL	89	30	6	M-IGHV	IGHV3-15*01 F
132	CLL	90	50		M-IGHV	IGHV4-4*07 F
132A	CLL	88	25	18		
156E	CLL	94	24		M-IGHV	IGHV5-51*01 F
156F	CLL	92	23			
156G	CLL	93	18			
156D	CLL	92	33	21		
276	CLL	73	1040		M-IGHV	IGHV3-23*01 F
276A	CLL	80	882			
276B	CLL	86	820			
276C	CLL	83	792			
276D	CLL	95	784			
279A	CLL	89	28	74	M-IGHV	IGHV3-30-3*01 F
348	CLL	93	84	3	M-IGHV	IGHV3-15*01 F
348A	CLL	93	66	4		
348C	CLL	96	35	21		
348D	CLL	98	53	4		
351C	CLL	96	34	79	M-IGHV	IGHV3-66*01 F, or IGHV3-66*04 F
368	CLL	92	81		M-IGHV	IGHV3-15*05 F
368A	CLL	91	40			
368B	CLL	83	41	46		
	CLL	93	62	45		
368D	CLL	97	52	35		
368E	CLL	97	31	36		
448	CLL	93	35		U-IGHV	IGHV3-49*05 F
448B	CLL	83	115	73		
470	CLL	84	15		M-IGHV	IGHV3-7*02 F, or IGHV3-7*03 F
470A	CLL	82	12			
470B	CLL	86	10			
475	CLL	61	53	2	M-IGHV	IGHV1-3*01 F
475A	CLL	81	33			
475C	CLL	91	12	10		
478A	CLL	63	45			

478C	**CLL**				**U-IGHV**	**IGHV1-69*01 F, or IGHV1-69D*01 F**
478D	**CLL**	**88**	**42**	**54**		
488	**CLL**	**69**	**22**	**15**	**M-IGHV**	**IGHV1-69*01 F**
496A	**CLL**	**79**	**55**			
496B	**CLL**	**84**	**43**	**5**	**M-IGHV**	**IGHV3-30*03**
496D	**CLL**	**91**	**46**	**8**		
496E	**CLL**	**74**	**32**	**8**		
496F	**CLL**	**75**	**32**	**14**		
511	**CLL**	**90**	**46**	**41**		
511A	**CLL**	**96**	**32**	**39**	**U-IGHV**	**IGHV3-72*01 F**
511B	**CLL**	**89**	**29**	**48**		
520	**CLL**	**81**	**25**	**2**	**U-IGHV**	**IGHV3-33*01 F, or IGHV3-33*06 F**
520B	**CLL**	**95**	**31**	**36**		
523	**CLL**	**93**	**31**	**4**	**M-IGHV**	**IGHV3-72*01 F**
523I	**CLL**	**93**	**102**			
523A	**CLL**	**89**	**50**	**62**		
523B	**CLL**	**94**	**26**	**14**		
523C	**CLL**	**83**	**75**	**56**		
523D	**CLL**	**95**	**48**	**65**		
523E	**CLL**	**95**	**120**	**5**		
523F	**CLL**	**96**	**31**	**25**		
523G	**CLL**	**96**	**23**	**13**		
523H	**CLL**	**92**	**45**	**39**		
530	**CLL**		**119**	**76**	**U-IGHV**	**IGHV3-66*01 F, or IGHV3-66*04 F**
530A	**CLL**	**95**	**91**	**85**		
530B	**CLL**	**97**	**115**	**74**		
531	**CLL**				**U-IGHV**	**IGHV4-39*01 F**
531AC	**CLL**	**95**	**82**			
531A	**CLL**	**97**	**40**	**43**		
531B	**CLL**	**97**	**50**	**5**		
550	**CLL**	**52**	**75**	**83**	**U-IGHV**	**IGHV4-34*01 F**
550B	**CLL**	**89**	**130**	**87**		
553	**CLL**	**34**	**26**	**19**	**U-IGHV**	**IGHV3-33*01 F, or IGHV3-33*06 F**
555	**CLL**	**99**	**38**	**68**	**U-IGHV**	**IGHV3-11*01 F**
561	**CLL**	**95**	**39**	**50**	**M-IGHV**	**IGHV3-48*03 F**
569						
573	**CLL**	**80**	**32**	**74**	**M-IGHV**	**IGHV1-3*01 F**
573A	**CLL**	**87**	**51**	**75**		
575	**CLL**	**89**	**56**	**62**	**M-IGHV**	**IGHV3-15*01 F**
575A	**CLL**	**91**	**67**	**64**		
575B	**CLL**	**97**	**87**	**64**		
575C	**CLL**	**96**	**117**	**66**		
575D	**CLL**	**98**	**116**	**52**		

575E	**CLL**	**95**	**99**	**69**		
581	**CLL**	**49**	**27**	**16**	**M-IGHV**	**IGHV1-3*01 F**
588	**CLL**	**86**	**31**	**4**	**M-IGHV**	**IGHV3-23*01 F (see comment)**
588A	**CLL**	**94**	**30**	**5**		
589	**CLL**	**94**	**65**	**82**	**M-IGHV**	**IGHV1-18*01 F**
595	**CLL**	**82**	**27**	**17**	**U-IGHV**	**IGHV3-30*01 F**
595E	**CLL**	**86**	**78**			
595A	**CLL**	**95**	**26**	**10**		
595B	**CLL**	**94**	**38**	**20**		
595C	**CLL**	**96**	**26**	**18**		
595D	**CLL**	**95**	**36**	**20**		
602A	**CLL**	**97**	**76**	**44**		
604	**CLL**	**94**	**31**	**42**	**M-IGHV**	**IGHV3-30*03 F, or IGHV3-30*05 F or IGHV3-30*06 F or IGHV3-30*13 F or IGHV3-30*18 F or IGHV3-30*19 F**
604A	**CLL**	**92**	**94**	**44**		
604B	**CLL**	**88**	**59**	**73**		
604C	**CLL**	**85**	**61**	**60**		
604D	**CLL**	**85**	**35**	**75**		
604E	**CLL**	**87**	**95**	**84**		
604F	**CLL**	**86**	**54**	**79**		
604G	**CLL**	**89**	**81**	**40**		
609	**CLL**	**88**	**25**	**57**	**M-IGHV**	**IGHV3-72*01 F**
609A	**CLL**	**87**	**37**			
615	**CLL**	**93**	**32**	**69**	**M-IGHV**	**IGHV4-39*01 F**
618	**CLL**	**85**	**24**	**58**	**U-IGHV**	**IGHV3-11*01 F**
618A	**CLL**	**87**	**145**	**68**		
620						
626	**CLL**	**68**	**25**	**29**	**M-IGHV**	**IGHV4-34*01 F, or IGHV4-34*02 F or IGHV4-34*07 F**
627	**CLL**	**68**	**146**	**86**	**M-IGHV**	**IGHV3-30*03 F, or IGHV3-30*18 F**
628	**CLL**	**94**	**32**	**22**	**U-IGHV**	**IGHV1-69*01 F, or IGHV1-69D*01 F**
632	**CLL**	**96**	**46**	**73**		
632A	**CLL**	**97**	**66**	**59**		
633	**CLL**	**82**	**45**	**59**	**M-IGHV**	**IGHV3-7*03 F**
635D	**CLL**	**95**	**50**	**78**		
636	**CLL**	**94**	**24**	**2**	**M-IGHV**	**IGHV4-34*02 F**
641	**CLL**	**80**	**139**	**37**	**M-IGHV**	**IGHV3-15*01 F**
643	**CLL**	**91**	**25**	**26**	**M-IGHV**	**IGHV6-1*01 F**
644	**CLL**	**90**	**48**	**31**	**U-IGHV**	**IGHV4-39*01 F**
644A	**CLL**	**93**	**51**	**47**		
645	**CLL**	**96**	**43**	**66**	**M-IGHV**	**IGHV1-18*04 F**
650	**CLL**	**79**	**45**	**10**	**M-IGHV**	**IGHV3-72*01 F**

650A	**CLL**	**82**	**71**	**18**		
653	**CLL**	**67**	**28**	**3**	**M-IGHV**	**IGHV3-7*01 F**
657	**CLL**	**91**	**24**	**0**	**M-IGHV**	**IGHV4-59*08 F**
657F	**CLL**	**85**	**22**			
657A	**CLL**	**66**	**16**	**2**		
657B	**CLL**	**83**	**18**	**2**		
664	**CLL**	**93**	**37**	**84**	**M-IGHV**	**IGHV3-21*01 F, or IGHV3-21*02 F**
665	**CLL**	**85**	**468**	**68**	**M-IGHV**	**IGHV3-11*01 F**
675		**88**	**70**	**53**	**U-IGHV**	**IGHV3-21*01 F**
676	**CLL**	**56**	**918**	**100**	**M-IGHV**	**IGHV6-1*02 F**
676A	**CLL**	**36**	**364**	**86**		
679	**CLL**	**80**	**70**	**21**	**M-IGHV**	**IGHV3-15*01 F**
680	**CLL**	**75**	**14**		**M-IGHV**	**IGHV4-59*01 F**
681	**CLL**	**96**	**212**	**60**	**M-IGHV**	**IGHV3-7*02 F, or Homsap IGHV3-7*03 F**
681A	**CLL**	**97**	**185**	**31**		
681B	**CLL**	**98**	**116**	**27**		
681C	**CLL**	**93**	**180**	**28**		
684	**CLL**	**94**	**29**	**7**	**M-IGHV**	**IGHV3-15*07 F**
684A	**CLL**	**90**	**31**	**14**		
684B	**CLL**	**85**	**28**	**14**		
684C	**CLL**	**92**	**25**	**13**		
684D	**CLL**	**94**	**33**	**21**		
690	**CLL**	**93**	**18**	**1**	**M-IGHV**	**IGHV4-61*02 F**
709	**CLL**	**92**	**101**	**46**	**M-IGHV**	**IGHV3-7*01 F**
709A	**CLL**	**76**	**50**	**63**		
715	**CLL**	**92**	**145**	**73**	**U-IGHV**	**IGHV1-2*02 F**
720	**CLL**	**92**	**63**	**11**	**U-IGHV**	**IGHV1-69*01 F**
722	**CLL**	**77**	**21**	**5**	**M-IGHV**	**IGHV5-51*01 F**
732	**CLL**	**91**	**85**	**47**	**U-IGHV**	**IGHV1-46*01 F, or Homsap IGHV1-46*03 F**
739	**CLL**	**98**	**99**	**76**	**U-IGHV**	**IGHV3-66*02 F**
739A	**CLL**	**97**	**83**	**75**		
767	**CLL**	**82**	**27**	**34**	**M-IGHV**	**IGHV3-7*01 F**
767A	**CLL**	**74**	**98**			
771	**CLL**	**96**	**94**	**73**	**U-IGHV**	**IGHV1-2*02 F**
772	**CLL**	**89**	**60**	**59**	**M-IGHV**	**IGHV1-46*01 F**
773	**CLL**	**86**	**58**	**75**		**NOT DETERMINED**
773A	**CLL**	**92**	**112**	**78**		
773B	**CLL**	**95**	**49**	**78**		
773C	**CLL**	**96**	**34**	**79**		
773D					**U-IGHV**	**IGHV3-48*03**
773E	**CLL**	**95**	**95**	**80**		
773F	**CLL**	**95**	**117**	**70**		
774	**CLL**	**96**	**80**	**27**	**U-IGHV**	**IGHV1-69*01 F**
774A	**CLL**	**97**	**40**	**25**		

775	**CLL**	**81**	**65**	**57**	**U-IGHV**	**IGHV4-4*07 F**
776	**CLL**	**92**	**67**	**39**	**U-IGHV**	**IGHV4-34*01 F**
778	**CLL**	**86**	**27**	**41**	**U-IGHV**	**IGHV3-33*01 F**
778A	**CLL**	**86**	**14**	**62**		
780	**CLL**	**99**	**65**	**81**		**IGHV3-21*01 F, or Homsap IGHV3-21*02 F**
780A	**CLL**	**99**	**81**	**81**		**IGHV3-21*01 F, or Homsap IGHV3-21*02 F**
780B	**CLL**	**98**	**47**	**81**	**U-IGHV**	**IGHV3-21*01 F, or Homsap IGHV3-21*02 F**
803	**CLL**	**95**	**33**	**30**	**U-IGHV**	**IGHV1-69*01**
803E	**CLL**	**95**	**60**			
803F	**CLL**	**96**	**74**			
803A	**CLL**	**94**	**33**	**31**		
803B	**CLL**	**93**	**38**	**20**		
803C	**CLL**	**95**	**30**	**31**		
816D	**CLL**	**82**	**43**			
888	**CLL**	**94**	**139**	**65**	**U-IGHV**	**IGHV3-21*01 F, or Homsap IGHV3-21*02 F**
888 rpt	**CLL**	**94**	**182**	**63**		
888B	**CLL**					
929	**CLL**	**90**	**134**	**58**	**U-IGHV**	**Homsap IGHV1-69*01 F, or Homsap IGHV1-69D*01 F**
1158	**CLL**	**99**	**83**		**U-IGHV**	**Homsap IGHV1-69*04 F**
1266	**CLL**	**92**	**43**		**U-IGHV**	**Homsap IGHV3-48*03 F**
1267	**CLL**	**99**	**58**		**U-IGHV**	**Homsap IGHV1-69*04 F**
1384	**CLL**	**84**	**82**	**21**	**M-IGHV**	**Homsap IGHV3-33*01 F, or Homsap IGHV3-33*06 F**
1427	**CLL**	**95**	**1268**	**83**	**U-IGHV**	**Homsap IGHV1-8*01 F**
1431	**CLL**	**97**	**50**	**76**	**U-IGHV**	**Homsap IGHV3-21*01 F, or Homsap IGHV3-21*02 F**

Appendix 2: RNA QC results for RNA-Sequencing

Sample	Treatment	Reference Genome	Sample Concentration	Units	Volume (µL)	Sample Mass (ng)	RIN
87B	6H DMSO + Control Ab Beads	GRCh37.EBVB95-8wt.ERCC	13.3	ng/µL	30	400.0	10.0
87B	6H DMSO + αIgM Beads	GRCh37.EBVB95-8wt.ERCC	13.3	ng/µL	30	400.0	10.0
87B	6H VPS34-IN1 + Control Ab Beads	GRCh37.EBVB95-8wt.ERCC	13.3	ng/µL	30	400.0	10.0
87B	6H VPS34-IN1 + αIgM Beads	GRCh37.EBVB95-8wt.ERCC	13.3	ng/µL	30	400.0	10.0
132A	6H DMSO + Control Ab Beads	GRCh37.EBVB95-8wt.ERCC	13.3	ng/µL	30	400.0	10.0
132A	6H DMSO + αIgM Beads	GRCh37.EBVB95-8wt.ERCC	13.3	ng/µL	30	400.0	10.0
132A	6H VPS34-IN1 + Control Ab Beads	GRCh37.EBVB95-8wt.ERCC	13.3	ng/µL	30	400.0	10.0
132A	6H VPS34-IN1 + αIgM Beads	GRCh37.EBVB95-8wt.ERCC	13.3	ng/µL	30	400.0	10.0
523G	6H DMSO + Control Ab Beads	GRCh37.EBVB95-8wt.ERCC	13.3	ng/µL	30	400.0	9.9
523G	6H DMSO + αIgM Beads	GRCh37.EBVB95-8wt.ERCC	13.3	ng/µL	30	400.0	9.4
523G	6H VPS34-IN1 + Control Ab Beads	GRCh37.EBVB95-8wt.ERCC	13.3	ng/µL	30	400.0	9.6
523G	6H VPS34-IN1 + αIgM Beads	GRCh37.EBVB95-8wt.ERCC	13.3	ng/µL	30	400.0	10.0
1384	6H DMSO + Control Ab Beads	GRCh37.EBVB95-8wt.ERCC	13.3	ng/µL	30	400.0	10.0
1384	6H DMSO + αIgM Beads	GRCh37.EBVB95-8wt.ERCC	13.3	ng/µL	30	400.0	9.9

1384	6H VPS34-IN1 + Control Ab Beads	GRCh37.EBVB95-8wt.ERCC	13.3	ng/µL	30	400.0	10.0
1384	6H VPS34-IN1 + αIgM Beads	GRCh37.EBVB95-8wt.ERCC	13.3	ng/µL	30	400.0	10.0
1427	6H DMSO + Control Ab Beads	GRCh37.EBVB95-8wt.ERCC	13.3	ng/µL	30	400.0	10.0
1427	6H DMSO + αIgM Beads	GRCh37.EBVB95-8wt.ERCC	13.3	ng/µL	30	400.0	10.0
1427	6H VPS34-IN1 + Control Ab Beads	GRCh37.EBVB95-8wt.ERCC	13.3	ng/µL	30	400.0	9.9
1427	6H VPS34-IN1 + αIgM Beads	GRCh37.EBVB95-8wt.ERCC	13.3	ng/µL	30	400.0	10.0
1431	6H DMSO + Control Ab Beads	GRCh37.EBVB95-8wt.ERCC	13.3	ng/µL	30	400.0	10.0
1431	6H DMSO + αIgM Beads	GRCh37.EBVB95-8wt.ERCC	13.3	ng/µL	30	400.0	10.0
1431	6H VPS34-IN1 + Control Ab Beads	GRCh37.EBVB95-8wt.ERCC	13.3	ng/µL	30	400.0	10.0
1431	6H VPS34-IN1 + αIgM Beads	GRCh37.EBVB95-8wt.ERCC	13.3	ng/µL	30	400.0	10.0
87B	24H DMSO + Control Ab Beads	GRCh37.EBVB95-8wt.ERCC	13.3	ng/µL	30	400.0	9.2
87B	24H DMSO + αIgM Beads	GRCh37.EBVB95-8wt.ERCC	13.3	ng/µL	30	400.0	10.0
87B	24H VPS34-IN1 + Control Ab Beads	GRCh37.EBVB95-8wt.ERCC	13.3	ng/µL	30	400.0	8.8
87B	24H VPS34-IN1 + αIgM Beads	GRCh37.EBVB95-8wt.ERCC	13.3	ng/µL	30	400.0	9.8
132A	24H DMSO +	GRCh37.EBVB95-8wt.ERCC	13.3	ng/µL	30	400.0	10.0

	Control Ab Beads						
132A	24H DMSO + αIgM Beads	GRCh37.EBVB95-8wt.ERCC	13.3	ng/µL	30	400.0	10.0
132A	24H VPS34-IN1 + Control Ab Beads	GRCh37.EBVB95-8wt.ERCC	13.3	ng/µL	30	400.0	10.0
132A	24H VPS34-IN1 + αIgM Beads	GRCh37.EBVB95-8wt.ERCC	13.3	ng/µL	30	400.0	10.0
523G	24H DMSO + Control Ab Beads	GRCh37.EBVB95-8wt.ERCC	13.3	ng/µL	30	400.0	10.0
523G	24H DMSO + αIgM Beads	GRCh37.EBVB95-8wt.ERCC	13.3	ng/µL	30	400.0	10.0
523G	24H VPS34-IN1 + Control Ab Beads	GRCh37.EBVB95-8wt.ERCC	13.3	ng/µL	30	400.0	9.6
523G	24H VPS34-IN1 + αIgM Beads	GRCh37.EBVB95-8wt.ERCC	13.3	ng/µL	30	400.0	10.0
1384	24H DMSO + Control Ab Beads	GRCh37.EBVB95-8wt.ERCC	13.3	ng/µL	30	400.0	10.0
1384	24H DMSO + αIgM Beads	GRCh37.EBVB95-8wt.ERCC	13.3	ng/µL	30	400.0	10.0
1384	24H VPS34-IN1 + Control Ab Beads	GRCh37.EBVB95-8wt.ERCC	13.3	ng/µL	30	400.0	10.0
1384	24H VPS34-IN1 + αIgM Beads	GRCh37.EBVB95-8wt.ERCC	13.3	ng/µL	30	400.0	10.0
1427	24H DMSO + Control Ab Beads	GRCh37.EBVB95-8wt.ERCC	13.3	ng/µL	30	400.0	10.0
1427	24H DMSO + αIgM Beads	GRCh37.EBVB95-8wt.ERCC	13.3	ng/µL	30	400.0	10.0

1427	24H VPS34-IN1 + Control Ab Beads	GRCh37.EBVB95-8wt.ERCC	13.3	ng/µL	30	400.0	10.0
1427	24H VPS34-IN1 + αIgM Beads	GRCh37.EBVB95-8wt.ERCC	13.3	ng/µL	30	400.0	10.0
1431	24H DMSO + Control Ab Beads	GRCh37.EBVB95-8wt.ERCC	6.7	ng/µL	30	200.0	8.7
1431	24H DMSO + αIgM Beads	GRCh37.EBVB95-8wt.ERCC	6.7	ng/µL	30	200.0	10.0
1431	24H VPS34-IN1 + Control Ab Beads	GRCh37.EBVB95-8wt.ERCC	6.7	ng/µL	30	200.0	8.3
1431	24H VPS34-IN1 + αIgM Beads	GRCh37.EBVB95-8wt.ERCC	6.7	ng/µL	30	200.0	10.0

Appendix 3 :Top 100 IPA pathways

Anti-IgM 6H UP top 100 canonical pathways IPA

Ingenuity Canonical Pathways	-log(p-value)	Ratio	z-score
Antigen Presentation Pathway	10.7	0.359	**#NUM!**
PD-1, PD-L1 cancer immunotherapy pathway	8.47	0.179	-1.604
MSP-RON Signaling In Macrophages Pathway	7.73	0.162	-1.886
Sirtuin Signaling Pathway	7.51	0.106	0.447
tRNA Charging	7.28	0.282	3.317
Th1 and Th2 Activation Pathway	6.91	0.128	**#NUM!**
B Cell Development	6.8	0.256	**#NUM!**
Purine Nucleotides De Novo Biosynthesis II	6.19	0.545	2.449
Th1 Pathway	6.01	0.139	3.051
Role of PKR in Interferon Induction and Antiviral Response	5.99	0.132	-0.5
Th2 Pathway	5.94	0.131	2.828
IL-4 Signaling	5.46	0.151	**#NUM!**
Endoplasmic Reticulum Stress Pathway	5.37	0.333	1.89
Role of Macrophages, Fibroblasts and Endothelial Cells in Rheumatoid Arthritis	5.05	0.0862	**#NUM!**
TREM1 Signaling	4.92	0.156	3.317
Unfolded protein response	4.91	0.144	2.714
Neuroinflammation Signaling Pathway	4.41	0.0825	4.583
5-aminoimidazole Ribonucleotide Biosynthesis I	4.39	1	**#NUM!**
Inosine-5'-phosphate Biosynthesis II	4.39	1	**#NUM!**

Aldosterone Signaling in Epithelial Cells	4.27	0.104	**#NUM!**
Coronavirus Pathogenesis Pathway	4.09	0.0936	-0.471
EIF2 Signaling	3.99	0.0893	0
Small Cell Lung Cancer Signaling	3.95	0.125	1.633
Ferroptosis Signaling Pathway	3.94	0.111	2.138
Cysteine Biosynthesis III (mammalia)	3.89	0.25	2.449
Glucocorticoid Receptor Signaling	3.89	0.0654	**#NUM!**
IL-9 Signaling	3.79	0.2	1.342
Role of JAK family kinases in IL-6-type Cytokine Signaling	3.78	0.24	**#NUM!**
IL-10 Signaling	3.77	0.139	**#NUM!**
Superpathway of Methionine Degradation	3.63	0.189	2.646
Acute Phase Response Signaling	3.63	0.0919	3
FAT10 Cancer Signaling Pathway	3.55	0.16	2.449
Crosstalk between Dendritic Cells and Natural Killer Cells	3.54	0.121	3
Hepatic Fibrosis Signaling Pathway	3.5	0.0692	3.8
Induction of Apoptosis by HIV1	3.43	0.138	1.414
Tetrahydrofolate Salvage from 5,10-methenyltetrahydrofolate	3.41	0.6	**#NUM!**
Pancreatic Adenocarcinoma Signaling	3.39	0.103	2.121
Colorectal Cancer Metastasis Signaling	3.35	0.0781	4.243
GADD45 Signaling	3.32	0.25	**#NUM!**
Tumor Microenvironment Pathway	3.32	0.0894	3.873
Cell Cycle: G1/S Checkpoint Regulation	3.29	0.132	-1.134
Cardiac Hypertrophy Signaling (Enhanced)	3.27	0.0632	4.849
NRF2-mediated Oxidative Stress Response	3.23	0.0802	2.887
TNFR2 Signaling	3.16	0.188	2
Methionine Degradation I (to Homocysteine)	3.11	0.227	2.236
IL-17 Signaling	3.11	0.0856	4
STAT3 Pathway	3.1	0.0963	1.265
Hepatic Cholestasis	3.06	0.0847	**#NUM!**
HIF1α Signaling	3.04	0.0817	2
4-1BB Signaling in T Lymphocytes	3.02	0.176	2
Chronic Myeloid Leukemia Signaling	2.94	0.103	**#NUM!**
PPAR Signaling	2.94	0.103	-3.162
Autophagy	2.93	0.0798	1.213
Spermidine Biosynthesis I	2.93	1	**#NUM!**
Erythropoietin Signaling Pathway	2.91	0.0847	-0.535
TWEAK Signaling	2.82	0.162	0.447
MYC Mediated Apoptosis Signaling	2.82	0.14	1.134
Antioxidant Action of Vitamin C	2.81	0.0991	-2.828
IL-6 Signaling	2.8	0.0938	2.714
Prostate Cancer Signaling	2.78	0.0982	**#NUM!**
Histidine Degradation III	2.7	0.375	**#NUM!**
RAN Signaling	2.64	0.235	2
BAG2 Signaling Pathway	2.62	0.107	0.816
Insulin Secretion Signaling Pathway	2.61	0.0709	3.441
p38 MAPK Signaling	2.6	0.0932	3.317
Differential Regulation of Cytokine Production in Macrophages and T Helper Cells by IL-17A and IL-17F	2.54	0.222	2
Folate Transformations I	2.53	0.333	**#NUM!**
MSP-RON Signaling In Cancer Cells Pathway	2.53	0.087	3.317
ERK5 Signaling	2.49	0.111	2.646
Ovarian Cancer Signaling	2.48	0.0823	2
CD27 Signaling in Lymphocytes	2.48	0.123	1.342

Aryl Hydrocarbon Receptor Signaling	2.46	0.0818	0.632
PI3K/AKT Signaling	2.42	0.0754	2.333
Apelin Pancreas Signaling Pathway	2.33	0.13	-2.236
PFKFB4 Signaling Pathway	2.33	0.13	2.449
IL-23 Signaling Pathway	2.33	0.13	1.342
Role of Osteoblasts, Osteoclasts and Chondrocytes in Rheumatoid Arthritis	2.31	0.0714	**#NUM!**
iNOS Signaling	2.28	0.128	2
Toll-like Receptor Signaling	2.27	0.103	2
Role of JAK2 in Hormone-like Cytokine Signaling	2.24	0.147	**#NUM!**
Factors Promoting Cardiogenesis in Vertebrates	2.22	0.0795	3.317
p53 Signaling	2.18	0.0918	1
Salvage Pathways of Pyrimidine Ribonucleotides	2.18	0.0918	3
Role of Tissue Factor in Cancer	2.17	0.0862	**#NUM!**
Glutathione Redox Reactions II	2.17	0.5	**#NUM!**
Proline Biosynthesis I	2.17	0.5	**#NUM!**
WNT/β-catenin Signaling	2.15	0.0751	1.155
Assembly of RNA Polymerase I Complex	2.15	0.25	**#NUM!**
JAK/STAT Signaling	2.14	0.0976	0.378
Differential Regulation of Cytokine Production in Intestinal Epithelial Cells by IL-17A and IL-17F	2.14	0.174	2
Hepatic Fibrosis / Hepatic Stellate Cell Activation	2.13	0.0722	**#NUM!**
CD40 Signaling	2.09	0.104	1.633
Cell Cycle Regulation by BTG Family Proteins	2.08	0.135	0
IL-22 Signaling	2.07	0.167	1
Iron homeostasis signaling pathway	2.06	0.0791	**#NUM!**
Remodeling of Epithelial Adherens Junctions	2.06	0.103	**#NUM!**
Cholesterol Biosynthesis I	2.05	0.231	**#NUM!**
Cholesterol Biosynthesis II (via 24,25-dihydrolanosterol)	2.05	0.231	**#NUM!**

Anti-IgM 6H down top 100 canonical pathways IPA

Ingenuity Canonical Pathways	-log(p-value)	Ratio	z-score
Leukotriene Biosynthesis	3.7	0.429	-2.236
Cardiac Hypertrophy Signaling (Enhanced)	3.5	0.11	-5.642
Axonal Guidance Signaling	3.46	0.111	**#NUM!**
Hepatic Fibrosis Signaling Pathway	3.12	0.112	-5.191
Senescence Pathway	3.12	0.121	-3.536
Phagosome Formation	3.09	0.102	-8.367
Molecular Mechanisms of Cancer	3.05	0.11	**#NUM!**
UVA-Induced MAPK Signaling	2.96	0.163	-3
Sphingosine-1-phosphate Signaling	2.9	0.153	-3
Cellular Effects of Sildenafil (Viagra)	2.84	0.141	**#NUM!**
Role of NFAT in Cardiac Hypertrophy	2.57	0.123	-4.264
Regulation of Cellular Mechanics by Calpain Protease	2.51	0.157	-1.89
Role of Macrophages, Fibroblasts and Endothelial Cells in Rheumatoid Arthritis	2.44	0.111	**#NUM!**
Ethanol Degradation IV	2.4	0.261	-2.449
PI3K Signaling in B Lymphocytes	2.33	0.133	-3.153
LPS/IL-1 Mediated Inhibition of RXR Function	2.33	0.116	1.387
Sperm Motility	2.26	0.114	-3.742
Superpathway of Inositol Phosphate Compounds	2.25	0.116	-4.796

Dilated Cardiomyopathy Signaling Pathway	2.24	0.13	2.138
GP6 Signaling Pathway	2.18	0.134	-4.123
Production of Nitric Oxide and Reactive Oxygen Species in Macrophages	2.17	0.12	-2.558
FAK Signaling	2.17	0.137	**#NUM!**
ERK/MAPK Signaling	2.14	0.117	-3.13
D-myo-inositol-5-phosphate Metabolism	2.14	0.12	-4.243
Glioblastoma Multiforme Signaling	2.12	0.123	-3.771
D-myo-inositol (1,4,5)-Trisphosphate Biosynthesis	2.12	0.231	-2.449
Calcium Signaling	2.09	0.116	-3.051
Hepatic Fibrosis / Hepatic Stellate Cell Activation	2.09	0.119	**#NUM!**
FLT3 Signaling in Hematopoietic Progenitor Cells	2.06	0.15	-2.714
Cardiac β-adrenergic Signaling	2.04	0.121	-1.387
Opioid Signaling Pathway	2.02	0.109	-3
HGF Signaling	2.01	0.129	-3.162
Inflammasome pathway	1.99	0.25	-2.236
IL-15 Production	1.97	0.13	-4
Thrombin Signaling	1.97	0.114	-3.638
WNT/Ca+ pathway	1.92	0.156	-3.162
Endothelin-1 Signaling	1.89	0.115	-3.71
Endocannabinoid Neuronal Synapse Pathway	1.89	0.122	-3.207
Kinetochore Metaphase Signaling Pathway	1.87	0.133	-2.111
FcγRIIB Signaling in B Lymphocytes	1.86	0.141	-1.342
Phospholipases	1.83	0.152	-3.162
nNOS Signaling in Skeletal Muscle Cells	1.79	0.167	**#NUM!**
TREM1 Signaling	1.78	0.143	-2.714
Xenobiotic Metabolism Signaling	1.78	0.104	**#NUM!**
Choline Biosynthesis III	1.77	0.267	-2
Semaphorin Neuronal Repulsive Signaling Pathway	1.77	0.119	-0.258
VDR/RXR Activation	1.74	0.141	-0.816
Apelin Cardiomyocyte Signaling Pathway	1.72	0.131	-3.606
Signaling by Rho Family GTPases	1.71	0.104	-3.441
Actin Cytoskeleton Signaling	1.7	0.106	-1.604
Protein Kinase A Signaling	1.68	0.097	-1.616
Role of Pattern Recognition Receptors in Recognition of Bacteria and Viruses	1.64	0.115	-3.317
CCR3 Signaling in Eosinophils	1.61	0.119	-2.828
RHOA Signaling	1.61	0.121	-1.807
Dopamine-DARPP32 Feedback in cAMP Signaling	1.59	0.11	-3.357
Acetate Conversion to Acetyl-CoA	1.58	0.5	**#NUM!**
Aryl Hydrocarbon Receptor Signaling	1.57	0.113	-1
G-Protein Coupled Receptor Signaling	1.56	0.101	**#NUM!**
Synaptic Long Term Depression	1.55	0.108	-3.578
cAMP-mediated signaling	1.55	0.105	-3.411
Fcγ Receptor-mediated Phagocytosis in Macrophages and Monocytes	1.54	0.128	-3.464
RAC Signaling	1.53	0.116	-3.162
GPCR-Mediated Nutrient Sensing in Enteroendocrine Cells	1.53	0.121	-3.742
Cyclins and Cell Cycle Regulation	1.53	0.131	1.134
VEGF Family Ligand-Receptor Interactions	1.53	0.131	-3.162
tRNA Splicing	1.52	0.159	-2.449
Leptin Signaling in Obesity	1.51	0.135	-2
Neuregulin Signaling	1.5	0.12	-2.121

G Beta Gamma Signaling	1.48	0.116	-3.464
P2Y Purigenic Receptor Signaling Pathway	1.48	0.116	-3.606
Primary Immunodeficiency Signaling	1.46	0.145	**#NUM!**
MIF-mediated Glucocorticoid Regulation	1.45	0.167	-2.449
Adrenomedullin signaling pathway	1.45	0.106	-4.243
Nitric Oxide Signaling in the Cardiovascular System	1.45	0.118	-2.53
IL-8 Signaling	1.45	0.104	-4.123
Xenobiotic Metabolism CAR Signaling Pathway	1.44	0.106	-3.13
GABA Receptor Signaling	1.43	0.115	**#NUM!**
Role of NANOG in Mammalian Embryonic Stem Cell Pluripotency	1.42	0.117	-2.236
Ephrin Receptor Signaling	1.41	0.104	-2.887
Integrin Signaling	1.41	0.103	-4.243
Eicosanoid Signaling	1.39	0.134	-2.236
Lysine Degradation II	1.38	0.4	**#NUM!**
Lysine Degradation V	1.38	0.4	**#NUM!**
Toll-like Receptor Signaling	1.37	0.128	-1.89
RHOGDI Signaling	1.37	0.102	2.309
Valine Degradation I	1.34	0.2	-2
Ceramide Signaling	1.34	0.122	-1.667
Leukocyte Extravasation Signaling	1.34	0.104	-2.668
Neuropathic Pain Signaling In Dorsal Horn Neurons	1.34	0.119	-3.464
Ovarian Cancer Signaling	1.33	0.108	-2.449
Gαq Signaling	1.32	0.106	-3.357
Glioma Signaling	1.32	0.113	-2.646
Chemokine Signaling	1.31	0.125	-2.333
Amyotrophic Lateral Sclerosis Signaling	1.26	0.113	-1.414
Gαi Signaling	1.26	0.109	-2.309
Actin Nucleation by ARP-WASP Complex	1.25	0.118	-1.342
Factors Promoting Cardiogenesis in Vertebrates	1.23	0.106	-4
Urea Cycle	1.22	0.333	**#NUM!**

Anti-IgM 24H up top 100 canonical pathways IPA

Ingenuity Canonical Pathways	-log(p-value)	Ratio	z-score
BAG2 Signaling Pathway	11.2	0.25	1.667
Superpathway of Cholesterol Biosynthesis	10.8	0.448	3.606
Inhibition of ARE-Mediated mRNA Degradation Pathway	8.5	0.155	2.673
Sirtuin Signaling Pathway	8.48	0.12	0
Antigen Presentation Pathway	7.81	0.308	**#NUM!**
Crosstalk between Dendritic Cells and Natural Killer Cells	7.18	0.187	3.464
FAT10 Signaling Pathway	6.79	0.232	**#NUM!**
Cholesterol Biosynthesis I	6.75	0.538	2.646
Cholesterol Biosynthesis II (via 24,25-dihydrolanosterol)	6.75	0.538	2.646
Cholesterol Biosynthesis III (via Desmosterol)	6.75	0.538	2.646
TNFR2 Signaling	6.67	0.312	2.449
Glycolysis I	6.66	0.36	3
Polyamine Regulation in Colon Cancer	6.24	0.21	**#NUM!**
Induction of Apoptosis by HIV1	5.99	0.2	1.155
Hepatic Cholestasis	5.91	0.122	**#NUM!**
tRNA Charging	5.79	0.256	3.162
Death Receptor Signaling	5.39	0.156	1.069
Mevalonate Pathway I	5.12	0.429	2.449

TWEAK Signaling	5.06	0.243	0
Unfolded protein response	5.05	0.156	3.317
Small Cell Lung Cancer Signaling	4.72	0.146	1.633
Role of PKR in Interferon Induction and Antiviral Response	4.69	0.125	-1
Protein Ubiquitination Pathway	4.56	0.0945	**#NUM!**
Ferroptosis Signaling Pathway	4.53	0.127	1
Purine Nucleotides De Novo Biosynthesis II	4.49	0.455	2.236
Gluconeogenesis I	4.48	0.28	2.646
4-1BB Signaling in T Lymphocytes	4.44	0.235	2
Th1 and Th2 Activation Pathway	4.4	0.11	**#NUM!**
Glucocorticoid Receptor Signaling	4.39	0.074	**#NUM!**
Superpathway of Geranylgeranyldiphosphate Biosynthesis I (via Mevalonate)	4.39	0.333	2.449
NRF2-mediated Oxidative Stress Response	4.28	0.097	2.673
Remodeling of Epithelial Adherens Junctions	4.25	0.162	**#NUM!**
CD27 Signaling in Lymphocytes	4.23	0.175	0.816
Erythropoietin Signaling Pathway	4.23	0.107	-1.886
HIF1α Signaling	4.21	0.101	1.789
GADD45 Signaling	4.1	0.3	**#NUM!**
UDP-N-acetyl-D-galactosamine Biosynthesis II	4.07	0.385	2.236
Huntington's Disease Signaling	3.98	0.089	0
Endoplasmic Reticulum Stress Pathway	3.96	0.286	2.449
MYC Mediated Apoptosis Signaling	3.95	0.18	1.667
Colanic Acid Building Blocks Biosynthesis	3.89	0.357	2.236
Cardiac Hypertrophy Signaling (Enhanced)	3.85	0.0725	5.24
Aryl Hydrocarbon Receptor Signaling	3.82	0.107	1.732
TNFR1 Signaling	3.81	0.173	2.646
Role of Macrophages, Fibroblasts and Endothelial Cells in Rheumatoid Arthritis	3.76	0.0831	**#NUM!**
April Mediated Signaling	3.75	0.19	0.378
B Cell Activating Factor Signaling	3.67	0.186	2
PD-1, PD-L1 cancer immunotherapy pathway	3.64	0.123	-1.155
CD40 Signaling	3.62	0.149	0.333
Lymphotoxin β Receptor Signaling	3.62	0.164	1.89
Th2 Pathway	3.56	0.109	2.121
PFKFB4 Signaling Pathway	3.46	0.174	2.121
Antioxidant Action of Vitamin C	3.44	0.117	-3.162
Role of Pattern Recognition Receptors in Recognition of Bacteria and Viruses	3.43	0.103	1
iNOS Signaling	3.4	0.17	2.449
Phagosome Maturation	3.34	0.101	**#NUM!**
Tetrahydrofolate Salvage from 5,10-methenyltetrahydrofolate	3.26	0.6	**#NUM!**
Neuroinflammation Signaling Pathway	3.23	0.0794	4.796
FAT10 Cancer Signaling Pathway	3.21	0.16	2.449
PI3K/AKT Signaling	3.12	0.0905	2.309
HMGB1 Signaling	3.1	0.0958	3.162
Th1 Pathway	3.05	0.107	3.317
Stearate Biosynthesis I (Animals)	3.04	0.151	2.828
LXR/RXR Activation	3.01	0.106	-0.447
Mitochondrial Dysfunction	2.99	0.0936	**#NUM!**
Zymosterol Biosynthesis	2.97	0.5	**#NUM!**
Sertoli Cell-Sertoli Cell Junction Signaling	2.95	0.0874	**#NUM!**
Cell Cycle: G1/S Checkpoint Regulation	2.92	0.132	-0.707

Pancreatic Adenocarcinoma Signaling	2.92	0.103	2.53
B Cell Development	2.92	0.163	**#NUM!**
Prostate Cancer Signaling	2.88	0.107	**#NUM!**
eNOS Signaling	2.88	0.0943	0.577
Endocannabinoid Cancer Inhibition Pathway	2.88	0.0979	-1.069
MIF Regulation of Innate Immunity	2.86	0.159	2.449
p53 Signaling	2.84	0.112	1.633
Epoxysqualene Biosynthesis	2.82	1	**#NUM!**
Tumor Microenvironment Pathway	2.78	0.0894	3.873
IL-10 Signaling	2.75	0.125	**#NUM!**
Superpathway of Serine and Glycine Biosynthesis I	2.74	0.429	**#NUM!**
Hepatic Fibrosis Signaling Pathway	2.71	0.0692	2.353
Osteoarthritis Pathway	2.71	0.0812	2
Hypoxia Signaling in the Cardiovascular System	2.66	0.122	2.646
Acute Phase Response Signaling	2.64	0.0865	2.673
Apoptosis Signaling	2.64	0.106	1.265
MIF-mediated Glucocorticoid Regulation	2.62	0.167	2.236
IL-17 Signaling	2.59	0.0856	4
Parkinson's Signaling	2.55	0.25	**#NUM!**
TREM1 Signaling	2.54	0.117	2.828
Estrogen-mediated S-phase Entry	2.54	0.192	1
Toll-like Receptor Signaling	2.51	0.115	1
IL-17A Signaling in Fibroblasts	2.5	0.158	**#NUM!**
IL-4 Signaling	2.5	0.108	**#NUM!**
IL-1 Signaling	2.46	0.106	2.828
Activation of IRF by Cytosolic Pattern Recognition Receptors	2.46	0.123	-0.378
RAN Signaling	2.45	0.235	2
Isoleucine Degradation I	2.45	0.235	**#NUM!**
14-3-3-mediated Signaling	2.42	0.0945	1.633
Folate Transformations I	2.39	0.333	**#NUM!**

Anti-IgM 24H down top 100 canonical pathways IPA

Ingenuity Canonical Pathways	-log(p-value)	Ratio	z-score
Sperm Motility	5.49	0.126	-3.606
Hepatic Fibrosis / Hepatic Stellate Cell Activation	4.6	0.129	#NUM!
cAMP-mediated signaling	4.23	0.118	-3.138
tRNA Splicing	4.18	0.227	-3
Cardiac Hypertrophy Signaling (Enhanced)	4.02	0.0911	-5.864
GP6 Signaling Pathway	4.01	0.142	-4
CREB Signaling in Neurons	3.65	0.0864	-6.782
Cardiac β-adrenergic Signaling	3.56	0.121	-2.496
Human Embryonic Stem Cell Pluripotency	3.41	0.12	#NUM!
Leukotriene Biosynthesis	3.3	0.357	-2
G-Protein Coupled Receptor Signaling	3.26	0.101	#NUM!
Endothelin-1 Signaling	3.02	0.11	-3.13
Relaxin Signaling	3.01	0.118	-2
Gαs Signaling	2.83	0.124	-2.53
Molecular Mechanisms of Cancer	2.74	0.0854	#NUM!
Axonal Guidance Signaling	2.73	0.083	#NUM!
nNOS Signaling in Neurons	2.58	0.17	#NUM!

Synaptic Long Term Depression	2.57	0.103	-3.441
Cellular Effects of Sildenafil (Viagra)	2.34	0.107	#NUM!
Role of NFAT in Cardiac Hypertrophy	2.28	0.0955	-4
G Protein Signaling Mediated by Tubby	2.15	0.159	#NUM!
Eicosanoid Signaling	2.13	0.134	-2
D-myo-inositol (1,4,5)-Trisphosphate Biosynthesis	2.01	0.192	-2.236
Dermatan Sulfate Degradation (Metazoa)	2	0.235	-2
Th1 Pathway	1.97	0.107	-1.897
Role of Macrophages, Fibroblasts and Endothelial Cells in Rheumatoid Arthritis	1.96	0.0831	#NUM!
Melatonin Signaling	1.93	0.125	-3
Factors Promoting Cardiogenesis in Vertebrates	1.93	0.0993	-3.357
PCP (Planar Cell Polarity) Pathway	1.93	0.133	-2.121
Phagosome Formation	1.8	0.0711	-7
Th1 and Th2 Activation Pathway	1.77	0.093	#NUM!
Protein Kinase A Signaling	1.74	0.0771	-2.746
VDR/RXR Activation	1.72	0.115	0.378
Sphingosine-1-phosphate Signaling	1.71	0.102	-2.111
Granulocyte Adhesion and Diapedesis	1.71	0.0899	#NUM!
Adipogenesis pathway	1.64	0.0963	#NUM!
Thrombin Signaling	1.6	0.0857	-2.887
Dopamine-DARPP32 Feedback in cAMP Signaling	1.58	0.0884	-3.317
Apelin Endothelial Signaling Pathway	1.55	0.0935	-2.121
TR/RXR Activation	1.53	0.107	#NUM!
VEGF Family Ligand-Receptor Interactions	1.53	0.107	-2.828
Agranulocyte Adhesion and Diapedesis	1.53	0.0841	#NUM!
HIPPO signaling	1.5	0.106	0.816
IL-10 Signaling	1.49	0.111	#NUM!
Basal Cell Carcinoma Signaling	1.49	0.111	-2.646
Selenocysteine Biosynthesis II (Archaea and Eukaryotes)	1.46	0.333	#NUM!
G Beta Gamma Signaling	1.45	0.093	-3.162
P2Y Purigenic Receptor Signaling Pathway	1.45	0.093	-3.162
MIF-mediated Glucocorticoid Regulation	1.44	0.139	-1.342
GPCR-Mediated Nutrient Sensing in Enteroendocrine Cells	1.42	0.0948	-3.317
GABA Receptor Signaling	1.4	0.0916	#NUM!
Dilated Cardiomyopathy Signaling Pathway	1.4	0.089	1.265
Colorectal Cancer Metastasis Signaling	1.39	0.0781	-3.873
Endocannabinoid Neuronal Synapse Pathway	1.38	0.0884	-2.887
Fc Epsilon RI Signaling	1.37	0.0932	-3
Virus Entry via Endocytic Pathways	1.37	0.0962	#NUM!
Thrombopoietin Signaling	1.36	0.111	-2.449
Nitric Oxide Signaling in the Cardiovascular System	1.35	0.0924	-1.667
Chondroitin Sulfate Degradation (Metazoa)	1.33	0.188	#NUM!
Adenine and Adenosine Salvage III	1.33	0.286	#NUM!
CCR3 Signaling in Eosinophils	1.32	0.0889	-2.449
STAT3 Pathway	1.32	0.0889	-2.449
α-Adrenergic Signaling	1.32	0.0943	#NUM!
Opioid Signaling Pathway	1.29	0.0761	-2.183
2-amino-3-carboxymuconate Semialdehyde Degradation to Glutaryl-CoA	1.29	1	#NUM!
Th2 Pathway	1.28	0.0876	-2.714
Breast Cancer Regulation by Stathmin1	1.28	0.0676	-6.164
Phospholipases	1.27	0.106	-2.646

IL-15 Production	1.26	0.0894	-3.317
IL-1 Signaling	1.26	0.0957	#NUM!
Gαi Signaling	1.26	0.087	-0.816
Superpathway of Inositol Phosphate Compounds	1.24	0.0776	-4
Purine Ribonucleosides Degradation to Ribose-1-phosphate	1.22	0.25	#NUM!
Glioblastoma Multiforme Signaling	1.21	0.0819	-3.317
Pregnenolone Biosynthesis	1.2	0.167	#NUM!
Primary Immunodeficiency Signaling	1.19	0.109	#NUM!
Hepatic Cholestasis	1.18	0.0794	#NUM!
Apelin Cardiomyocyte Signaling Pathway	1.15	0.0909	-3
D-myo-inositol-5-phosphate Metabolism	1.13	0.0781	-3.606
Role of Osteoblasts, Osteoclasts and Chondrocytes in Rheumatoid Arthritis	1.13	0.0759	#NUM!
Atherosclerosis Signaling	1.13	0.0846	#NUM!
Role of Hypercytokinemia/hyperchemokinemia in the Pathogenesis of Influenza	1.11	0.093	-2.121
Neuropathic Pain Signaling In Dorsal Horn Neurons	1.11	0.0891	-3
Ephrin B Signaling	1.1	0.0972	-2.236
p70S6K Signaling	1.09	0.0833	-1.897
Inflammasome pathway	1.09	0.15	#NUM!
Neuregulin Signaling	1.09	0.0855	-1.89
Regulation of the Epithelial-Mesenchymal Transition Pathway	1.09	0.0769	#NUM!
Leptin Signaling in Obesity	1.06	0.0946	#NUM!
CXCR4 Signaling	1.03	0.0778	-2.121
Ceramide Signaling	1.03	0.0889	-1.633
White Adipose Tissue Browning Pathway	1.02	0.0809	-2.714
Type II Diabetes Mellitus Signaling	1.02	0.0789	-2
nNOS Signaling in Skeletal Muscle Cells	0.996	0.104	#NUM!
Alanine Degradation III	0.996	0.5	#NUM!
Taurine Biosynthesis	0.996	0.5	#NUM!
Alanine Biosynthesis II	0.996	0.5	#NUM!
Sulfate Activation for Sulfonation	0.996	0.5	#NUM!

Appendix 4 : Top 100 differentially expressed genes Control DMSO vs αIgM DMSO 6H

Gene Name	logFC	AveExpr	t	P Value	FDR	B
LIF	6.956639	1.142677	2.595808	0.016	0.028351	-2.98231
XIRP1	5.32844	-2.51849	4.244318	0.000294	0.000833	-0.53299
LINC02156	4.759261	0.088766	7.176033	2.31E-07	1.99E-06	6.41526
LINC02416	4.677266	1.237616	7.789542	5.81E-08	6.77E-07	8.259111
SERPINE2	4.61692	4.013756	7.173837	2.32E-07	2.00E-06	7.135716
IL6R-AS1	4.498956	-0.77469	6.707903	6.83E-07	4.77E-06	4.768627
AL160408.1	4.342292	-1.32029	7.875461	4.81E-08	5.85E-07	5.978933
AC004264.1	4.327698	-3.78659	3.635378	0.001349	0.003167	-1.46287
NPTX1	4.323184	1.663587	2.962993	0.006867	0.01334	-2.37477
AL160408.3	4.291613	1.261019	11.60513	3.24E-11	3.53E-09	14.32416
MYCN	4.230318	0.616586	7.436054	1.28E-07	1.24E-06	7.136372
FOSL1	4.201675	2.817178	6.123534	2.75E-06	1.52E-05	4.760683
CCL4L2	4.179343	3.220168	3.519243	0.001796	0.004082	-1.447
COL4A2	4.124211	3.89911	9.359757	2.13E-09	5.42E-08	11.64009
CSF1	4.066688	3.65627	6.992816	3.52E-07	2.80E-06	6.711676
CCL4	3.996877	5.09356	3.703695	0.001139	0.002723	-1.26188
C12orf77	3.973687	-0.70574	6.378626	1.49E-06	9.05E-06	4.480071
CBARP	3.923179	2.575673	6.806032	5.43E-07	3.95E-06	6.307679
PIF1	3.849216	2.144319	4.911427	5.49E-05	0.000193	1.903526
PYCR1	3.7976	4.23241	9.834586	8.37E-10	2.80E-08	12.60938
HLA-DPB2	3.755977	0.514645	6.762127	6.01E-07	4.30E-06	5.916302
NPW	3.700973	-0.97392	4.109776	0.000413	0.001123	0.031362
SPTBN4	3.697377	4.134095	6.796088	5.55E-07	4.02E-06	6.255213
PDGFA	3.684327	4.363354	12.05492	1.50E-11	2.40E-09	16.46955
CILP2	3.661077	0.033429	3.938725	0.000634	0.001633	-0.26675
STRIP2	3.637363	2.175235	7.048571	3.09E-07	2.53E-06	6.858854
AC092723.5	3.584632	-0.62339	5.276192	2.20E-05	8.77E-05	2.497024
LINC01181	3.556273	-1.75798	6.105619	2.87E-06	1.57E-05	3.453245
NHLRC1	3.555406	-3.30228	5.005675	4.33E-05	0.000157	0.660648
VGF	3.519748	2.450219	4.884456	5.87E-05	0.000205	1.827704
MYC	3.508419	6.516489	6.723496	6.58E-07	4.62E-06	5.888219
CNKSR3	3.478394	1.128044	5.253639	2.33E-05	9.22E-05	2.752562
NCS1	3.447354	3.854859	8.579568	1.06E-08	1.82E-07	10.12696
SLC6A17	3.394528	-2.44039	3.570032	0.001585	0.003658	-1.26674
ASS1	3.362096	-1.97176	4.538681	0.00014	0.000436	0.587487
HIVEP3	3.340083	4.178062	7.494613	1.12E-07	1.12E-06	7.786701
OLFML2A	3.338398	-1.95036	3.73555	0.001052	0.002539	-0.82416
SH2D5	3.31979	2.996861	7.548593	9.92E-08	1.02E-06	7.955268
CPNE7	3.294364	0.582329	5.692289	7.86E-06	3.66E-05	3.746278
GJC1	3.259691	-0.42599	4.375569	0.000211	0.000627	0.671761
CHAC1	3.244096	2.949065	7.506831	1.09E-07	1.09E-06	7.863506
KLK1	3.196998	2.545284	2.519052	0.018995	0.033003	-3.39152
SLC7A5	3.140825	8.389827	9.102098	3.59E-09	7.88E-08	11.06676
AP000941.1	3.127083	-2.52024	4.238587	0.000299	0.000844	-0.13824

MIR132	3.11484	-1.12167	3.3726	0.002572	0.005598	-1.5048
HLA-DPA3	3.08867	-3.02377	3.5667	0.001598	0.003685	-1.33241
NME1	3.079714	1.201822	11.12322	7.58E-11	5.88E-09	14.28249
CSF2	3.067449	-2.76639	2.611926	0.01543	0.027466	-2.97296
ULBP1	3.06055	-0.49704	4.845243	6.48E-05	0.000223	1.617936
LINC02365	3.023762	5.932425	6.108232	2.85E-06	1.56E-05	4.513984
BX640514.2	3.021891	-1.99449	4.640782	0.000108	0.00035	0.803659
EPOP	2.992681	2.868619	8.16992	2.53E-08	3.54E-07	9.279704
HOXB9	2.991032	-2.12912	5.346147	1.85E-05	7.53E-05	2.430605
HSD11B2	2.987944	-1.13774	5.780202	6.34E-06	3.07E-05	3.444713
CCL3L1	2.986403	2.081087	2.944124	0.007179	0.013871	-2.59974
GZMB	2.933705	2.734003	5.65264	8.67E-06	3.97E-05	3.563573
METTL1	2.919997	3.226819	12.67723	5.35E-12	1.34E-09	17.3741
B4GALT2	2.915094	4.436934	11.4387	4.33E-11	4.23E-09	15.50448
MIR221	2.91116	-2.61228	3.133699	0.00458	0.009324	-2.07825
EGR3	2.909673	4.827903	6.088411	2.99E-06	1.63E-05	4.48324
SLC29A1	2.908266	5.047276	10.78284	1.40E-10	8.42E-09	14.36357
SLAMF7	2.869531	9.608067	7.96483	3.95E-08	5.00E-07	8.647978
LDHAL6B	2.868534	-0.75038	5.547285	1.12E-05	4.93E-05	2.921928
RAMP2-AS1	2.846667	-1.78705	3.080744	0.005197	0.010431	-2.0754
CEP170B	2.840387	2.58915	7.389651	1.42E-07	1.35E-06	7.61005
BCAT1	2.839129	4.396397	8.311159	1.87E-08	2.82E-07	9.5346
PPIAP45	2.834348	-2.41652	3.755435	0.001001	0.002428	-0.86752
HSPA5	2.833031	9.791681	14.60007	2.77E-13	3.38E-10	20.5101
AL162724.2	2.815913	-2.01853	6.321533	1.71E-06	1.01E-05	3.661036
BAALC-AS2	2.809945	-1.6312	4.93393	5.19E-05	0.000184	1.654625
RASL10B	2.80807	-1.16166	3.910554	0.00068	0.001737	-0.37218
MIR222HG	2.795209	0.234879	6.427372	1.33E-06	8.26E-06	5.271953
STEAP3	2.79377	1.287254	7.620954	8.44E-08	9.00E-07	8.067411
CD1C	2.793379	1.404146	3.650523	0.001299	0.003061	-1.03944
DTX1	2.792334	4.610431	6.669507	7.47E-07	5.12E-06	5.938148
USP2-AS1	2.780351	-2.21313	3.253883	0.00343	0.007224	-1.81117
MIR155HG	2.766153	6.448947	6.199467	2.29E-06	1.30E-05	4.604173
LINC02362	2.764942	1.395193	6.686667	7.18E-07	4.97E-06	5.993823
HIC1	2.764689	3.234799	5.47724	1.34E-05	5.71E-05	3.173946
B4GALNT1	2.762184	-2.65516	4.293298	0.00026	0.000749	0.184353
PDIA5	2.752954	2.19722	6.512761	1.08E-06	7.00E-06	5.65275
GPSM1	2.745353	3.371221	7.549263	9.91E-08	1.02E-06	7.949148
SNHG4	2.739224	3.953095	11.01116	9.27E-11	6.46E-09	14.74447
TNFRSF9	2.737958	2.855358	4.667603	0.000101	0.00033	1.18894
RASAL1	2.730534	3.494212	7.261068	1.90E-07	1.72E-06	7.307002
TRIB3	2.730524	5.591505	11.38308	4.78E-11	4.56E-09	15.42367
AC090617.5	2.72578	1.172482	4.110769	0.000412	0.001121	0.085103
ANKRD13B	2.723163	4.591246	10.01332	5.93E-10	2.18E-08	12.94661
COL8A2	2.696723	2.048206	8.278175	2.01E-08	2.98E-07	9.475846
SPTBN2	2.686465	4.398739	10.64259	1.82E-10	9.85E-09	14.1106
AC009041.2	2.68413	2.349059	4.960897	4.85E-05	0.000174	2.015185
TFPI2	2.679396	-0.67742	2.898371	0.007991	0.015235	-2.43705
CGN	2.675687	1.284926	8.25465	2.11E-08	3.09E-07	9.28646

BIRC7	2.671514	-4.37418	2.873484	0.008469	0.016055	-2.59819
PHEX	2.659446	4.255242	5.835126	5.54E-06	2.73E-05	3.835653
FAM131C	2.653022	-2.8447	2.948771	0.007101	0.01374	-2.34199
MTHFD1L	2.646541	6.375906	10.94595	1.04E-10	7.02E-09	14.63067
SLC24A3	2.639497	-1.52119	3.55358	0.00165	0.003793	-1.17432
RCN1	2.632488	1.536055	10.18379	4.28E-10	1.70E-08	12.93705
TNFSF14	2.625817	4.461551	6.53111	1.04E-06	6.77E-06	5.556853
LINC01480	2.60961	3.935911	6.004367	3.67E-06	1.93E-05	4.352796

Appendix 5 : Top 100 differentially expressed genes Control DMSO vs αIgM DMSO 24H

Gene Name	logFC	AveExpr	t	P Value	FDR	B
CCL4L2	7.714787	1.429966	2.658069	0.014051	0.023739	-2.88756
CCL4	6.853661	3.808345	5.300617	2.22E-05	7.73E-05	2.786722
XIRP1	6.834367	-2.52441	4.158215	0.00038	0.000938	-1.64608
CCL3L1	6.255662	0.155217	3.002954	0.006346	0.011641	-2.38889
BIRC7	5.950574	-2.52582	2.925044	0.007615	0.013708	-2.7466
CD1C	5.791345	3.288319	6.936355	4.53E-07	2.91E-06	6.404319
CCL3	5.690111	-0.85914	3.519912	0.001837	0.003832	-1.76514
AL357992.1	5.444845	-2.60359	3.338491	0.002853	0.005689	-2.25023
RAMP2-AS1	5.4234	-0.75812	3.747955	0.00105	0.00232	-1.26396
MYCN	5.392524	1.302753	4.245414	0.000305	0.000772	0.237549
NPW	5.140589	-1.05311	4.949659	5.28E-05	0.000165	0.513613
FAM131C	5.106756	-0.76787	4.930542	5.54E-05	0.000172	0.491552
C12orf77	5.038214	-0.40248	4.962896	5.11E-05	0.00016	1.118946
PDGFA	4.944838	3.436997	9.047317	4.88E-09	9.70E-08	10.48691
EGR4	4.939297	-2.69827	4.448732	0.000184	0.000493	-0.90476
LINC02156	4.869319	-1.03322	5.320231	2.12E-05	7.41E-05	1.596822
LIF	4.849514	-1.50566	2.506218	0.019721	0.032205	-3.23137
CCL22	4.832794	5.594329	7.923857	5.05E-08	5.15E-07	8.609715
PYCR1	4.826256	2.718976	4.956918	5.19E-05	0.000162	2.013674
EGR1	4.813129	4.736166	7.281272	2.07E-07	1.55E-06	7.252051
C6orf223	4.761121	-0.64421	3.980319	0.000591	0.001395	-0.88796
TNFRSF9	4.75988	1.839492	2.977168	0.006742	0.012293	-2.33722
IL4I1	4.70125	3.770006	5.336572	2.03E-05	7.14E-05	2.874397
B4GALNT1	4.64547	-1.28731	5.328622	2.07E-05	7.27E-05	1.535528
EPOP	4.48583	2.93039	6.13485	2.94E-06	1.37E-05	4.688661
DACT3	4.479883	0.028408	4.668024	0.000106	0.000305	0.868908
GJC1	4.443413	-1.26981	3.597579	0.001519	0.003232	-1.56676
SERPINE2	4.421835	2.127435	3.191285	0.004062	0.007815	-1.87874
EGR3	4.418021	4.867158	7.477455	1.34E-07	1.10E-06	7.655681
LINC02416	4.394444	0.756046	3.362167	0.002694	0.005404	-1.52166
MYC	4.377232	5.612284	11.23873	8.08E-11	9.31E-09	14.87556
HMGN2P15	4.373027	-2.80555	4.969166	5.03E-05	0.000158	-0.07697
CILP2	4.302347	-0.61079	3.35422	0.002746	0.0055	-1.66802
HSPB7	4.283126	-2.50842	5.989291	4.16E-06	1.84E-05	1.70287

LINC02362	4.206467	0.988937	3.74369	0.001061	0.002342	-0.76105
EBI3	4.185971	1.28741	4.440982	0.000188	0.000502	0.744462
HUNK	4.172072	-1.82635	3.544542	0.001729	0.003636	-1.64322
LGALS9C	4.129474	1.349893	4.926862	5.59E-05	0.000174	1.907928
HOXB9	4.107069	-3.39447	3.337368	0.002861	0.005702	-2.33617
CPNE7	4.059017	0.855981	4.440054	0.000188	0.000503	0.654346
FOSL1	4.042079	0.876198	4.193447	0.000348	0.000867	0.253645
SCD	4.015313	6.685078	12.8197	5.84E-12	4.75E-09	17.48303
KIF7	3.91881	-1.07067	5.915823	4.96E-06	2.15E-05	2.015969
TNFRSF4	3.898035	5.090923	6.372372	1.67E-06	8.53E-06	5.147019
PANX2	3.830161	0.555473	6.082729	3.33E-06	1.52E-05	3.849112
CBARP	3.804533	1.183824	4.383944	0.000216	0.000568	0.65038
HRAT92	3.787755	0.171389	8.492131	1.52E-08	2.12E-07	7.264778
USP2-AS1	3.762732	-3.80614	4.76324	8.40E-05	0.000247	-0.79549
CHAC1	3.751561	1.049224	4.394875	0.00021	0.000555	0.717083
INHBA	3.723103	0.296989	3.103539	0.005005	0.009404	-2.05093
LINC02365	3.688671	5.885123	9.310761	2.89E-09	6.88E-08	11.40875
PTGIR	3.678222	3.140634	6.423952	1.48E-06	7.71E-06	5.364837
HIVEP3	3.664038	4.552072	7.263323	2.16E-07	1.60E-06	7.207507
AL160408.1	3.657353	-2.81462	4.637505	0.000115	0.000325	-0.36581
IGSF3	3.654098	7.080733	10.72829	2.00E-10	1.40E-08	14.02516
SOX5	3.641274	-2.34101	3.924553	0.000678	0.001576	-1.5498
SAMSN1-AS1	3.611652	0.31669	3.525762	0.001811	0.003785	-1.20593
MIR3142HG	3.609831	3.275495	7.144191	2.82E-07	1.98E-06	6.93811
PIGR	3.586421	3.418902	6.643591	8.88E-07	5.01E-06	5.851351
LINC00158	3.578635	-1.8348	5.379416	1.83E-05	6.52E-05	1.114235
OAS3	3.566401	6.182199	13.5525	1.88E-12	3.57E-09	18.59696
NME1	3.557562	0.178731	6.047893	3.62E-06	1.63E-05	3.676238
PPIAP45	3.55475	-2.72015	4.14884	0.000388	0.000958	-0.87335
VEGFA	3.529471	4.837458	4.829798	7.12E-05	0.000214	1.463357
TNFRSF18	3.521146	6.328567	6.369897	1.68E-06	8.57E-06	5.029352
MYCNOS	3.425224	-2.65101	3.539799	0.00175	0.003673	-1.79032
CNKSR3	3.410138	-0.32239	4.487722	0.000167	0.000452	0.692357
STUM	3.392054	5.909977	12.55993	8.84E-12	5.04E-09	17.04725
ANKRD13B	3.386023	3.590031	9.800186	1.12E-09	3.77E-08	12.17685
MCM10	3.38456	-1.37347	4.192244	0.000349	0.000869	-0.53522
RASAL1	3.378069	4.488721	9.547393	1.82E-09	5.20E-08	11.78953
MT1G	3.372414	-3.196	3.395325	0.002486	0.005023	-1.96488
TERT	3.369126	-2.72594	2.697542	0.01285	0.021886	-3.11734
MSI1	3.348507	-3.9398	2.387837	0.02555	0.040639	-3.5279
SLC7A5	3.347474	6.091293	7.868287	5.69E-08	5.61E-07	8.424165
FAM189A1	3.339353	-2.45059	4.059342	0.000485	0.00117	-1.0301
AC104564.2	3.303305	-2.11998	3.803095	0.000916	0.002056	-1.09331
CLCNKA	3.296595	-2.00021	6.377718	1.65E-06	8.44E-06	3.572343
SH2D5	3.287282	2.205759	6.73995	7.11E-07	4.17E-06	5.978672
CPNE2	3.260195	3.873731	7.596478	1.03E-07	8.91E-07	7.929948
PSAT1	3.225261	1.65707	3.953659	0.000631	0.00148	-0.34028
MYOCD	3.213003	-2.51306	2.467259	0.021487	0.034777	-3.28287
GNG8	3.195851	0.596748	3.641005	0.001366	0.00294	-0.94124

CX3CL1	3.190933	-3.2157	5.102133	3.62E-05	0.000119	-0.19532
HES1	3.185997	-2.42175	4.470035	0.000174	0.00047	-0.38018
HMOX1	3.175616	7.558487	6.944659	4.44E-07	2.87E-06	6.325012
AC003092.1	3.16523	-1.11799	5.472297	1.46E-05	5.36E-05	2.020021
MAFG-DT	3.163882	-2.56627	4.456166	0.000181	0.000485	-0.20981
AC009090.4	3.160314	-1.0876	5.729111	7.79E-06	3.16E-05	2.444409
AC083837.1	3.159248	-1.01232	4.483005	0.000169	0.000457	0.536873
VWCE	3.125059	0.020826	5.174879	3.03E-05	0.000101	1.962743
DUPD1	3.120409	-2.36432	5.119393	3.47E-05	0.000114	1.002651
RASL10B	3.100728	-0.84552	5.376708	1.84E-05	6.55E-05	1.694326
NAP1L4P1	3.082759	1.417979	6.202457	2.50E-06	1.19E-05	4.722511
AC104699.1	3.064236	-1.4563	6.195079	2.55E-06	1.21E-05	3.342927
INA	3.051242	-3.42736	4.841856	6.91E-05	0.000208	-0.5659
MIR155HG	3.02184	5.275002	7.213787	2.41E-07	1.75E-06	6.999604
HSD11B2	3.015821	-2.32074	5.040575	4.22E-05	0.000135	0.722124
GFI1	3.012375	4.147195	10.94498	1.35E-10	1.21E-08	14.27481
SEMA7A	3.007454	5.994751	7.421022	1.52E-07	1.21E-06	7.442734
AC026310.2	2.994016	-1.28017	3.889822	0.000739	0.001702	-0.73898

Appendix 6 : Top 100 differentially expressed genes control DMSO versus anti-IgM VPS34-IN1 at 6 hr

	logFC	AveExpr	t	PValue	FDR	B
SERPINE2	4.755817	4.013756	7.372308	1.48E-07	1.79E-06	7.571236
AL160408.1	4.750677	-1.32029	8.48686	1.29E-08	2.94E-07	6.387363
NPTX1	4.549146	1.663587	3.083199	0.005166	0.010788	-2.10602
AL160408.3	4.49224	1.261019	12.05588	1.50E-11	5.02E-09	14.68163
CBARP	4.416344	2.575673	7.609714	8.65E-08	1.18E-06	8.0078
PIF1	4.35064	2.144319	5.520168	1.20E-05	5.97E-05	3.36636
LINC02156	4.3166	0.088766	6.531314	1.04E-06	8.03E-06	5.106751
KLK4	4.138203	0.23127	2.496402	0.019974	0.035096	-3.15322
LINC02416	4.118416	1.237616	6.885796	4.51E-07	4.14E-06	6.366668
IL6R-AS1	3.981127	-0.77469	5.96914	3.99E-06	2.42E-05	3.377222
SPTBN4	3.887839	4.134095	7.168305	2.35E-07	2.55E-06	7.110483
HLA-DPB2	3.776763	0.514645	6.768342	5.93E-07	5.12E-06	5.854878
NCS1	3.679451	3.854859	9.189838	3.00E-09	1.11E-07	11.33007
SH2D5	3.652112	2.996861	8.326376	1.81E-08	3.73E-07	9.57572
XIRP1	3.605226	-2.51849	3.005868	0.006207	0.012639	-2.45397
FOSL1	3.494165	2.817178	5.095104	3.46E-05	0.000144	2.337601
CILP2	3.465825	0.033429	3.728503	0.001071	0.002747	-0.72952
PYCR1	3.464968	4.23241	9.011727	4.32E-09	1.42E-07	11.00309
MYCN	3.461651	0.616586	6.126258	2.73E-06	1.79E-05	4.483126
CNKSR3	3.376101	1.128044	5.099104	3.43E-05	0.000143	2.392235
COL4A2	3.338449	3.89911	7.571883	9.42E-08	1.26E-06	8.003996
AP000941.1	3.268712	-2.52024	4.434779	0.000182	0.000595	0.118319
CCL4	3.196657	5.09356	2.962147	0.006881	0.013831	-2.93743
CSF2	3.177852	-2.76639	2.711701	0.012303	0.023002	-2.83146

MIR132	3.172883	-1.12167	3.422049	0.002279	0.005286	-1.42348
SLAMF7	3.169685	9.608067	9.06078	3.91E-09	1.33E-07	10.98734
KLK1	3.152997	2.545284	2.482934	0.020579	0.036046	-3.43018
CCL4L2	3.14154	3.220168	2.644034	0.01435	0.026275	-3.34221
GJB2	3.069529	-0.10303	3.869651	0.000753	0.002025	-0.43104
BLVRB	3.058361	3.593884	6.337801	1.64E-06	1.17E-05	5.221449
C12orf77	3.035275	-0.70574	4.926729	5.28E-05	0.000206	1.629005
MYC	3.012798	6.516489	5.870028	5.09E-06	2.97E-05	3.862227
PDGFA	2.985432	4.363354	9.762073	9.64E-10	5.28E-08	12.4549
LDHAL6B	2.924513	-0.75038	5.638542	8.97E-06	4.69E-05	3.002741
HSPA5	2.923744	9.791681	15.53083	7.39E-14	2.53E-10	21.80275
SLC7A5	2.922278	8.389827	8.71671	7.94E-09	2.18E-07	10.2774
INHBA	2.902028	1.932266	3.798425	0.0009	0.002362	-0.75253
CD274	2.854497	5.270763	7.29703	1.75E-07	2.02E-06	7.288722
TRIB3	2.836096	5.591505	12.02724	1.57E-11	5.07E-09	16.51735
LINC01181	2.827332	-1.75798	4.8977	5.68E-05	0.000219	1.237479
SLC29A1	2.823495	5.047276	10.59298	1.99E-10	1.94E-08	14.02064
HLA-DPA3	2.819211	-3.02377	3.259127	0.003387	0.007461	-1.90824
HLA-DQB2	2.782061	0.251385	4.696675	9.42E-05	0.000339	1.457988
CPNE7	2.769049	0.582329	4.789452	7.46E-05	0.000278	1.672189
HLA-DQA2	2.76845	-0.03397	3.170054	0.004198	0.009003	-2.04484
KIF26B	2.764861	1.447345	3.812435	0.000869	0.002291	-0.61655
STUM	2.751812	5.858304	9.367961	2.10E-09	8.63E-08	11.67873
TNFRSF9	2.724626	2.855358	4.680077	9.82E-05	0.000352	1.243107
MET	2.723577	2.515028	5.524338	1.19E-05	5.93E-05	3.357479
LINC02365	2.710234	5.932425	5.51913	1.20E-05	5.98E-05	3.106911
OLFML2A	2.699518	-1.95036	3.043432	0.005678	0.011712	-2.16738
CHAC1	2.697772	2.949065	6.226202	2.15E-06	1.47E-05	4.973864
METTL1	2.689069	3.226819	11.70344	2.73E-11	6.47E-09	15.80408
DTX1	2.688606	4.610431	6.461743	1.22E-06	9.23E-06	5.471033
GJA3	2.640644	-1.11169	3.271731	0.003285	0.007274	-1.71703
B4GALT2	2.63442	4.436934	10.39934	2.85E-10	2.47E-08	13.66176
STRIP2	2.630546	2.175235	5.058637	3.79E-05	0.000155	2.247213
NME1	2.620638	1.201822	9.45057	1.78E-09	7.79E-08	11.43519
HLA-DQB1-AS1	2.610306	1.269777	5.419023	1.54E-05	7.34E-05	3.137289
AC090617.5	2.592861	1.172482	3.919111	0.000666	0.001821	-0.34506
GIPR	2.590837	2.693607	7.308205	1.71E-07	1.98E-06	7.430931
CSF1	2.585347	3.65627	4.406961	0.000195	0.000632	0.562283
ULBP1	2.574148	-0.49704	4.080194	0.000445	0.001282	-0.02408
NPW	2.566799	-0.97392	2.891454	0.008121	0.016003	-2.44108
EPOP	2.564639	2.868619	6.985764	3.57E-07	3.49E-06	6.714741
CCL3L1	2.563802	2.081087	2.525754	0.018714	0.033155	-3.43023
PHLDB1	2.562243	4.75799	8.043357	3.33E-08	5.78E-07	8.966338
PPIAP45	2.555489	-2.41652	3.384859	0.002496	0.005734	-1.59224
SNHG4	2.550806	3.953095	10.30726	3.39E-10	2.71E-08	13.47772
AC104564.2	2.543932	-0.02919	5.032973	4.04E-05	0.000164	2.145947
GJC1	2.525805	-0.42599	3.403916	0.002382	0.005498	-1.42014
PHEX	2.512482	4.255242	5.57653	1.05E-05	5.31E-05	3.227663

HPDL	2.500321	0.30768	4.305866	0.000252	0.000787	0.559181
AL157871.2	2.487493	0.987601	8.290336	1.95E-08	3.96E-07	9.291642
GPSM1	2.478937	3.371221	6.827782	5.16E-07	4.60E-06	6.34665
HLA-DQA1	2.465815	9.398641	7.927651	4.29E-08	6.99E-07	8.574025
RAMP2-AS1	2.462236	-1.78705	2.67333	0.013427	0.024809	-2.84221
FFAR1	2.459429	2.491796	5.885402	4.90E-06	2.88E-05	4.197882
TNFSF14	2.434805	4.461551	6.103258	2.89E-06	1.87E-05	4.562247
SNORA73B	2.433424	-0.96395	5.437826	1.47E-05	7.07E-05	2.877719
HLA-L	2.416064	5.167125	10.05503	5.47E-10	3.67E-08	13.01049
MIR155HG	2.40936	6.448947	5.519791	1.20E-05	5.97E-05	2.961001
AC092723.5	2.406006	-0.62339	3.55941	0.001627	0.003941	-1.10945
HIC1	2.40389	3.234799	4.759564	8.04E-05	0.000296	1.452673
AL663070.1	2.401587	0.537354	6.584341	9.13E-07	7.27E-06	5.682179
AKR7A2P1	2.399377	-1.36448	4.797593	7.30E-05	0.000273	1.348064
PDIA5	2.395685	2.19722	5.660004	8.51E-06	4.49E-05	3.674144
SESN2	2.394921	5.485136	10.31188	3.36E-10	2.71E-08	13.49377
RYR1	2.386095	3.495317	6.694275	7.05E-07	5.90E-06	6.012467
DDIT4	2.385375	4.753181	8.072104	3.13E-08	5.55E-07	9.021534
CAVIN1	2.379965	1.174842	4.454064	0.000174	0.000571	0.805327
UBASH3B	2.379905	5.402254	9.809103	8.80E-10	5.03E-08	12.53899
CEP170B	2.37026	2.58915	6.147464	2.59E-06	1.71E-05	4.812259
MFSD2A	2.365794	4.092017	6.948897	3.89E-07	3.72E-06	6.553901
ANKRD13B	2.361882	4.591246	8.731348	7.70E-09	2.15E-07	10.42359
CGN	2.356945	1.284926	7.261546	1.90E-07	2.15E-06	7.23135
CORO6	2.356605	7.791657	5.192382	2.71E-05	0.000117	2.107152
NAP1L4P1	2.35359	2.128793	7.243877	1.98E-07	2.22E-06	7.283977
AC126696.2	2.351606	-1.59208	4.221097	0.000312	0.000945	0.129171
AKAP12	2.349963	2.46429	3.880632	0.000733	0.00198	-0.59204
TEKT5	2.341795	-2.07324	3.700456	0.001148	0.002922	-0.89309

Appendix 7 : Top 100 differentially expressed genes control DMSO versus anti-IgM VPS34-IN1 at 24 hr

	logFC	AveExpr	t	PValue	FDR	B
CCL4L2	7.331638	1.429966	2.482523	0.020779	0.037964	-3.19514
CCL4	6.59284	3.808345	4.959457	5.16E-05	0.000228	1.979143
EGR1	5.967712	4.736166	8.952165	5.91E-09	4.27E-07	10.62796
XIRP1	5.778497	-2.52441	3.524421	0.001817	0.004594	-2.55135
CCL3	5.589344	-0.85914	3.377494	0.002596	0.006237	-2.17528
CCL3L1	5.588326	0.155217	2.651743	0.014253	0.027356	-3.00175
EGR4	5.522174	-2.69827	4.772859	8.20E-05	0.000335	-1.03391
EGR3	5.25087	4.867158	8.946996	5.97E-09	4.28E-07	10.68359
CD1C	5.04774	3.288319	5.891828	5.26E-06	3.77E-05	4.086378
TNFRSF9	5.024297	1.839492	3.04865	0.005699	0.012274	-2.15683
MYCN	4.947873	1.302753	3.827151	0.000863	0.002429	-0.69485
PDGFA	4.749485	3.436997	8.475127	1.57E-08	7.28E-07	9.227572
GJC1	4.711169	-1.26981	3.690988	0.001208	0.003243	-1.67533
CILP2	4.704111	-0.61079	3.543432	0.001734	0.00441	-1.4758

LINC02156	4.661632	-1.03322	4.973673	4.98E-05	0.000222	0.664648
RAMP2-AS1	4.644449	-0.75812	3.169772	0.004276	0.009583	-2.31166
MIR132	4.568611	-3.75101	5.704457	8.27E-06	5.31E-05	-0.45689
C12orf77	4.530904	-0.40248	4.385272	0.000215	0.000746	-0.13033
CCL22	4.487168	5.594329	7.428598	1.49E-07	2.87E-06	7.565948
SERPINE2	4.470432	2.127435	3.13575	0.004637	0.010258	-1.97748
OLR1	4.450068	-2.54055	3.184054	0.004133	0.009296	-2.678
FAM131C	4.423005	-0.76787	4.222455	0.000323	0.001059	-0.85246
LINC02416	4.377211	0.756046	3.253659	0.003499	0.008049	-1.74658
CBARP	4.375153	1.183824	4.849951	6.77E-05	0.000285	1.50208
IL4I1	4.330029	3.770006	4.814903	7.39E-05	0.000307	1.678709
AC025259.3	4.294946	-1.88973	4.586863	0.00013	0.000491	-0.13476
PYCR1	4.268092	2.718976	4.2901	0.000273	0.000917	0.490916
NR4A1	4.205273	5.768466	10.4255	3.46E-10	1.02E-07	13.48841
INHBA	4.14364	0.296989	3.344169	0.002814	0.006675	-1.65791
MYC	4.14039	5.612284	10.79039	1.79E-10	7.48E-08	14.06718
DACT3	4.127314	0.028408	4.21915	0.000326	0.001067	-0.15846
AL357992.1	4.0952	-2.60359	2.534375	0.01853	0.0344	-3.35717
EBI3	4.093484	1.28741	4.23798	0.000311	0.001024	0.227152
TNFRSF4	3.970146	5.090923	6.58136	1.03E-06	1.12E-05	5.66976
CCL24	3.911607	1.608435	4.519872	0.000154	0.000564	1.013169
NPW	3.864501	-1.05311	3.736987	0.001078	0.002944	-1.5107
EPOP	3.844638	2.93039	5.1753	3.02E-05	0.000148	2.506347
TNFRSF18	3.758087	6.328567	7.317038	1.91E-07	3.43E-06	7.220253
HMGN2P15	3.727983	-2.80555	4.197326	0.000344	0.001116	-1.37123
AL160408.1	3.723833	-2.81462	4.611117	0.000123	0.000467	-0.81365
CPNE7	3.703517	0.855981	3.976031	0.000597	0.001777	-0.38638
HSD11B1	3.699544	-0.63586	4.287058	0.000275	0.000922	-0.05417
HOXB9	3.688497	-3.39447	2.955175	0.007098	0.014863	-2.96897
EGR2	3.668945	4.924377	8.00408	4.25E-08	1.31E-06	8.785234
PPIAP45	3.657323	-2.72015	4.150333	0.000387	0.001232	-1.20636
LINC02362	3.647078	0.988937	3.200517	0.003974	0.008991	-1.87385
CXCL5	3.590775	-1.87264	2.426597	0.023486	0.042185	-3.37135
HIVEP3	3.538733	4.552072	6.975625	4.14E-07	5.93E-06	6.588457
KIF7	3.459896	-1.07067	5.155478	3.17E-05	0.000154	0.529994
SAMSN1-AS1	3.438513	0.31669	3.286072	0.003237	0.007522	-1.71856
GNG8	3.435204	0.596748	3.819792	0.000879	0.002466	-0.56053
CSF2	3.421591	-4.37322	4.511131	0.000157	0.000575	-1.44911
PTGIR	3.406964	3.140634	5.859213	5.69E-06	4.00E-05	4.085903
C6orf223	3.376276	-0.64421	2.853245	0.008995	0.018262	-2.7375
ARNTL2	3.32492	-0.07037	7.162338	2.71E-07	4.35E-06	4.754932
SEMA7A	3.311893	5.994751	8.69383	1.00E-08	5.87E-07	10.16862
AC104564.2	3.265108	-2.11998	3.685916	0.001223	0.003278	-1.48662
LINC02365	3.258169	5.885123	8.406765	1.81E-08	7.96E-07	9.615715
CHAC1	3.22992	1.049224	3.731588	0.001093	0.002979	-0.74546
HBEGF	3.1974	-1.94416	4.837502	6.98E-05	0.000293	-0.02887
ITGAD	3.188647	-0.0139	2.491705	0.020363	0.037288	-3.17694
SCD	3.187436	6.685078	10.90375	1.46E-10	7.12E-08	14.33826

STUM	3.182031	5.909977	12.19359	1.60E-11	2.53E-08	16.43358
FOSL1	3.169403	0.876198	3.26337	0.003418	0.007895	-1.7225
MYCNOS	3.156575	-2.65101	3.221082	0.003783	0.008606	-2.41614
SH2D5	3.146196	2.205759	6.349688	1.77E-06	1.69E-05	5.060688
LINC00158	3.145446	-1.8348	4.672611	0.000105	0.000411	-0.25207
IL1B	3.140664	-1.56716	2.979508	0.006705	0.014144	-2.45553
AKAP12	3.132631	1.82572	3.934484	0.000662	0.00194	-0.31056
CORO6	3.124885	6.793679	10.31177	4.27E-10	1.07E-07	13.27193
MIR6775	3.114238	-4.04465	5.470264	1.46E-05	8.34E-05	-0.5432
IGSF3	3.07979	7.080733	10.13729	5.91E-10	1.26E-07	12.94707
NR6A1	3.069785	-0.9134	4.362408	0.000228	0.000783	-0.09629
DUPD1	3.055924	-2.36432	4.936004	5.47E-05	0.000239	0.347046
MIR3142HG	3.052856	3.275495	5.985133	4.20E-06	3.20E-05	4.367995
DUSP2	3.040301	7.204	9.818326	1.08E-09	1.66E-07	12.33722
HRAT92	3.038043	0.171389	6.738872	7.12E-07	8.73E-06	4.246996
MMP7	3.026127	0.382702	4.392828	0.000211	0.000735	0.685577
CSF1	2.98945	4.846821	5.748003	7.44E-06	4.88E-05	3.695996
IER3	2.970871	2.180958	7.09162	3.18E-07	4.90E-06	6.673131
INHBC	2.969193	-1.76858	4.153688	0.000384	0.001224	-0.82799
ESPL1	2.964717	2.541054	6.733348	7.21E-07	8.77E-06	5.969083
B4GALNT1	2.925436	-1.28731	3.403411	0.002438	0.005917	-1.78102
DUSP4	2.923341	7.422575	8.056645	3.80E-08	1.23E-06	8.77268
CNN1	2.911199	-2.86955	3.189893	0.004076	0.00919	-2.55372
ANKRD13B	2.905601	3.590031	8.331105	2.12E-08	8.62E-07	9.343685
CPNE2	2.878789	3.873731	6.661243	8.53E-07	9.86E-06	5.894803
SLC7A5	2.863476	6.091293	7.160057	2.72E-07	4.36E-06	6.887472
EIF5AP2	2.855647	-2.03062	3.578346	0.001592	0.004111	-1.44912
MRC1	2.851036	3.23173	4.553905	0.000141	0.000525	0.953024
HCG20	2.847481	-3.39747	4.113234	0.000425	0.001331	-1.32362
NR4A3	2.845134	6.106359	9.42	2.33E-09	2.39E-07	11.59496
TMEM88	2.8398	0.380802	7.220703	2.38E-07	3.94E-06	5.959119
ICAM5	2.839719	0.321542	5.160857	3.13E-05	0.000153	2.094554
PRRG4	2.832863	-1.47326	4.479767	0.00017	0.000613	-0.01294
TREM1	2.8258	-2.57361	2.706697	0.012586	0.024496	-3.00478
LINC02498	2.795153	-2.18336	4.128355	0.000409	0.001288	-0.80634
USP2-AS1	2.786532	-3.80614	3.528037	0.001801	0.004556	-2.42198
G0S2	2.782897	0.225922	3.349134	0.00278	0.00661	-1.55477
NME1	2.764646	0.178731	4.659186	0.000109	0.000422	0.868286
MIR155HG	2.763289	5.275002	6.923131	4.66E-07	6.44E-06	6.37388

Appendix 8 : Top 100 differentially expressed genes control antibody DMSO versus control antibody VPS34-IN1 at 6 hr

	logFC	AveExpr	t	PValue	FDR	B
F3	3.069677	-2.01399	4.010749	0.000529	0.023381	-1.12151
TNFAIP6	2.2441	-0.39786	4.064735	0.000462	0.021709	-0.23555
LINC02365	2.14091	5.932425	4.40738	0.000195	0.014384	0.611928

TGM2	2.087891	1.250242	5.395684	1.64E-05	0.003411	3.000496
MET	2.07374	2.515028	4.194453	0.000334	0.018283	0.299927
ITGB8	1.949183	1.427967	4.402646	0.000198	0.014432	0.750613
SERPINB2	1.925472	1.368758	4.65067	0.000106	0.010329	1.348828
IL1R1	1.924632	1.334471	4.632431	0.000111	0.010469	1.298056
CCL7	1.897122	-2.13539	4.139004	0.000384	0.019459	-0.5545
CXCL3	1.881893	1.525951	4.096581	0.000427	0.020784	0.069003
TLR5	1.815573	-1.55487	4.149842	0.000373	0.019396	-0.25733
EREG	1.797429	0.86174	3.781547	0.000938	0.031547	-0.61541
CXCL2	1.722202	1.783928	4.63197	0.000111	0.010469	1.307756
PTX3	1.691781	1.222418	4.75234	8.19E-05	0.008429	1.567993
AQP9	1.676049	2.825102	4.410934	0.000193	0.014319	0.775299
NID1	1.667016	0.396763	3.906716	0.000687	0.026443	-0.35739
AC245297.1	1.622195	1.64167	5.387829	1.67E-05	0.003436	3.025466
ARHGEF10	1.618039	-2.36743	3.544349	0.001688	0.04426	-1.62756
CXCL8	1.601033	5.034529	4.088464	0.000435	0.020914	-0.21626
SLAMF7	1.581459	9.608067	4.817275	6.95E-05	0.00803	1.40592
VNN1	1.547407	-0.103	3.889999	0.000716	0.026752	-0.48392
CD300E	1.507016	3.854113	4.868556	6.11E-05	0.00757	1.768664
STUM	1.496663	5.858304	5.146977	3.04E-05	0.005174	2.363669
THBS1	1.467527	5.467923	3.909426	0.000682	0.026443	-0.77737
PID1	1.456639	0.912698	4.314006	0.000247	0.016399	0.578069
WDFY3	1.419895	0.520322	4.256687	0.000285	0.017608	0.436396
PLA2G7	1.386383	2.594188	3.903849	0.000692	0.026452	-0.4463
LY9	1.373834	10.12917	7.786894	5.84E-08	9.08E-05	8.418454
AC099489.1	1.36709	4.722014	6.584249	9.14E-07	0.000591	5.782631
DMXL2	1.364515	2.595404	4.173323	0.000352	0.018687	0.19724
PLAUR	1.325048	2.94759	4.456181	0.000173	0.013352	0.84804
CD244	1.324881	5.060417	6.016193	3.56E-06	0.001692	4.456271
AC138932.5	1.323789	-0.27551	5.751707	6.79E-06	0.002273	3.321109
AC113208.2	1.307688	-1.98743	3.787822	0.000924	0.031335	-0.87235
RSAD2	1.297498	0.636546	4.473383	0.000165	0.012979	0.92569
LINC02427	1.278994	1.028261	4.403473	0.000197	0.014432	0.771696
GK-AS1	1.27088	1.106689	4.256966	0.000285	0.017608	0.441686
MN1	1.254596	0.507649	4.286665	0.000265	0.016884	0.497793
KIF9-AS1	1.249235	0.920745	4.481281	0.000162	0.01288	0.961454
LVRN	1.206272	-1.02007	4.917352	5.41E-05	0.007164	1.595704
EMP1	1.19661	3.053124	4.23272	0.000303	0.017965	0.331424
AC023825.2	1.19342	0.724992	4.528079	0.000144	0.012248	1.050745
AC127496.2	1.187171	-1.60427	4.366361	0.000216	0.015291	0.554758
AC138932.3	1.182858	-0.39426	4.820365	6.90E-05	0.008022	1.494341
LINC01108	1.181759	-0.68492	4.173926	0.000351	0.018687	0.085651
IFI30	1.175205	1.66974	4.029616	0.000505	0.022831	-0.07251
AL356750.1	1.174714	1.717017	3.821957	0.000848	0.029847	-0.52818
AC112496.1	1.173326	1.208821	4.054606	0.000474	0.022053	-0.00781
THBS4	1.171586	0.370917	4.301632	0.000255	0.016631	0.549825
HCAR3	1.162769	-1.67056	3.444902	0.002155	0.049465	-1.56871
CDHR5	1.143646	-0.74054	4.514101	0.000149	0.012439	0.78362
BACE2	1.140307	7.676514	8.888111	5.56E-09	2.38E-05	10.74894

DOCK4	1.139923	2.912206	5.216052	2.56E-05	0.004861	2.650785
MX1	1.137722	6.69767	7.558579	9.70E-08	0.000128	7.93889
MAP1A	1.128669	1.285669	3.698749	0.001153	0.035443	-0.79516
C3AR1	1.1257	1.450319	3.517619	0.001803	0.045596	-1.24407
IFIT3	1.104459	0.815859	3.712715	0.001113	0.034985	-0.77794
AL157935.1	1.096087	0.880152	4.129587	0.000393	0.019735	0.151478
WDR63	1.094148	-0.37211	3.688134	0.001183	0.036079	-0.81612
HNRNPH1P1	1.086258	-1.17044	4.270445	0.000276	0.017195	0.186652
ACP4	1.071587	1.080657	4.283617	0.000267	0.016891	0.482152
KLHDC8B	1.06788	2.791663	4.808656	7.10E-05	0.008097	1.602406
CARD14	1.061141	1.21669	10.26145	3.70E-10	3.16E-06	12.47654
RENBP	1.058558	5.312185	6.659628	7.65E-07	0.000568	5.947158
C5AR1	1.051881	3.92087	4.113273	0.000409	0.020218	-0.07069
FCER1G	1.049925	1.310815	4.101272	0.000422	0.020599	0.093317
RRAGD	1.034658	2.866303	4.216632	0.000316	0.01806	0.343788
AC020904.2	1.030554	-1.37474	3.527497	0.00176	0.045175	-1.22496
ANPEP	1.029704	3.91306	3.450562	0.002126	0.049267	-1.6464
AC073111.1	1.029093	2.193778	4.748159	8.27E-05	0.008429	1.569708
AL136988.2	1.027751	1.121289	5.64233	8.89E-06	0.002642	3.572896
PDXDC1	1.024578	8.017984	8.327443	1.81E-08	4.90E-05	9.584813
JAKMIP3	1.019372	-0.93574	3.621655	0.001395	0.039813	-1.00341
SPRED3	1.018775	1.060676	7.136439	2.53E-07	0.000254	6.702289
CSF3R	1.017165	1.32293	3.43855	0.002189	0.049767	-1.40855
NBEAL2	1.015067	8.044038	6.488206	1.15E-06	0.000676	5.466597
NPIPA7	1.011537	-1.11808	3.895645	0.000706	0.026701	-0.62595
NPIPA1	1.008526	4.408887	7.230865	2.03E-07	0.000217	7.261719
RBM44	1.004872	1.240668	6.575407	9.33E-07	0.000591	5.667675
OASL	1.00397	2.059587	4.782966	7.58E-05	0.0082	1.652566
CTD-2201I18.1	1.003939	0.025371	4.066476	0.00046	0.021674	0.016586
CYP2C8	-1.00575	-0.57045	-3.47203	0.002017	0.048096	-1.33958
COL5A2	-1.01848	-0.39922	-4.2032	0.000326	0.018189	0.230067
COL19A1	-1.02494	1.308227	-4.28337	0.000267	0.016891	0.495998
AP000553.7	-1.02979	-2.18475	-3.79009	0.000919	0.031221	-0.85925
LINC02576	-1.05049	1.347409	-4.35911	0.00022	0.015323	0.639792
PYCARD	-1.0508	-0.58128	-3.89294	0.000711	0.026749	-0.42916
AL596202.1	-1.05338	-0.19982	-5.47066	1.36E-05	0.003076	2.851089
WNT6	-1.05807	-0.0759	-3.64848	0.001306	0.038551	-0.90191
KLHL14	-1.06119	4.218489	-4.38625	0.000206	0.014726	0.493682
C10orf25	-1.06253	-0.6698	-3.45035	0.002127	0.049267	-1.36624
UBQLNL	-1.07656	-2.21	-4.01265	0.000527	0.023381	-0.53412
METTL7A	-1.07856	4.0148	-5.03352	4.04E-05	0.005953	2.081789
FCRLB	-1.07901	1.026607	-4.98133	4.60E-05	0.006399	2.115345
TNFSF10	-1.08199	0.86612	-4.83161	6.71E-05	0.007961	1.765791
KLHL32	-1.08569	0.037185	-4.27211	0.000274	0.017186	0.475039
CHIT1	-1.08721	1.662562	-5.16138	2.93E-05	0.005074	2.537226
SIGLEC10	-1.09382	2.775253	-3.87306	0.000747	0.027461	-0.57018
TCEA3	-1.09471	-1.81874	-3.55869	0.00163	0.043467	-1.30451
GZMA	-1.11872	-1.32304	-3.71731	0.001101	0.034786	-0.83074

GSTM4	-1.12499	0.713681	-4.21876	0.000314	0.01806	0.3613

Appendix 9 : Top 100 differentially expressed genes control antibody DMSO versus control antibody VPS34-IN1 at 24 hr

	logFC	AveExpr	t	PValue	FDR	B
LRP2	2.847086	-4.51642	3.724198	0.001113	0.023665	-2.55196
PTPRD	2.811371	-4.15879	3.466235	0.002093	0.033219	-2.78422
PPARGC1A	2.736857	-3.61837	3.474874	0.00205	0.032872	-2.76399
NRXN3	2.735098	-4.74	3.603512	0.001497	0.02714	-2.7923
ATRNL1	2.730284	-3.15258	4.271309	0.000286	0.011049	-1.80151
NOS1	2.718713	-3.9146	3.611401	0.001468	0.02682	-2.3317
LINC02365	2.708834	5.885123	6.85331	5.47E-07	0.000273	6.319267
MCM10	2.694863	-1.37347	3.349599	0.002777	0.03924	-2.31808
CATSPERD	2.523383	-4.66874	3.277989	0.0033	0.043603	-2.87827
NOVA2	2.420971	-4.95654	3.227553	0.003725	0.046892	-3.07981
GK-IT1	2.354536	-4.07924	4.24847	0.000303	0.011434	-1.96716
PIEZO2	2.312579	-4.20455	3.533805	0.001775	0.030231	-2.813
HBEGF	2.294557	-1.94416	3.554686	0.001687	0.029134	-2.12738
OLIG2	2.267217	-1.79314	3.249026	0.003538	0.04565	-2.03023
SLAMF7	2.213377	8.55871	6.872562	5.24E-07	0.000273	6.308757
CNTNAP3	2.135846	-4.46922	3.757386	0.001026	0.02264	-2.6021
GABRB3	2.108431	-4.34588	3.429057	0.002291	0.034787	-2.92942
GALNT18	2.099571	-4.37004	3.555064	0.001686	0.029134	-2.79033
AP001610.1	2.096717	-0.47508	4.157894	0.00038	0.013139	-0.1547
LINC01567	2.023601	0.600115	4.620258	0.00012	0.00653	1.033979
AR	2.014058	-3.93236	3.65338	0.001325	0.02559	-2.44541
SERPINB2	1.980894	-3.90121	3.701808	0.001176	0.024107	-2.32696
STUM	1.960425	5.909977	7.248447	2.23E-07	0.000194	7.183157
COL4A2	1.956482	4.189677	4.054721	0.000491	0.015073	-0.07358
MX1	1.936339	7.024997	8.646325	1.10E-08	4.71E-05	10.10019
GNAI1	1.935575	-3.81114	3.351793	0.002763	0.039097	-2.66792
PLAC4	1.902864	-0.47206	3.667981	0.001278	0.025089	-1.15981
DNAH8	1.816234	-3.41224	3.209649	0.003888	0.048199	-2.32428
RHBDF1	1.786256	3.358241	3.97463	0.000599	0.016702	-0.24359
C3	1.764648	2.000473	3.739047	0.001073	0.023279	-0.7433
LINC00589	1.763033	0.192202	4.551763	0.000142	0.00726	0.6528
LINC02099	1.72045	4.245802	4.672809	0.000105	0.006132	1.307747
EPHB1	1.688179	-2.40876	3.650881	0.001333	0.025689	-1.73153
TGM2	1.630393	2.575921	3.869162	0.000778	0.01943	-0.45534
BACE2	1.619669	6.929629	9.153617	3.95E-09	2.25E-05	11.10415
THBS1	1.59076	0.946305	4.396687	0.000209	0.008974	0.731356
ARHGEF10	1.560627	-2.11442	3.394277	0.002493	0.036897	-2.19424
ADGRV1	1.546124	-2.07312	3.484301	0.002003	0.032523	-1.73871
BNC2	1.5344	-2.90464	3.584657	0.001568	0.027833	-1.54498
CAB39L	1.480678	3.837645	6.234772	2.32E-06	0.000631	4.934604
RRAGD	1.463626	3.203132	4.022675	0.000532	0.015727	-0.12075

LDLR	1.413094	2.520526	3.672773	0.001263	0.024934	-0.91319
CORO6	1.366713	6.793679	4.135926	0.000401	0.013501	-0.20558
AC138932.3	1.364575	-0.02347	3.286095	0.003237	0.043115	-1.67891
SLC5A11	1.353577	-0.13737	4.829697	7.12E-05	0.004927	1.323192
LY6E-DT	1.338193	-0.82352	3.712098	0.001147	0.023876	-1.07094
AC009690.1	1.3381	2.93246	7.305044	1.97E-07	0.000194	7.220265
DOCK4	1.332475	1.783121	3.788052	0.000951	0.021713	-0.63049
AL139246.2	1.322314	1.920625	4.145755	0.000391	0.01328	0.167937
HELLPAR	1.319593	0.195445	3.73785	0.001076	0.023288	-0.74443
LY9	1.319166	9.423501	5.443986	1.56E-05	0.002022	2.984745
KLHDC8B	1.291677	4.222271	4.82283	7.24E-05	0.004929	1.523479
AC026150.2	1.273617	-0.94562	3.413367	0.00238	0.035693	-1.57922
PI4K2A	1.258169	6.59722	7.90242	5.29E-08	0.000124	8.562291
USP32P3	1.252667	-0.73435	3.56171	0.001658	0.028857	-1.34573
RENBP	1.223641	6.207489	6.07181	3.42E-06	0.000779	4.456113
KLF10	1.215211	6.256627	3.787321	0.000953	0.021713	-1.05178
CCDC81	1.205585	-1.33741	4.62021	0.00012	0.00653	0.096127
NPIPA1	1.188603	4.153233	6.842489	5.61E-07	0.000273	6.292998
ARHGAP27P2	1.172268	3.985628	3.476086	0.002044	0.032837	-1.58384
LINC02427	1.137735	0.972661	4.5703	0.000136	0.007101	1.058644
LINC01762	1.108446	-0.18408	3.301637	0.003118	0.042236	-1.76714
MCOLN3	1.106917	1.672318	4.16731	0.000371	0.013079	0.213743
SETDB2	1.105165	6.277094	6.842428	5.61E-07	0.000273	6.234747
MTSS1L	1.104079	2.193023	3.445362	0.002202	0.033857	-1.47879
AC124283.4	1.103708	-1.24696	3.916063	0.000693	0.018289	-0.85863
FZD5	1.099551	2.950505	8.194838	2.83E-08	8.07E-05	8.931233
RAPSN	1.087634	0.86523	3.571886	0.001618	0.02848	-1.10184
ALS2CR12	1.086641	1.851871	4.130072	0.000407	0.01354	0.114202
CTD-2201I18.1	1.080346	0.754513	3.546854	0.00172	0.029488	-1.16483
PDXDC1	1.063783	7.746221	6.543814	1.12E-06	0.000427	5.556331
Sep-03	1.060311	-0.64849	3.596994	0.001521	0.02726	-1.20742
PDCD1LG2	1.038678	0.18305	4.042561	0.000506	0.015286	-0.1317
SLC26A11	1.034858	6.293577	4.153221	0.000384	0.013139	-0.18978
AC007823.1	1.027142	-1.11867	3.216017	0.003829	0.04778	-2.02228
WDR63	1.024112	-0.05652	3.204481	0.003936	0.048693	-1.8409
AC141586.1	1.009292	4.743553	6.470911	1.33E-06	0.000445	5.42993
NEK6	1.005505	6.358023	6.299857	1.99E-06	0.000576	5.002838
FCRL1	-1.00385	6.144537	-3.91735	0.000691	0.018275	-0.75376
ADTRP	-1.00566	6.320413	-3.3165	0.003008	0.041208	-2.17282
SYNE3	-1.00741	6.777275	-8.35439	2.02E-08	6.91E-05	9.504951
GGNBP1	-1.00858	0.274858	-4.85421	6.70E-05	0.004693	1.4147
AC139149.1	-1.01622	-0.02671	-5.1066	3.58E-05	0.003047	1.563558
DENND6B	-1.0228	3.862882	-4.52077	0.000154	0.007683	0.870762
FAM111B	-1.0239	3.047699	-3.35984	0.002709	0.038715	-1.90002
RASL10A	-1.02392	-0.15269	-3.20981	0.003886	0.048199	-1.83106
AL138781.1	-1.02567	-0.06404	-3.97093	0.000605	0.016779	-0.39122
AP005131.6	-1.026	0.834882	-3.60843	0.001479	0.026947	-1.06
SERPINB9P1	-1.02987	1.651726	-3.25618	0.003478	0.045214	-1.76994

SUSD3	-1.03078	2.964882	-3.94671	0.000642	0.017321	-0.42727
AL139020.1	-1.04033	0.192292	-3.1915	0.00406	0.049616	-1.86753
MAP2K6	-1.04658	3.700316	-4.19741	0.000344	0.01248	0.114504
AL357033.1	-1.04999	0.470792	-3.23076	0.003696	0.046641	-1.80519
AC025034.1	-1.05266	0.00444	-4.13386	0.000403	0.013529	-0.0416
TMPRSS13	-1.05353	3.032388	-7.17736	2.62E-07	0.000203	6.976676
AC021127.1	-1.05397	-0.24498	-3.842	0.000832	0.020005	-0.56678
TCL1A	-1.06052	6.03221	-5.69798	8.40E-06	0.001382	3.58098
VWA7	-1.06167	0.623601	-3.32525	0.002945	0.040543	-1.61418
TRAJ56	-1.06707	-0.50103	-3.45881	0.002131	0.033677	-1.57896
IGHD	-1.06744	6.811231	-3.95944	0.000622	0.017058	-0.6534
AL121835.2	-1.07569	-0.54015	-3.52225	0.001826	0.030825	-1.24957

References

Adler, L.N. *et al.* (2017) 'The Other Function: Class II-Restricted Antigen Presentation by B Cells', *Front Immunol*, 8, p. 319.

Aguilar-Hernandez, M.M. *et al.* (2016) 'IL-4 enhances expression and function of surface IgM in CLL cells', *Blood*, 127(24), pp. 3015-25.

Ahuja, S.K. and Murphy, P.M. (1996) 'The CXC chemokines growth-regulated oncogene (GRO) alpha, GRObeta, GROgamma, neutrophil-activating peptide-2, and epithelial cell-derived neutrophil-activating peptide-78 are potent agonists for the type B, but not the type A, human interleukin-8 receptor', *J Biol Chem*, 271(34), pp. 20545-50.

Aita, V.M. *et al.* (1999) 'Cloning and genomic organization of beclin 1, a candidate tumor suppressor gene on chromosome 17q21', *Genomics*, 59(1), pp. 59-65.

Al-Alwan, L.A. *et al.* (2013) 'Differential roles of CXCL2 and CXCL3 and their receptors in regulating normal and asthmatic airway smooth muscle cell migration', *J Immunol*, 191(5), pp. 2731-41.

Alemu, E.A. *et al.* (2012) 'ATG8 family proteins act as scaffolds for assembly of the ULK complex: sequence requirements for LC3-interacting region (LIR) motifs', *J Biol Chem*, 287(47), pp. 39275-90.

Alers, S. *et al.* (2011) 'Atg13 and FIP200 act independently of Ulk1 and Ulk2 in autophagy induction', *Autophagy*, 7(12), pp. 1423-33.

Alers, S. *et al.* (2012) 'Role of AMPK-mTOR-Ulk1/2 in the regulation of autophagy: cross talk, shortcuts, and feedbacks', *Mol Cell Biol*, 32(1), pp. 2-11.

Allman, D. and Pillai, S. (2008) 'Peripheral B cell subsets', *Curr Opin Immunol*, 20(2), pp. 149-57.

Anderson, M.A. *et al.* (2016) 'The BCL2 selective inhibitor venetoclax induces rapid onset apoptosis of CLL cells in patients via a TP53-independent mechanism', *Blood*, 127(25), pp. 3215-24.

Arbogast, F. *et al.* (2018) 'ATG5 is required for B cell polarization and presentation of particulate antigens', *Autophagy*, pp. 1-15.

Arnold, J. *et al.* (2016) 'Autophagy is dispensable for B-cell development but essential for humoral autoimmune responses', *Cell Death Differ*, 23(5), pp. 853-64.

Arroyo, D.S. *et al.* (2020) 'Increased Expression of Autophagy Protein LC3 in Two Patients With Progressing Chronic Lymphocytic Leukemia', *Front Endocrinol (Lausanne)*, 11, p. 321.

Arruga, F. *et al.* (2020) 'Immune Response Dysfunction in Chronic Lymphocytic Leukemia: Dissecting Molecular Mechanisms and Microenvironmental Conditions', *Int J Mol Sci*, 21(5).

Asma, G.E., Langlois van den Bergh, R. and Vossen, J.M. (1984) 'Development of pre-B and B lymphocytes in the human fetus', *Clin Exp Immunol*, 56(2), pp. 407-14.

Avsec, D. *et al.* (2021) 'Targeting Autophagy Triggers Apoptosis and Complements the Action of Venetoclax in Chronic Lymphocytic Leukemia Cells', *Cancers*, 13(18).

Badoux, X.C. *et al.* (2011) 'Fludarabine, cyclophosphamide, and rituximab chemoimmunotherapy is highly effective treatment for relapsed patients with CLL', *Blood*, 117(11), pp. 3016-24.

Balkwill, F. (2004) 'Cancer and the chemokine network', *Nat Rev Cancer*, 4(7), pp. 540-50.

Baquero, P. *et al.* (2019) 'Targeting quiescent leukemic stem cells using second generation autophagy inhibitors', *Leukemia*, 33(4), pp. 981-994.

Basquin, C. *et al.* (2013) 'The signalling factor PI3K is a specific regulator of the clathrin-independent dynamin-dependent endocytosis of IL-2 receptors', *J Cell Sci*, 126(Pt 5), pp. 1099-108.

Batista, F.D. and Harwood, N.E. (2009) 'The who, how and where of antigen presentation to B cells', *Nat Rev Immunol*, 9(1), pp. 15-27.

Batista, F.D., Iber, D. and Neuberger, M.S. (2001) 'B cells acquire antigen from target cells after synapse formation', *Nature*, 411(6836), pp. 489-94.

Batista, F.D. and Neuberger, M.S. (2000) 'B cells extract and present immobilized antigen: implications for affinity discrimination', *EMBO J*, 19(4), pp. 513-20.

Berridge, M.J. (1993) 'Inositol trisphosphate and calcium signalling', *Nature*, 361(6410), pp. 315-25.

Billadeau, D.D. and Leibson, P.J. (2002) 'ITAMs versus ITIMs: striking a balance during cell regulation', *J Clin Invest*, 109(2), pp. 161-8.

Blombery, P. *et al.* (2019) 'Acquisition of the Recurrent Gly101Val Mutation in BCL2 Confers Resistance to Venetoclax in Patients with Progressive Chronic Lymphocytic Leukemia', *Cancer Discov*, 9(3), pp. 342-353.

Bolland, S. *et al.* (1998) 'SHIP modulates immune receptor responses by regulating membrane association of Btk', *Immunity*, 8(4), pp. 509-16.

Bologna, C. *et al.* (2016) 'SLAMF1 regulation of chemotaxis and autophagy determines CLL patient response', *J Clin Invest*, 126(1), pp. 181-94.

Bologna, C. and Deaglio, S. (2018) 'Linking SLAMF1 to autophagy and sensitivity to therapy in chronic lymphocytic leukemia', *Mol Cell Oncol*, 5(3), p. e1143077.

Boniface, J.J. *et al.* (1998) 'Initiation of signal transduction through the T cell receptor requires the multivalent engagement of peptide/MHC ligands [corrected]', *Immunity*, 9(4), pp. 459-66.

Botbol, Y., Guerrero-Ros, I. and Macian, F. (2016) 'Key roles of autophagy in regulating T-cell function', *Eur J Immunol*, 46(6), pp. 1326-34.

Brenner, H., Gondos, A. and Pulte, D. (2008) 'Trends in long-term survival of patients with chronic lymphocytic leukemia from the 1980s to the early 21st century', *Blood*, 111(10), pp. 4916-21.

Brier, L.W. *et al.* (2019) 'Regulation of LC3 lipidation by the autophagy-specific class III phosphatidylinositol-3 kinase complex', *Mol Biol Cell*, 30(9), pp. 1098-1107.

Brown, B.K. and Song, W. (2001) 'The actin cytoskeleton is required for the trafficking of the B cell antigen receptor to the late endosomes', *Traffic*, 2(6), pp. 414-27.

Brown, G.D. and Crocker, P.R. (2016) 'Lectin Receptors Expressed on Myeloid Cells', *Microbiol Spectr*, 4(5).

Burger, J.A. and Chiorazzi, N. (2013) 'B cell receptor signaling in chronic lymphocytic leukemia', *Trends Immunol*, 34(12), pp. 592-601.

Burger, J.A. *et al.* (2009) 'The microenvironment in mature B-cell malignancies: a target for new treatment strategies', *Blood*, 114(16), pp. 3367-75.

Burman, C. and Ktistakis, N.T. (2010) 'Regulation of autophagy by phosphatidylinositol 3-phosphate', *FEBS Lett*, 584(7), pp. 1302-12.

Burshtyn, D.N. *et al.* (1997) 'A novel phosphotyrosine motif with a critical amino acid at position -2 for the SH2 domain-mediated activation of the tyrosine phosphatase SHP-1', *J Biol Chem*, 272(20), pp. 13066-72.

Caballero, A. *et al.* (2006) 'Functional and structural requirements for the internalization of distinct BCR-ligand complexes', *Eur J Immunol*, 36(12), pp. 3131-45.

Caligaris-Cappio, F. (2003) 'Role of the microenvironment in chronic lymphocytic leukaemia', *Br J Haematol*, 123(3), pp. 380-8.

Caligaris-Cappio, F. (2014) 'Anergy: the CLL cell limbo', *Blood*, 123(21), pp. 3214-5.

Calsou, P. *et al.* (2003) 'Coordinated assembly of Ku and p460 subunits of the DNA-dependent protein kinase on DNA ends is necessary for XRCC4-ligase IV recruitment', *J Mol Biol*, 326(1), pp. 93-103.

Cambier, J.C. *et al.* (2007) 'B-cell anergy: from transgenic models to naturally occurring anergic B cells?', *Nat Rev Immunol*, 7(8), pp. 633-43.

Capolla, S. *et al.* (2016) 'A new approach for the treatment of CLL using chlorambucil/hydroxychloroquine-loaded anti-CD20 nanoparticles', *Nano Research*, 9(2), pp. 537-548.

Carrasco, Y.R. and Batista, F.D. (2006) 'B cell recognition of membrane-bound antigen: an exquisite way of sensing ligands', *Curr Opin Immunol*, 18(3), pp. 286-91.

Cerutti, A. *et al.* (2002) 'Ongoing in vivo immunoglobulin class switch DNA recombination in chronic lymphocytic leukemia B cells', *J Immunol*, 169(11), pp. 6594-603.

Chang, Z. *et al.* (2013) 'Dual PI3K/mTOR inhibitor NVP-BEZ235-induced apoptosis of hepatocellular carcinoma cell lines is enhanced by inhibitors of autophagy', *Int J Mol Med*, 31(6), pp. 1449-56.

Chen, S.S. *et al.* (2016) 'BTK inhibition results in impaired CXCR4 chemokine receptor surface expression, signaling and function in chronic lymphocytic leukemia', *Leukemia*, 30(4), pp. 833-43.

Cho, Y.B. *et al.* (2012) 'CC chemokine ligand 7 expression in liver metastasis of colorectal cancer', *Oncol Rep*, 28(2), pp. 689-94.

Choi, Y.S. *et al.* (2011) 'ICOS receptor instructs T follicular helper cell versus effector cell differentiation via induction of the transcriptional repressor Bcl6', *Immunity*, 34(6), pp. 932-46.

Chu, H.H. *et al.* (2010) 'Negative selection and peptide chemistry determine the size of naive foreign peptide-MHC class II-specific CD4+ T cell populations', *J Immunol*, 185(8), pp. 4705-13.

Clarke, A.J. *et al.* (2018) 'B1a B cells require autophagy for metabolic homeostasis and self-renewal', *J Exp Med*, 215(2), pp. 399-413.

Codogno, P., Mehrpour, M. and Proikas-Cezanne, T. (2011) 'Canonical and non-canonical autophagy: variations on a common theme of self-eating?', *Nat Rev Mol Cell Biol*, 13(1), pp. 7-12.

Coelho, V. *et al.* (2013) 'Identification in CLL of circulating intraclonal subgroups with varying B-cell receptor expression and function', *Blood*, 122(15), pp. 2664-72.

Crighton, D. *et al.* (2006) 'DRAM, a p53-induced modulator of autophagy, is critical for apoptosis', *Cell*, 126(1), pp. 121-34.

Crotty, S. (2011) 'Follicular helper CD4 T cells (TFH)', *Annu Rev Immunol*, 29, pp. 621-63.

Crotty, S. (2014) 'T follicular helper cell differentiation, function, and roles in disease', *Immunity*, 41(4), pp. 529-42.

Crotzer, V.L. and Blum, J.S. (2009) 'Autophagy and its role in MHC-mediated antigen presentation', *J Immunol*, 182(6), pp. 3335-41.

Crowley, M.T. *et al.* (1997) 'A critical role for Syk in signal transduction and phagocytosis mediated by Fcgamma receptors on macrophages', *J Exp Med*, 186(7), pp. 1027-39.

Currie, K.S. *et al.* (2014) 'Discovery of GS-9973, a selective and orally efficacious inhibitor of spleen tyrosine kinase', *J Med Chem*, 57(9), pp. 3856-73.

D'Avola, A. *et al.* (2016) 'Surface IgM expression and function are associated with clinical behavior, genetic abnormalities, and DNA methylation in CLL', *Blood*, 128(6), pp. 816-26.

Dal Bo, M. *et al.* (2015) 'The SIRT1/TP53 axis is activated upon B-cell receptor triggering via miR-132 up-regulation in chronic lymphocytic leukemia cells', *Oncotarget*, 6(22), pp. 19102-17.

Dal Porto, J.M. *et al.* (2004) 'B cell antigen receptor signaling 101', *Mol Immunol*, 41(6-7), pp. 599-613.

Damle, R.N. *et al.* (1999) 'Ig V gene mutation status and CD38 expression as novel prognostic indicators in chronic lymphocytic leukemia', *Blood*, 94(6), pp. 1840-7.

Danielsson, R. and Eriksson, H. (2021) 'Aluminium adjuvants in vaccines - A way to modulate the immune response', *Semin Cell Dev Biol*, 115, pp. 3-9.

Datan, E. *et al.* (2014) 'mTOR/p70S6K signaling distinguishes routine, maintenance-level autophagy from autophagic cell death during influenza A infection', *Virology*, 452-453, pp. 175-190.

de Rooij, M.F. *et al.* (2015) 'Ibrutinib and idelalisib synergistically target BCR-controlled adhesion in MCL and CLL: a rationale for combination therapy', *Blood*, 125(14), pp. 2306-9.

De Silva, N.S. and Klein, U. (2015) 'Dynamics of B cells in germinal centres', *Nat Rev Immunol*, 15(3), pp. 137-48.

Dennis, P.B. *et al.* (2001) 'Mammalian TOR: a homeostatic ATP sensor', *Science*, 294(5544), pp. 1102-5.

Denzin, L.K. and Cresswell, P. (1995) 'HLA-DM induces CLIP dissociation from MHC class II alpha beta dimers and facilitates peptide loading', *Cell*, 82(1), pp. 155-65.

Dighiero, G. *et al.* (1980) 'Individual cell-by-cell quantitation of lymphocyte surface membrane Ig in normal and CLL lymphocyte and during ontogeny of mouse B lymphocytes by immunoperoxidase assay', *Blood*, 55(1), pp. 93-100.

Ding, L. *et al.* (2018) 'Targeting the autophagy in bone marrow stromal cells overcomes resistance to vorinostat in chronic lymphocytic leukemia', *Onco Targets Ther*, 11, pp. 5151-5170.

DiPaola, R.S. *et al.* (2008) 'Therapeutic starvation and autophagy in prostate cancer: a new paradigm for targeting metabolism in cancer therapy', *Prostate*, 68(16), pp. 1743-52.

Dooley, H.C. *et al.* (2014) 'WIPI2 links LC3 conjugation with PI3P, autophagosome formation, and pathogen clearance by recruiting Atg12-5-16L1', *Mol Cell*, 55(2), pp. 238-52.

Duckworth, A. *et al.* (2014) 'Variable induction of PRDM1 and differentiation in chronic lymphocytic leukemia is associated with anergy', *Blood*, 123(21), pp. 3277-85.

Dupont, N. *et al.* (2017) 'Molecular Mechanisms of Noncanonical Autophagy', *Int Rev Cell Mol Biol*, 328, pp. 1-23.

Egan, D.F. *et al.* (2015) 'Small Molecule Inhibition of the Autophagy Kinase ULK1 and Identification of ULK1 Substrates', *Mol Cell*, 59(2), pp. 285-97.

Fang, W. *et al.* (1998) 'Self-reactive B lymphocytes overexpressing Bcl-xL escape negative selection and are tolerized by clonal anergy and receptor editing', *Immunity*, 9(1), pp. 35-45.

Fernald, K. and Kurokawa, M. (2013) 'Evading apoptosis in cancer', *Trends Cell Biol*, 23(12), pp. 620-33.

Ferrer, G. *et al.* (2014) 'B cell activation through CD40 and IL4R ligation modulates the response of chronic lymphocytic leukaemia cells to BAFF and APRIL', *Br J Haematol*, 164(4), pp. 570-8.

Florey, O. *et al.* (2015) 'V-ATPase and osmotic imbalances activate endolysosomal LC3 lipidation', *Autophagy*, 11(1), pp. 88-99.

Florey, O. *et al.* (2011) 'Autophagy machinery mediates macroendocytic processing and entotic cell death by targeting single membranes', *Nat Cell Biol*, 13(11), pp. 1335-43.

Florey, O. and Overholtzer, M. (2012) 'Autophagy proteins in macroendocytic engulfment', *Trends Cell Biol*, 22(7), pp. 374-80.

Fracchiolla, D. *et al.* (2020) 'A PI3K-WIPI2 positive feedback loop allosterically activates LC3 lipidation in autophagy', *Journal of Cell Biology*, 219(7).

Frick, R. *et al.* (2021) 'A high-affinity human TCR-like antibody detects celiac disease gluten peptide-MHC complexes and inhibits T cell activation', *Science Immunology*, 6(62).

Fujiwara, N. *et al.* (2016) 'Regulation of Beclin 1 Protein Phosphorylation and Autophagy by Protein Phosphatase 2A (PP2A) and Death-associated Protein Kinase 3 (DAPK3)', *J Biol Chem*, 291(20), pp. 10858-66.

Futterer, K. *et al.* (1998) 'Structural basis for Syk tyrosine kinase ubiquity in signal transduction pathways revealed by the crystal structure of its regulatory SH2 domains bound to a dually phosphorylated ITAM peptide', *J Mol Biol*, 281(3), pp. 523-37.

Gacon, G. *et al.* (1983) 'Tyrosine phosphorylation in human T lymphoma cells', *Biochem Biophys Res Commun*, 117(3), pp. 843-50.

Gade, P. *et al.* (2016) 'Death-associated Protein Kinase-1 Expression and Autophagy in Chronic Lymphocytic Leukemia Are Dependent on Activating Transcription Factor-6 and CCAAT/Enhancer-binding Protein-beta', *J Biol Chem*, 291(42), pp. 22030-22042.

Gao, J. *et al.* (2012) 'Novel functions of murine B1 cells: active phagocytic and microbicidal abilities', *Eur J Immunol*, 42(4), pp. 982-92.

Gao, W. *et al.* (2013) 'E1-like activating enzyme Atg7 is preferentially sequestered into p62 aggregates via its interaction with LC3-I', *PLoS One*, 8(9), p. e73229.

Garcia-Garcia, E., Rosales, R. and Rosales, C. (2002) 'Phosphatidylinositol 3-kinase and extracellular signal-regulated kinase are recruited for Fc receptor-mediated phagocytosis during monocyte-to-macrophage differentiation', *J Leukoc Biol*, 72(1), pp. 107-14.

Gauld, S.B. *et al.* (2005) 'Maintenance of B cell anergy requires constant antigen receptor occupancy and signaling', *Nat Immunol*, 6(11), pp. 1160-7.

Gay, D. *et al.* (1993) 'Receptor editing: an approach by autoreactive B cells to escape tolerance', *J Exp Med*, 177(4), pp. 999-1008.

Geisberger, R., Lamers, M. and Achatz, G. (2006) 'The riddle of the dual expression of IgM and IgD', *Immunology*, 118(4), pp. 429-37.

Geisler, C.H. *et al.* (1991) 'Prognostic importance of flow cytometric immunophenotyping of 540 consecutive patients with B-cell chronic lymphocytic leukemia', *Blood*, 78(7), pp. 1795-802.

Ghia, P. *et al.* (2002) 'Chronic lymphocytic leukemia B cells are endowed with the capacity to attract CD4+, CD40L+ T cells by producing CCL22', *Eur J Immunol*, 32(5), pp. 1403-13.

Ghimire, T.R. (2015) 'The mechanisms of action of vaccines containing aluminum adjuvants: an in vitro vs in vivo paradigm', *Springerplus*, 4, p. 181.

Gluschko, A. *et al.* (2018) 'The beta2 Integrin Mac-1 Induces Protective LC3-Associated Phagocytosis of Listeria monocytogenes', *Cell Host Microbe*, 23(3), pp. 324-337 e5.

Gonzalez-Rodriguez, A.P. *et al.* (2010) 'Prognostic significance of CD8 and CD4 T cells in chronic lymphocytic leukemia', *Leuk Lymphoma*, 51(10), pp. 1829-36.

Goodnow, C.C. *et al.* (1988) 'Altered immunoglobulin expression and functional silencing of self-reactive B lymphocytes in transgenic mice', *Nature*, 334(6184), pp. 676-82.

Grawunder, U. *et al.* (1995) 'Down-regulation of RAG1 and RAG2 gene expression in preB cells after functional immunoglobulin heavy chain rearrangement', *Immunity*, 3(5), pp. 601-8.

Grawunder, U. *et al.* (1998) 'DNA ligase IV is essential for V(D)J recombination and DNA double-strand break repair in human precursor lymphocytes', *Mol Cell*, 2(4), pp. 477-84.

Grawunder, U., Zimmer, D. and Lieber, M.R. (1998) 'DNA ligase IV binds to XRCC4 via a motif located between rather than within its BRCT domains', *Curr Biol*, 8(15), pp. 873-6.

Grucza, R.A. *et al.* (1999) 'Thermodynamic study of the binding of the tandem-SH2 domain of the Syk kinase to a dually phosphorylated ITAM peptide: evidence for two conformers', *Biochemistry*, 38(16), pp. 5024-33.

Grunwald, D.S. *et al.* (2020) 'GABARAPs and LC3s have opposite roles in regulating ULK1 for autophagy induction', *Autophagy*, 16(4), pp. 600-614.

Gwinn, D.M. *et al.* (2008) 'AMPK phosphorylation of raptor mediates a metabolic checkpoint', *Mol Cell*, 30(2), pp. 214-26.

Hagn, M. *et al.* (2014) 'B-CLL cells acquire APC- and CTL-like phenotypic characteristics after stimulation with CpG ODN and IL-21', *Int Immunol*, 26(7), pp. 383-95.

Hall, A.M. *et al.* (2005) 'Rh autoantigen presentation to helper T cells in chronic lymphocytic leukemia by malignant B cells', *Blood*, 105(5), pp. 2007-15.

Hallek, M. *et al.* (2018) 'iwCLL guidelines for diagnosis, indications for treatment, response assessment, and supportive management of CLL', *Blood*, 131(25), pp. 2745-2760.

Hallek, M. *et al.* (2008) 'Guidelines for the diagnosis and treatment of chronic lymphocytic leukemia: a report from the International Workshop on Chronic Lymphocytic Leukemia updating the National Cancer Institute-Working Group 1996 guidelines', *Blood*, 111(12), pp. 5446-56.

Hamblin, T.J. *et al.* (1999) 'Unmutated Ig V(H) genes are associated with a more aggressive form of chronic lymphocytic leukemia', *Blood*, 94(6), pp. 1848-54.

Hamel, K.M., Liarski, V.M. and Clark, M.R. (2012) 'Germinal center B-cells', *Autoimmunity*, 45(5), pp. 333-47.

Hartley, S.B. *et al.* (1991) 'Elimination from peripheral lymphoid tissues of self-reactive B lymphocytes recognizing membrane-bound antigens', *Nature*, 353(6346), pp. 765-9.

Healy, J.I. *et al.* (1997) 'Different nuclear signals are activated by the B cell receptor during positive versus negative signaling', *Immunity*, 6(4), pp. 419-28.

Heckmann, B.L. *et al.* (2017) 'LC3-Associated Phagocytosis and Inflammation', *J Mol Biol*, 429(23), pp. 3561-3576.

Heesters, B.A. *et al.* (2016) 'Antigen Presentation to B Cells', *Trends Immunol*, 37(12), pp. 844-854.

Helgason, G.V. *et al.* (2013) 'Autophagy in chronic myeloid leukaemia: stem cell survival and implication in therapy', *Curr Cancer Drug Targets*, 13(7), pp. 724-34.

Henry, J.Y. *et al.* (2013) 'Enhanced cross-priming of naive CD8+ T cells by dendritic cells treated by the IMiDs(R) immunomodulatory compounds lenalidomide and pomalidomide', *Immunology*, 139(3), pp. 377-85.

Herve, M. *et al.* (2005) 'Unmutated and mutated chronic lymphocytic leukemias derive from self-reactive B cell precursors despite expressing different antibody reactivity', *J Clin Invest*, 115(6), pp. 1636-43.

Hombach, J. *et al.* (1990) 'Molecular components of the B-cell antigen receptor complex of the IgM class', *Nature*, 343(6260), pp. 760-2.

Hoogeboom, R. *et al.* (2018) 'Myosin IIa Promotes Antibody Responses by Regulating B Cell Activation, Acquisition of Antigen, and Proliferation', *Cell Rep*, 23(8), pp. 2342-2353.

Hoogeboom, R. and Tolar, P. (2016) 'Molecular Mechanisms of B Cell Antigen Gathering and Endocytosis', *Curr Top Microbiol Immunol*, 393, pp. 45-63.

Hornberger, T.A. *et al.* (2007) 'mTOR is the rapamycin-sensitive kinase that confers mechanically-induced phosphorylation of the hydrophobic motif site Thr(389) in p70(S6k)', *FEBS Lett*, 581(24), pp. 4562-6.

Hosokawa, N. *et al.* (2009) 'Atg101, a novel mammalian autophagy protein interacting with Atg13', *Autophagy*, 5(7), pp. 973-9.

Howlader N, N.A., Krapcho M, Miller D, Bishop K, Kosary CL, Yu M, Ruhl J, Tatalovich Z, Mariotto A, Lewis DR, Chen HS, Feuer EJ, Cronin KA (2015) 'SEER Cancer Statistics Review, 1975-2014'. Available at: https://seer.cancer.gov/csr/1975_2014/.

Huang, T. *et al.* (2017) 'MST4 Phosphorylation of ATG4B Regulates Autophagic Activity, Tumorigenicity, and Radioresistance in Glioblastoma', *Cancer Cell*, 32(6), pp. 840-855 e8.

Huang, W.C. and Chen, C.C. (2005) 'Akt phosphorylation of p300 at Ser-1834 is essential for its histone acetyltransferase and transcriptional activity', *Mol Cell Biol*, 25(15), pp. 6592-602.

Huang, Z.Y. *et al.* (2006) 'Differential kinase requirements in human and mouse Fc-gamma receptor phagocytosis and endocytosis', *J Leukoc Biol*, 80(6), pp. 1553-62.

Huang, Z.Y. *et al.* (2003) 'The effect of phosphatases SHP-1 and SHIP-1 on signaling by the ITIM- and ITAM-containing Fcgamma receptors FcgammaRIIB and FcgammaRIIA', *J Leukoc Biol*, 73(6), pp. 823-9.

Hubbard, V.M. *et al.* (2010) 'Macroautophagy regulates energy metabolism during effector T cell activation', *J Immunol*, 185(12), pp. 7349-57.

Hus, I. and Rolinski, J. (2015) 'Current concepts in diagnosis and treatment of chronic lymphocytic leukemia', *Contemp Oncol (Pozn)*, 19(5), pp. 361-7.

Ibanez-Vega, J. *et al.* (2019) 'Proteasome Dependent Actin Remodeling Facilitates Antigen Extraction at the Immune Synapse of B Cells', *Front Immunol*, 10, p. 225.

Ibanez-Vega, J. *et al.* (2021) 'Ecm29-Dependent Proteasome Localization Regulates Cytoskeleton Remodeling at the Immune Synapse', *Front Cell Dev Biol*, 9, p. 650817.

Ichimura, Y. *et al.* (2013) 'Phosphorylation of p62 activates the Keap1-Nrf2 pathway during selective autophagy', *Mol Cell*, 51(5), pp. 618-31.

Inaba, A. *et al.* (2020) 'B Lymphocyte-Derived CCL7 Augments Neutrophil and Monocyte Recruitment, Exacerbating Acute Kidney Injury', *J Immunol*, 205(5), pp. 1376-1384.

Ishibashi, K. *et al.* (2011) 'Atg16L2, a novel isoform of mammalian Atg16L that is not essential for canonical autophagy despite forming an Atg12-5-16L2 complex', *Autophagy*, 7(12), pp. 1500-13.

Jaber, N. *et al.* (2012) 'Class III PI3K Vps34 plays an essential role in autophagy and in heart and liver function', *Proc Natl Acad Sci U S A*, 109(6), pp. 2003-8.

Jacquin, E. *et al.* (2017) 'Pharmacological modulators of autophagy activate a parallel noncanonical pathway driving unconventional LC3 lipidation', *Autophagy*, 13(5), pp. 854-867.

Jain, P. *et al.* (2015) 'Outcomes of patients with chronic lymphocytic leukemia after discontinuing ibrutinib', *Blood*, 125(13), pp. 2062-7.

Janeway CA, T.P., Walport M, Shlomchik MJ (2001) 'Immunobiology: The Immune System in Health and Disease

', in *Immunobiology: The Immune System in Health and Disease* 5th edition edn. Available at: https://www.ncbi.nlm.nih.gov/books/NBK27142/ (Accessed: 25/04/2019).

Janji, B. *et al.* (2020) 'Lighting up the fire in cold tumors to improve cancer immunotherapy by blocking the activity of the autophagy-related protein PIK3C3/VPS34', *Autophagy*, 16(11), pp. 2110-2111.

Jaumouille, V. *et al.* (2014) 'Actin cytoskeleton reorganization by Syk regulates Fcgamma receptor responsiveness by increasing its lateral mobility and clustering', *Dev Cell*, 29(5), pp. 534-546.

Joachim, J. *et al.* (2015) 'Activation of ULK Kinase and Autophagy by GABARAP Trafficking from the Centrosome Is Regulated by WAC and GM130', *Mol Cell*, 60(6), pp. 899-913.

Johnston, R.J. *et al.* (2009) 'Bcl6 and Blimp-1 are reciprocal and antagonistic regulators of T follicular helper cell differentiation', *Science*, 325(5943), pp. 1006-10.

Jung, C.H. *et al.* (2009) 'ULK-Atg13-FIP200 complexes mediate mTOR signaling to the autophagy machinery', *Mol Biol Cell*, 20(7), pp. 1992-2003.

Kabeya, Y. *et al.* (2000) 'LC3, a mammalian homologue of yeast Apg8p, is localized in autophagosome membranes after processing', *EMBO J*, 19(21), pp. 5720-8.

Kabeya, Y. *et al.* (2004) 'LC3, GABARAP and GATE16 localize to autophagosomal membrane depending on form-II formation', *J Cell Sci*, 117(Pt 13), pp. 2805-12.

Kaminskyy, V., Abdi, A. and Zhivotovsky, B. (2011) 'A quantitative assay for the monitoring of autophagosome accumulation in different phases of the cell cycle', *Autophagy*, 7(1), pp. 83-90.

Kim, J. *et al.* (2011) 'AMPK and mTOR regulate autophagy through direct phosphorylation of Ulk1', *Nat Cell Biol*, 13(2), pp. 132-41.

Kim, J.Y. *et al.* (2013) 'Noncanonical autophagy promotes the visual cycle', *Cell*, 154(2), pp. 365-76.

Kipps, T.J. *et al.* (2017a) 'Chronic lymphocytic leukaemia', *Nat Rev Dis Primers*, 3, p. 16096.

Kipps, T.J. *et al.* (2017b) 'Chronic lymphocytic leukaemia', *Nat Rev Dis Primers*, 3, p. 17008.

Kiss, A.L. and Botos, E. (2009) 'Endocytosis via caveolae: alternative pathway with distinct cellular compartments to avoid lysosomal degradation?', *J Cell Mol Med*, 13(7), pp. 1228-37.

Klionsky, D.J. *et al.* (2021) 'Guidelines for the use and interpretation of assays for monitoring autophagy (4th edition)1', *Autophagy*, 17(1), pp. 1-382.

Klionsky, D.J. *et al.* (2008) 'Guidelines for the use and interpretation of assays for monitoring autophagy in higher eukaryotes', *Autophagy*, 4(2), pp. 151-75.

Klionsky, D.J., Meijer, A.J. and Codogno, P. (2005) 'Autophagy and p70S6 kinase', *Autophagy*, 1(1), pp. 59-60; discussion 60-1.

Komatsu, M. and Ichimura, Y. (2010) 'Physiological significance of selective degradation of p62 by autophagy', *FEBS Lett*, 584(7), pp. 1374-8.

Kong, Y.L. *et al.* (2018) 'Expression of autophagy related genes in chronic lymphocytic leukemia is associated with disease course', *Leuk Res*, 66, pp. 8-14.

Koster, S. *et al.* (2017) 'Mycobacterium tuberculosis is protected from NADPH oxidase and LC3-associated phagocytosis by the LCP protein CpsA', *Proc Natl Acad Sci U S A*, 114(41), pp. E8711-E8720.

Kraus, M. *et al.* (2004) 'Survival of resting mature B lymphocytes depends on BCR signaling via the Igalpha/beta heterodimer', *Cell*, 117(6), pp. 787-800.

Krisenko, M.O. *et al.* (2015) 'Syk Is Recruited to Stress Granules and Promotes Their Clearance through Autophagy', *J Biol Chem*, 290(46), pp. 27803-15.

Kristensen, L. *et al.* (2015) 'High expression of PI3K core complex genes is associated with poor prognosis in chronic lymphocytic leukemia', *Leuk Res*, 39(6), pp. 555-60.

Krysov, S. *et al.* (2012) 'Surface IgM stimulation induces MEK1/2-dependent MYC expression in chronic lymphocytic leukemia cells', *Blood*, 119(1), pp. 170-9.

Krysov, S. *et al.* (2014) 'Stimulation of surface IgM of chronic lymphocytic leukemia cells induces an unfolded protein response dependent on BTK and SYK', *Blood*, 124(20), pp. 3101-9.

Kumari, S., Mg, S. and Mayor, S. (2010) 'Endocytosis unplugged: multiple ways to enter the cell', *Cell Res*, 20(3), pp. 256-75.

Lamprinaki, D. *et al.* (2017) 'LC3-Associated Phagocytosis Is Required for Dendritic Cell Inflammatory Cytokine Response to Gut Commensal Yeast Saccharomyces cerevisiae', *Front Immunol*, 8, p. 1397.

Lanemo Myhrinder, A. *et al.* (2008) 'A new perspective: molecular motifs on oxidized LDL, apoptotic cells, and bacteria are targets for chronic lymphocytic leukemia antibodies', *Blood*, 111(7), pp. 3838-48.

Lanham, S. *et al.* (2003) 'Differential signaling via surface IgM is associated with VH gene mutational status and CD38 expression in chronic lymphocytic leukemia', *Blood*, 101(3), pp. 1087-93.

Le Roux, D. *et al.* (2007) 'Syk-dependent actin dynamics regulate endocytic trafficking and processing of antigens internalized through the B-cell receptor', *Mol Biol Cell*, 18(9), pp. 3451-62.

Lebecque, S.G. and Gearhart, P.J. (1990) 'Boundaries of somatic mutation in rearranged immunoglobulin genes: 5' boundary is near the promoter, and 3' boundary is approximately 1 kb from V(D)J gene', *J Exp Med*, 172(6), pp. 1717-27.

Lee, E.J. and Tournier, C. (2011) 'The requirement of uncoordinated 51-like kinase 1 (ULK1) and ULK2 in the regulation of autophagy', *Autophagy*, 7(7), pp. 689-95.

Lee, I.H. and Finkel, T. (2009) 'Regulation of autophagy by the p300 acetyltransferase', *J Biol Chem*, 284(10), pp. 6322-8.

Lee, I.H. *et al.* (2012) 'Atg7 modulates p53 activity to regulate cell cycle and survival during metabolic stress', *Science*, 336(6078), pp. 225-8.

Lee, S.K. *et al.* (2011) 'B cell priming for extrafollicular antibody responses requires Bcl-6 expression by T cells', *J Exp Med*, 208(7), pp. 1377-88.

Leuenberger, M. *et al.* (2010) 'AID protein expression in chronic lymphocytic leukemia/small lymphocytic lymphoma is associated with poor prognosis and complex genetic alterations', *Mod Pathol*, 23(2), pp. 177-86.

Li, Y. *et al.* (2008) 'Efficient cross-presentation depends on autophagy in tumor cells', *Cancer Res*, 68(17), pp. 6889-95.

Ligeon, L.A. *et al.* (2021) 'Oxidation inhibits autophagy protein deconjugation from phagosomes to sustain MHC class II restricted antigen presentation', *Nat Commun*, 12(1), p. 1508.

Liu, E.Y. *et al.* (2015) 'Loss of autophagy causes a synthetic lethal deficiency in DNA repair', *Proc Natl Acad Sci U S A*, 112(3), pp. 773-8.

Loi, M. *et al.* (2016) 'Macroautophagy Proteins Control MHC Class I Levels on Dendritic Cells and Shape Anti-viral CD8(+) T Cell Responses', *Cell Rep*, 15(5), pp. 1076-1087.

MacCallum, S.F. *et al.* (2013) 'Dysregulation of autophagy in chronic lymphocytic leukemia with the small-molecule Sirtuin inhibitor Tenovin-6', *Sci Rep*, 3, p. 1275.

Mahoney, E., Byrd, J.C. and Johnson, A.J. (2013) 'Autophagy and ER stress play an essential role in the mechanism of action and drug resistance of the cyclin-dependent kinase inhibitor flavopiridol', *Autophagy*, 9(3), pp. 434-5.

Mahoney, E., Johnson, A. J., Wagner, A. J., Hessler, J., Gupta, S. V., Herman, S. E., Andritsos, L., Jones, J. A., Flynn, J. M., Lucas, D. M., Grever, M. R., & Byrd, J. C. (2010) 'Autophagy Is a Relevant Cellular Process In CLL and Contributes to Drug Resistance of Flavopiridol', *Blood*, 116(21), p. 691.

Mahoney, E. *et al.* (2012) 'ER stress and autophagy: new discoveries in the mechanism of action and drug resistance of the cyclin-dependent kinase inhibitor flavopiridol', *Blood*, 120(6), pp. 1262-73.

Malhotra, S. *et al.* (2009) 'B cell antigen receptor endocytosis and antigen presentation to T cells require Vav and dynamin', *J Biol Chem*, 284(36), pp. 24088-97.

Mandik-Nayak, L. *et al.* (2008) 'Role of B cells in systemic lupus erythematosus and rheumatoid arthritis', *Curr Opin Immunol*, 20(6), pp. 639-45.

Mansilla, E. *et al.* (2010) 'The lysosomotropic agent, hydroxychloroquine, delivered in a biodegradable nanoparticle system, overcomes drug resistance of B-chronic lymphocytic leukemia cells in vitro', *Cancer Biother Radiopharm*, 25(1), pp. 97-103.

Maric, M.A., Taylor, M.D. and Blum, J.S. (1994) 'Endosomal aspartic proteinases are required for invariant-chain processing', *Proc Natl Acad Sci U S A*, 91(6), pp. 2171-5.

Marrack, P. *et al.* (2008) 'Evolutionarily conserved amino acids that control TCR-MHC interaction', *Annu Rev Immunol*, 26, pp. 171-203.

Martin, V.G. *et al.* (2016) 'Transitional B Cells in Early Human B Cell Development - Time to Revisit the Paradigm?', *Front Immunol*, 7, p. 546.

Martinez-Martin, N. *et al.* (2017) 'A switch from canonical to noncanonical autophagy shapes B cell responses', *Science*, 355(6325), pp. 641-647.

Martinez-Riano, A. *et al.* (2018) 'Antigen phagocytosis by B cells is required for a potent humoral response', *EMBO Rep*, 19(9).

Martinez, J. *et al.* (2011) 'Microtubule-associated protein 1 light chain 3 alpha (LC3)-associated phagocytosis is required for the efficient clearance of dead cells', *Proc Natl Acad Sci U S A*, 108(42), pp. 17396-401.

Martinez, J. *et al.* (2015) 'Molecular characterization of LC3-associated phagocytosis reveals distinct roles for Rubicon, NOX2 and autophagy proteins', *Nat Cell Biol*, 17(7), pp. 893-906.

Mauthe, M. *et al.* (2018) 'Chloroquine inhibits autophagic flux by decreasing autophagosome-lysosome fusion', *Autophagy*, 14(8), pp. 1435-1455.

McBlane, J.F. *et al.* (1995) 'Cleavage at a V(D)J recombination signal requires only RAG1 and RAG2 proteins and occurs in two steps', *Cell*, 83(3), pp. 387-95.

McGreal, E.P. *et al.* (2006) 'The carbohydrate-recognition domain of Dectin-2 is a C-type lectin with specificity for high mannose', *Glycobiology*, 16(5), pp. 422-30.

McLeod, I.X. *et al.* (2011) 'The class III kinase Vps34 promotes T lymphocyte survival through regulating IL-7Ralpha surface expression', *J Immunol*, 187(10), pp. 5051-61.

Meffre, E. and Nussenzweig, M.C. (2002) 'Deletion of immunoglobulin beta in developing B cells leads to cell death', *Proc Natl Acad Sci U S A*, 99(17), pp. 11334-9.

Mercer, C.A., Kaliappan, A. and Dennis, P.B. (2009) 'A novel, human Atg13 binding protein, Atg101, interacts with ULK1 and is essential for macroautophagy', *Autophagy*, 5(5), pp. 649-62.

Mettlen, M. *et al.* (2009) 'Dissecting dynamin's role in clathrin-mediated endocytosis', *Biochem Soc Trans*, 37(Pt 5), pp. 1022-6.

Mezzaroba, N. *et al.* (2013) 'New potential therapeutic approach for the treatment of B-Cell malignancies using chlorambucil/hydroxychloroquine-loaded anti-CD20 nanoparticles', *PLoS One*, 8(9), p. e74216.

Minton, A.R. *et al.* (2022) 'B-cell receptor dependent phagocytosis and presentation of particulate antigen by chronic lymphocytic leukemia cells', *Exploration of Targeted Anti-tumor Therapy*, 3(1), pp. 37-49.

Mizushima, N. and Yoshimori, T. (2007) 'How to interpret LC3 immunoblotting', *Autophagy*, 3(6), pp. 542-5.

Mkaddem, S.B. *et al.* (2017) 'Lyn and Fyn function as molecular switches that control immunoreceptors to direct homeostasis or inflammation', *Nat Commun*, 8(1), p. 246.

Mockridge, C.I. *et al.* (2007) 'Reversible anergy of sIgM-mediated signaling in the two subsets of CLL defined by VH-gene mutational status', *Blood*, 109(10), pp. 4424-31.

Moens, L., Kane, A. and Tangye, S.G. (2016) 'Naive and memory B cells exhibit distinct biochemical responses following BCR engagement', *Immunol Cell Biol*, 94(8), pp. 774-86.

Moss, C.X., Tree, T.I. and Watts, C. (2007) 'Reconstruction of a pathway of antigen processing and class II MHC peptide capture', *EMBO J*, 26(8), pp. 2137-47.

Mrakovcic, M. and Frohlich, L.F. (2018) 'p53-Mediated Molecular Control of Autophagy in Tumor Cells', *Biomolecules*, 8(2).

Muehlinghaus, G. *et al.* (2005) 'Regulation of CXCR3 and CXCR4 expression during terminal differentiation of memory B cells into plasma cells', *Blood*, 105(10), pp. 3965-71.

Munz, C. (2012) 'Antigen Processing for MHC Class II Presentation via Autophagy', *Front Immunol*, 3, p. 9.

Muzio, M. *et al.* (2008) 'Constitutive activation of distinct BCR-signaling pathways in a subset of CLL patients: a molecular signature of anergy', *Blood*, 112(1), pp. 188-95.

Natkanski, E. *et al.* (2013) 'B cells use mechanical energy to discriminate antigen affinities', *Science*, 340(6140), pp. 1587-90.

Nazarko, V.Y. and Zhong, Q. (2013) 'ULK1 targets Beclin-1 in autophagy', *Nat Cell Biol*, 15(7), pp. 727-8.

Ni, Z. *et al.* (2017) 'AKT-mediated phosphorylation of ATG4B impairs mitochondrial activity and enhances the Warburg effect in hepatocellular carcinoma cells', *Autophagy*, pp. 1-43.

Nick McElhinny, S.A. *et al.* (2000) 'Ku recruits the XRCC4-ligase IV complex to DNA ends', *Mol Cell Biol*, 20(9), pp. 2996-3003.

Niiro, H. *et al.* (2004) 'The B lymphocyte adaptor molecule of 32 kilodaltons (Bam32) regulates B cell antigen receptor internalization', *J Immunol*, 173(9), pp. 5601-9.

Nojima, H. *et al.* (2003) 'The mammalian target of rapamycin (mTOR) partner, raptor, binds the mTOR substrates p70 S6 kinase and 4E-BP1 through their TOR signaling (TOS) motif', *J Biol Chem*, 278(18), pp. 15461-4.

Noman, M.Z. *et al.* (2020) 'Inhibition of Vps34 reprograms cold into hot inflamed tumors and improves anti-PD-1/PD-L1 immunotherapy', *Sci Adv*, 6(18), p. eaax7881.

O'Brien, S. *et al.* (2018) 'Single-agent ibrutinib in treatment-naive and relapsed/refractory chronic lymphocytic leukemia: a 5-year experience', *Blood*, 131(17), pp. 1910-1919.

O'Neill, S.K. *et al.* (2011) 'Monophosphorylation of CD79a and CD79b ITAM motifs initiates a SHIP-1 phosphatase-mediated inhibitory signaling cascade required for B cell anergy', *Immunity*, 35(5), pp. 746-56.

Oliver, P.M. *et al.* (2006) 'Loss of the proapoptotic protein, Bim, breaks B cell anergy', *J Exp Med*, 203(3), pp. 731-41.

Onabajo, O.O. *et al.* (2008) 'Actin-binding protein 1 regulates B cell receptor-mediated antigen processing and presentation in response to B cell receptor activation', *J Immunol*, 180(10), pp. 6685-95.

Ono, M. *et al.* (1997) 'Deletion of SHIP or SHP-1 reveals two distinct pathways for inhibitory signaling', *Cell*, 90(2), pp. 293-301.

Orchard, J.A. *et al.* (2004) 'ZAP-70 expression and prognosis in chronic lymphocytic leukaemia', *Lancet*, 363(9403), pp. 105-11.

Os, A. *et al.* (2013) 'Chronic lymphocytic leukemia cells are activated and proliferate in response to specific T helper cells', *Cell Rep*, 4(3), pp. 566-77.

Packham, G. *et al.* (2014) 'The outcome of B-cell receptor signaling in chronic lymphocytic leukemia: proliferation or anergy', *Haematologica*, 99(7), pp. 1138-48.

Palma, M. *et al.* (2017) 'T cells in chronic lymphocytic leukemia display dysregulated expression of immune checkpoints and activation markers', *Haematologica*, 102(3), pp. 562-572.

Panayiotidis, P. *et al.* (1993) 'Interleukin-4 inhibits apoptotic cell death and loss of the bcl-2 protein in B-chronic lymphocytic leukaemia cells in vitro', *Br J Haematol*, 85(3), pp. 439-45.

Parekh, V.V. *et al.* (2017) 'Autophagy-related protein Vps34 controls the homeostasis and function of antigen cross-presenting CD8alpha(+) dendritic cells', *Proc Natl Acad Sci U S A*, 114(31), pp. E6371-E6380.

Parra, D. *et al.* (2012) 'Pivotal advance: peritoneal cavity B-1 B cells have phagocytic and microbicidal capacities and present phagocytosed antigen to CD4+ T cells', *J Leukoc Biol*, 91(4), pp. 525-36.

Pasquier, B. (2015) 'SAR405, a PIK3C3/Vps34 inhibitor that prevents autophagy and synergizes with MTOR inhibition in tumor cells', *Autophagy*, 11(4), pp. 725-6.

Patten, P.E. *et al.* (2012) 'IGHV-unmutated and IGHV-mutated chronic lymphocytic leukemia cells produce activation-induced deaminase protein with a full range of biologic functions', *Blood*, 120(24), pp. 4802-11.

Petherick, K.J. *et al.* (2015a) 'Pharmacological inhibition of ULK1 kinase blocks mammalian target of rapamycin (mTOR)-dependent autophagy', *J Biol Chem*, 290(18), pp. 11376-83.

Petherick, K.J. *et al.* (2015b) 'Pharmacological inhibition of ULK1 kinase blocks mammalian target of rapamycin (mTOR)-dependent autophagy', *J Biol Chem*, 290(48), p. 28726.

Pizzolo, G. *et al.* (1983) 'Immunohistologic study of bone marrow involvement in B-chronic lymphocytic leukemia', *Blood*, 62(6), pp. 1289-96.

Puente, C., Hendrickson, R.C. and Jiang, X. (2016) 'Nutrient-regulated Phosphorylation of ATG13 Inhibits Starvation-induced Autophagy', *J Biol Chem*, 291(11), pp. 6026-35.

Qi, S. *et al.* (2015) 'Structure of the Human Atg13-Atg101 HORMA Heterodimer: an Interaction Hub within the ULK1 Complex', *Structure*, 23(10), pp. 1848-57.

Qu, X. *et al.* (2003) 'Promotion of tumorigenesis by heterozygous disruption of the beclin 1 autophagy gene', *J Clin Invest*, 112(12), pp. 1809-20.

Quach, T.D. *et al.* (2016) 'Human B-1 and B-2 B Cells Develop from Lin-CD34+CD38lo Stem Cells', *J Immunol*, 197(10), pp. 3950-3958.

Quijano, S. *et al.* (2008) 'Impact of trisomy 12, del(13q), del(17p), and del(11q) on the immunophenotype, DNA ploidy status, and proliferative rate of leukemic B-cells in chronic lymphocytic leukemia', *Cytometry B Clin Cytom*, 74(3), pp. 139-49.

Rameh, L.E. and Cantley, L.C. (1999) 'The role of phosphoinositide 3-kinase lipid products in cell function', *J Biol Chem*, 274(13), pp. 8347-50.

Ramsay, A.G. *et al.* (2008) 'Chronic lymphocytic leukemia T cells show impaired immunological synapse formation that can be reversed with an immunomodulating drug', *J Clin Invest*, 118(7), pp. 2427-37.

Ravetch, J.V. and Lanier, L.L. (2000) 'Immune inhibitory receptors', *Science*, 290(5489), pp. 84-9.

Rejman, J. *et al.* (2004) 'Size-dependent internalization of particles via the pathways of clathrin- and caveolae-mediated endocytosis', *Biochem J*, 377(Pt 1), pp. 159-69.

Reth, M. (1989) 'Antigen receptor tail clue', *Nature*, 338(6214), pp. 383-4.

Reversat, A. *et al.* (2015) 'Polarity protein Par3 controls B-cell receptor dynamics and antigen extraction at the immune synapse', *Mol Biol Cell*, 26(7), pp. 1273-85.

Ribes, S. *et al.* (2010) 'Toll-like receptor stimulation enhances phagocytosis and intracellular killing of nonencapsulated and encapsulated Streptococcus pneumoniae by murine microglia', *Infect Immun*, 78(2), pp. 865-71.

Riches, J.C. *et al.* (2013) 'T cells from CLL patients exhibit features of T-cell exhaustion but retain capacity for cytokine production', *Blood*, 121(9), pp. 1612-21.

Richter, J.D. and Sonenberg, N. (2005) 'Regulation of cap-dependent translation by eIF4E inhibitory proteins', *Nature*, 433(7025), pp. 477-80.

Ritvo, P.G. and Klatzmann, D. (2019) 'Interleukin-1 in the Response of Follicular Helper and Follicular Regulatory T Cells', *Front Immunol*, 10, p. 250.

Roberts, A.D. *et al.* (2020) 'Structurally distinct endocytic pathways for B cell receptors in B lymphocytes', *Mol Biol Cell*, 31(25), pp. 2826-2840.

Rogov, V.V. *et al.* (2017) 'Structural and functional analysis of the GABARAP interaction motif (GIM)', *EMBO Rep*, 18(8), pp. 1382-1396.

Rolink, A.G. *et al.* (1999) 'B cell development in the mouse from early progenitors to mature B cells', *Immunol Lett*, 68(1), pp. 89-93.

Rolli, V. *et al.* (2002) 'Amplification of B cell antigen receptor signaling by a Syk/ITAM positive feedback loop', *Mol Cell*, 10(5), pp. 1057-69.

Romao, S. *et al.* (2013) 'Autophagy proteins stabilize pathogen-containing phagosomes for prolonged MHC II antigen processing', *J Cell Biol*, 203(5), pp. 757-66.

Romero Mendez, I.Z. *et al.* (2007) 'Potentiation of the immune response to non-adsorbed antigens by aluminum-containing adjuvants', *Vaccine*, 25(5), pp. 825-33.

Rosenspire, A.J. and Chen, K. (2015) 'Anergic B Cells: Precarious On-Call Warriors at the Nexus of Autoimmunity and False-Flagged Pathogens', *Front Immunol*, 6, p. 580.

Rosenwald, A. *et al.* (2001) 'Relation of gene expression phenotype to immunoglobulin mutation genotype in B cell chronic lymphocytic leukemia', *J Exp Med*, 194(11), pp. 1639-47.

Ross, S.H. and Cantrell, D.A. (2018) 'Signaling and Function of Interleukin-2 in T Lymphocytes', *Annu Rev Immunol*, 36, pp. 411-433.

Rostislavleva, K. *et al.* (2015) 'Structure and flexibility of the endosomal Vps34 complex reveals the basis of its function on membranes', *Science*, 350(6257), p. aac7365.

Rudack, C. *et al.* (2003) 'The primary role in biologic activity of the neutrophil chemokines IL-8 and GRO-alpha in cultured nasal epithelial cells', *J Interferon Cytokine Res*, 23(2), pp. 113-23.

Russell, R.C. *et al.* (2013) 'ULK1 induces autophagy by phosphorylating Beclin-1 and activating VPS34 lipid kinase', *Nat Cell Biol*, 15(7), pp. 741-50.

Sancak, Y. *et al.* (2007) 'PRAS40 is an insulin-regulated inhibitor of the mTORC1 protein kinase', *Mol Cell*, 25(6), pp. 903-15.

Sanjuan, M.A. *et al.* (2007) 'Toll-like receptor signalling in macrophages links the autophagy pathway to phagocytosis', *Nature*, 450(7173), pp. 1253-7.

Sasai, M. *et al.* (2017) 'Essential role for GABARAP autophagy proteins in interferon-inducible GTPase-mediated host defense', *Nat Immunol*, 18(8), pp. 899-910.

Sato, K. *et al.* (2006) 'Dectin-2 is a pattern recognition receptor for fungi that couples with the Fc receptor gamma chain to induce innate immune responses', *J Biol Chem*, 281(50), pp. 38854-66.

Scharenberg, A.M. *et al.* (1998) 'Phosphatidylinositol-3,4,5-trisphosphate (PtdIns-3,4,5-P3)/Tec kinase-dependent calcium signaling pathway: a target for SHIP-mediated inhibitory signals', *EMBO J*, 17(7), pp. 1961-72.

Schjetne, K.W. *et al.* (2002) 'A mouse C kappa-specific T cell clone indicates that DC-SIGN is an efficient target for antibody-mediated delivery of T cell epitopes for MHC class II presentation', *Int Immunol*, 14(12), pp. 1423-30.

Schroder, B. (2016) 'The multifaceted roles of the invariant chain CD74--More than just a chaperone', *Biochim Biophys Acta*, 1863(6 Pt A), pp. 1269-81.

Schulz, H. *et al.* (2002) 'Phase 2 study of a combined immunochemotherapy using rituximab and fludarabine in patients with chronic lymphocytic leukemia', *Blood*, 100(9), pp. 3115-20.

Sedlik, C. *et al.* (2003) 'A critical role for Syk protein tyrosine kinase in Fc receptor-mediated antigen presentation and induction of dendritic cell maturation', *J Immunol*, 170(2), pp. 846-52.

Sharma, S., Orlowski, G. and Song, W. (2009) 'Btk regulates B cell receptor-mediated antigen processing and presentation by controlling actin cytoskeleton dynamics in B cells', *J Immunol*, 182(1), pp. 329-39.

Simon, A.K. and Clarke, A.J. (2016) 'Non-canonical autophagy LAPs lupus', *Cell Death Differ*, 23(8), pp. 1267-8.

Sini, P. *et al.* (2010) 'Simultaneous inhibition of mTORC1 and mTORC2 by mTOR kinase inhibitor AZD8055 induces autophagy and cell death in cancer cells', *Autophagy*, 6(4), pp. 553-4.

Sintes, J. *et al.* (2017) 'mTOR intersects antibody-inducing signals from TACI in marginal zone B cells', *Nat Commun*, 8(1), p. 1462.

Skalet, A.H. *et al.* (2005) 'Rapid B cell receptor-induced unfolded protein response in nonsecretory B cells correlates with pro- versus antiapoptotic cell fate', *J Biol Chem*, 280(48), pp. 39762-71.

Skytte Rasmussen, M. *et al.* (2017) 'ATG4B contains a C-terminal LIR motif important for binding and efficient cleavage of mammalian orthologs of yeast Atg8', *Autophagy*, 13(5), pp. 834-853.

Slobodkin, M.R. and Elazar, Z. (2013) 'The Atg8 family: multifunctional ubiquitin-like key regulators of autophagy', *Essays Biochem*, 55, pp. 51-64.

Smith-Garvin, J.E., Koretzky, G.A. and Jordan, M.S. (2009) 'T cell activation', *Annu Rev Immunol*, 27, pp. 591-619.

Smith, L. *et al.* (2015) 'Biological Significance of B Cell Receptor Mediated Regulation of Autophagy in Chronic Lymphocytic Leukemia', *Blood*, 126(23), p. 4130.

Smith, L.D. *et al.* (2020) 'BCR signaling contributes to autophagy regulation in chronic lymphocytic leukemia', *Leukemia*, 34(2), pp. 640-644.

Smith, M.D. *et al.* (2018) 'CCPG1 Is a Non-canonical Autophagy Cargo Receptor Essential for ER-Phagy and Pancreatic ER Proteostasis', *Dev Cell*, 44(2), pp. 217-232 e11.

Solvik, T. and Debnath, J. (2016) 'At the crossroads of autophagy and infection: Noncanonical roles for ATG proteins in viral replication', *J Cell Biol*, 214(5), pp. 503-5.

Spillane, K.M. and Tolar, P. (2017) 'B cell antigen extraction is regulated by physical properties of antigen-presenting cells', *J Cell Biol*, 216(1), pp. 217-230.

Spillane, K.M. and Tolar, P. (2018) 'DNA-Based Probes for Measuring Mechanical Forces in Cell-Cell Contacts: Application to B Cell Antigen Extraction from Immune Synapses', *Methods Mol Biol*, 1707, pp. 69-80.

Sprenkeler, E.G., Gresnigt, M.S. and van de Veerdonk, F.L. (2016) 'LC3-associated phagocytosis: a crucial mechanism for antifungal host defence against Aspergillus fumigatus', *Cell Microbiol*, 18(9), pp. 1208-16.

Stevenson, F.K. and Caligaris-Cappio, F. (2004) 'Chronic lymphocytic leukemia: revelations from the B-cell receptor', *Blood*, 103(12), pp. 4389-95.

Stevenson, F.K. *et al.* (2011) 'B-cell receptor signaling in chronic lymphocytic leukemia', *Blood*, 118(16), pp. 4313-20.

Stoddart, A. *et al.* (2002) 'Lipid rafts unite signaling cascades with clathrin to regulate BCR internalization', *Immunity*, 17(4), pp. 451-62.

Stolz, A., Ernst, A. and Dikic, I. (2014) 'Cargo recognition and trafficking in selective autophagy', *Nat Cell Biol*, 16(6), pp. 495-501.

Strawbridge, A.B. and Blum, J.S. (2007) 'Autophagy in MHC class II antigen processing', *Curr Opin Immunol*, 19(1), pp. 87-92.

Su, H. *et al.* (2017) 'VPS34 Acetylation Controls Its Lipid Kinase Activity and the Initiation of Canonical and Non-canonical Autophagy', *Mol Cell*, 67(6), pp. 907-921 e7.

Tabata, H. *et al.* (2020) 'Syk facilitates phagosome-lysosome fusion by regulating actin-remodeling in complement-mediated phagocytosis', *Sci Rep*, 10(1), p. 22086.

Taherbhoy, A.M. *et al.* (2011) 'Atg8 transfer from Atg7 to Atg3: a distinctive E1-E2 architecture and mechanism in the autophagy pathway', *Mol Cell*, 44(3), pp. 451-61.

Tan, Q. *et al.* (2016) 'Role of Autophagy as a Survival Mechanism for Hypoxic Cells in Tumors', *Neoplasia*, 18(6), pp. 347-55.

Tang, F. *et al.* (2017) 'SBI0206965, a novel inhibitor of Ulk1, suppresses non-small cell lung cancer cell growth by modulating both autophagy and apoptosis pathways', *Oncol Rep*, 37(6), pp. 3449-3458.

Tay, M.Z., Wiehe, K. and Pollara, J. (2019) 'Antibody-Dependent Cellular Phagocytosis in Antiviral Immune Responses', *Front Immunol*, 10, p. 332.

Ten Hacken, E. *et al.* (2016) 'Functional Differences between IgM and IgD Signaling in Chronic Lymphocytic Leukemia', *J Immunol*, 197(6), pp. 2522-31.

Tisch, R., Roifman, C.M. and Hozumi, N. (1988) 'Functional differences between immunoglobulins M and D expressed on the surface of an immature B-cell line', *Proc Natl Acad Sci U S A*, 85(18), pp. 6914-8.

Tolar, P. and Spillane, K.M. (2014) 'Force generation in B-cell synapses: mechanisms coupling B-cell receptor binding to antigen internalization and affinity discrimination', *Adv Immunol*, 123, pp. 69-100.

Tresckow, J.V. *et al.* (2019) 'The Treatment of Chronic Lymphatic Leukemia', *Dtsch Arztebl Int*, 116(4), pp. 41-46.

Tse, S.M. *et al.* (2003) 'Differential role of actin, clathrin, and dynamin in Fc gamma receptor-mediated endocytosis and phagocytosis', *J Biol Chem*, 278(5), pp. 3331-8.

Tubo, N.J. *et al.* (2013) 'Single naive CD4+ T cells from a diverse repertoire produce different effector cell types during infection', *Cell*, 153(4), pp. 785-96.

Tze, L.E. *et al.* (2000) 'Ig light chain receptor editing in anergic B cells', *J Immunol*, 165(12), pp. 6796-802.

Ubelhart, R. *et al.* (2015) 'Responsiveness of B cells is regulated by the hinge region of IgD', *Nat Immunol*, 16(5), pp. 534-43.

van Attekum, M.H.A. *et al.* (2017) 'CD40 signaling instructs chronic lymphocytic leukemia cells to attract monocytes via the CCR2 axis', *Haematologica*, 102(12), pp. 2069-2076.

van der Straten, L. *et al.* (2020) 'Survival continues to increase in chronic lymphocytic leukaemia: a population-based analysis among 20 468 patients diagnosed in the Netherlands between 1989 and 2016', *Br J Haematol*, 189(3), pp. 574-577.

Van Kaer, L. *et al.* (2019) 'Role of autophagy in MHC class I-restricted antigen presentation', *Mol Immunol*, 113, pp. 2-5.

Vangapandu, H.V. *et al.* (2017) 'B-cell Receptor Signaling Regulates Metabolism in Chronic Lymphocytic Leukemia', *Mol Cancer Res*, 15(12), pp. 1692-1703.

Vazquez, G. *et al.* (2002) 'An inositol 1,4,5-trisphosphate receptor-dependent cation entry pathway in DT40 B lymphocytes', *EMBO J*, 21(17), pp. 4531-8.

Venkitaraman, A.R. *et al.* (1991) 'The B-cell antigen receptor of the five immunoglobulin classes', *Nature*, 352(6338), pp. 777-81.

Verfaillie, T. *et al.* (2010) 'Linking ER Stress to Autophagy: Potential Implications for Cancer Therapy', *Int J Cell Biol*, 2010, p. 930509.

Vicinanza, M. *et al.* (2015) 'PI(5)P regulates autophagosome biogenesis', *Mol Cell*, 57(2), pp. 219-34.

Vos, Q. *et al.* (2000) 'B-cell activation by T-cell-independent type 2 antigens as an integral part of the humoral immune response to pathogenic microorganisms', *Immunol Rev*, 176, pp. 154-70.

Waldron, M., Winter, A. and Hill, B.T. (2017) 'Pharmacokinetic and Pharmacodynamic Considerations in the Treatment of Chronic Lymphocytic Leukemia: Ibrutinib, Idelalisib, and Venetoclax', *Clin Pharmacokinet*, 56(11), pp. 1255-1266.

Walker, S. *et al.* (2008) 'Making autophagosomes: localized synthesis of phosphatidylinositol 3-phosphate holds the clue', *Autophagy*, 4(8), pp. 1093-6.

Wallot-Hieke, N. *et al.* (2018) 'Systematic analysis of ATG13 domain requirements for autophagy induction', *Autophagy*, 14(5), pp. 743-763.

Wan, W. *et al.* (2017) 'mTORC1 Phosphorylates Acetyltransferase p300 to Regulate Autophagy and Lipogenesis', *Mol Cell*, 68(2), pp. 323-335 e6.

Watanabe, K. and Tsubata, T. (2009) 'Autophagy connects antigen receptor signaling to costimulatory signaling in B lymphocytes', *Autophagy*, 5(1), pp. 108-10.

Watts, C. (2001) 'Antigen processing in the endocytic compartment', *Curr Opin Immunol*, 13(1), pp. 26-31.

Weidberg, H. *et al.* (2010) 'LC3 and GATE-16/GABARAP subfamilies are both essential yet act differently in autophagosome biogenesis', *EMBO J*, 29(11), pp. 1792-802.

Wenger, T. *et al.* (2012) 'Autophagy inhibition promotes defective neosynthesized proteins storage in ALIS, and induces redirection toward proteasome processing and MHCI-restricted presentation', *Autophagy*, 8(3), pp. 350-63.

White, E. (2015) 'The role for autophagy in cancer', *J Clin Invest*, 125(1), pp. 42-6.

White, E. (2016) 'Autophagy and p53', *Cold Spring Harb Perspect Med*, 6(4), p. a026120.

Woyach, J.A. (2013) 'Survival of the weak (signalers): anergy in CLL', *Blood*, 121(19), pp. 3781-3.

Woyach, J.A. *et al.* (2017) 'BTK(C481S)-Mediated Resistance to Ibrutinib in Chronic Lymphocytic Leukemia', *J Clin Oncol*, 35(13), pp. 1437-1443.

Wu, W. *et al.* (2015) 'PINK1-Parkin-Mediated Mitophagy Protects Mitochondrial Integrity and Prevents Metabolic Stress-Induced Endothelial Injury', *PLoS One*, 10(7), p. e0132499.

Xiong, Q. *et al.* (2018) 'The Role of ATG16 in Autophagy and The Ubiquitin Proteasome System', *Cells*, 8(1).

Xu, Y. *et al.* (2007) 'Toll-like receptor 4 is a sensor for autophagy associated with innate immunity', *Immunity*, 27(1), pp. 135-44.

Yam-Puc, J.C. *et al.* (2018) 'Role of B-cell receptors for B-cell development and antigen-induced differentiation', *F1000Res*, 7, p. 429.

Yamamoto, K. *et al.* (2020) 'Autophagy promotes immune evasion of pancreatic cancer by degrading MHC-I', *Nature*, 581(7806), pp. 100-105.

Yan, M.M. *et al.* (2015) 'Interplay between unfolded protein response and autophagy promotes tumor drug resistance', *Oncol Lett*, 10(4), pp. 1959-1969.

Yang, G. *et al.* (2021) 'Autophagy-related protein PIK3C3/VPS34 controls T cell metabolism and function', *Autophagy*, 17(5), pp. 1193-1204.

Yang, W. *et al.* (2001) 'Regulation of transcription by AMP-activated protein kinase: phosphorylation of p300 blocks its interaction with nuclear receptors', *J Biol Chem*, 276(42), pp. 38341-4.

Yeomans, A. *et al.* (2016) 'Engagement of the B-cell receptor of chronic lymphocytic leukemia cells drives global and MYC-specific mRNA translation', *Blood*, 127(4), pp. 449-57.

Yoshimori, T. *et al.* (1991) 'Bafilomycin A1, a specific inhibitor of vacuolar-type H(+)-ATPase, inhibits acidification and protein degradation in lysosomes of cultured cells', *J Biol Chem*, 266(26), pp. 17707-12.

Youle, R.J. and Narendra, D.P. (2011) 'Mechanisms of mitophagy', *Nat Rev Mol Cell Biol*, 12(1), pp. 9-14.

Yu, L. *et al.* (2010) 'Termination of autophagy and reformation of lysosomes regulated by mTOR', *Nature*, 465(7300), pp. 942-6.

Yuan, L.W. and Gambee, J.E. (2000) 'Phosphorylation of p300 at serine 89 by protein kinase C', *J Biol Chem*, 275(52), pp. 40946-51.

Yuan, N. *et al.* (2015) 'Autophagy collaborates with ubiquitination to downregulate oncoprotein E2A/Pbx1 in B-cell acute lymphoblastic leukemia', *Blood Cancer J*, 5, p. e274.

Yun, C.W. and Lee, S.H. (2018) 'The Roles of Autophagy in Cancer', *Int J Mol Sci*, 19(11).

Yuseff, M.I. and Lennon-Dumenil, A.M. (2015) 'B Cells use Conserved Polarity Cues to Regulate Their Antigen Processing and Presentation Functions', *Front Immunol*, 6, p. 251.

Yuseff, M.I. *et al.* (2011) 'Polarized secretion of lysosomes at the B cell synapse couples antigen extraction to processing and presentation', *Immunity*, 35(3), pp. 361-74.

Zhang, F. and Yu, X. (2011) 'WAC, a functional partner of RNF20/40, regulates histone H2B ubiquitination and gene transcription', *Mol Cell*, 41(4), pp. 384-97.

Zhang, Y. *et al.* (2018) 'Plasma cell output from germinal centers is regulated by signals from Tfh and stromal cells', *J Exp Med*, 215(4), pp. 1227-1243.

Zhao, M. and Klionsky, D.J. (2011) 'AMPK-dependent phosphorylation of ULK1 induces autophagy', *Cell Metab*, 13(2), pp. 119-20.

Zhou, D. *et al.* (2005) 'Lamp-2a facilitates MHC class II presentation of cytoplasmic antigens', *Immunity*, 22(5), pp. 571-81.

Zhu, J., Yamane, H. and Paul, W.E. (2010) 'Differentiation of effector CD4 T cell populations (*)', *Annu Rev Immunol*, 28, pp. 445-89.